

Open Research Online

The Open University's repository of research publications and other research outputs

Decellularised Normal and Tumour Scaffolds for Cancer Organoid Cultures as a Model of Colorectal Peritoneal Metastases

Thesis

How to cite:

Varinelli, Luca (2022). Decellularised Normal and Tumour Scaffolds for Cancer Organoid Cultures as a Model of Colorectal Peritoneal Metastases. PhD thesis The Open University.

For guidance on citations see [FAQs](#).

© 2021 Luca Varinelli



<https://creativecommons.org/licenses/by-nc-nd/4.0/>

Version: Version of Record

Link(s) to article on publisher's website:
<http://dx.doi.org/doi:10.21954/ou.ro.000142a3>

Copyright and Moral Rights for the articles on this site are retained by the individual authors and/or other copyright owners. For more information on Open Research Online's data [policy](#) on reuse of materials please consult the policies page.

oro.open.ac.uk



The Open University
Milton Keynes, United Kingdom

L'ONCOLOGIA ITALIANA È NATA QUI

Sistema Socio Sanitario



Fondazione IRCCS
Istituto Nazionale dei Tumori

via Venezian, 1 20133 Milano



Regione
Lombardia

Affiliated Research Centre
Fondazione IRCCS Istituto Nazionale dei Tumori
Milano, Italia

Decellularised Normal and Tumour Scaffolds for Cancer

Organoid Cultures as a Model of Colorectal Peritoneal Metastases

Thesis presented for the degree of Doctor of Philosophy
The Open University, Milton Keynes (UK)

School of Life, Health and Chemical Sciences

Luca Varinelli

Personal Identifier: G4609795

October 2021

... “*This one means the most to me
Stays here for eternity
A ship that always stays the course
An anchor for my every choice

A rose that shines down from above
I signed and sealed these words in blood
I heard them once, sung in a song
It played again and we sang along

You'll always be there with me
Even if you're gone
You'll always have my love
Our memory will live on” ...

To my grandpa,
with love
Luca

1	
1. Abbreviations	5
10. References	164
11. Appendix	186
2	
2. Declaration	11
3	
3. Abstract	14
4	
4. Introduction	16
4.1 Colorectal cancer	16
4.10 Pathophysiology and molecular features of PM disease	36
4.11 The peritoneal metastatic cascade	38
4.12 The Extracellular matrix: involvement in cancer	49
4.13 ECM and its involvement in the cellular signaling	56
4.14 Biomechanical properties and functions of the ECM in cancer	60
4.15 Conclusions	64
4.16 The need for preclinical models to study PM disease	65
4.17 Patient-derived 3D organoids cultures	67
4.18 Role of organoids in translational cancer research	73
4.19 Organoids and their role in basic cancer research	79
4.2 Pathogenesis of Colorectal cancers	17
4.20 Conclusions	84
4.21 Decellularised ECM for bioengineering cancer	85
4.22 Decellularisation methodologies	86
4.23 dECMs for <i>in vitro</i> tumour modelling	90
4.3 Left-sided and right-sided CRC: main molecular features	19
4.4 Consensus molecular subtypes of CRC	21
4.5 Metastatic Colorectal Cancer	25
4.6 The metastatic niche	25
4.7 The peritoneal metastasis disease	30
4.8 Epidemiology of PM disease	31
4.9 Current treatment approaches for PM diseases	32
5	
5. Hypothesis alongside the project and specific aims	96

6	
6. Materials and Methods	96
6.1 Human tissues	97
6.10 ECM component quantification	109
6.11 Nanoindentation measurements by AFM	110
6.12 Stem cell maintenance, proliferation, and apoptosis assays	111
6.13 RNA-seq analysis	112
6.14 Gene Set Enrichment Analysis	113
6.15 Treatment with cytotoxic drugs	113
6.16 <i>ex vivo</i> PM lesion to test HIPEC efficacy <i>in vitro</i>	113
6.17 MMT Assay and 3D-dECMs lyophilization	115
6.18 Statistical analyses	115
6.2 Development of PM-derived organoids	98
6.3 Preparation of 3D-dECMs	102
6.4 <i>ex vivo</i> engineered PM lesion	104
6.5 Nucleic acid extraction	105
6.6 Histochemistry (HC), IHC and IF	106
6.7 DNA sequencing	108
6.8 Morphological evaluation of the decellularised matrices	108
6.9 Nanoscale topographical analysis of 3D-dECMs	109
7	
7. Results	116
7.1 Development of PM-derived organoids	116
7.10 HIPEC treatments lead to apoptosis in PM-derived organoids	154
7.2 PM-derived organoid characterisation	117
7.3 Development of 3D decellularised scaffolds	122
7.4 3D-dECMs: morphological features and mechanical properties	127
7.5 Decellularised scaffolds sustain PM-derived organoid growth	134
7.6 3D decellularised scaffolds support the proliferation of organoids	136
7.7 <i>ex vivo</i> engineered PM lesions reproduce the patient's PM	139
7.8 Gene expression analysis of engineered PM lesions	142
7.9 3D-dECMs decrease the efficacy of HIPEC treatments	149
8	
8. Discussion	158
9	
9. Conclusions	162

1. Abbreviations

3D; Three Dimensions

3D-dECM; Three Dimensional decellularised-Extracellular Matrix

A83-01; anti-p38 inhibitor

ADAM; Adamylisins

AFM; Atomic Force Microscopy

ANOVA; Analysis of Variance

APC; Adenomatous Polyposis Coli gene

aSCs; Organ-Restricted Adult Stem Cells

ASPN; Asporin

ATM; Serine-protein kinase ATM

BARD1; BRCA1-associated RING domain protein 1

BMDCs; Bone Marrow-Derived Cells

BMP; Bone Morphogenetic Proteins

BMP4; Bone Morphogenic Protein 4

BMPRI1A; Bone Morphogenetic Protein Receptor type-1A

BRAF; Serine/threonine-protein kinase B-raf gene

BRCA1-2; Breast Cancer type 1-2 susceptibility protein

BRIP1; Fanconi anaemia group J protein

CAF; Cancer-related Activated Fibroblasts

CAMK2A; Calcium/calmodulin-dependent protein kinase type II subunit alpha

CCL2; Chemokine (C-C motif) Ligand 2

CCL21; Chemokine (C-C motif) Ligand 21

CCR; Effectiveness of Cytoreduction

CD43; Cluster Differentiation 43

CD44; Cluster Differentiation 44

CDH1; Fizzy-related protein homolog

CDK4; Cyclin-dependent kinase 4

CDKN2A; Cyclin-dependent kinase inhibitor 2A

CDX2; Homeobox protein CDX-2

CHEK2; Serine/threonine-protein kinase Chk2

CHIR; GSK inhibitor

CK AE1/AE3; Cytokeratin AE1/AE3

CK19; Cytokeratin-19

CK20; Cytokeratin-20

c-MET; Hepatocyte growth factor receptor

CMS; Consensus Molecular Subtypes

CO₂; Carbon Dioxide

COL1A2; Collagen Type-1-alpha-2

COL3A1; Collagen Type-3-alpha-1

CpG; CpG island

CRC; Colorectal Cancer

CRISPR-Cas9; Clustered Regularly Interspaced Short Palindromic Repeats

CRS; Cytoreductive Surgery

CTLA4; Cytotoxic T-lymphocyte-Associated Protein 4,

CTNNA1; Catenin alpha 1

CXCL12; Chemokine (C-X-C-motif) Ligand 12

CXCL2-3-8; Chemokine (C-X-C-motif) Ligand 2-3-8

CXCR3/CCR5; Chemokine (C-X-C motif) Receptor 3/C-C Chemokine Receptor Type 5

CXCR4; Chemokine (C-X-C motif) Receptor 4

DAPI; 4',6-Diamidino-2-Phenylindole

DCN; Decorin

DDR1-2; Discoidin Domain-Containing Receptors 1

dECM; decellularized-Extracellular Matrix

DEGs; Differentially Expressed Genes

DMEM-F12; Dulbecco's Modified Medium Eagle F12

dMMR; Mismatch Repair Mechanism

DMSO; Dimethyl sulfoxide

DPT; Dermatopontin

ECM; Extracellular Matrix

EDIL3; EGF-like repeat and discoidin I-like domain-containing protein 3

EDTA; Ethylenediamine tetraacetic acid

EFEMP1; EGF-containing fibulin-like extracellular matrix protein 1

EGFR; Epidermal Growth Factor Receptor

EMT; Epithelial-to-Mesenchymal Transition

EPCAM; Epithelial cell adhesion molecule

ERBB2; Receptor tyrosine-protein kinase erbB-2

ERK; Mitogen-activated protein kinase

ES; Embryonic Pluripotent Stem Cells

EVs; Extracellular Vesicles

FAK; Focal adhesion kinase protein

FANCM; Fanconi anaemia group M protein

FBN2; Fibrillin-2

FBS; Fetal Bovine Serum

FCS; Fetal Calf Serum

FCs; Simply Force Curves

FFPE; Formalin-Fixed, Paraffin-Embedded

FGF4; Fibroblast growth factor 4

GAG; Glycosaminoglycan

GO; Gene Ontology

GSEA; Gene Set Enrichment Analysis

GSEA; Gene Set Enrichment Analysis

GSK; Glycogen synthase kinase

HC; Histochemistry

HCL; Hydrogen Chloride

HCM; Human Cancer Models Initiative

HEPES; N-2-Hydroxyethylpiperazine-N'-2-Ethanesulfonic Acid

HER; Receptor tyrosine-protein kinase erbB

HER2; Receptor tyrosine-protein kinase erbB-2

HGF; Hepatocyte growth factor

HGFR; Hepatocyte growth factor receptor

HIF-1; Hypoxia-inducible factor 1- α

HIPEC; Hyperthermic Intraperitoneal Chemotherapy

HTRA3; Serine protease HTRA3

ICAM1; Intracellular Adhesion Molecule-1

ICAM-1; Intracellular Adhesion Molecule-1

IDO1; Indoleamine-Pyrrole 2,3-Dioxygenase,

IF; Immunofluorescence

IGF-1; Insulin Like Growth Factor-1

IGFBP1; Insulin-like growth factor-binding protein 1

IgG; Immunoglobulin G

IHC; Immunohistochemical

IL-1 β ; Interleukin-1 β

IL-6; Interleukin-6

INF γ ; Interferon- γ

iPS; Synthetic Induced Pluripotent Stem Cells

Ki-67; Marker of Proliferation Ki-67

KRAS; GTPase KRas gene

LAIR; Leukocyte-Associated Immunoglobulin-like Receptor 1

LGR5; Leucine-rich repeat-containing G-protein coupled receptor 5

LOXs; Extracellular Lysyl Oxidases

MAPK; Mitogen-activated protein kinase

MEK; Dual specificity mitogen-activated protein kinase kinase

MErT; Reverse Mesenchymal-to-Epithelial Transition

MFAP4; Microfibril-associated glycoprotein 4

MgCl₂; Magnesium Chloride

MGP; Matrix Gla protein

MLH1; DNA mismatch repair protein Mlh1

MMC; Mitomycin-c

MMP-1; Metalloproteases-1

MMP-13; Metalloproteases-13

MMP-14; Metalloproteases-14

MMP-2; Metalloproteases-2

MMP3; Metalloprotease-3

MMP-7; Metalloproteases-7

MMP-9; Metalloproteases-9

MMPs; Metalloproteases

MN; Metastatic Niche

MSH2; DNA mismatch repair protein Mlh2

MSH3; DNA mismatch repair protein Mlh3

MSH6; DNA mismatch repair protein Mlh6

MSI; Instability of Microsatellites

MSI-H; High Instability of Microsatellites

MT1M; Metallothionein-1M

MTT; 3-(4, 5-Dimethylthiazol-2-yl)-2, 5-Diphenyltetrazolium Bromide) assay

MUTYH; Adenine DNA glycosylase

NBN; Nibrin

NNMT; Nicotinamide N-methyltransferase

Notch; Neurogenic locus notch homolog protein

NTHL1; Excision Repair Nth Like DNA Glycosylase 1

O₂; Oxygen

OCT; Optimal cutting temperature compound

OSCAR; Osteoclast-Associated Immunoglobulin-Like Receptor

OXL; Oxaliplatin

p38; Mitogen-activated protein kinase p38

p53; Cellular tumour antigen p53

PALB2; Partner and localizer of BRCA2

PARP; Poly (ADP-ribose) Polymerase (PARP) Inhibitors

PBS; Phosphate Buffer Saline

PC1; Epithelial Polycystins 1

PC2; Epithelial Polycystins 2

PD1; Programmed Death Protein 1,

PDOs; Patient-Derived Organoids

PDTX; Patient-Derived Tumour Xenografts

PECAM-1; Platelet-Endothelial Cell Adhesion Moelcule-1

PI3KCA; Phosphoinositide 3-kinase gene

PLEK; Pleckstrin

PM; Peritoneal Metastasis

PMI; Patient's Peritoneal Body Index

PMS; Pro-Metastatic Secretome

PMS2; Mismatch repair endonuclease PMS2

POLD1; DNA polymerase delta catalytic subunit

POLE; DNA polymerase epsilon catalytic subunit A

POSTN; Periostin

PSCs; Pluripotent Stem Cells

PTEN; Phosphatidylinositol 3,4,5-trisphosphate 3-phosphatase and dual-specificity protein phosphatase PTEN

RAD51C; DNA repair protein RAD51 homolog 3

RAD51D; DNA repair protein RAD51 homolog 4

RAF; RAF proto-oncogene serine/threonine-protein kinase

RAS; GTPase KRas

RER; small Rough Endoplasmic Reticles

RhoA; Transforming protein RhoA

RNA-seq; RNA Sequencing

RNF43; E3 ubiquitin-protein ligase RNF43

ROCK; Rho-associated protein kinase 1

RT; Room Temperature

S100A; Protein S100-A

S100A12; Protein S100-A12

S100A8; Protein S100-A8

SB202190; anti-ROCK inhibitor

SDS; Sodium Dodecyl Sulphate

SEM; Standard error of the mean

SERPFIN1; Serphine 1

SFRP2; Secreted frizzled-related protein 2

sGAG; sulphated Glycosaminoglycan

SMAD2; Mothers against decapentaplegic homolog 2 gene

SMAD4; Mothers against decapentaplegic homolog 4 gene

SMAD4; Mothers against decapentaplegic homolog 4

SNAIL-1; Zinc finger protein SNAI1

SRC; Proto-oncogene tyrosine-protein kinase Src

SRGN; Serglycin

STAT; Signal transducer and activator of transcription

STK11; Serine/threonine-protein kinase STK11

TA; Transiently Amplified

TAZ; Tafazzin

TDO; Tumour-Derived Organoid

TGF α ; Tumour Growth Factor Alpha

TGF- β ; Transforming Growth Factor Beta

THBS2; Thrombospondin-2

THY1; Thy-1 membrane glycoprotein

TIMPs; Inhibitors of Metalloproteinases

TNF α ; Tumour Necrosis Factor Alpha

TNR; Tenascin-R

TP53; Cellular tumour antigen 53 gene

TWIST; Twist-related protein 1

uPAR; urokinase Plasminogen Activator Receptor

UPARAP; Syndecans Urokinase-type Plasminogen Activator Receptor- Associated Protein

VCAM-1; Vascular cell adhesion protein 1

VCAMs; Vascular cell adhesion proteins

VEGF; Vascular endothelial growth factor A

VEGFR; Vascular endothelial growth factor A receptor

VWF; von Willebrand factor

WGA; Wheat Germ Agglutinin

WHO; World Health Organisation

Wnt; Protein wnt

WNT3a; Protein Wnt-3a

WNT7A; Protein Wnt-7a

YAP; Transcriptional coactivator YAP1

YM; Young Moduls

Zeb1; Zinc finger E-box-binding homeobox 1

2. Declaration

The data presented in this thesis are original, were not previously used for any other PhD degree and were originated by myself and by the cited below collaborators. During my PhD I worked in the Genetic Epidemiology and Pharmacogenomics unit in the Department of Research, at the IRCCS Foundation, Istituto Nazionale dei Tumori di Milano, Milan, Italy (INT). My director of studies was Dr. Manuela Gariboldi (PhD) and my supervisors were Dr. Gabriella Sozzi (PhD) and Dr. Luca Roz (PhD).

This work was funded by funds obtained through an Italian law that allows taxpayers to allocate 0.5 percent of their tax to a research institution (INT) of their choice.

- Peritoneal tissues were collected and selected by Dr. Marcello Guaglio (MD), Peritoneal Malignancies Unit, IRCCS Foundation, Istituto Nazionale dei Tumori di Milano, Milan, Italy.
- The histopathological evaluation of peritoneal tissues were performed by Dr. Massimo Milione (MD) and Dr. Laura Cattaneo (MD), Pathology and Laboratory Medicine Department, IRCCS Foundation, Istituto Nazionale dei Tumori di Milano, Milan, Italy.
- Immunohistochemistry, immunofluorescence and fluorescence analyses included in this thesis were performed in collaboration with Dr. Silvia Brich (PhD), Pathology and Laboratory Medicine Department, IRCCS Foundation, Istituto Nazionale dei Tumori di Milano, Milan, Italy. My contribution was samples preparation and data interpretation.
- Formalin-fixed, paraffin-embedded blocks and slices used in this thesis were developed by Dr. Silvia Brich (PhD), Pathology and Laboratory Medicine Department, IRCCS Foundation, Istituto Nazionale dei Tumori di Milano, Milan, Italy.

- DNA sequencing analyses on organoids derived from peritoneal metastasis were conducted by Dr. Sara Volorio (MsC) and Dr. Stefano Fortuzzi, (MsC) from the DNA Sequencing Facility, Cogentech Ltd, Benefit Corporation with a Sole Shareholder, Milan, Italy. My contribution was sample preparation, including DNA extraction, and data interpretation.
- Confocal and polarized-light microscopy analyses on peritoneal-derived 3D decellularized matrices included in this thesis were performed by Dr. Elisa Costa, Technological Development Unit, the FIRC Institute of Molecular Oncology, IFOM, Milan, Italy. My contribution was data interpretation.
- The topographical evaluation of the peritoneal-derived 3D decellularized matrices presented in this thesis was performed through Atomic Force Microscopy, by Dr. Amanda Oldani (PhD), Technological Development Unit, the FIRC Institute of Molecular Oncology, IFOM, Milan, Italy. My contribution was samples preparation and data interpretation.
- Atomic Force Microscopy mechanical analyses of peritoneal-derived 3D decellularized matrices used in this thesis were performed by Prof. Alessandro Podestà (PhD) and Dr. Matteo Chighinzola (PhD), .CI.Ma.I.Na. and Department of Physics “Giuseppe Occhialini”, University of Milan, Milan, Italy. My contribution was samples preparation and data evaluation.
- RNA sequencing analyses on peritoneal metastasis-derived organoids and on peritoneal-derived 3D decellularised matrices repopulated with organoids used in this thesis, were performed by Dr. Simone Minardi (PhD), RNA Sequencing Facility, Cogentech Ltd, Benefit Corporation with a Sole Shareholder, Milan, Italy. My contribution was samples preparation, including RNA extraction.
- Gene set Enrichment Analysis on differentially expressed genes obtained from RNA sequencing analyses, presented in this thesis, were performed by Dr.

Federica Zanardi (PhD) and Dr. Ivan Iannelli (PhD), Bioinformatics Core Unit, IFOM, the FIRC Institute of Molecular Oncology, Milan, Italy. My contribution was data interpretation.

The results obtained in this thesis are included in the following manuscript: L. Varinelli *et al.* **“Decellularized Normal and Tumor Scaffolds for Cancer Organoid Cultures as a Model of Colorectal Peritoneal Metastases”** *BioRxiv*, 2021; 2021.07.15.452437

3. Abstract

Peritoneal metastasis (PM) is one of the most common routes of dissemination for colorectal cancer and remains a lethal disease. PM development is caused by a cross-talk between invading cancer cells and the rearrangement of the extracellular matrix (ECM). This interplay is governed by biochemical and biomechanical events that allow the development of a specific microenvironment: the so-called metastatic niche. ECM remodeling may be critical for PM spread. In fact, it has been demonstrated that ECMs are not only able to provide structural support to the exfoliated neoplastic cells, but also to trigger specific molecular pathways, paving the path for the seed of cancer cells, directly to their "pre-educated" soil. The mechanisms that determine the interactions within cancer cells and the ECM are still obscure and could be elucidated by an *in vitro* 3D-culture system that integrates all the elements involved in PM development. Cancer organoids have shown a profound impact in the field of oncology since they better reflect the main characteristics of the native organs compared to the traditional cell culture models. However, they still fail to represent the heterogeneity of the microenvironment. Methodologies have been recently established to remove cells from tissues and obtain matrices in which ECM and tissue architecture are maintained (dECM models), that could be used as the most representative scaffold on which implant 3D cultures.

I aimed to obtain a 3D-model that closely recapitulates the microenvironment where the PM develops and includes d-ECM repopulated with PM-derived organoids (3D-dECM model). I removed the cellular component of ECMs derived from peritoneal cavity obtained from both PM samples and r matched normal peritoneum using detergents and enzymatic methods. dECMs analyses demonstrated that the procedure maintained the specific characteristics of their tissue of origin also in terms of distribution, localization, and architectural organization of ECM-related proteins. The obtained dECMs showed a different spatial rearrangement between normal and PM-derived peritoneum, suggesting that dECM scaffolds closely

recapitulate the native PM microenvironment. Moreover, when I repopulated dECMs with PM-derived organoids I found that PM- and normal peritoneum-derived dECMs differentially regulated the localization and organization of the seeded organoids, which was the same as in the original tissue. The two 3D-ECM models presented different ability in supporting cell proliferation, where PM-derived 3D-dECMs showed a higher proliferation index and a major ability to maintain the stemness phenotype. PM- and normal peritoneum-derived 3D-dECMs differently modulated cell homeostasis and proliferation ratio.

A gene expression analysis of organoids, grown on different substrates reflected faithfully the clinical and biological characteristics of the organoids. The impact of the ECM on the response to standard chemotherapy treatment for PM was also observed.

This demonstrated the value of ex vivo 3D models obtained by combining patient-derived extracellular matrices depleted of cellular components and organoids to mimic the metastatic niche, which could provide tools to develop new therapeutic strategies in a biologically relevant context, to personalize treatments and increase their efficacy.

4. Introduction

4.1 Colorectal cancer

Colorectal cancer (CRC) accounts for about 10% of all cancers diagnosed each year with a mortality rate of 10% worldwide. It is the second most diagnosed malignancy in women and the third in men. Of note, mortality from CRC in women is 25% lower than in men. The death rate varies widely geographically, with developed countries having higher rates than developing countries. It is estimated that in industrialized states, approximately 2.5 million new cases of CRC will be diagnosed by 2035 (F. Bray *et al.* 2018, M. Arnold *et al.* 2017). In highly industrialized countries the development of national screening programs and the continuous increase in diagnoses through colonoscopy, in addition to changes in lifestyle and nutrition that have emerged in recent decades towards a healthier lifestyle, have led to a stabilization of incidence and mortality (E. Dekker *et al.* 2019, D. Ait Ouakrim *et al.* 2015). On the other hand, there is an increase in cases of CRC in young subjects, under 50 years of age, especially carcinomas of the rectum and left colon (R.L Siegel *et al.* 2017, P.M. Kasi *et al.* 2019). Genetic factors, lifestyle, obesity, and environmental factors seem to be involved, but the reasons for this increase have not yet been fully understood (E. Dekker *et al.* 2019).

4.2 Pathogenesis of Colorectal cancers

Most of CRCs arise from the onset of polyps along the intestinal tract. The process of carcinogenesis begins with the formation of aberrant colon lesions which over time evolve into pre-neoplastic lesions which can then, usually after about 10-15 years, lead to the development of colorectal cancer (E. Dekker *et al.* 2019). The cells involved in the development of most diagnosed CRCs are the stem cell or stem cell-like cells (J.P. Medema 2013, D. Nassar & C. Blanpain 2016). These stem cells are the result of the progressive

accumulation of both genetic and epigenetic alterations that evade or alter the various tumour suppression mechanisms normally active in healthy cells, also contributing to increase the expression of proto-oncogenes. From a biological point of view, stem cells are positioned at the base of the crypt of the intestinal tract and play a fundamental role in triggering and maintaining the neoplastic process (J.P. Medema 2013; D. Nassar & C. Blanpain 2016; M. Shimokawa *et al.* 2017). Two distinct types of lesions can originate, both governed by specific pathways (Figure 1): the traditional pathway linked to the development of adenomas and carcinomas, characterised by strong chromosomal instability, which affects about 70-90% of CRC cases, and the pathway of serrated neoplasia, which, on the other hand, represents about 10-20% of all diagnosed CRCs. These pathways are characterised by specific and distinct genetic and epigenetic events that occur in a well-defined sequential order (Cancer Genome Atlas Network 2012). CRCs with characteris chromosome instability usually develop because of genomic events that begin with the mutation of the *APC* gene, followed by activation of the RAS pathway or loss of function of the *TP53* gene. Conversely, the serrated neoplasia pathway is correlated with the onset of mutations in *RAS* and *RAF* genes, and also with epigenetic changes that induce microsatellite instability such as CpG Island methylation (E. Dekker *et al.* 2019). Recently, thanks to large genome-wide studies, new interactors have been identified that lead to the development of CRC from the mutated phenotype. The main characteristics involved in these subtypes of CRC are the presence of mutations in the genes that code for polymerase- ϵ or for POLE, or defects in the repair mechanisms governed by the genes coding for proteins involved in the mismatch repair (dMMR) mechanism (E. Dekker *et al.* 2019).

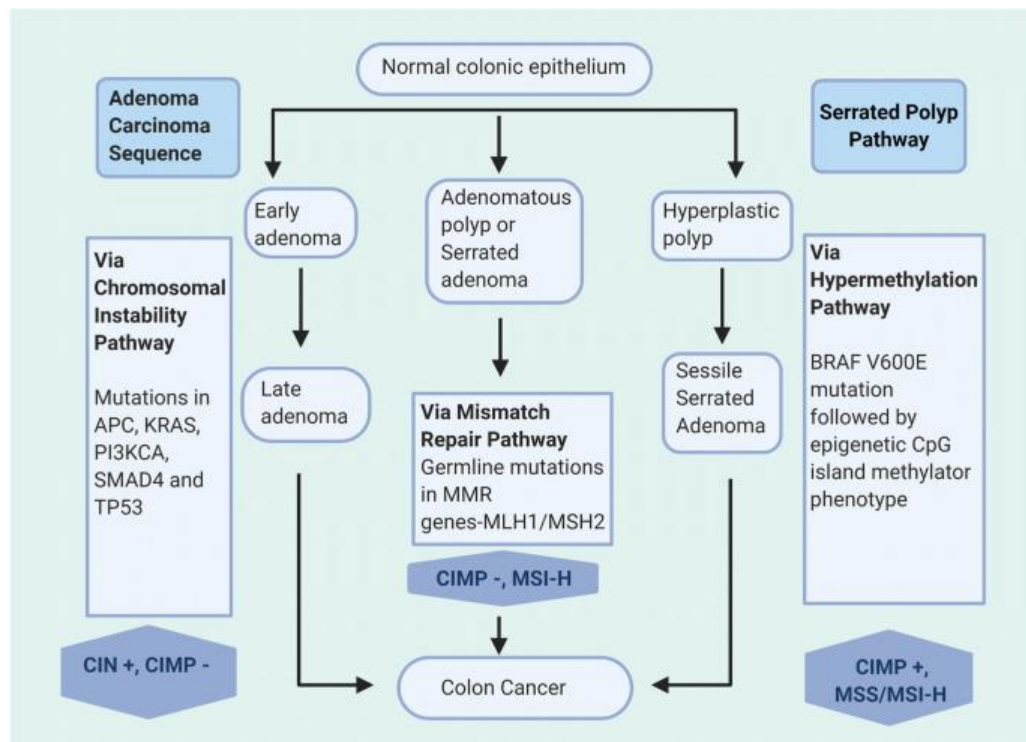


Figure 1. The figure summarizes the main molecular pathways that sustain the CRC development. Figure taken from “**Molecular Pathogenesis and Classification of Colorectal Carcinoma**” by A Kasi *et al.* *Current Colorectal Cancer Reports*. **16**, 97–106 (2020)

4.3 Left-sided and right-sided CRC: main molecular features

CRC can occur in both the proximal (right colon) and distal part of the colon (left colon). Depending on the localization of the onset, CRCs have specific and different molecular characteristics to be considered two clinically distinct diseases (Figure 2) (A. Kasi *et al.* 2020). Several theories have been formulated to explain this disparity, ranging from differences during embryonic development to the presence of different immune infiltrates, differences in the composition of the gut microbiota and delayed diagnosis, especially for right colon cancers (S. Stintzing *et al.* 2017, A. Bertotti & F. Sassi 2015). From a molecular point of view, right colon cancers are more associated with high microsatellite instability, defects in the mismatch repair genes, the presence of methylations along the CpG Islands and

mutations affecting the *BRAF* oncogene (Q. Peng, K. Lin *et al.* 2018, M.E. Salem *et al.* 2017, F. Petrelli *et al.* 2017). Except for microsatellite instability, the rest of these genetic and epigenetic aberrations are always associated with poor survival (J. Tabernero *et al.* 2018). As for left side colon cancers, they are characterised by a marked chromosomal instability and generally present mutations in the classic genes mutated in CRC, such as *APC*, *KRAS*, *PI3KCA*, *SMAD2*, *SMAD4* and *TP53* (F. Petrelli *et al.* 2017). The phenotype characterised by high instability of microsatellites (MSI-H) characteristic of right colon cancer, confers a high degree of immunogenicity, due to the extensive mutational rate of neoantigens that promote the infiltration of T lymphocytes, explaining why it responds to therapeutic strategies based on immune check-point inhibitors. Left CRCs have instead a low degree of immuno-infiltration and are generally considered “cold” from this point of view. It is noteworthy that the mutational status of the *KRAS* and *BRAF* genes is related to significant differences in patients, where wild type right cancers have a worse prognosis when compared to left CRCs (J. Tabernero *et al.* 2018). Also, from the morphological point of view, left and right-side cancers have very different characteristics: left side cancers usually present tubular or villous adenocarcinomas, while cancers in the right site frequently appear as adenocarcinoma lesions of the mucinous and sessile type. In addition, the latter grow "flat" or laterally with respect to the organ. All this makes this subtype difficult to diagnose at an early stage through endoscopic screening. Nonetheless, left side colon cancers remain the most diagnosed, with approximately 70% of CRCs even if they present a risk of death less than 19% compared to right CRCs (P. Jess *et al.* 2013).

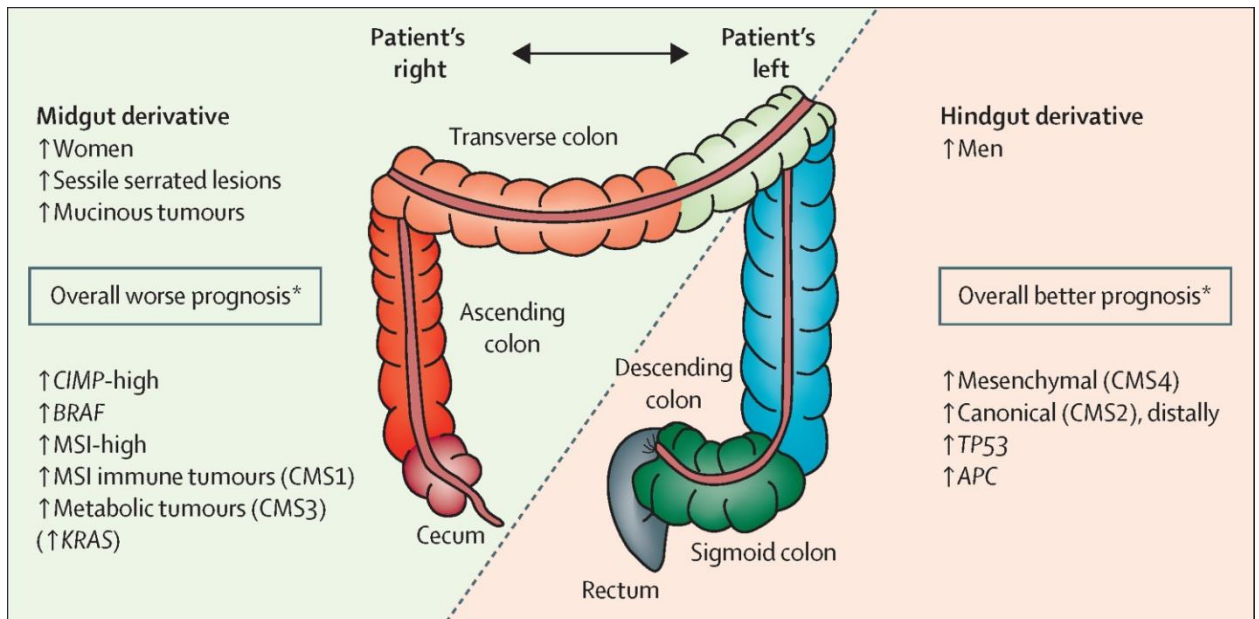


Figure 2. The picture shows a schematic representation of the main characteristics and features of right-sided CRC and left-sided CRC. Figure taken from “Colorectal Cancer” by E. Dekker *et al. Lancet.* **394**, 1467-80 (2019).

4.4 Consensus molecular subtypes of CRC

With the advent of the “era of transcriptomics” and the development of more precise gene expression techniques, a better classification of CRC has been achieved, which has also led to explain the great heterogeneity between the different patients, also helping to direct the therapeutic and diagnostic process. In 2014, based on gene expression analysis, the CRC subtyping consortium allowed the classification of CRC on the basis of a single classification system known as the Consensus Molecular Subtypes (CMS, Figure 3) (A. Kasi *et al.* 2020) that classified CRC into four different subgroups:

CMS1: 14% of all CRC cases fall into this subgroup. Most of them are sporadic, while a small percentage are associated with hereditary syndromes, such as Lynch syndrome (J. Guinney *et al.* 2015). The CMS1 phenotype is associated with high mutation levels, due to a high rate of hypermethylation and/or mutations in promoter genes of dMMR genes. This subtype is also characterised by the presence of a high rate of somatic copy number alteration. They often have mutations in the *BRAF* gene, and this type of tumours usually originates in the proximal tract of the colon (D. Barras *et al.* 2017). One of the peculiar characteristics of the CMS1 subtype is that of presenting a high expression of genes that regulate the immunoinfiltrate and the trafficking of T-cell helper 1 and cells with cytotoxic activity, which in turn involves the activation of immune escape mechanisms, making this subgroup responsive to treatments based on immunotherapy (W. Gang *et al.* 2018).

2 CMS2: The CMS2 subtype is the most represented molecular subgroup and comprises 39% of all diagnosed cases of CRCs. For this reason, CMS2 is also referred to as the "canonical subtype", which is characterised by chromosomal instability, a high rate of copy number alterations and a low number of mutations. This subtype is the one closest to the canonical description of CRC development based on the adenoma-adenocarcinoma progression model, where the first mutational event includes mutation of the *APC* gene, followed by mutation of *KRAS* and then mutation of the *TP53* gene, described by Wolgstein (A. Kasi *et al.* 2020). CMS2 is associated with tumours affecting the left side of the colon and has the best prognosis with a mean 5-year survival of approximately 77% (K. Thanki *et al.* 2017).

3 CMS3: This subtype comprises about 13% of CRC cases and is also called the "metabolic subtype". Chromosomal instability is markedly lower respect to CMS2 and CMS4 subtypes. The main feature of CMS3 is that it has a lower MSI than CMS1 but clearly higher when compared with the CMS3 and CMS4 subtypes (r J. Guinney *et al.* 2015). Furthermore, mutations in *KRAS* gene are very common, with a frequency of 68% of all cases diagnosed as CMS3, showing a survival rate of around 75% (D. Barras *et al.* 2017).

4 CMS4: This subtype is also known as the “mesenchymal subtype” and comprises approximately 24% of CRCs. Compared to the other subtypes, the CMS4 subtype tends to be diagnosed late with advanced disease and for this reason has the lowest 5-year survival rate and poorer prognosis. This subtype originates from serrated pathways and exhibits a high rate of somatic copy number alterations and a low mutation frequency (J.B Bramsen *et al.* 2017). Gene expression data have also shown that CMS4 has high expression of a series of genes coding for proteins that modulate mesenchymal stromal infiltration (A. Kasi *et al.* 2020).

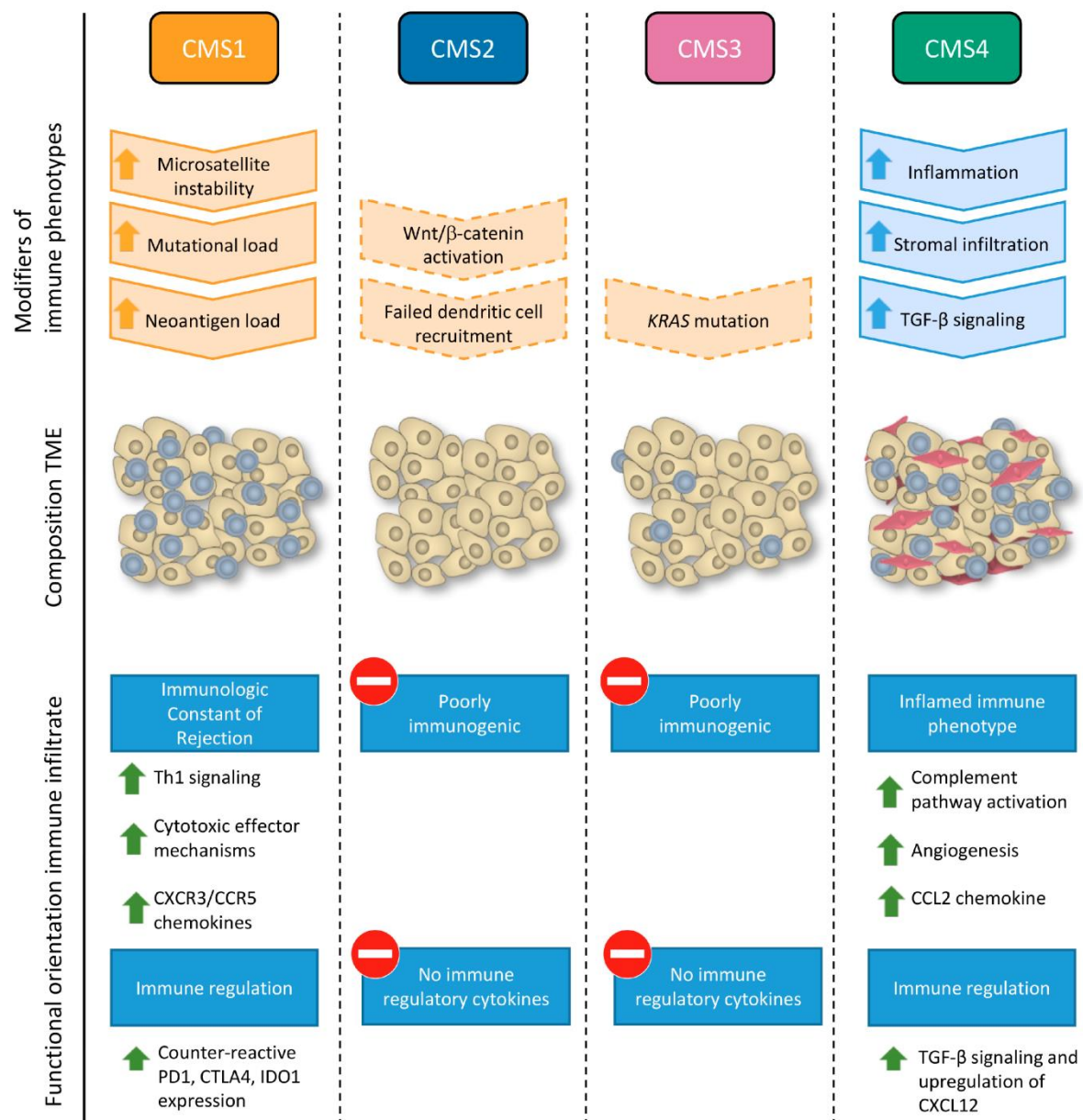


Figure 3. Consensus Molecular Subtypes (CMS) and their specific characteristics in CRC. **Legend** TGF-β: Transforming growth factor beta, complement CXCR3/CCR5: Chemokine (C-X-C motif) receptor 3/C-C chemokine receptor type 5, PD1: programmed death protein 1, CTLA4: cytotoxic T-lymphocyte-associated protein 4, IDO1: Indoleamine-pyrrole 2,3-dioxygenase, CCL2: chemokine (C-C motif) ligand 2, CXCL12: Chemokine (C-X-C-motif) ligand 12. Figure taken from “**Immunogenomic Classification of Colorectal Cancer and Therapeutics Implications**” by J. Roelands *et al.* *International Journal of Molecular Science*. *18*(10), 2229 (2017).

4.5 Metastatic Colorectal Cancer

Metastases from CRC represent an open clinical question, given the high mortality rate associated with CRC-derived neoplastic cells at distant organs. The main sites of metastasis of CRC are the liver, with a frequency of about 70% with an overall survival of 25 months, followed by the peritoneal cavity, with a frequency around 25% and an overall survival of 14 months, and by lung metastases, with an average frequency of 5% and an overall survival of 30 months (D. Baratti *et al.* 2016). Regarding the biology that governs the metastatic spread, little is known and many of the biological mechanisms involved remain elusive. As regards the management of hepatic and lung metastases, significant progress has been made in recent years, thanks to the development of new surgical techniques and to the discovery of different key molecular player involved in the metastatic spread in the liver and lung (D. Baratti *et al.* 2016).

4.6 The metastatic niche

Recently, it has been demonstrated that organs where metastases develop are not passive receivers of circulating tumour cells, but are actively modified by the primary tumour before the occurrence of metastatic spread. The metastatic process is caused by a crosstalk between cancer cells and the microenvironment, involving several steps, known as "metastatic cascade". This cascade is governed by a *fine-tuned* interaction between biochemical factors, released from the tumour and biomechanical events, such as remodeling of the extracellular matrix (ECM), which allow the formation of the so-called "pre-metastatic and metastatic niche" (Figure 4) (C.M. Ghajar 2015, R.S. Lindoso *et al.* 2016).

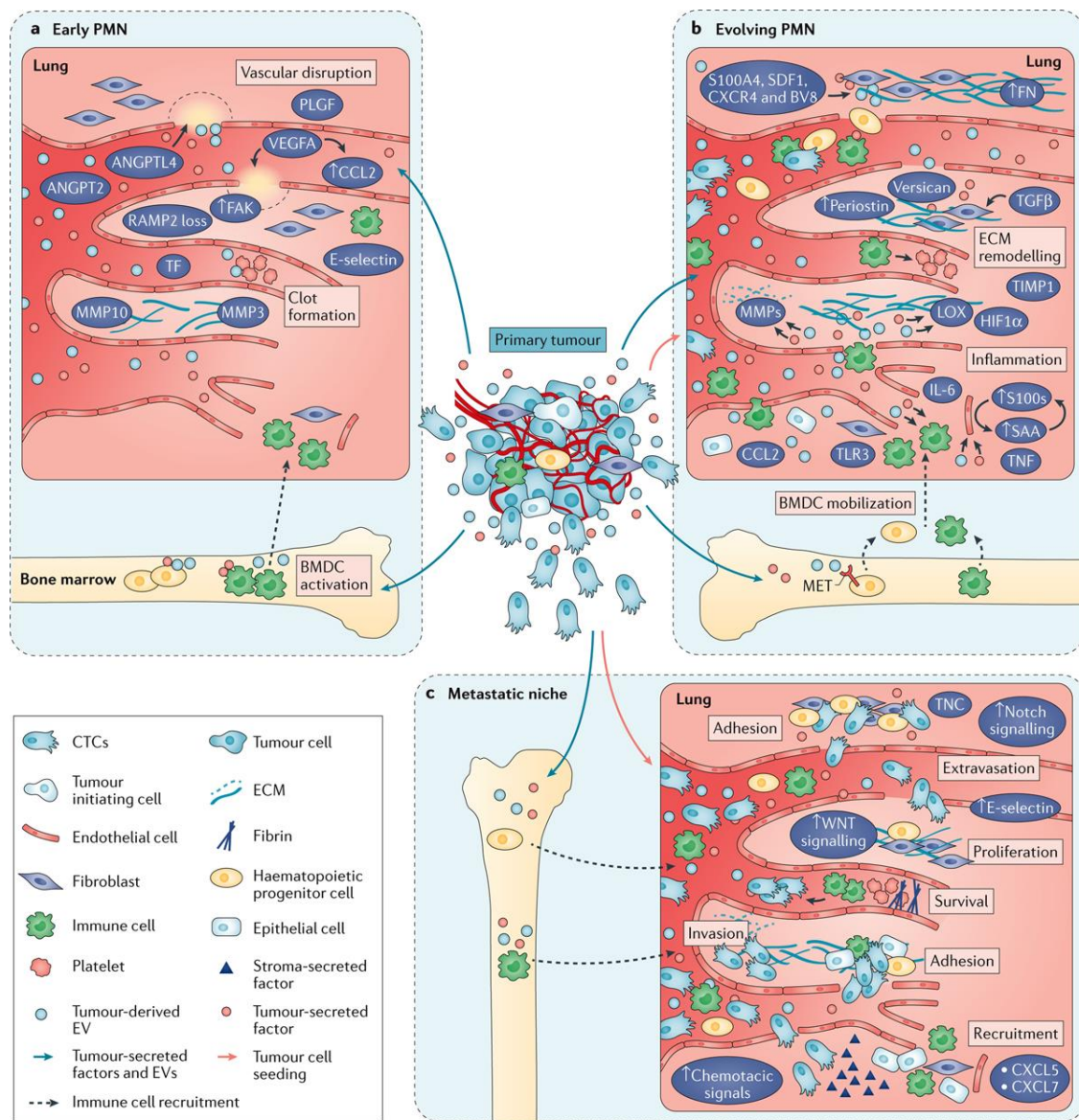


Figure 4. The figure schematically shows the evolution that leads to the formation and development of the pre-metastatic and metastatic niche. **a)** The early step of the process is characterised by the clot formation and fenestration of blood vessels mediated by the upregulation of angiogenic proteins and inflammatory processes. **b)** the evolution of the niche subsequently sees the reshaping of the ECM and a significant increase in inflammation levels with consequent recruitment of bone marrow-derived cells (BMDCs), **c)** all this leads to favoring the adhesion of circulating metastatic cells to the target organ via processes mediated by specific adhesion proteins. In this context, cancer cells will find a microenvironment favorable to their growth, capable of supporting several of their main functions. Figure taken “**Pre-metastatic niches: organ-specific homes for metastases**” by H. Peinado *et al.* *Nature Reviews Cancer*, **17**, pages302–317 (2017)

Some key molecular players in the metastatic cascade involving the development of hepatic and lung metastases are known: detachment from primary tumour is promoted by down-regulation of E-cadherin, and up-regulation of N-cadherin following by the upregulation of Zeb1 and SNAIL-1 related genes (E. Batlle *et al.* 2000, A. Cano *et al.* 2000, J. Comijn *et al.* 2001, J. Yang *et al.* 2004). All favor epithelial-to-mesenchymal transition (EMT) which, together with its reverse mesenchymal-to-epithelial transition (MET), is a hallmark of cancer metastases (E. Pretzsch *et al.* 2019). The risk of development of metastases, in particular to the liver and lung, seems to be related with high- microsatellite instability (MSI) levels, CpG island methylation and presence of BRAF mutations (M. Fujii *et al.* 2016, D. Caccia *et al.* 2013). The existence of the pre-metastatic microenvironment has been clearly demonstrated in several cancer tissues, which are characterised by specific molecular events allowing the organotropism of the metastatic process (E. Pretzsch *et al.* 2019). In fact, the development of the metastatic niche facilitates organotropic metastasis by directly promoting cancer stem cells survival, taking advantage from the so-called pro-metastatic secretome (PMS) (R.F. Lindoso *et al.* 2016, E. Pretzsch *et al.* 2019). PMS can increase metastases by inducing a remodeling of the surrounding microenvironment that could favor the organotropism process (L. Rivoltini *et al.* 2016, A. Hoshino *et al.* 2015). Regarding hepatic and lung metastases, several aspects of their development are promoted by a re-education program of the stromal cells compartment. These cells can recruit exfoliated cancer cells with a mechanism involving the expression of CD43 and intracellular adhesion molecule-1 (ICAM1) (C. Millan *et al.* 2018). Moreover, stromal cells frequently display early senescence associated with high fibrosis, which could promote adhesion of CRC circulating cells with an increased production of fibronectin and integrin on their surface via TGF- β 1-dependent induction of p38 (K. Ksiazek *et al.* 2010, E. Pretzsch *et al.* 2019). Moreover, they may also regulate tumour progression by directly reprogramming their secretory phenotype, leading to an increased production of pro-angiogenic factors, which directly stimulate the vascular endothelium of liver and the lung.

(J. Mikula-Pietrasik *et al.* 2018, E. Pretzsch *et al.* 2019). Cancer-related activated fibroblasts (CAF) are another fundamental cell subpopulation that actively contributes to the remodeling of the microenvironment of the pre-metastatic and metastatic niche. CAF have a pro-tumorigenic role in the remodeling of the tumour microenvironment and could be involved in the perturbation of peritoneal homeostasis by TGF- β 1-dependent activation (A.H. Yang *et al.* 2003, E. Pretzsch *et al.* 2019). An emerging number of studies have focused especially on extracellular vesicles (EVs) directly released into the secretome by neoplastic cells as a tool for the modeling, and also the development, of the metastatic niche (MN) (J. Pagetti *et al.* 2015, A. Hoshino *et al.* 2015, B. Costa-Silva *et al.* 2015). EVs are a heterogeneous family of vesicles of different size and origins. Among them, exosomes, membrane vesicles of endosomal origin ranging from 30 to 150 nm (E.I. Andaloussi *et al.* 2013), are emerging key players in intercellular communication between cancer cells and their microenvironment since they can transfer fundamental information through their cargo, typically consisting in proteins, DNA, mRNA and miRNAs (H. Peinado *et al.* 2011, C. Tetta *et al.* 2013). It has been shown that the formation of the MN also depends on tumour-derived exosomes (H. Peinado *et al.* 2012, L. Hood *et al.* 2011). In fact, in pancreatic cancer and in liver-related metastasis, exosomes play a fundamental role in the sequential steps involved in the induction of the liver pre-metastatic niche (B. Costa-Silva *et al.* 2015). Moreover, proteomics analysis of the exosomal content has revealed distinct integrin expression profiles in several models of cancer cell lines: exosomal integrins $\alpha_6\beta_1$ are related to lung metastasis while integrins $\alpha_v\beta_5$ are linked to liver metastasis (A. Hoshino *et al.* 2015) (Figure 5).

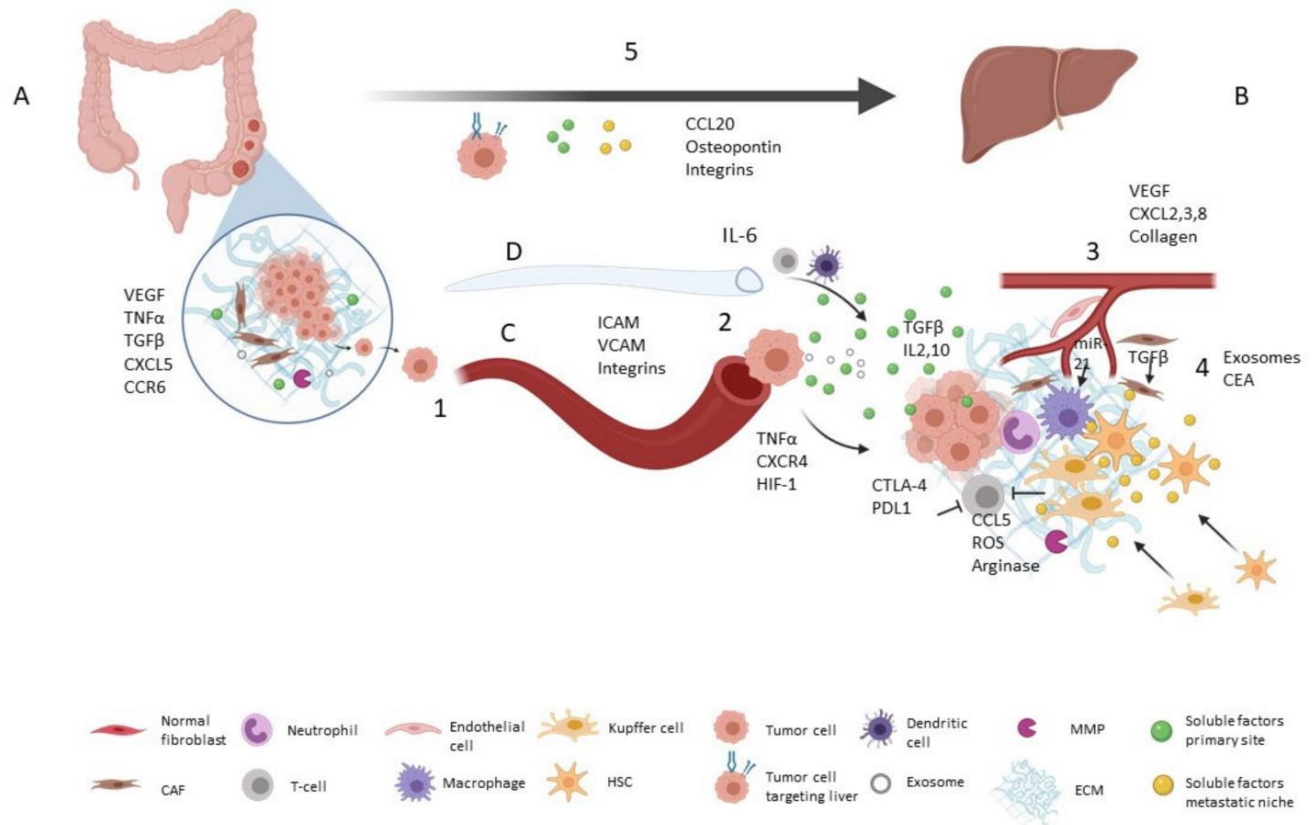


Figure 5. The figure shows the process of the formation of metastases in the liver. The primary tumour secretes a series of soluble factors capable of pre-educating the target organ. The tumour cells exfoliated from the primitive site enter the blood and / or lymphatic circulation, thanks also to a profound remodeling of the ECM. The extravasation process is mediated by ICAM adhesion molecules and by vascular molecules such as VCAMs. In addition, there is an increase in the levels of $\text{TNF}\alpha$, of the CXCR4 receptor, of HIF-1. The neovascularization of the pre-metastatic niche is promoted by the specific expression of VEGF and by the upregulation of specific chemokines, such as CXCL2-3-8. At the level of the metastasis site, there are soluble factors, high levels of cytokines and chemokines, specific recruitment of stromal cells, remodeling of the ECM and favor the engraftment of circulating neoplastic cells. Figure taken from “**Tumour Microenvironment in Metastatic Colorectal Cancer: The Arbitrator in Patients’ Outcome**” by C. Galindo-Plumarino *et al. Cancers*, 13(5), 1130 (2021).

However, how primary CRC is able to spread directly into the peritoneum cavity and how the metastatic niche develops still remains unknown and data derived from the literature still

remain elusive. For these reasons the identification of biological markers to integrate with clinical-pathological features to guide additional therapeutic interventions is strongly needed.

4.7 The peritoneal metastasis disease

Metastatic dissemination to the peritoneal cavity is a common event in patients with advanced CRC. This stage of the disease has always been indicated as terminal, amenable only to palliative care aimed at reducing pain and increasing quality of life, through systemic chemotherapy or supportive therapies (D. Baratti *et al.* 2016, Sugarbaker and Ryan 2012). In the studies conducted in recent years on the various mechanisms of metastatic dissemination and on the course of patients with PM disease it is evident that peritoneal metastasis can also occur in the absence of dissemination through the bloodstream (D. Baratti *et al.* 2016). Moreover, PM can be considered a locoregional disease and new therapeutic approaches have emerged, which improve the prognosis and outcome. These strategies are based on an aggressive surgical intervention using cytoreductive surgery (CRS), aimed at the removal of all metastatic nodules visible on the surface of the peritoneum, followed by hyperthermic intraperitoneal chemotherapy (HIPEC), with the aim of eradicating the minimal residual disease, which is not eliminated with the surgical approach (M. Deraco *et al.* 2009). However, despite the abundance of randomized clinical trials, the ever-increasing number of data derived from retrospective analyses, and the increase of studies that have helped to highlight various biological aspects that govern the development of metastases to the peritoneum (T. Weber *et al.* 2012, D. Baratti *et al.* 2016), the treatment of PM remains critical, mainly due to the lack of high quality controlled studies and the lack of standardized therapeutic protocols (Sugarbaker and Ryan, 2012).

4.8 Epidemiology of PM disease

Three large population studies have highlighted the frequencies of occurrence of metastases to the peritoneum, following a diagnosis of CRC (J. Segelman *et al.* 2012, V.E. Lemmens *et al.* 2011, Y.R. van Gestel *et al.* 2014). In the first study, 11124 patients with CRC were observed between 1995 and 2007. Of these patients, 924 had synchronous or metachronous metastases to the peritoneum, corresponding to 8.3% of the subjects examined, while isolated lesions to the peritoneum were present in 4.8% of the subjects examined (J. Segelman *et al.* 2012). The second study considered 18738 CRC patients that had surgery between 1995 and 2008 and found that 904 of them had synchronous PM, equal to 3.8% of the total. The data also revealed that the peritoneum was the second most common site of metastasis after the liver, followed by the lung, with $n = 395$, $n = 2086$ and $n = 102$ events respectively (V.E. Lemmens *et al.* 2011). The third study, conducted on a cohort of 5671 patients, showed that 3.5% of them had PM after standard curative treatments (Y.R. van Gestel *et al.* 2014). In these studies an average survival rate of only 6 to 8 months was shown. In a German epidemiological study, carried out on 2406 CRC cases between 1986 and 2009, synchronous and metachronous PM were present in 4.8% and 5.9% of patients respectively, highlighting that the peritoneum was the only one site of metastasis with an incidence of 59% (A.G. Kerscher *et al.* 2013). On the basis of the data collected over the years, it is possible to state that metastases to the peritoneum are diagnosed in 4 - 19% of CRC patients after curative surgery, while they rise to 44% in case of disease relapse. It is very interesting to note how autopsy studies have highlighted the presence of metastases in the peritoneal cavity in 40 - 80% of cases (M.J. Koppe *et al.* 2006), underlining the large diagnostic gap that still affects the diagnosis of PM.

4.9 Current treatment approaches for PM diseases

Current therapeutic approaches for PM disease include CRS coupled with the treatment of the remained loco-regional metastases using HIPEC. Local administration of chemotherapy is effective with lesions about 2-3 mm thick; therefore, CRS maximizes the response to chemotherapy treatment in the peritoneal cavity (P.H. Sugarbaker 1995).

- **CRS Surgery.** Cytoreductive Surgery (CRS) manually removes all visible neoplastic nodules, leaving less local trauma, which could be beneficial for the recovery of patients after surgery (D. Baratti *et al.* 2016). The introduction of the CRS/HIPEC therapeutic approach has improved the prognosis of the disease, ensuring an acceptable quality of life compared to the previously used palliative care. The effectiveness of cytoreduction (CCR) is classified according to the rules developed by Sugarbaker, according to 4 specific scores: CCR0 indicates the complete resection of the lesions at a macroscopic level, CCR1 indicates a residual disease less than 2.5 mm in each region of the peritoneum, CCR2 indicates the presence of residual disease between 2.5 and 25 mm, while CCR3 indicates the presence of minimal residual disease greater than 25 mm (P. Jaquet & P.H. Sugarbaker, 1996).

- **HIPEC Technique.** Hyperthermic intraperitoneal chemotherapy (HIPEC) is used for the loco-regional treatment of PM (S. Gonzalez-Moreno *et al.* 2012). One of the major advantages of intra-abdominal administration of drugs is that of being able to use pharmacological concentrations significantly higher than those used by the intravenous systemic route, due to the presence of a semi-permeable barrier that covers the peritoneal layer, allowing a scarce diffusion of the drug, and therefore low toxicity, at systemic level (M. Deraco *et al.* 2009K. Van der Speeten *et al.* 2012). In addition, a moderate hyperthermia, ranging from 40 to 43 ° C, has a cytotoxic effect on neoplastic lesions through a series of

specific molecular mechanisms, such as DNA repair impairment, protein denaturation, inhibition of oxidative metabolism with consequent increase in apoptosis rates. Hyperthermia also considerably increases the efficacy and penetration into the tissues of mitomycin-c and platinum-based compounds, typically cisplatin and oxaliplatin (R.P. Sticca & B.W. Dach 2006, S. Kusamura *et al.* 2008). To date, there is no general standardization of the HIPEC technique and protocols for HIPEC vary greatly depending on the hospital centers. This variability ranges from the choice of the abdominal administration technique (with open or stitched up abdomen), from which drugs to use, pharmacological concentrations, temperatures used for the hyperthermia phase, duration of treatment and choice of the volume of carrier solutions (D. Baratti *et al.* 2016, S. Van Ruth *et al.* 2003). The choice of antitumoral drugs for HIPEC is based on their clinical efficacy and their pharmacokinetics. The ideal drug for HIPEC should have the following characteristics: i) be hydrophilic, ii) have a high molecular weight to limit as much as possible its passage through the peritoneal-plasma layer, iii) have a high clearance in plasma and iv) a mechanism of action that can be enhanced by hyperthermia (S. Kusamura *et al.* 2008). Two HIPEC-based treatment schemes are currently widely used. The first consists of open abdominal intraperitoneal lavage with oxaliplatin combined with irinotecan with simultaneous intravenous administration of 5-fluorouracil and folic acid. The second involves intraperitoneal lavage with closed or open abdomen, with mitomycin-c given alone or in combination with other drugs, such as cisplatin (Figure 6) (D. Baratti *et al.* 2016, S. Kusamura *et al.* 2008, S. Van Ruth *et al.* 2003, D. Elias *et al.* 2002).

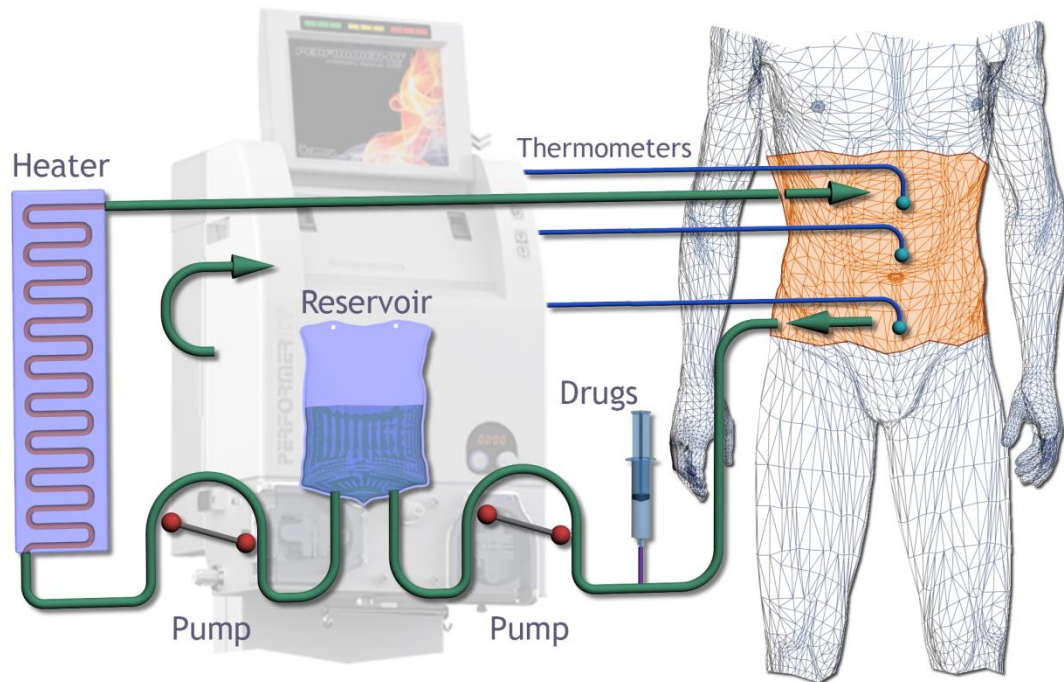


Figure 6. Representative scheme of HIPEC for the treatment of PM disease. The washing of the peritoneal cavity is performed with the abdomen open or sewn up using a perfusion pump that sprays the solution containing the antitlastic drug (s) (mitomycin-c, irinotecan, cisplatin and oxalipatin). The perfusion volume is calculated based on the patient's peritoneal body index (PMI). Washing times vary from 30 minutes to 2 hours depending on the drug treatment. HIPEC is commonly carried out with the washing liquid maintained at 42.5 °C. Figure taken from the following link: https://en.wikipedia.org/wiki/File:Schema_HIPEC.png

Given the technical complexity, the considerable economic costs and the high risk of post-operative problems, CRS/HIPEC can only be used on a small number of candidate patients. It is therefore essential to optimize outcomes of CRS / HIPEC in order to obtain an acceptable morbidity related to the intervention (T.C. Chua *et al.* 2009, D. Baratti *et al.* 2010). The selection of candidates for HIPEC involves a careful evaluation of factors related to the patient, the type of treatment and the characteristics of the tumour. CRS / HIPEC surgery lasts from 8 - 14 h, patients undergo extensive stripping of the peritoneum, multi-organ resections and locoregional chemotherapy treatment in hyperthermic conditions (P.H. Sugarbaker, 1995). Older age, poor performance index (World Health Organization score ≥ 2), significant

co-morbidities, renal insufficiency, heart, lung and bone marrow dysfunction are all exclusion criteria for CRS/HIPEC. Also obesity represents a risk, especially since it could lead to complications in the lungs, although to date, it does not represent an absolute exclusion criterion (P.M. Polanco *et al.*, 2014). Furthermore, in some critical areas of the peritoneum, such as the area of the small intestine, is more difficult to obtain a complete CRS making CRS/HIPEC treatment ineffective and completely superfluous. (D. Baratti *et al.*, 2016). All this leads to a notable decrease in the number of patients who can access CRS/HIPEC treatment, thus also increasing the overall mortality rate of PM disease. However, it is now well established that the introduction of CRS/HIPEC has led to a significant increase in the mean 5-year survival rates among patients eligible for the treatment. In fact, the average overall survival is about 30.1 months, while the 5-year survival rate is about 27%. (D. Elias *et al.*, 2010). A complete cytoreduction of metastatic lesions is essential to see an increase of median survival rates. In patients with a CCR index of 0, the median survival is 33 months, but it decreases to 20 months in patients with index of 1 and to only 7 months in patients who have benefited from only a gross reduction in malignant lesions (D. Baratti *et al.*, 2010). Over the years a good complete cytoreduction rate has been obtained, thanks also to the advent of new surgical techniques, the greater experience of the operating teams and the creation of large networks to share data on CRS/HIPEC. Today it is possible to appreciate an average survival ranging from 16 to 51 months and a five-year survival ranging from 22% to 50.5% (D. Elias *et al.* 2010, G. Passot *et al.*, 2012, C.Q. Huang *et al.*, 2014b, A.U. Blackham *et al.*, 2014, D. Baratti *et al.*, 2014, A.M. Kuijpers *et al.*, 2013, Y. Yonemura *et al.*, 2013, E.I. Benizri *et al.*, 2012). Despite this, about 60 % of patients still experience peritoneal recurrence after CRS/HIPEC. Furthermore, the added value of HIPEC has been questioned by the Prodiges-7 randomized trial, which showed no survival benefit by adding oxaliplatin (OXL)-based HIPEC to complete CRS/HIPEC (W. Ceelen *et al.*, 2019). For these reasons, a deeper characterisation of the molecular events underlying CRC-derived peritoneal

metastases (CRC-PM) development could help in define the biological players of PM disease, also improving patient care.

4.10 Pathophysiology and molecular features of PM disease

The peritoneum is a colonisation site of neoplastic cells exfoliated from primary CRCs. It consists of large and complex serous membrane of the human body (J.B. van der Wal & J. Jeekel, 2007). The visceral peritoneum forms a continuous layer with the parietal peritoneum connected with the abdominal floor and with the cavities of the pelvis (J.B. van der Wal & J. Jeekel, 2007). The peritoneum is basically composed of a monolayer of mesothelial cells that rest on a basement membrane, bounded by a connective tissue floor, also called submesothelium (Figure 7) (P.H. Sugarbaker, 2007). The mesothelium is a monolayer made up of cells that take on a peculiar morphology, ranging from flattened and elongated squamous to cuboidal cells. This morphology is found in other anatomical regions, such as in the liver, in the spleen, in the so-called milk spots of the omentum and in the side facing of the diaphragm of the peritoneum (K. Michailova *et al.*, 1999).

Squamous and cuboidal mesothelial cells can be distinguished through specific ultrastructural characteristics. Squamous cells generally contain few mitochondria, an underdeveloped Golgi apparatus and small rough endoplasmic reticles (RER), which usually are in close contact with the nucleus, which in turn takes on a rounded or oval shape (S.E. Mutsaers & S. Wilkosz, 2007). Cuboidal cells are characterised by a large nucleus in a central position with respect to the cytoplasm, by the presence of numerous mitochondria and RERs, by a highly developed Golgi apparatus and also by the marked presence of microtubules and microfilaments (J.W. Dobbie, 1989).

The luminal surface of the mesothelial cells has numerous microvilli of different shape, size and density depending on the peritoneal areas, which serve to increasing the surface area of the peritoneum (S.E. Mutsaers *et al.* 1996). The main functions of the mesothelium are to form a dynamic layer that determines the main characteristics of the structure, functioning and homeostasis of the peritoneum (L. Lemoine *et al.*, 2016).

The peritoneal basement membrane is formed by a thin layer consisting mainly of type I and type IV collagen, laminin, proteoglycans and glycoproteins. It acts as a highly selective barrier for a whole series of macromolecules that cross the submesothelial layer (S.E. Mutsaers & S. Wilkosz, 2007). As for the submesothelium, it is mainly made up of a complex network of ECMs, such as different types of collagen, glycoproteins, glycoaminoglycans and proteoglycans. In this region, different cell subtypes such as fibroblasts, macrophages and mast cells, can be identified. Furthermore, this layer is characterised by the presence of a dense blood and lymphatic microcirculation (J.B. van der Wal & J. Jeekel, 2007). The main function of the peritoneum is to facilitate the transport of fluids and cells through the serous cavities (M.E. Fedorko *et al.*, 1971). The microvilli of the luminal surface of the mesothelial cells play a fundamental role in this process, since they contribute to increasing the uptake surface of the peritoneum and by binding the fluids that pass through the glycocalyx regions, enriched in glycosaminoglycans with an absorbent function (N.S. Wang, 1974).

The peritoneum provides a slippery and non-adhesive surface that allows the peristalsis (P.H. Sugarbaker, 2007), through the secretion of small quantities of sterile fluid containing phosphatidylcholine, produced in turn by the mesothelial cells.

Indeed, the peritoneum contributes to providing the first line of defense against external pathogenic (S. Varghese *et al.*, 2007) and is also involved in tissue repair through the direct release of specific growth factors (R. Warn *et al.*, 2001). For all these reasons, the peritoneum

is considered a sort of “organ”, characterised by both structural and protective functions for the abdominal cavity (A.P. Wasnik *et al.*, 2015).

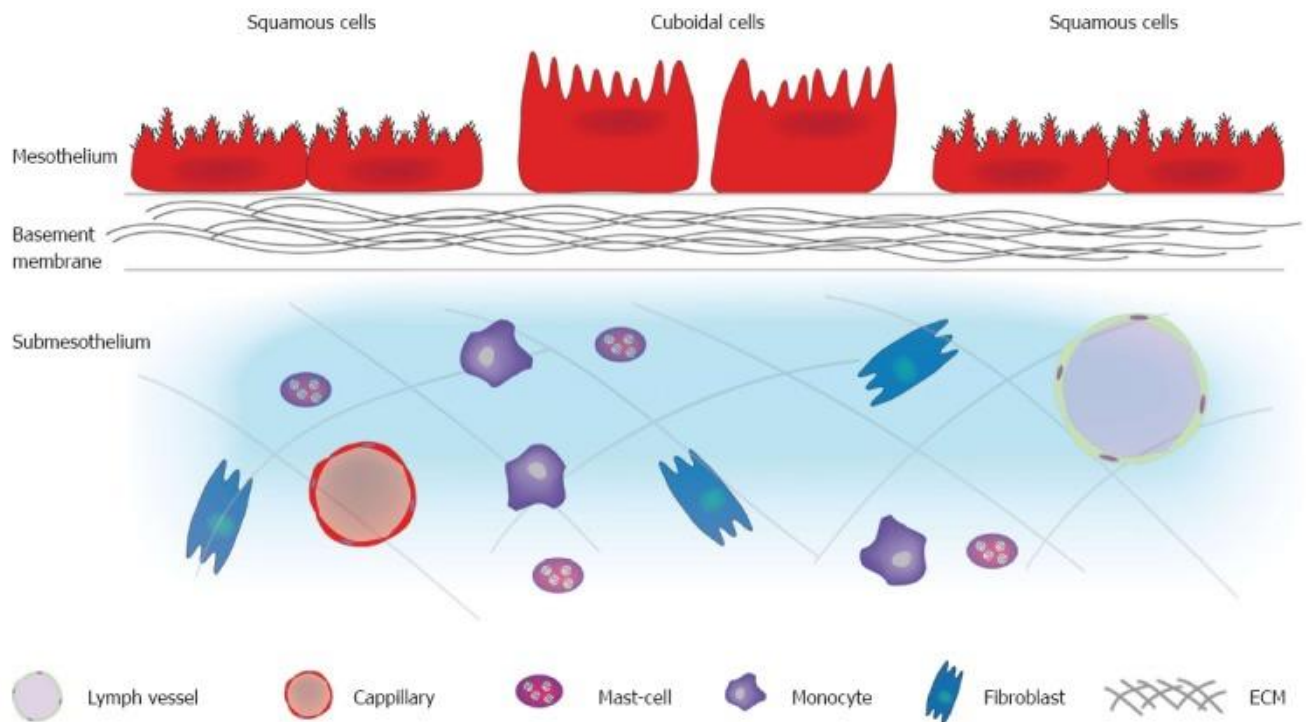


Figure 7. Structure and composition of the human peritoneum. Figure taken from “ **Pathophysiology of colorectal peritoneal carcinomatosis: Role of the peritoneum**” by L Leimoine *et al.* *World Journal of Gastroenterology*, **14**, 22(34): 7692-7707, (2016).

4.11 The peritoneal metastatic cascade

- **Introduction.** The development of peritoneal metastases from primary CRC is the result of fine-tuned molecular interactions and continuous crosstalk between tumour cells and the host microenvironment, which includes several well-defined steps. First, single cells or group of cells detach from the primary tumour and enter the peritoneal cavity. Subsequently, these free circulating cells come into contact with the normal peritoneal transport circle. At this point, these cells are distributed along the peritoneal wall at different points where they

will then invade the peritoneal space. The connective tissue located below the subperitoneal space plays a crucial role in the metastatic process, providing the scaffold for tumour development and proliferation (L. Lemoine *et al.*, 2016). Finally, the activation of angiogenic mechanisms that support the proliferation of neoplastic cells allows the further development of metastases (D. Jayne, 2007). All these processes converge in the phenomenon commonly called "peritoneal metastatic cascade" (Figure 8).

- The detachment of neoplastic cells.

The detachment of single cells or groups of cells from the primary tumour may be due to a spontaneous exfoliation of the neoplastic cells that have previously completely invaded the intestinal wall, colonizing also the layers of the serosa (D. Jayne, 2007, M.J. Koppe *et al.*, 2014). Spontaneous exfoliation is promoted through a downregulation of intracellular adhesion molecules that are present on the surface of cancer cells. In detail, downregulation of E-Cadherin, which belongs to the sub-family of type 1 cadherins, may be observed (M.E. Bracke, 2007). Furthermore, it has been shown that low levels of E-cadherin are associated with specific processes of differentiation, progression and development of metastases in CRC (M. Pocard *et al.*, 2001). Decrease of cell-cell adhesion mechanisms through loss of expression of E-cadherin and upregulation of N-Cadherin is an established hallmark of the epithelial to mesenchyme transition (EMT) (M. Yilmaz & G. Christofori, 2009). This process is reversible and programmable and allows cells to separate from each other and to lose their apico-basal polarization, also demonstrating a strong resistance to all apoptotic mechanisms, thus reversing towards a mesenchymal phenotype characterised by a high motility (T.M. Bodenstine & D.R. Welch, 2008). This mechanism seems to be fundamental in invasion and development processes of PM disease.

Another important phenomenon involved in the first steps of the metastatic process towards the peritoneal cavity is the overexpression of two membrane-spanning proteins: the epithelial polycystins PC1 and PC2. PC1 is a mechanical sensor conjugated to a G-protein receptor with the function of perceiving mechanical signals coming from the extracellular environment, transducing them in biochemical responses (G. Dalagiorgou *et al.*, 2010). PC2 constitutes a mechanosensor that forms a calcium channel (H. Hoffmeister *et al.* 2011). They both contribute to inducing alterations related to the EMT phenomenon, modifying the expression levels of E-cadherin, N-cadherin Snail and TWIST. Furthermore, they seem to be involved in the migration processes of circulating tumour cells (A.N. Gargalionis *et al.*, 2015).

Tumour cells that have spontaneously detached from the primary tumour are also involved in the phenomenon of increasing the pressure of the interstitial fluids present in the peritoneal cavity. The pressure at the tumour level is a very important factor, not only for increasing the number of shed cells, but also for determining the size of the emboli in the lymphatic vessels around the primary tumour (K. Hayashi *et al.*, 2007). Interstitial hypertension contributes to giving rise to a high osmotic pressure, leads to an increase in vascular permeability, to the perfusion of fluids, to a rapid cell proliferation, to the lack of lymph node drainage, to the formation of hyperplasia around the blood vessels and to a marked increase of the ECM remodeling (I.A. Khawar *et al.*, 2015). Finally, it would seem that even the surgery itself can promote the accidental detachment of tumour cells from the primary tumour, when for example the primary mass is inadvertently injured or through cuts of lymphatic and blood vessels during the course of the surgical intervention (E. Hansen *et al.*, 1995).

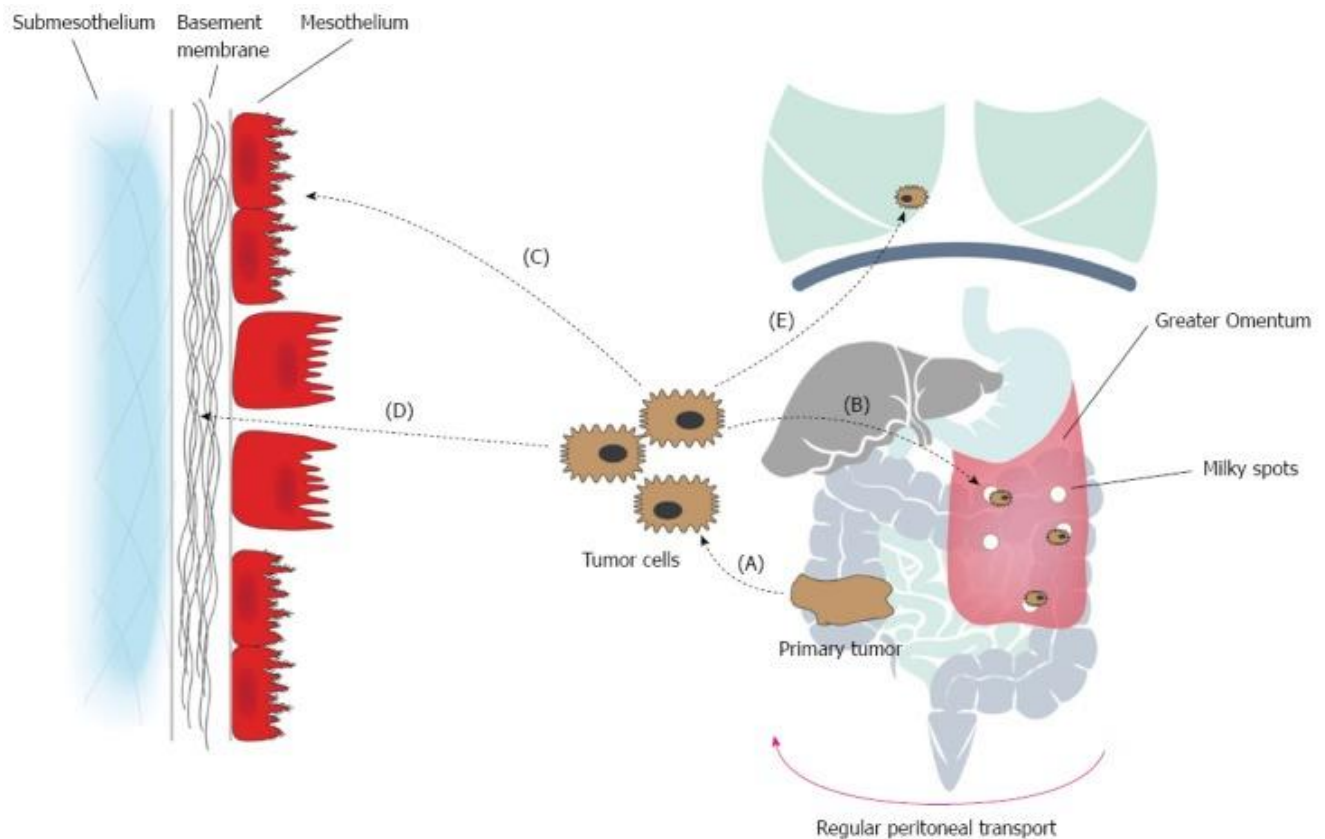


Figure 8. The main steps of the peritoneal metastatic cascade. The process begins with the exfoliation of the neoplastic cells from the primary tumour. Thereafter, the single cells or cell clumps come in contact with the peritoneal cavity through the peritoneal transport flow. Once they reach the cavity of the peritoneum, the neoplastic cells bind the mesothelial layer through very specific mechanisms such as transmesothelial metastasis and translymphatic metastasis. In the first case, the tumour cells adhere directly to the adhesion molecules to the peritoneum. In the second case, the circulating cells colonize the submesothelial layer through the lymphatic system. Once the mesothelium is reached, the tumour cells interact with the laminar network present in the basement membrane through integrin bonds. Finally, the subsequent invasion of the submesothelium is mediated by the production of specific metalloproteases (MMPs).

- Transport of detached tumour cells through the peritoneum. Once the neoplastic cells have detached from the primary tumour and have colonized the peritoneal cavity, they enter directly into the regular peritoneal transport. Initially, the development of metastases at the level of the peritoneal cavity was considered a random process independent of physical

and biological factors, also for the type of primary tumour from which the metastases originated and for the interaction with the site of colonization of the metastases (P.H. Sugarbaker, 1996). In recent years, evidence has emerged that have clarified how the direction taken by the circulating cells and their final destination depends on the anatomical position of the primary tumour and on the continuous cephalic circulation, responsible for the clearance of the peritoneal fluid (N. Hugen *et al.*, 2014). The latter is due to changes in intra-abdominal pressure due to respiration, gravity and intestinal peristalsis, which causes the formation of a flow gradient towards the pelvis, which passes along the right gutter and through the subdiaphragmatic space and, finally, across the pelvis again (C.P. Carmignani & T.A. Sugarbaker, 2003). All these characteristics imply that some areas of the peritoneal cavity may present a greater risk of developing metastatic lesions (P.H. Sugarbaker, 1996). Furthermore, the presence of mucinous ascites facilitates the massive colonization of large areas of the peritoneum also showing specific metastatic patterns (N. Hugen *et al.*, 2014). During the EMT process, circulating malignant cells acquire migratory and invasive characteristics that result in a profound reorganization of actin microfilaments activity, which involves the formation of actin-rich membrane protrusion domains, generally known as lamellipodia and filipodia phenomena. All these processes are favored by the pathological expression of growth factors, their respective receptors and by the activation of specific signal transduction pathways that are the result of the activation of certain proto-oncogenes (U. Lindberg *et al.*, 2008).

- Attachement of the metastatic cells to distant areas of the peritoneum. The final site of engraftment of metastatic cells along the peritoneal wall depends not only on the physical and biological properties of the same free circulating cells, but also on the tissue from which the metastatic implant originates. Engraftment of CRC metastatic cells occurs

through two well-defined biological mechanisms (Figure 9): transmesothelial or translymphatic metastasis. As for the first case, the cells that have detached from the primary tumour are able to adhere directly to distant areas of the mesothelium, which is located between the peritoneal layer (L. Lemoine *et al.*, 2016). This process is promoted by adhesion molecules expressed by the mesothelial cells, in particular molecules belonging to the immunoglobulin superfamily, such as intracellular adhesion molecule-1 (ICAM-1), platelet-endothelial cell adhesion molecule-1 (PECAM-1) and vascular adhesion molecule-1 (VCAM-1) (N.A. Alkhamesi *et al.*, 2005). The secretion of several pro-inflammatory cytokines, released during the operative phase or by circulating neoplastic cells, such as TNF α , interleukin-1 β (IL-1 β), interleukin-6 (IL-6) and interferon- γ (INF γ), favors the formation of a “prone” microenvironment which facilitates the interaction between mesothelial and metastatic cells (K. Ksiazek *et al.*, 2010, L. Lemoine *et al.*, 2016). These cytokines promote the increase of the expression levels of ICAM-1 and VCAM-1 by mesothelial cells, inducing their contraction. Contraction makes the areas of the basement membrane available (D.G. Jayne *et al.* 1999). In these areas, interaction with cancer cells occurs through the β 1 integrin subunit, which favors the uptake and implantation of the metastatic cells at the final sites (W.M. van Grevenstein *et al.*, 2007).

During the development of PM, mesothelial cells secrete a huge quantities of glycosaminoglycans and hyaluronan that that will be assembled together to form pericellular coats (L. Lemoine *et al.*, 2016). These coats protect the mesothelium from viral infections and from the cytotoxic effects of lymphocytes; in a pathological environment they are also involved in the mediation of adhesion between mesothelium and neoplastic cells through the interaction with the CD44 receptor expressed by tumour cells (N. Harada *et al.*, 2001). This interaction is a fundamental step in the peritoneal metastatic cascade of CRC, as it favors the migration of exfoliated cells and the determination of the final site of formation of the various metastatic lesions in the peritoneal cavity (C.Z. Li *et al.*, 2008). As for translymphatic

dissemination, metastatic cells have access to the sub mesothelial lymphatic vessels, through the opening of the junctions between two or more mesothelial cells, taking the route of the lymphatic stomata. The latter are characterised by a micro fenestration of open lymphatic capillaries which are normally involved in the drainage and active absorption of fluids and cells that derive from the serous cavities (L. Lemoine *et al.*, 2016). Other structures involved in the engraftment phase of neoplastic cells to the peritoneum include the so-called milk spots, which are distributed along the lymphatic stomata and are made up of immunocompetent cellular aggregates that act as access routes and supply the abdominal cavity with macrophages (L. Cao *et al.*, 2011). They provide a highly vascularized microenvironment that allows the survival of circulating cells that soon arrive at their site. At the level of milky spots, the mesothelial cells are also induced to produce VEGF, favouring angiogenesis and contributing to the preference by neoplastic cells of these specific areas of the peritoneum, demonstrating that tumour growth occurs preferentially at the level of immunoaggregates (S.A. Gerber *et al.*, 2006).

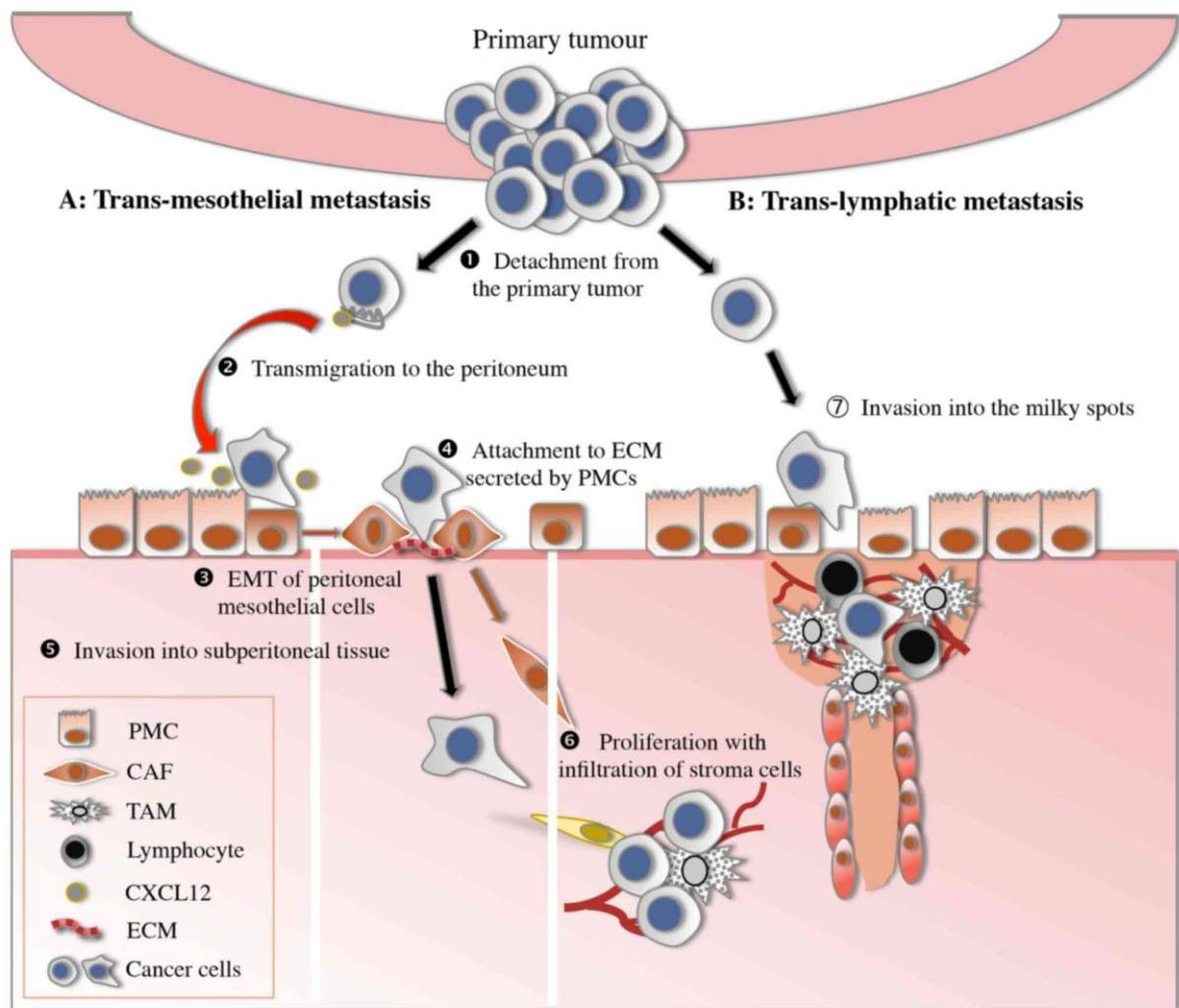


Figure 9. Main mechanisms of dissemination of PM disease. The first step sees the detachment of tumour cells mediated by the upregulation of E-cadherin and S100A. Migration to the peritoneal cavity is mediated by CXCR4/CXCL2 receptors. At this point the cells undergo EMT, thanks to the presence of CD44 and high levels of TGF β . The engraftment of metastatic cells is then mediated by the presence of integrin receptors, followed by the invasion of the deep layers of the peritoneum thanks to the activation of MMPs, at this point the process of cellular invasion and proliferation begins.

- Invasion of the subperitoneal space during PM development. Once they reach the peritoneal wall, the metastatic cells begin to invade the “deep” layer of the peritoneum, or the subperitoneal space. To do this, cancer cells must first penetrate through the mesothelial layer. Mesothelial invasion can occur in two distinct ways: cells can invade the intracellular spaces

between rounded mesothelial cells, or they can actively destroy the mesothelial cell monolayer (L. Lemoine *et al.*, 2016). Invasion of the space between rounded cells occurs in response to various pro-inflammatory stimuli mediated by specific cytokines that allow the exposure of the basal matrix of the mesothelium, thanks to the stretching of the mesothelial cells. These mechanisms appear to be also mediated by the hepatocyte growth factor/scatter factor (HGF/SF) produced by mesothelial cells which induces detachment, motility and proliferation of these cells during the mesothelial wound repair process (R. Warn *et al.*, 2001). Furthermore, the binding of HGF, with its respective tyrosine kinase receptor, involves the activation of an invasion program, as this receptor is encoded by the protooncogene c-MET (P.C. Ma *et al.*, 2003). The destruction of the mesothelial monolayer can occur through the activation of apoptotic mechanisms induced by the tumour cells themselves. Once they reach the mesothelium, most of the neoplastic cells show high proliferative abilities but poor invasive abilities. At this point, some cells manage to invade the mesothelium inducing apoptosis to the mesothelial cells through the Fas-ligand pathway (R.M. Heath *et al.*, 2004). After invading the mesothelium, cancer cells adhere to the basement membrane by promoting integrin bonds (L. Lemoine *et al.*, 2016). The subsequent invasion of the peritoneal-blood barrier, which represents the submesothelial tissue between the peritoneal mesothelium and between the submesothelial arterial blood capillaries, occurs thanks to the action of proteases (L. Lemoine *et al.*, 2016). In fact, tumour cells, mesothelial cells, fibroblasts, inflammatory cells and the same macrophages present in the peritoneum, secrete matrix metalloproteinases (MMPs), which are responsible for the degradation of various components of the ECM (L. Lemoine *et al.*, 2016). Increase of MMP-1, MMP-2, MMP-7, MMP-9, MMP-13 and MMP-14 levels is associated with the development processes of metastases from CRC to the peritoneal cavity (X. Garcia-Albeniz *et al.*, 2011). High MMP-1 levels have been associated with the development of metastases as well as a drastic reduction in overall and/or disease-free survival (L. Lemoine *et al.*, 2016).

Of note, a bidirectional signaling was observed between mesothelial and tumour cells. In fact, the interaction between ICAM and its ligand CD43 plays a fundamental role both in adhesion to the peritoneum and in the preparation of an adequate environment for the subsequent invasion of neoplastic cells, through the production of MMPs by the mesothelial cells (N.A. Alkhamesi *et al.*, 2007). Several studies have shown that MMP-7 is strongly involved in the spread of circulating CRC cells to the peritoneum. MMP-7 helps to degrade the basement membrane and various components of the submesothelium, also promoting the progression of cancer cells by inhibiting apoptosis, decreasing cell adhesion and inducing angiogenesis (M. Li *et al.*, 2006). Another mediator of the degradation of the peritoneal-blood barrier is the urokinase plasminogen activating system that includes the urokinase plasminogen activator receptor (uPAR) and the urokinase plasminogen activator (uPA). UPA is a serine protease that, when activated, catalyzes the conversion reaction of plasminogen into plasmin, which in turn is responsible for the degradation of various components of the ECM and for the activation of multiple pro-MMPs (U. Klinge *et al.*, 2007).

- Role of proliferation and angiogenesis during PM development. Cancer cells are characterised by a marked proliferative capacity. Proliferation is activated by the production of growth factors that interact directly with the tumour cells and with the stromal cells, generating autocrine and paracrine loops (N.A. Bhowmick *et al.*, 2004). Both epidermal growth factor receptor (EGFR) and insulin like growth factor-1 (IGF-1) are involved in this process (L. Lemoine *et al.*, 2016). In fact, intestinal tumours that present a synchronous expression of EGF and EGFR have a higher malignant potential and secrete autocrine factors that promote the self-replication of neoplastic cells at the metastatic sites (M. Tampellini *et al.*, 2007). In addition, when TGF β binds its receptor it can activate an autocrine circuit that makes CRC independent from growth factors (C.S. Fuchs *et al.*, 2008). Furthermore, CRCs

with peritoneal metastases show suppression of both EGFR and TGF α , giving rise to immunoreactive reactions capable of modulating the immune microenvironment in favor of metastatic cells (M. Tampellini *et al.*, 2007). Regarding IGF-1, it has been found upregulated only in CRCs with peritoneal metastases, indicating its importance in the proliferative processes of metastatic CRC cells in the peritoneal cavity (C.S. Fuchs *et al.*, 2008).

Angiogenesis, which consists in the development of new blood vessels starting from vessels already present in the tissues, is another fundamental characteristic of cancer. To survive, cancer cells need oxygen from the blood vessels already present in the tissue they have invaded and nutrients from stromal cells. Nevertheless, when the tumour cells are more than 150 μ m from the capillaries of the submesothelium, oxygen and nutrients are no longer able to pass the peritoneal-blood barrier, causing an apoptotic process mediated by hypoxia (M.M. Olcina *et al.*, 2016). To survive, cancer cells induce angiogenesis through the production of angiogenic factors. The main proteins involved in these biological mechanisms are the hypoxia inducible factor-1 (HIF-1) and VEGF. Expression of HIF-1 increases exponentially with the lowering of oxygen levels in the cells and is strongly upregulated in case of PM disease (L. Lemoine *et al.*, 2016). VEGF is able to promote the survival of tumour endothelial cells, as well as their proliferation and differentiation, while its expression depends on that of HIF-1 (L. Lemoine *et al.*, 2016).

- **Conclusions.** Peritoneal metastases are the result of complex molecular interactions between tumour cells and the peritoneal microenvironment, mediated by paracrine cell-cell interactions through the secretion of specific factors by tumour cells. To date, several molecular mechanisms underlying the development of PM disease are known and have greatly contributed to increasing our knowledge of this peculiar oncological disease, leading to a significant increase in patient's survival, thanks also to the implementation of innovative

surgical techniques such as CRS / HIPEC. Despite this, PM disease still remains elusive and deserves to be studied in depth as numerous biological mechanisms that lead to the colonization of the peritoneum by circulating CRC cells still remain unknown. In recent times, the concept that metastatic cells operate in a variegated context, formed by the microenvironment, which is now known to play a fundamental role in the metastatic process and in the formation of the metastatic niche, has become increasingly popular. In particular, the focus is on the ECM, which in addition to playing a passive role of scaffolding, actively participates in the promotion of metastases to the respective target organs. Given the profound remodeling and primary role of ECM during the formation of colorectal metastases in the peritoneal cavity, future studies based on characterising the precise role of ECM in PM disease could open new scenarios for understanding the disease and its treatment.

4.12 The Extracellular matrix: involvement in cancer

Introduction. The ExtraCellular Matrix (ECM) is an ubiquitous acellular component present in all tissues of the body constituted by molecules that are secreted and assembled to form specific insoluble components that play a fundamental role during the processes that underlie organ development, the repair of damaged tissues, and in the maintenance of tissue and organ homeostasis during the entire life of the organism. Furthermore, the ECM has a whole series of cues that are able to regulate several processes such as cell proliferation, survival, migration and cell invasion as well as providing the resident cells with the correct architectural support and mechanical properties (T.R. Cox, 2021). The ECM is made up of hundreds of different proteins that interact with each other to form a complex 3D architecture. Moreover, thanks to the numerous post-translational modifications or the presence of specific mRNAs that code for proteins of the matrix, the human body is able to produce an almost infinite quantity and variety of ECMs (T.R. Cox, 2021). The matrix is also a "dynamic"

entity, characterized by a continuous remodeling process in response to external and/or internal stimuli (T.R. Cox, 2021).

There is a reciprocal interaction between the ECM and the cells, which involves numerous cellular activities, such as the deposition of cells along the 3D architecture of the ECM, specific and selective remodeling of the matrix and, at the same time, the ECM itself significantly affects the cellular well-being. These complex and mutual interactions are defined as "dynamic reciprocity", indicating how the ECM can be considered an important entity for the entire physiology of tissues and organs (T.R. Cox & J.T. Erler, 2014). In cancer, the ECM goes against a strong deregulation, actively participating both in the tumorigenesis process, but also, on the other hand, by helping to play an anticarcinogenic role (T.R. Cox, 2021) (Figure 10). Furthermore, tumour desmoplasia is a common feature in several solid tumours, acquiring many of the characteristics that distinguish states of tissue fibrosis (T.R. Cox & J.T. Erler, 2014). The loss of the correct organization of the ECM is now regarded as a major sign of cancer development. It is important to consider how both tumour cells and non-malignant stromal cells contribute to, and consequently are also affected by, the deposition and active remodeling of the ECM during cancer (T.R. Cox, 2021). In the last 30 years, the interest in ECM and its involvement in neoplastic processes has increased exponentially and, in the last decade, it has emerged that the matrix can act as a prognostic and diagnostic index, as a biomarker and also as a possible therapeutic target for various solid tumours (T.R. Cox, 2021).

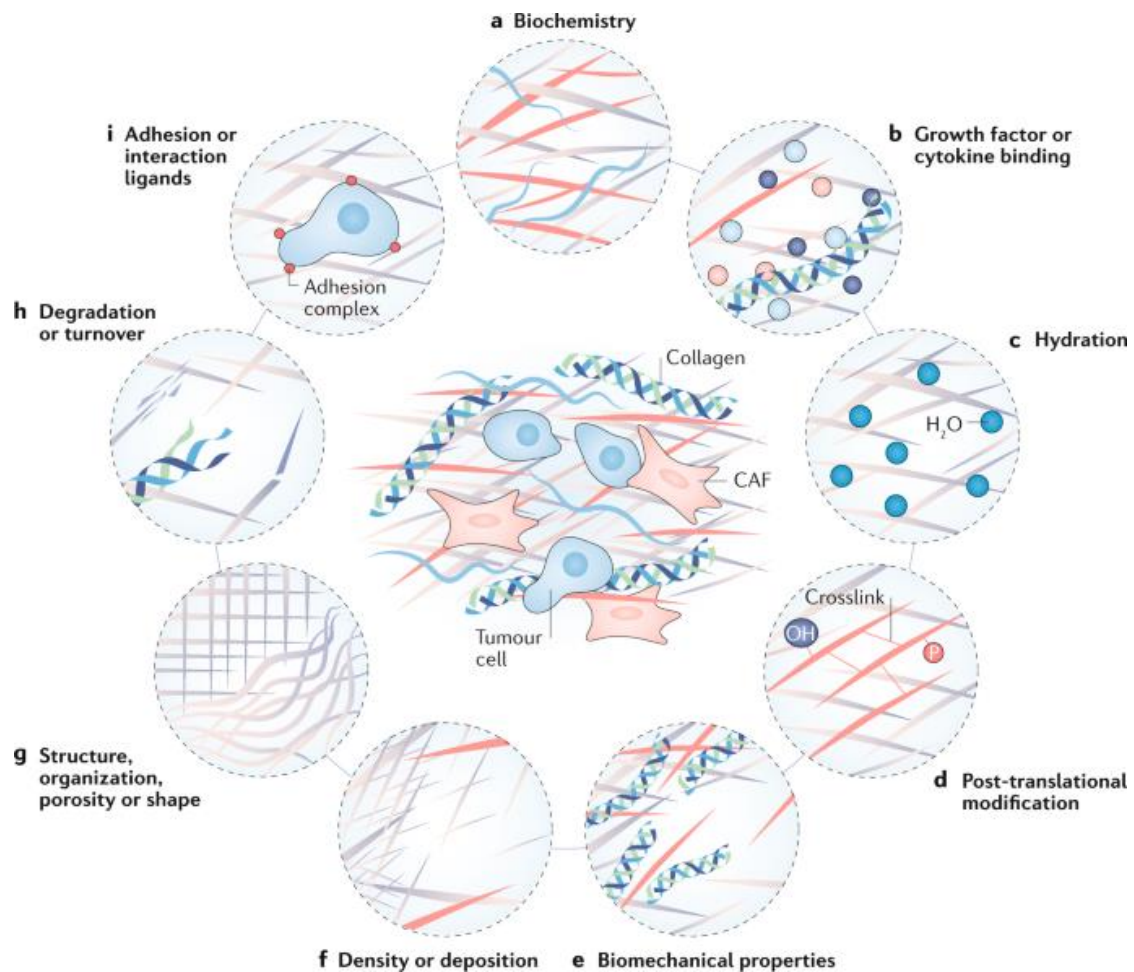


Figure 10: Changes that the ECM undergoes during tumour development. Both the neoplastic cells and the non-malignant cells of the stromal component are involved, which in turn will be mutually influenced by the modifications of the matrix.. These types of modifications include **a)** biochemic aspects, **b)** secretion of specific growth factors, **c)** changes in matrix hydration states, **d)** post-translational changes, **e)** changes in biomechanical properties such as increased stiffness, **f)** massive deposition of collagen fibers with consequent increase of the fibrotic state, **g)** alterations in the structural organization with changes in the porosity of the ECM, **h)** deregulation of the turnover rhythms of the degradation of the structural components of the matrix and **i)** perforation of adhesion interactions between cells due to expression of binding proteins. Figure taken from “**The matrix in cancer**” by Thomas R. Cox, *Nature Reviews Cancers*, **21**, 217-238, (2021).

- **The principal components of the ECM.** All ECM proteins, are commonly classified within the so-called "human matrisome" (A. Naba *et al.*, 2012). There are about 1000 specific genes of the matrix included in the matrisome of mammals, which can be substantially divided into different macro-areas: molecules belonging to what is defined as

core-matrisome, which includes about 300 genes, and molecules and proteins associated with the matrisome, included in the subgroup of the matrisome-associated molecules, which includes approximately 800 genes (A. Naba *et al.*, 2012). The genes coding for the matrisome-proteins comprise about 4% of the entire human proteome.

The ECMs, in turn, can be divided into two major classes: the interstitial matrices and the highly specialized organ or tissue-specific matrices, such as the basal lamina (T.R. Cox, 2021). Both these classes are highly compartmentalized and ordered according to their functions, which vary from the conferment of elastic properties to the formation of fibrillar, reticular or plate-like networks of molecules involved in the determination of stiffness and compressive strength. The macromolecules that constitute the different ECMs of organs and tissues are classified according to their composition. A complete view of these molecules, is shown in table 1. Some of these classes, such as collagen proteins, account for 30% of the total proteins of the whole body, reaching 90% in some particular tissues, such as connective tissue (K.E. Kadler *et al.*, 2007). Each matrix is characterised in a unique manner, and their properties have been locally or globally understood through their biochemical and biophysical characteristics (T.R. Cox, 2021). The biophysical properties allow the matrix to provide support as a scaffold and to mediate different mechanical forces, while the biochemical properties allow the ECM to present ligands useful for cell behaviour and cell-matrix interactions (J.T. Parsons *et al.*, 2010). Finally, the various types of collagen and glycoproteins are the two major classes of proteins that constitute the ECM.

ECM's molecules functions	Protein members
Fibrillar and fibrillar-like collagens	Collagens I, II, III, V, XI, XXIV, XXVII
Network-forming collagens	Collagens IV, VIII, X, XV, XVII
Filament-forming collagens	Collagens VI, XXVI
Transmembrane and membrane-bound collagens	Collagens XIII, XVII, XXII, XXIII, XXV
Glycoproteins	Agrin, fibronectin, fibrinogen, laminin, matrilins, nidogens, osteopontin, osteonectin, periostin, tenascins, trombospondins, vitronectin
Proteoglycans	Aggrecan, brevican, biglycan, decorin, lumican, neurocan, perlecan, versican

Table 1: classification of the main ECM components based on their function and location within the ECM. Table adapted from “**The matrix in cancer**” by *Thomas R. Cox, Nature Reviews Cancers, 21, 217-238, (2021).*

- **Post-translational modifications of the ECM.** The physicomechanical and biochemical properties of the ECM are often modulated by post-translational modifications. These modifications affect the interactions between the molecules of the matrix and the receptors placed on the its surface and include hydroxylation, glycosylation, transglutamination, sulfation and the formation of new cross-links, as well as the cleavage and degradation of the structural components of the ECM (M.D. Roycik *et al.*, 2009). . Post-translational modifications are mediated by several families of intracellular and extracellular enzymes, such as intracellular collagen prolyl hydroxylase 3 and prolyl hydroxylase 4, lysine

hydroxylases, the extracellular lysyl oxidases (LOXs), transglutaminases, sulfatases, pepsins and heparanase (T.R. Cox, 2021). These modifications play a fundamental role in maintaining the dynamics of the ECM, allowing the continuous renewal and shelter of the tissue microenvironment; deregulation of post-translational modification mechanisms can lead to significant changes in the matrix that can result in cancer promotion and development (T.R. Cox, 2021).

- **Crosslinking functions of the ECM.** All the components of the ECM can undergo crosslinking through various mechanisms that usually lead to the formation of a dense network of molecules constituted by the matrix coupled to a progressive increase in the stiffness of the tissue that has undergone the modifications mediated by crosslinking (B. Piersma *et al.*, 2020). The stiffness of the ECM plays a fundamental role, as it can alter the activation of mechanosensor programs in both cancerous and non-cancerous cells. Furthermore, the generation of crosslinking bonds can reduce the turnover of the ECM and increase the half-life of the molecules associated with the pro-tumour type matrix at the level of the extracellular space (E.C. Filipe *et al.*, 2020). The crosslinking present in the ECM can generate strong or weak bonds; weak bonds usually coexist with strong covalent bonds of a stable type, allowing the ECM to assume peculiar characteristics of viscoelasticity that facilitate reactions to deformation stress (T.R. Cox, 2021).

- **ECM remodeling: degradation and turnover.** One of the main characteristics of the ECM is that of its degradation and, above all, of its turnover. Insufficient degradation, as well as excessive degradation of the matrix can lead to fibrotic conditions and at the same time both situations favour cancer development (T.R. Cox, 2021). ECM turnover is operated by different enzymatic classes, the most important of which is represented by the family of MMPs, adamalysins (ADAM), cathepsins, hyaluronidase and heparanase (T.R. Cox, 2021).

Tumours have often high ECM turnover , which in turn leads to high degradation of the healthy matrix, facilitating its replacement, with a tumour-type matrix that reinforces the aggressive characteristics of the tumour (T.R. Cox, 2021). Furthermore, the degradation of the ECM results in the loss of physical barriers and thus, the destruction of the healthy ECM leads to metastatic dissemination (T.R. Cox, 2021). Growth factors that bind to the matrix make it an important reservoir of ligands. Cleavage of the ECM causes the local release of these factors which can activate specific signal transduction pathways by stimulating their target cells (R.O. Hynes, 2009). In addition to being a reservoir of growth factors, cytokines and chemokines, ECM is also a supporting supplier of inorganic molecules, such as ions, for example calcium and zinc ions. Their release during ECM degradation facilitates the transport of ions across the membranes and can also modulate the activities of various enzymes, such as MMPs (T.R. Cox, 2021). Finally, the activity of the enzymes involved in the degradation and regulation of ECM turnover is modulated by specific inhibitors, typically the tissue inhibitors of metalloproteinases (TIMPs), cystatins and serpins (T.R. Cox, 2021). Also in this case, deregulation of these inhibitors is at the basis of tumour progression and metastatic dissemination.

- Changes in the ECM during cancer. As previously described, many solid tumours are highly fibrotic. Recently, it has emerged that the ECM at the tumour site is mainly produced by cells of the stromal microenvironment, in particular by cancer-activated fibroblasts (CAFs) (T. Liu *et al.*, 2019). A considerable variety of CAFs have been described in different types of tumours, although the precise origin of many CAFs subtypes still remains poorly understood (B.A. Pereira *et al.*, 2019). CAFs are resident fibroblasts that are activated and directly influenced by the growing tumour cells. This influence also triggers other cells of the stromal compartment, such as adipocytes and mesothelial cells, giving rise to a complex network of cells, capable of remodeling and removing the ECM, favouring the development

of the tumour (R. Kalluri, 2016). Exosomes are one of the main interactors in the modulation of CAFs and other cells of the stroma, which are able to mediate the cross-talk between tumour cells and cells of the microenvironment, reprogramming the latter through the transport of pathways activators such as TGF β (J.P. Webber *et al.*, 2015). Furthermore, it has been shown that in several solid tumours an increase in the number of CAFs correlates with poor prognosis, indicating that there may be a specific spatial and temporal segregation of the factors released by CAFs and other cells of the stroma that remodel the ECM (L. Liu *et al.*, 2016). The high variability of CAFs subtypes means that, based on their localization within the tissues, they are able to secrete particular types of molecules that can induce fibrosis, thus contributing to carry out a multifactorial activity in the remodeling of the ECM, partly explaining the great heterogeneity of the matrix in cancer (T.R. Cox, 2021). In addition, CAFs appear to possess a transient phenotype, which can be influenced by various growth factors and cytokines, such as TGF β and interleukin-1 (IL-1) through the RAS-STAT pathways (G. Vasiukov *et al.*, 2020). For these reasons, CAFs, and other cells in the microenvironment are the major source of ECM deposition in cancer and many of the components of the matrix deposited by CAFs are fibrotic-like molecules (C. Tian *et al.*, 2019). Nevertheless, it is still necessary to understand how the composition of the ECM contributes to the cancer or anti-cancer processes. Due to the activity of CAFs and other cells of the stroma, their reprogramming, rather than their depletion, could represent a good therapeutic strategy (T.R. Cox, 2021).

4.13 ECM and its involvement in the cellular signaling

- **Introduction.** Tumour ECM undergoes a large number of biochemical and biomechanical modifications. These changes support fundamental functions for neoplastic cells, such as proliferation and cell survival, as well as their resistance to chemotherapy treatments (L. Wei *et al.*, 2018). The profound changes provoked by the continuous

remodeling of the ECM influence the cellular interactions mediated by the surface receptors, allowing the activation of specific intracellular inputs mediated by matrix changes. For these reasons, the cells present within the ECM receive a series of stimuli both in time and space (J.F. Hastings *et al.*, 2019). The various components of the ECM are characterised by a heterogeneous longevity: some of them degrade in a short time, typically after a few days, while others can last for months. This indicates how some biological phenomena mediated by the ECM can be activated even after some time with respect to the initial deposit and production of the various molecules associated with the ECM (T.R. Cox, 2021). Finally, the dynamic nature of the matrix indicates that the cells themselves actively participate in its remodeling, generating continuous changes in the activation of surface receptors, with consequent activation of multiple cellular signaling pathways (Figure 11) (O. Chaudhuri *et al.*, 2015).

- **The role of growth factors in ECM-mediated signaling.** The influence that the ECM has on intracellular signaling leads to the development of a complex network of interactions that causes cross-regulation and reciprocal influence of other cell signaling pathways that are not directly mediated by the matrix. For example, integrin-mediated signaling is strongly influenced by ECM stiffness, which increases the activity of these molecules through the increase of signaling mediated by tyrosin-kinase receptors such as EGFR, ERBB2, VEGFR and HGFR both in normal cells and especially in cancer (W. Guo *et al.*, 2006). Moreover, it has been shown that mechanosensitisation due to remodeling of the ECM is a driver factor for the activation of EGF-mediated signaling in some types of cancer (E.M. Grasset *et al.*, 2018). Another signal transduction pathway influenced by ECM stiffness is the ERBB2 signaling, whose activation leads to enhancement of resistance to standard therapy (B. Weigelt *et al.*, 2010). Other pathways activated by changes in tumour ECM structure include MAPK- and YAP-TAZ-mediated signaling pathways. Both pathways, are

associated with the onset of chemoresistance linked with the molecular and mechanical changes of the matrix (C.D. Nguyen & C. Yi, 2019). It has recently emerged that signal transduction acting through the ROCK pathways plays an important role in the modulation of the ECM and in the response to stimuli associated with its remodeling, both in tumour cells and in stromal-associated CAFs (Figure 11) (C. Vennin *et al.*, 2017).

- Integrins function as ECM receptors. The expression of specific integrin patterns, related to the remodulation of the tumour ECM, plays a pivotal role during the neoplastic development. Integrins are heterodimers that represent the major mediators of cell-ECM communications, activating numerous signaling pathways (J.Z. Kechagia *et al.*, 2019). Different integrins are overexpressed in several types of tumours and usually mediate cell invasion and the development of metastases through the formation of matrix-dependent bonds (H. Hamidi & J. Ivaska, 2018). The expression of specific integrin heterodimers, with their spatial location in certain sectors of the ECM, involves the development of phenomena of resistance to therapeutic treatments, also promoting cell survival. Therefore, the specific expression of integrins, which interact with a strongly remodeled matrix, is involved in the onset of resistance phenotypes in different types of solid tumours (A. Madamanchi *et al.*, 2014). For example, it has been shown how the expression of the integrin heterodimers $\alpha\text{v}\beta 3$ promotes binding with fibronectin. The latter undergoes remodeling during tumour development. This involves the activation of intracellular processes that favour the survival of cancer cells (J.L. Young *et al.*, 2020).

Overexpression of the $\alpha 5\beta 1$ dimer leads to the activation of CAFs, promoting tumour fibrosis, acting as a protective scaffold towards the permeation of treatments at the neoplastic lesion (P.R. Kuninty *et al.*, 2019). Given the complexity of integrin-ECM interactions and the vast plethora of intracellular signals they are able to regulate, the role of integrins in cancer development depends on both the cell type from which they are expressed and the

biochemical properties of the ECM. During EMT transition, when there is a switch between E-cadherin and N-cadherin, the switch of the $\alpha 6 \beta 4$ dimer into $\beta 1$ and $\beta 3$ integrin heterodimers is simultaneously observed (M. Janiszewska *et al.*, 2020). This change allows cancer cells to switch from a cell-cell type to a cell-ECM type connection, facilitating adhesion to type I collagen fibers and, consequently, promoting neoplastic invasion (M.J. Wheelock *et al.*, 2008). For this reason many adhesion complexes formed by integrins and cadherins, accompanied by modifications of the cellular cytoskeleton, lead to the development of a complex network that allows cancer cells to respond to stress signals, to trigger in the various biochemical and biomechanical processes that occur in the surrounding microenvironment (Figure 11) (A. Zuidema *et al.*, 2020).

- Other non-integrin ECM-binding receptors and their functions. The ECM also forms bonds with molecules other than integrins. For example, other receptors able to bind to the matrix include the discoidin domain-containing receptors 1 (DDR1) and DDR2, the osteoclast-associated immunoglobulin-like receptor (OSCAR), the syndecans, urokinase-type plasminogen activator receptor-associated protein (UPARAP) and the leukocyte-associated immunoglobulin-like receptor 1 (LAIR), which are able to coordinate the transfer of information generated by the interactions between the extracellular and intracellular environments, with the consequent activation of downstream signaling programs (T.R. Cox, 2021). DDR1 and DDR2, once activated in a tumour context or in CAFs, promote an increase in ECM stiffness and the deposition of a new matrix, favouring metastatic dissemination and impairing the response to chemotherapy (S.V. Bayer *et al.*, 2019). Syndecan-4, which is usually deregulated in solid tumours, in turn tunes intracellular signaling in response to localized ECM fibers, through mechanochemical signaling involving the action of $\beta 1$ integrin and YAP-mediated signaling (Figure 11) (A. Chronopoulos *et al.*, 2020).

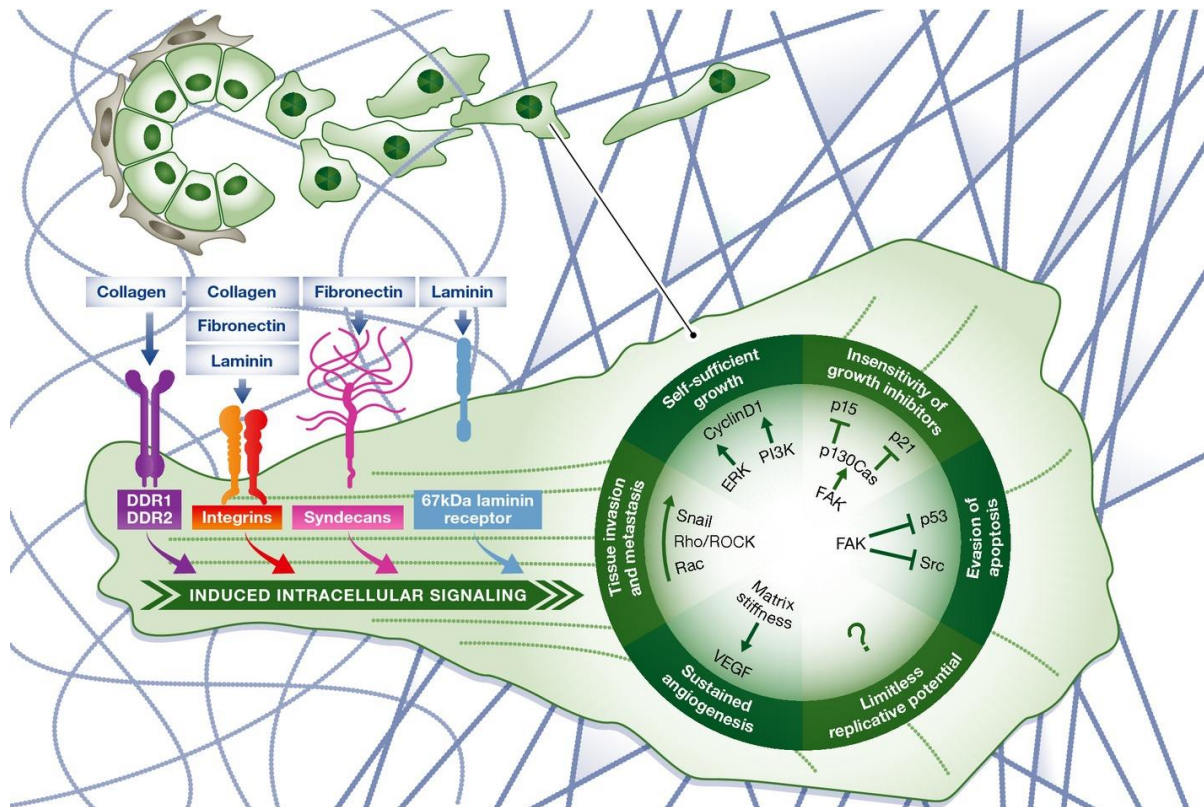


Figure 11. Modulation of the main hallmarks of cancer by the ECM. The remodeling of the ECM during the development of cancer allows the formation of bonds between the proteins and the molecules that make up the matrix, such as collagen, laminin, fibronectin and laminin with different receptors present on the cell surface. The formation of these bonds leads to the activation of intracellular signaling that promote various pro-tumour actions, such as survival, proliferation, the development of neoangiogenic processes, metastasis and resistance to chemotherapy. Figure taken from “**The extracellular matrix modulates the hallmarks of cancer**” by M.W. Pickup et al. *EMBO reports*, **15**, 1243-1253, (2014).

4.14 Biomechanical properties and functions of the ECM in cancer

- Introduction. The functions promoted by the biomechanical properties of the matrix have a key role in understanding the biological mechanisms that lead to cancer formation and colonization of the metastatic sites by circulating cancer cells. It is now known that cells are influenced by both biochemical factors and mechanical forces capable of activating specific signal transduction pathways at the intracellular level, thanks to the conversion of mechanical inputs into biochemical inputs. Biochemical and biomechanical stimuli do not operate separately and are often influenced by each other, generating a complex network of

intracellular signals. The conversion of certain mechanical inputs into biochemical intracellular signals is the so-called mechanotransduction. Mechanotransduction is involved in several biological functions, favouring the activation of many mechanisms fundamental for cellular behaviour (A. Miller *et al.*, 2020).

- **ECM mechanical properties and cancer.** Mechanotransduction is involved in processes that regulate development, such as the regulation of cell polarity, the regulation of gene expression and the differentiation of stem cells towards their lineage of commission (L.R. Smith *et al.*, 2018). The biomechanical properties of the tumour ECM can influence the behavior of neoplastic cells, of CAFs and of many stromal cells and immune cells, including macrophages, underlining how mechano-modulation influences several fundamental aspects of cancer biology (E.J. Hoffmann & S. Ponik, 2020). The ECM shows complex mechanical properties, such as viscoelasticity, mechanical plasticity and non-linear plasticity (E.J. Hoffmann & S. Ponik, 2020). The result of this complexity is that many of the cellular responses influenced by the ECM are biphasic, regulated on specific time scales and in a bidirectional manner through ECM-cell interactions (Z. Gong *et al.*, 2018). The main biological mediators of the biomechanical functions of the ECM include FAK-SRC, MEK-ERK, YAP-TAZ and ROCK signal transduction pathways (S.J.P. Pratt *et al.*, 2020). They are strongly deregulated in cancer and have key roles in the so called "cancer hallmarks", helping to generate phenotypes of resistance, immuno-escape, enhancement of invasion (and therefore metastasis), survival and cell proliferation.

Differences in ECM architecture and physical properties, such as tissue stiffness and 3D conformation, have been associated with some important features of cancer progression and cancer stem cells behavior. Data from the literature have highlighted the prominent role of both morphological aspects and mechanical properties of the ECM in the regulation/modification of asymmetric division and differentiation of the stem cells,

epithelial-mesenchymal transition, modulation of cell migration and spreading and also in differentiation and proliferation of the neoplastic cell subpopulation, both at primary and metastatic sites (T.R. Cox, 2021). It has been demonstrated how the tumour process is able to induce several changes in the surrounding ECM (T.R. Cox, 2021), such as conformation changes, expression of specific structural and non-structural proteins, presence of specific growth factors and also marked increase in rigidity due to the fibrotic process (T.R. Cox, 2021). The stiffness itself is directly involved in the development of the metastatic spread, favouring the generation of a microenvironment more suitable for the neoplastic cells, able to favour tumour development and also drug resistance (T.R. Cox, 2021). Atomic force microscopy (AFM) technique in indentation mode is a technology used to study changes in the stiffness of the ECM. It is a high-resolution non-optical imaging technique that allows the characterisation of the morphology of different biological samples. It was developed by Binnig, Quate and Gerber in 1985 (G. Binnig *et al.* 1985) to perform measurements of the surface of different organic and non-organic samples. AFM consents to accurately and non-destructively measure the topographical properties of a sample surface with very high resolution in air, liquids or ultra-high vacuum (O. Marti *et al.* 1987). Basically, this method allows measurements of the stiffness of the 3D-dECMs with an AFM tip of selected geometry and dimension that applies a specific force from the bending of the AFM cantilever (indentation mode). Fitting the force-indentation curve to the Hertz model for the corresponding tip geometry can give quantitative measurements of the ECM's stiffness in terms of Young Modulus, which represent a mechanical property that measures the tensile stiffness of a solid material (G. Thomas *et al.* 2013).

- **The role of ECM in development of metastases.** The metastatic process requires the acquisition of a whole series of specific characteristics, such as motility, the ability to invade, the ability to modulate the metastatic sites and the local microenvironment,

characteristics of plasticity and the ability to colonize distant sites (T.R. Cox, 2021). The ECM plays a very important role in the regulation of all these processes and is one of the main actors of the metastatic development. Tumours usually have linear and thickened collagen fibres, with a radial orientation with respect to the tumour mass. This pattern predisposes to metastasis; in fact it acts as a sort of "highway" for tumour cells, facilitating their migration from the primary tumour (M.W. Conklin *et al.*, 2018). Type I collagen is the protein most involved in this process, both at the metastatic and at primary tumour sites. This suggests that ECM remodeling is a dynamic process (A.E. Mayorca- Guiliani *et al.*, 2017). Moreover, proteolytic programs mediated by MMPs facilitate the invasion processes of circulating tumour cells (T.Y. Feinberg *et al.*, 2018). ECM can promote the development of metastases also by activating a non-canonical pathway mediated by the DDR1 protein, which allows the collagen I present in the interstitial matrix to be exploited to promote survival in the metastatisation sites (H. Gao *et al.*, 2016). Matrix remodeling during metastatic development activates mechanisms that promote the phenomenon of "invadopodia". It consists in the generation of actin-rich ECM protrusions that, interacting with integrin receptors and forming focal adhesions, direct tumour invasion through the localized degradation of the ECM by means of MMPs (T. Beaty & J. Condeelis, 2014). The stiffness of the ECM helps to increase tumour invasion by guiding the assembly of focal adhesions (A. Parekh *et al.*, 2011). Once the physical barriers surrounding the tumour mass are compromised, migration of neoplastic cells is activated. This phenomenon is mediated by the activity of Rho and Rac GTPases (M. Parri & P. Chiarugi, 2011; V. Sanz-Moreno *et al.*, 2008). The Ras oncogene stimulates the activity of Rho to promote a phenotype that induces an amoeboid-like migration, while the tumour suppressor p53 inhibits cell migration by reducing the activity of RhoA (M. Xia & H. Land, 2007). Once the parenchyma of the target organ is reached, the metastatic cells must "navigate" through the vascularization of the tissue to be able to extravasate in the secondary sites (T. Celià-Terrassa *et al.*, 2012). In this context,

the metastatic potential of transformed cells is favoured by the EMT switch, which is promoted by a strong exposure to the TGFβ factor, secreted by the immune cells of the infiltrate, or by local degradation of the ECM (M.W. Pickup1 *et al.*, 2014). A strong increase in the stiffness of the ECM promotes TGFβ-induced EMT, favouring a basal-like phenotype of tumour cells, wichstimulate the metastatic process (Figure 12) (J.L. Leight *et al.*, 2012).

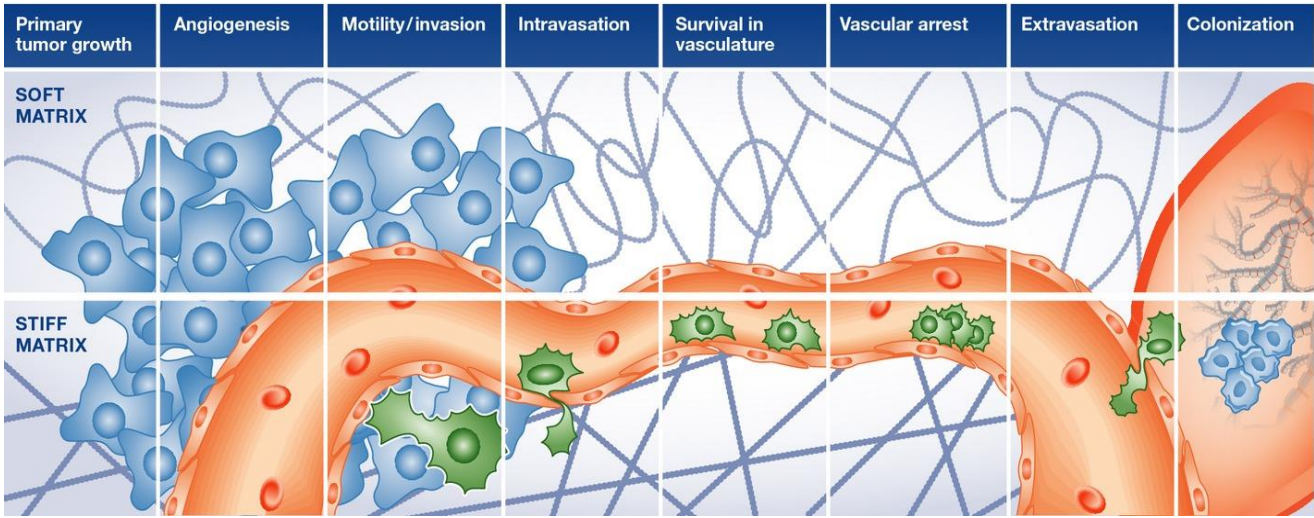


Figure 12. I Involvement of the ECM during the various stages of the metastasis process. The dissemination and engraftment of circulating neoplastic cells are controlled by numerous biochemical and biomechanical processes, which lead to the induction of an invasive phenotype, cell migration through the parenchyma, intravasation into the bloodstream, survival in the circulation followed by extravasation and secondary organ growth and survival. Adhesion to the ECM by tumour cells is able to regulate and influence each of these stages of the metastatic cascade. Figure taken from “**The extracellular matrix modulates the hallmarks of cancer**” by M.W. Pickup *et al.* *EMBO reports*, **15**, 1243-1253, (2014).

4.15 Conclusions

Tumour ECM is very heterogeneous among the various types of solid tumours, which in turn show multiple variability in matrix deposition and stiffness. The influence of ECM on tumour development is one of the main unsolved questions that has yet to be answered. Furthermore, the presence of conflicting data on the role of the matrix in cancer suggests that the influence of the ECM on the main hallmarks of cancer cannot be effectively extended for

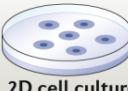






all types of cancer. These potentially conflicting results indicate that further studies are needed to understand the dynamic changes that occur in the biochemical and biophysical properties of the ECM during tumour progression. Given the need for the ECM to increase its stiffness to guide the different pro-tumour effects on the matrix itself, it becomes essential to determine how these properties of the ECM can be related to tumour progression or how they can be a random factor in promoting cancer, particularly in the early stages of the carcinogenic process.

4.16 The need for preclinical models to study PM disease

One of the main problems in the development of new therapies is the transfer of scientific knowledge from the desk to the bed (J. Drost & H. Clevers, 2018), mainly because many models for the study of cancer are unable to fully recapitulate patient-derived tumours (J. Drost & H. Clevers, 2018). As a consequence, several drugs that work well in the currently used models often fail in their later stages of development on patients (A. Kamb, 2005). Although animal models have contributed significantly to increasing the knowledge on the biological basis of cancer, it is still a matter of debate whether they can fully recapitulate the pathogenetic processes of the disease (G. Caponigro & W.R. Sellers, 2011). The models commonly used for cancer studies include cell lines and patient-derived tumour xenografts (PDX). Two dimensional (2D) cancer cell lines are usually developed from material derived from patients' tumours. However, their generation is highly inefficient and involves extensive adaptation and selection that focuses on growth conditions (J. Drost & H. Clevers, 2018). In fact, cell clones that are able to expand and that can be kept in culture for various passages are rare, as 2D cell lines often have changes in their genetic landscape and are unable to maintain the heterogeneity of their tumour of origin. Other limitations of 2D lines is the absence of cellular controls derived from healthy tissue and, most of all, the lack of the stromal compartment (Table 2) (D.J. Cheon & S. Orsulic, 2011). PDXs have the advantage of

mimicking the biological characteristics of human tumours much better than 2D *in vitro* cell models. PDXs are developed through a series of subcutaneous or orthotopic transplant of fresh patient-derived material in immunodeficient mice (J. Drost & H. Clevers, 2018). The possibility of being transplanted into many mice, lacking of immune microenviroment, allows them to be used effectively in the development of new therapies (Figure 13). The main limitations of PDXs include the use of the animals themselves and the limited efficiency of the engraftment process for some tumour subsets. Furthermore, the development of PDXs is very expensive and takes a remarkably long time to complete, and PDXs may also undergo tumour-mimicking evolutions, specific to mice and not to humans (U. Ben- David *et al.*, 2017).

In recent years, innovative new culture methods based on growth in three dimensions (3D) have been developed, leading to the rise of new, and more representative, cellular models of healthy and cancerous human tissues. These 3D models are able to self-organize into complex tropic organ structures and are commonly called patient-derived organoids (PDOs) (J. Drost & H. Clevers, 2018).

	 2D cell culture	 <i>C.elegans</i>	 <i>D. melanogaster</i>	 <i>D. rerio</i>	 <i>M. musculus</i>	 PDX	 Human organoids
Ease of establishing system	✓/✗	✓	✓	✓	✓	✓	✓
Ease of maintenance	✓	✓	✓	✓	✓	✓	✓
Recapitulation of developmental biology	✗	✓	✓	✓	✓	✗	✓
Duration of experiments	✓	✓	✓	✓	✓	✓	✓
Genetic manipulation	✓	✓	✓	✓	✓	✗	✓
Genome-wide screening	✓	✓	✓	✓	✗	✗	✓
Physiological complexity	✗	✓	✓	✓	✓	✓	✓
Relative cost	✓	✓	✓	✓	✓	✓	✓
Recapitulation of human physiology	✓	✓	✓	✓	✓	✓	✓

✓ Best ✓ Good ✓ Partly suitable ✗ Not suitable

Figure 13. The main features of the principal preclinical cancer models. Relative scores are represented as being the best (dark green tick), good (light green tick), partly suitable (yellow tick) and not suitable (red cross).

“Human organoids: model systems for human biology and medicine”, by . Kim *et al.*, *Nature Reviews Molecular Cell Biology*, **21**, 571–584 (2020).

4.17 Patient-derived 3D organoids cultures

- **Introduction.** Organoids began to find more and more use in biomedical research between the 60s and 80s, when they were commonly used in developmental biology to describe the processes of organogenesis through cell dissociation and re-aggregation experiments (M.A. Lancaster & J.A Knoblich, 2014). The last decade has seen an enormous increase in interest from the scientific community towards organoids, but with a different point of view. In fact, nowadays, an organoid is defined as a 3D structure that can grow thanks to the presence of stem cells, consisting of specific cell subtypes that are able to autonomously organize in organ-like structures through a cell sorting and a spatially restricted lineage commitment (M. Eiraku & Y. Sasai, 20). Organoids can be derived from two main types of stem cells: i) embryonic pluripotent stem cells (ES) and their synthetic induced pluripotent stem cells (iPS); ii) organ-restricted adult stem cells (aSCs). Both the approaches are able to "capture" the infinite theoretical expansion potential of stem cells when they are cultured *in vitro* (H. Clevers, 2016). This potential was a fundamental prerequisite for the discovery for ES and iPS cells, commonly called pluripotent stem cells (PSCs). Conversely, aSCs were believed to be unable to proliferate outside the body. The development of cocktails of growth factors that mimic the different niches of the stem cells of different organs has allowed to expand the aSCs *in vitro* (H. Clevers, 2016). When PSCs and aSCs are induce to differentiate *in vitro*, they demonstrate a marked ability to self-organize into structures that reflect fundamental aspects of the tissue from which they are derived (H. Clevers, 2016).

- **PSC-derived organoids.** ES and iPS pluripotent cells, were initially used for developmental biology studies, to obtain different differentiated cell subtypes (K.G. Chen *et*

al., 2014) and to study the different spatial and morphogenetic patterns (M. Eiraku & Y. Sasai, 2012). Today it is possible to obtain organoids from ES and iPS that recapitulate various organs, including the brain, retina, pituitary gland, stomach, lung, thyroid, liver and intestine (Figure 14) (H. Clevers, 2016).

-Small intestine-derived Organoids from ES and iPS: The signals mediated by the Wnt and FGF factors are known to specifically define the toward mid/hindgut fate. To generate organoids derived from the intestinal tract, human PSCs cells activated by Activin are usually used, and cultured with medium supplemented with FGF4 and WNT3a. After initial steps of growth in two dimensions, spheroids are formed that recapitulate the Mid/hindgut protruding from the two-dimensional layer of epithelial cells. Spheroids are then grown in Matrigel with specific pro-intestinal factors that recapitulate the biological characteristics of the intestinal niche (T. Sato *et al.*, 2011). These organoids were expanded from 1 to 3 months to finally obtain villus- and crypt-like structures with proliferative zones and containing all the major subtypes of epithelial cells starting from a polarized epithelial pattern. Furthermore, within these structures, areas rich in myofibroblasts and smooth muscle cells surrounding the epithelial cells were observed (K.W. McCracken *et al.*, 2014).

- aSC-derived organoids. aSCs can be induced to form organoids through the development of conditions that mimic the environment of the niches in which stem cells are found during normal physiological conditions of self-renewal or during repair from exogenous or endogenous damages. The Wnt pathway, initially described for the first time within the intestinal gut, emerged as the major driver of epithelial aSC cells (H. Clevers, 2016). Furthermore, the LGR5 receptor, which acts as a receptor for R-spondin, whose secretion is induced by the Wnt pathway, is expressed in many aSCs, although not in all. For this reason, all activators of Wnt, such as Wnt3A factors, R-spondins, or small molecules such

as GSK3 or CHIR, are key components of many aSC-derived organoid culture protocols. Protocols have been currently developed to obtain, starting from aSCs, organoids from different tissues such as colon, stomach, liver, pancreas, prostate, breast, ovary and esophagus (Figure 14),(H. Clevers, 2016).

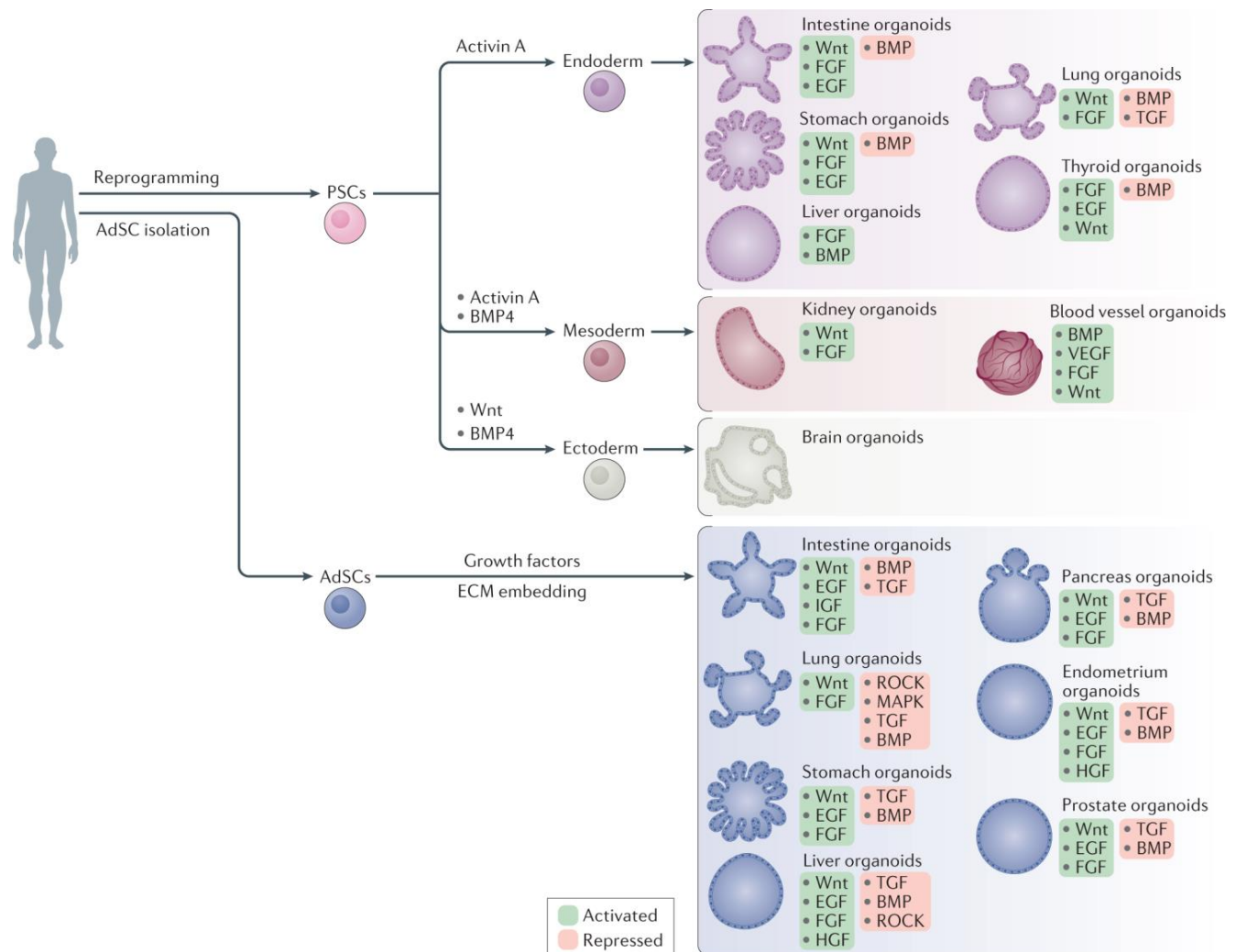


Figure 14. Schematic representation of the different organoids that can be developed starting from PSC and aSC cells and the different growth factors necessary for their obtainment. **Legend:** Signalling components that are important for guided differentiation and niche function are shown; activated signalling pathways are shown in green, and inhibited ones in red. BMP, bone morphogenetic protein; EGF, epidermal growth factor; FGF, fibroblast growth factors; HGF, hepatocyte growth factor; IGF, insulin-like growth factor; ROCK, RHO-associated protein kinase; TGF, transforming growth factor; VEGF, vascular endothelial growth factor.

Figure taken from “**Human organoids: model systems for human biology and medicine**”, by . Kim *et al.*, *Nature Reviews Molecular Cell Biology*, **21**, 571–584 (2020).

- **Small intestine organoids from aSCs.** The epithelium present in the intestinal tract, corresponding to the small intestine, has an extremely high and fast renewal properties. In fact, within 5 days, the epithelial component differentiates, develops, undergoes cell death and is replaced. All this because the region of the small intestine is continuously subjected to stress due to the process of digestion and metabolization of food (H. Clevers, 2016). The actively proliferating stem cells at the base of the intestinal villi, form the so-called stem cell crypt. The fundamental characteristic of the cells at the basis of the crypt is that they express the LGR5 receptor, which is therefore universally accepted as a specific marker of intestinal stem cells (N. Barker *et al.*, 2010). These stem cells, identified as transiently amplified (TA) cells are in a state of high proliferation and divide very rapidly until they differentiate through BMP4 signaling. They occupy the apical portions of the stem crypt and after differentiation move towards the sides of the villus going up towards the apical part, where they eventually undergo cell death and are replaced by a new pool of differentiated cells (H. Clevers, 2016). The differentiated epithelial cells positioned along the walls of the villi are many; they include enterocytes with the function of absorption of food metabolites, different types of secretory cells, such as paneth cells, goblet cells, enteroendocrine cells that secrete neurotransmitters, tuft cells and M cells, which form the so-called Peyer's plaques (H. Clevers, 2013). The differentiation and fate of crypt stem cells is regulated by four signaling pathways: the Wnt pathway, the Notch pathway, the EGF-mediated pathway and the BMP pathway. Wnt constitutes the key pathway for the maintenance of stem cells and guides the proliferation of both stem cells and TA cells. The Notch pathway helps to keep proliferating stem cells and TA cells in an undifferentiated state. In fact, when the Notch pathway is blocked, the cells differentiate into goblet cells. EGF-mediated signaling exerts a strong mitogenic effect on

both stem cells and TAs. Finally, the BMPs are usually active along the apical regions of the intestinal villi, and their inhibition is essential to generate a crypt-permissive environment (Figure 15), (H. Clevers, 2013).

Since LGR5-positive stem cells of the crypt can undergo hundreds of cell divisions *in vivo*, protocols have been developed to establish cell culture systems that allow the growth of organoids of the epithelial type starting from a single LGR5-positive stem cell (T. Sato *et al.*, 2009). The current protocols for culturing organoids from the intestine tract, are based on the mechanical and enzymatic isolation of the crypts or single LGR5-positive cells, which are then grown inside the Matrigel, which is able to provide them with the optimal structural support, helping them to organize in 3D structures. The isolated cells are then cultured using serum-free media and supplemented with three different recombinant proteins: R-spondin-1, an activator of the Wnt stem pathway, as well as the ligands for LGR5, EGF and Noggin, an inhibitor of the BMP-mediated pathway. Wnt3A protein is also usually added to obtain organoids from the non-tumour epithelium, as the epithelial cells of the colon are not able to amplify well (H. Clevers, 2016). Finally, to obtain long-term colon organoid cell cultures, Alk and p38 inhibitors are added to the culture media (H. Clevers, 2016, H. Clevers, 2013). The organoids obtained according to this procedure can be considered heterogeneous cellular entities in which it is possible to find all various subtypes of epithelial cells also present *in vivo* (ref Grun 2015, ref sato 2009). They are constituted by a highly polarized simple epithelium closely connected to a central lumen with crypt-like structures that protrudes outwards (T. Sato *et al.*, 2009; T. Sato *et al.* 2011). The basal portion of the cells usually faces the surrounding Matrigel. The enterocytes form the luminary surface, while the secretory cells are found within the lumen.

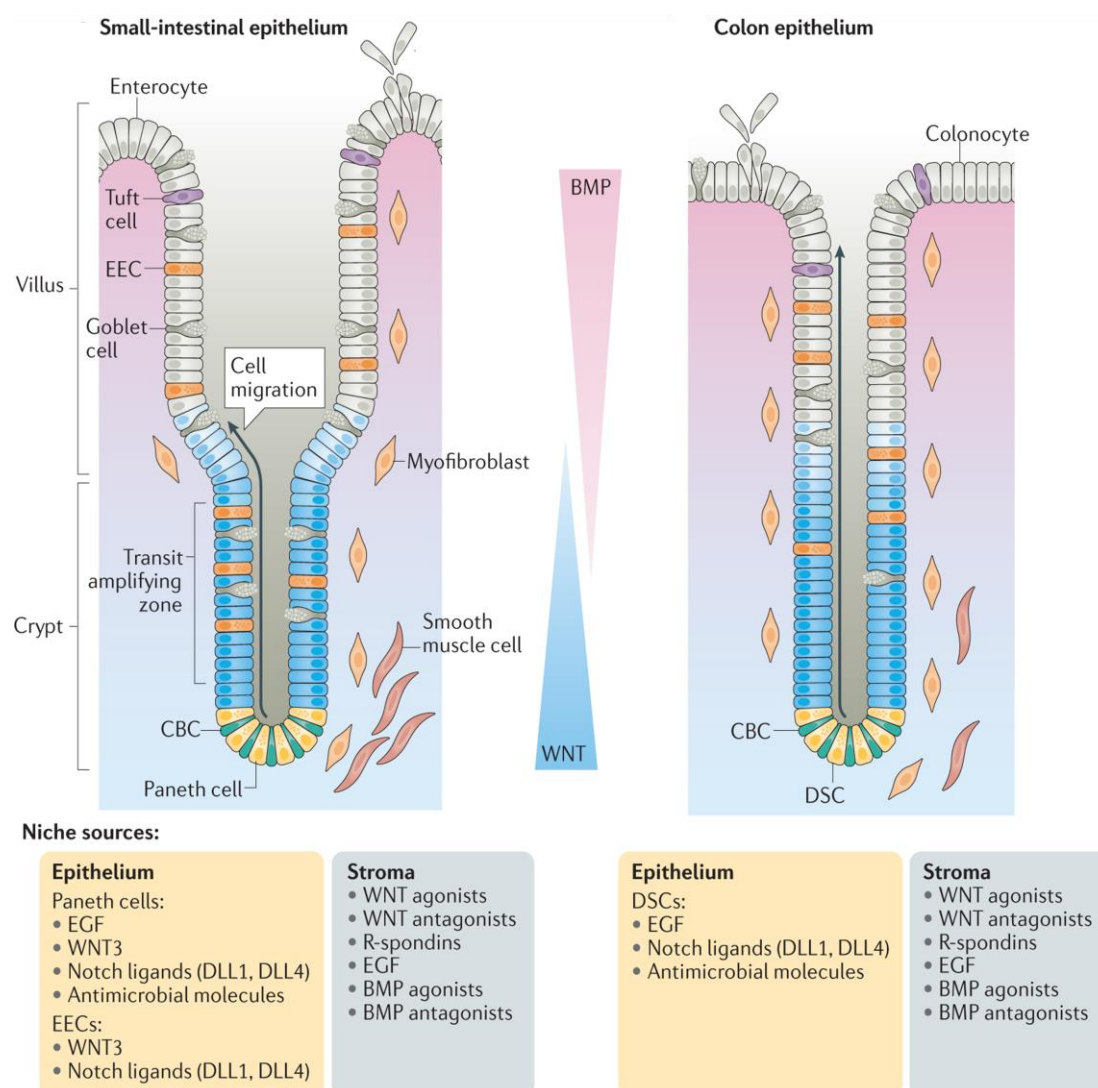


Figure 15. Organization of the intestine and colon epithelium. In the intestine, epithelial cells are organized in units called crypts, which are the sites of active proliferation, and in villi. Cells at the base of the crypt (CBCs) positive for LGR5, represent the stem cell pool. They are intercalated by Paneth cells, which provide ligands for the Wnt and Notch pathways and for EGF-mediated signaling. The daughter cells of the stem compartment migrate towards the apical part of the crypt. At this level there is a gradual shutdown of the Wnt pathway, while the signals mediated by the BMPs begin to increase. The BMPs negatively regulate the stemness and the activation/shutdown levels of the Wnt and BMPs pathways are constantly regulated by the differential expression of agonists and antagonists of these signaling pathways constantly secreted along the crypt-villus axis. At the crypt level, TA cells and secretory cells are also present. At the level of the villous region, cell proliferation is absent, and differentiated cells with absorbent and secretory activity can be found. At the end of their life cycle, the cells are released in the apical area and undergo cell death, typically through anoikis mechanisms. Both the stromal and epithelial compartments actively collaborate in providing niche factors to establish a morphogenic gradient. The stromal niche is composed of mesenchymal cells, myofibroblast and

smooth muscle cells that promote the secretions of BMPs and their respective inhibitors. The colon, unlike the small intestine, loses the ultrastructure of the villus and the colonicites are responsible for the absorption of water. Many of the cells that make up the colon are the same as those that make up the small intestine, except for Paneth cells which are absent in the colon. Morphogenic gradients similar to those observed in the small intestine are also found in the colon. Figure taken and adapted from “**Cell fate specification and differentiation in the adult mammalian intestine**” by J. Beumer and H. Clevers, *Nature Reviews Molecular Cell Biology*, **22**, 39–53 (2021)

4.18 Role of organoids in translational cancer research

- **Development of TDO-derived biobanks.** The development of protocols for the growth of organoids from different human tissues has allowed the generation of 3D models that recapitulate complex diseases, including cancer. Strategies have been developed to obtain organoids from almost all the different cancers (H. Clevers, 2016) and it has been demonstrated that tumour derived organoids (TDO) recapitulate the main phenotypic and genetic characteristics of their tumours of origin (J.Drost & H. Clevers, 2018). To obtain TDO, it is necessary to start from a pool made up of pure cancer cells, avoiding the possible contaminations of normal epithelial and stromal cells, and culture the samples using specific selective growth conditions that depend on the characteristics of the tumour from which they are derived. For example, TDO derived from tumours harbouring activating mutations of the Wnt pathway, that are very common in CRC (Cancer Genome Atlas, 2012), can be obtained using culture media without the supplementation of Wnt and R-spondin-1-related factors (T. Sato *et al.*, 2011). While tumours carrying mutations in the EGF receptor (EGFR), can be grow without EGF supplementation (M. Fujii *et al.*, 2016). Currently, the development of large libraries of TDO and their matched healthy controls has exploded, leading to the establishment of organoid biobanks (Figure 16), (J. Drost & H. Clevers, 2018). These libraries can be used as a resource to determine how TDO can predict the response to a specific drug treatment at the individual patient level. One of the first examples of the development of a

TDO biobank was the generation of a collection of 3D cultures derived from CRCs that have demonstrated their value in translational research applied to cancer (J. Drost & H. Clevers, 2018). These TDO were used to demonstrate the susceptibility of certain subgroups of CRC to inhibitors of non-canonical Wnt pathways (B. Chen *et al.*, 2009) and also to demonstrate susceptibility to different drugs, even independently of the genetic landscape of the tumours of origin (M. Maimets *et al.*, 2016).

TDO libraries are useful in defining the biological mechanisms underlying the disease, highlighting the dependence on specific pathways of particular tumour subtypes. For example, a collection of 55 CRCs demonstrated that the development of certain tumour subtypes depends on specific growth conditions (M. Fujii *et al.*, 2016). It has also been shown that TDO are able to maintain stable their mutational profile and their histopathological characteristics even after having been xenografted into immunocompromised mice (M. Fujii *et al.*, 2016). These findings underline how the biobanks of TDO can be used to develop xenograft transplantations to validate pharmacological responses *in vitro*, in a more complex *in vivo* context (J. Drost & H. Clevers, 2018). Recently, using a biobank of more than 100 TDO faithfully representing the heterogeneity of breast cancer, it was possible to develop a proof-of-principle of a drug screening using various drugs against HER-mediated signaling, demonstrating how sensitivity to drug treatment generally correlated with HER2 status (N. Sachs *et al.*, 2017). This was possible as TDO retained most of the histopathological and genetic characteristics of their tumours of origin (N. Sachs *et al.*, 2017). Several biobanks of TDO derived from rectal tumours showed how the response to standard drug treatment correlated with the responses shown by the patients from whom the TDO were obtained (J. Drost & H. Clevers, 2018). One main challenge is to significantly increase the number of TDO biobanks, to obtain greater statistical representativeness in order to be able to correlate genetic markers with sensitivity to certain drugs. A combined effort of several institutes working on TDO, known as the Human Cancer Models Initiative (HCMI), is developing a

bank of TDO from different cancer types accessible to the whole scientific community (J. Drost & H. Clevers, 2018).

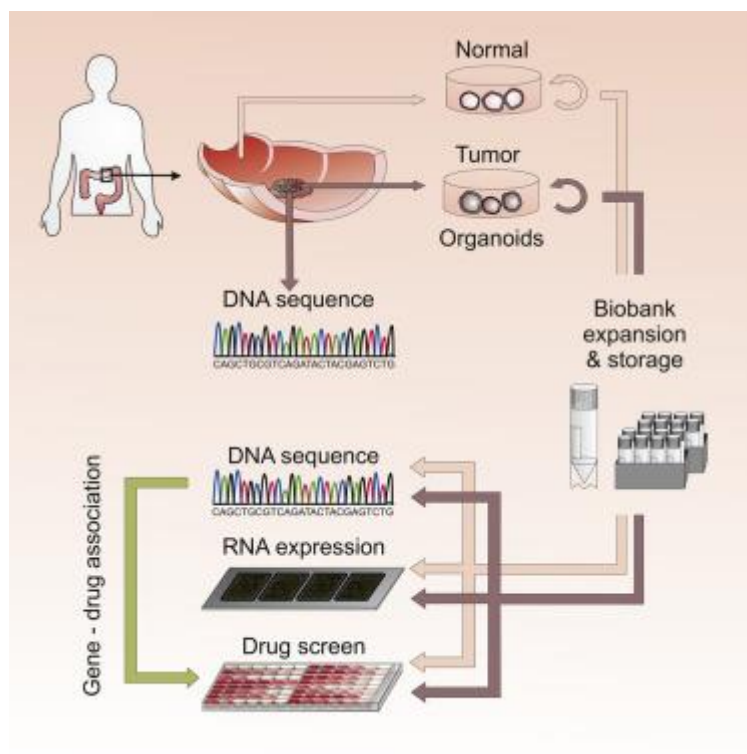


Figure 16. 3D TDO cultures derived from different biobanks that resemble the main features of different types of cancer are used for developing drug screenings in order to identify novel potential therapeutic markers that may facilitate patient's tailored therapy. Figure taken from **"Prospective derivation of a living organoid biobank of colorectal cancer patients"** by M. van de Wetering *et al.*, *Cell*, 161: 933-945, (2015).

- **Personalized therapy and drug screening using TDO.** TDO recapitulate the characteristics of their tumours of origin much better than other models and thus they could be considered a model suitable for identifying and testing new anticancer drugs (Figure 17). The implementation of high-throughput drug screening methods based on TDO is still under development, and the potential of organoids in these applications has just begun to be evaluated (J. Drost & H. Clevers, 2018). Low-scale screenings performed using TDO have given very promising results (Figure 17), (N. Sachs *et al.*, 2017, M. van de Wetering *et al.*, 2015, D. Gao *et al.*, 2014). TDO profiling could be useful to discover random epigenetic

and/or genetic changes that would modulate the response to drug treatments, and which could also be used to stratify patients to undergo a specific personalized drug treatment regimen (J. Drost & H. Clevers, 2018). For example, it has been shown in CRC how the combined treatment by MEK and ERK inhibitors leads to cell growth arrest (via block of cell cycle) in *KRAS*-mutated cancers (Figure 17), (C.S. Verissimo *et al.*, 2016), opening new scenarios on the effectiveness of the combined treatment for this type of CRCs. Also, the combined treatment based on targeting EGFR made *KRAS*-mutated tumours sensitive to treatment again, suggesting a therapeutic alternative (C.S. Verissimo *et al.*, 2016). Another study using TDO derived from patients with metastatic CRC undergoing different chemotherapies, aimed to determine whether organoids are able to predict the patient's response to drug treatment. TDO were assayed with a library of compounds already used in clinical practice or currently in clinical trials. Comparison of response to treatment of TDO and of the patient from which they were derived showed that TDO had a predictive index of 88% (G. Vlachogiannis *et al.*, 2018). Furthermore, a pharmacological screening program on TDO obtained from primary liver tumours has shown the inhibition of the ERK pathway could be a new therapeutic approach for the treatment of these types of tumours (G. Vlachogiannis *et al.*, 2018). TDO from prostate cancer patients have been used to demonstrate how *CDH1* gene deletions induce sensitivity to DNA damage mediating agents (L. Broutier *et al.*, 2017; T.R. Shenoy *et al.*, 2017). The possibility to obtain TDO from both the tumour and the healthy tissue of the same patient allows to determine whether the drugs selectively target cancer cells only, leading to the development of drugs with significantly lower cytotoxic than those currently used (Figure 17) (J. Drost & H. Clevers, 2018). In fact, drug-induced failure caused by hepatotoxicity is one of the major causes of drug failure during clinical trials (F. Ballet, 1997). For this reason, biobanks of liver organoids could be used for preclinical testing of new pharmaceutical compounds, to measure their hepatotoxicity (T. Katsuda *et al.*, 2016). Similarly, biobanks of iPSC-derived cardiac organoids could be employed to test

cardiotoxicity induced by chemotherapeutic agents (M. Takasato *et al.*, 2015). Based on all these promising data, the idea of using TDO in common hospital diagnostic pipelines (J. Drost & H. Clevers, 2018) is increasingly being considered.

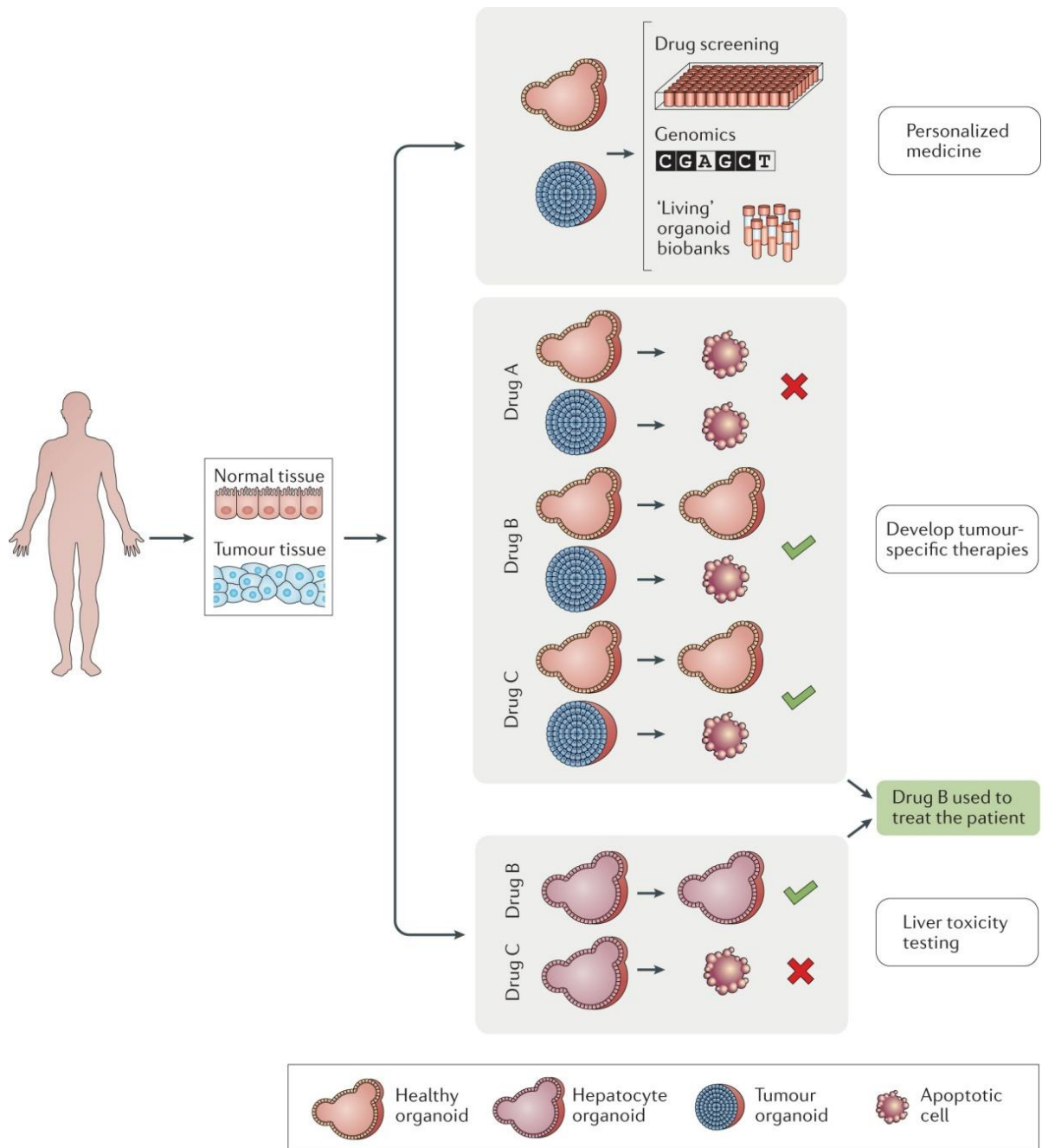


Figure 17. How organoids can be used for personalized cancer treatment and drug development. Organoids are developed from patient-derived tissue, both healthy and cancerous. Once the organoids have been established, they can be characterised from a genetic point of view and used to develop drug screening, in order to correlate the genetic landscape of the tumour with the pharmacological response. The development of healthy organoids allows to select less toxic drugs by screening for compounds that can selectively kill cancer cells only. In addition, organoids derived from healthy liver tissue can be used to test the hepatotoxicity of new drugs. Figure taken from “**Organoids in cancer research**” by J. Drost and H. Clevers, *Nature Reviews Cancer*, 18: 407-418, (2018).

4.19 Organoids and their role in basic cancer research

- **TDO for modeling tumorigenesis.** It has been widely demonstrated that cancer is caused by accumulation over time of a series of mutations affecting specific genes that act as driver of the disease (M.R. Stratton *et al.*, 2009). The high genetic stability of TDO derived from healthy tissue allows the study of mutagenic processes (Figure 18) (S. Behjati *et al.*, 2014). For example, the use of clonal organoids derived from the intestine, liver and colon has shown how the high turnover of crypt stem cells can be involved in the onset of mutagenic events induced by deamination processes, leading to the acquisition of a specific mutational signature (F. Blokzijl *et al.*, 2016). Indeed, these types of mutations are often found in the genes drivers for CRC, while the driver mutations of the same genes originate through different mechanisms in liver cancer (F. Blokzijl *et al.*, 2016). This evidence suggests that organ-specific mutational mechanisms are the product of the accumulation of certain somatic mutations during the neoplastic process (S. Behjati *et al.*, 2014). The importance of understanding how specific mutational signatures originate in cancer was recently demonstrated using organoids derived from the mammary gland where it has been shown that deficiency in the *BRCA1* and *BRCA2* genes can be predicted by the mutational signature of tumour. This result led to path the way for selecting subgroup of patients who could benefit from the treatment based on the use of poly (ADP-ribose) polymerase (PARP) inhibitors (H. Davies *et al.*, 2017).

Several mutational processes are active in neoplastic cells, making difficult to study the origins of the specific mutational signatures of different cancer types. The genetic stability of healthy organoids provides the ideal platform for attributing a specific mutational process with a specific mutational signature (J. Drost & H. Clevers, 2018). Studies on healthy organoids obtained from colon tissue have shown the prominent role of 30 specific mutations in the development of hereditary family-type cancers. These mutations affected the genes involved in the mechanisms of excision repair, like DNA glycosylase 1 (NTHL1) (J. Drost *et*

al., 2017). A similar approach could be used to study the effects of chemotherapy and radiotherapy on mutation rates using TDO. It should be noted that most tumours develop an unstable genome and consequently lead to the development of intratumoural heterogeneity (J. Drost & H. Clevers, 2018). Intratumoural heterogeneity seems to play a fundamental role in cancer progression, and in the development of treatment resistance; however tumour heterogeneity still remains poorly understood (C. Greenman *et al.*, 2007). Organoids maintain tumour heterogeneity, even after several passages (N. McGranahan *et al.*, 2017; C. Pauli *et al.*, 2017). For example, CRC-derived TDO obtained from different regions of the same tumour have been used to determine the sensitivity to drugs of the different subclones (J. Drost & H. Clevers, 2018).

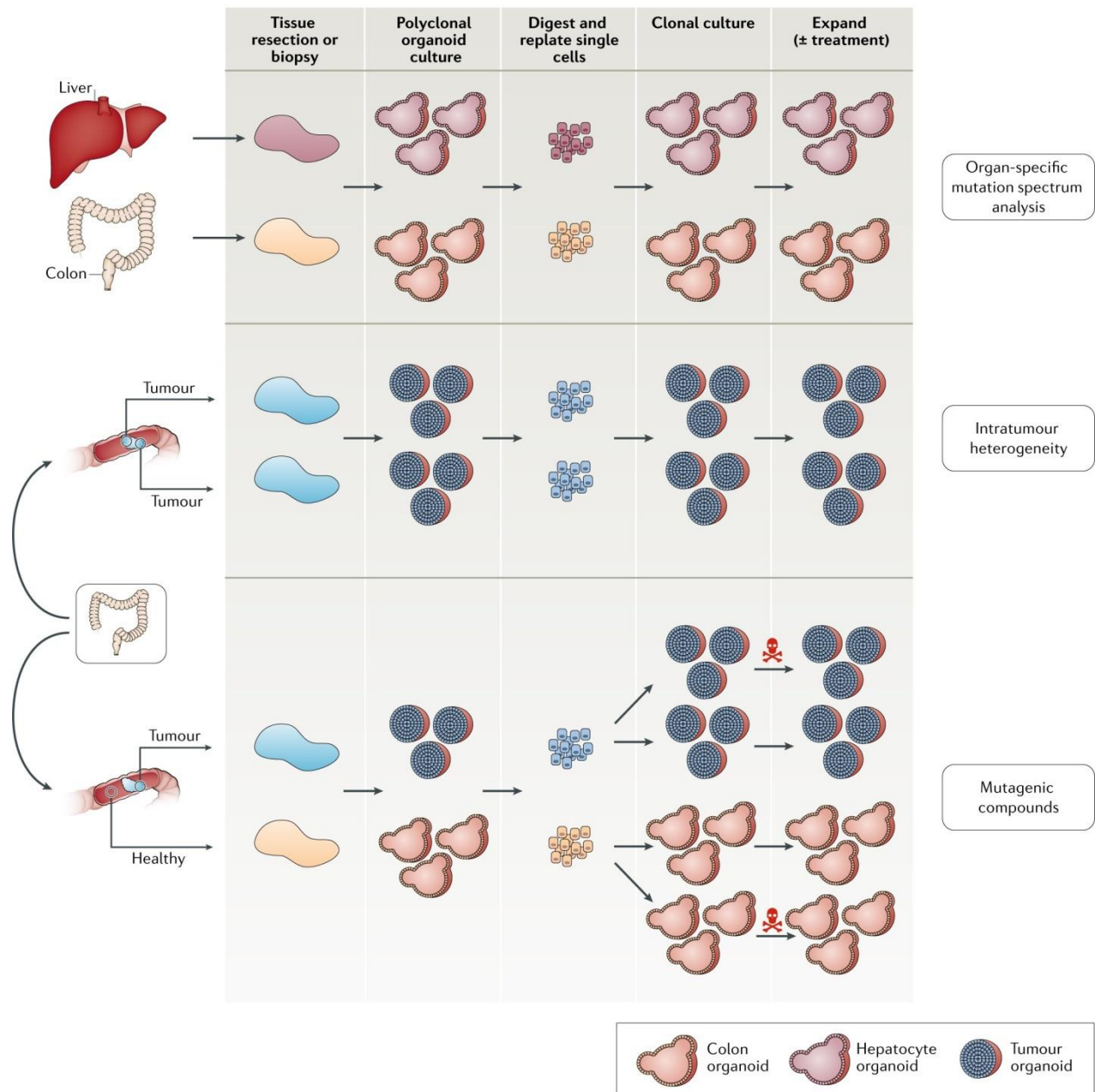


Figure 18. Clonal organoids from different healthy tissues followed by whole genomic sequencing lead to the study of the specific mutational spectrum of these tissues when they are affected by cancer. Organoids can also be used to study intratumour heterogeneity through the culture of clonal organoids obtained from different regions of the same tumour. Finally, organoids can be used to study the effects of a given compound on the mutational profile of both healthy and neoplastic cells. Figure taken from “**Organoids in cancer research**” by J. Drost and H. Clevers, *Nature Reviews Cancer*, 18: 407-418, (2018).

- **TDO for genetic cancer modeling.** Another field of application for TDO in cancer research is the study of the processes that define the initial stages of the disease and its progression. With the advent of the CRISPR-Cas9 genomic editing technology, which permits to introduce specific mutations in well-defined sites of the genome, TDO have been used to develop models of neoplastic progression of cancer (Figure 19), (M. Matano *et al.*, 2015). With this models, it was possible to demonstrate how neoplastic progression in CRC leads to tumour growth independent from factors that regulate the intestinal stem cell niche. Indeed, the TDO used in this study, which expressed activating mutations in the *KRAS* genes, and inactivating mutations in the *APC*, *TP53* and *SMAD4* genes, were able to grow independently of the growth factors Wnt, EGF, R-Spondin-1 and noggin (M. Matano *et al.*, 2015). Furthermore, using CRISPR-Cas9 technology, it has been shown that loss of function of the *APC* and the *TP53* genes led to the development of an aneuploid phenotype, characterised by strong chromosomal instability, which represent one of the main hallmarks of cancer (X. Li *et al.*, 2014). Orthotopical transplants of genetically modified organoids has demonstrated that the major contributions in the colonization of metastatic sites by neoplastic cells is the loss of dependence from the signal transduction pathways present at the level of the stem cell niche (A. Fumagalli *et al.*, 2017). The importance of transplanting tissues within an orthotopical environment was found to be fundamental for understanding the importance of mutations in CRC driver genes (*Apc*, *Kras*, *Trp53* and *Smad4*) are involved in the development of the metastatic process (A. Fumagalli *et al.*, 2017). Organoid technology can also be used to study cancer-related processes governed by precise signal transduction pathways. For example, in gastric cancer, the use of TDO has shown that the recurrent expression of hotspot mutations in the *RHOA* protein led to resistance to cell death mechanisms mediated by anoikis (K. Wang *et al.*, 2014). Furthermore, using a cellular model based on TDO engineered by CRISPR-Cas9 technology, it was possible to demonstrate that TGF β -mediated signalling, involved the development of serrated colon adenocarcinomas (E. Fessler *et al.*, 2016), can led

to the activation of signaling mediated by Wnt and β -catenin (H. Yan *et al.*, 2016). Furthermore, patients affected by serrated colon neoplasia carrying RNF43 mutations are sensitive to treatment with porcupine O-acyltransferase inhibitors, which inhibits the secretion of Wnt (B. Koo *et al.*, 2016). Finally, recent revolution in the genome editing given by the development of the CRISP-Cas9 technology could provide a useful platform for studying mutations affecting the main genes involved in CRC development. TDO engineered by CRISP-Cas9 have been used to test the repair of some mutations, affecting oncogenes, reversing the pro-tumour phenotype (J. Drost & H. Clevers, 2018).

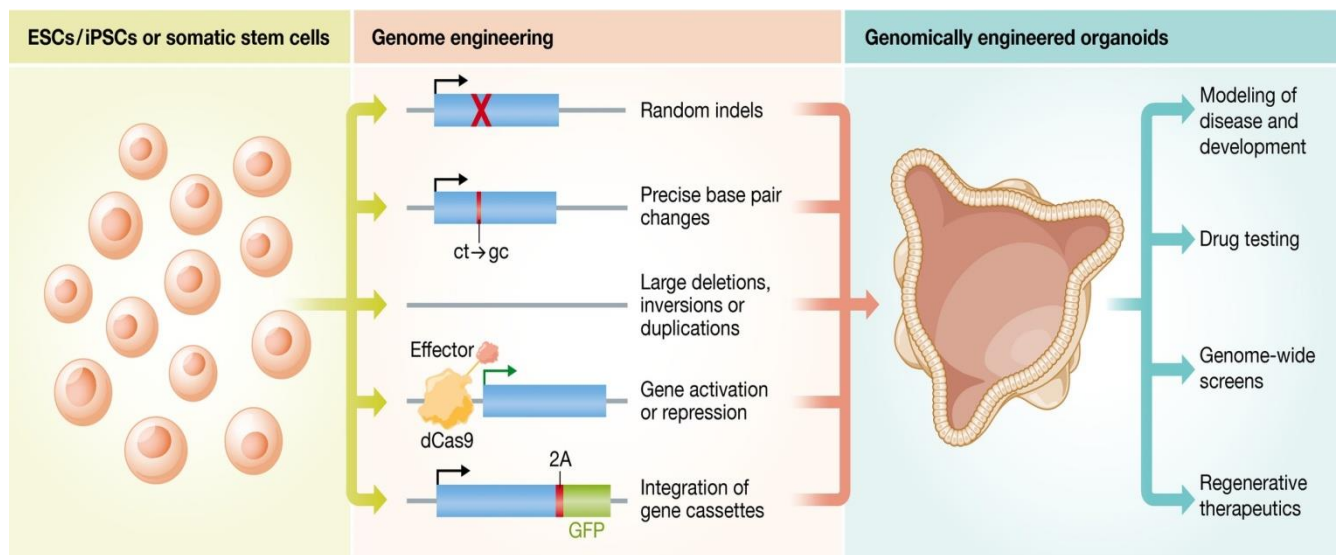


Figure 19. The figure shows the workflow to obtain modified organoids through genome editing. The development of engineered 3D models allows to carry out different types of studies, in particular based on understanding the genetic mechanisms that lead to the development of the disease. Figure taken from “**Organoid technologies meet genome engineering**” by J. Nie and E. Hashino, *EMBO Reports*, 18: 367-376, (2017).

4.20 Conclusions

Organoids have demonstrated their potential in cancer research. In fact, they represent a physiological model of the tumour from which they are derived, and can be developed with high efficiency starting from patient’s tissue samples. These peculiarities make TDO useful

for translational applications and for the development of personalized pharmacological therapies (J. Drost & H. Clevers, 2018t).

Although TDO have generated very promising data, they still have some limitations. The most relevant is that they lack the stroma, blood vessels and cells of the immune system. New studies are needed to develop co-culture systems to obtain organoids that also include the various cellular subpopulations of the microenvironment (X. Yin *et al.*, 2016). Furthermore, growth of TDO requires the presence of mouse-derived ECM, such as Matrigel, and, in some cases, of fetal calf serum (FCS), required for the production of WNT-conditioned medium. These two elements incorporate a series of intrinsic factors that could affect the experiment results. The development of synthetic ECMs able to support the growth of organoids derived from human tissues could represent a valid alternative to a mouse-derived ECM (N. Gjorevski *et al.*, 2016). Nonetheless, synthetic ECMs still need to be optimized and standardized. Finally, TDO obtained from advanced stage cancer often grow very slowly compared to TDO obtained from normal epithelium or early stage cancer, probably because advanced stage tumours have a high rate of mitotic failure which leads to cell death (J. Drost & H. Clevers, 2018). New culture systems supported by specific protocols must be developed, to obtain models integrating TDO with the different components of the tumour microenvironment, to obtain an *ex vivo* model more representative of the disease. These statements are true, for example, for PM disease, which is a complex disease where interactions between TDO and its surrounding environment are observed, ranging from cell-cell, cell-matrix interactions, ECM-remodeling and development of angiogenesis.

4.21 Decellularised ECM for bioengineering cancer

The hallmarks of cancer and the onsets of resistance to chemotherapy are due to changes in the structural components of the ECM and of the microenvironment (L.P. Ferreira *et al.* 2020). During tumour development, the accumulation of mutations affecting neoplastic

cells and the simultaneous deregulation of stromal cells lead to both biomechanical and functional changes in the tumour ECM (R. Kalluri. 2016). Alterations of the ECM in solid tumours have been found associated with increase in disease progression and poor prognosis. They are mainly characterised by a marked increase in invasiveness of cancer cells in colonizing the surrounding tissues and, also, resistance to standard therapies (H. Hamidi & J. Ivaska, 2018; T. Brabletz *et al.* 2018). The development of ECMs that mimic those found in solid tumours still remains an open question, given the complexity and dynamics that drive the main mechanical and biological characteristics of the tumour microenvironment (L.P. Ferreira *et al.* 2020). There is an increasing research interest on the development of protocols to obtain specific decellularised ECMs (dECMs), given the fact that the dECMs are able to "mimic" the tissues of origin very well. Recent advances in their production, extraction and processing have allowed to derive cell-derived and tissue-derived dECMs to be used as new scaffolds for bioengineering 3D tumour-ECM mimicking *in vitro* models (Figure 20), (F. Sensi *et al.* 2018).

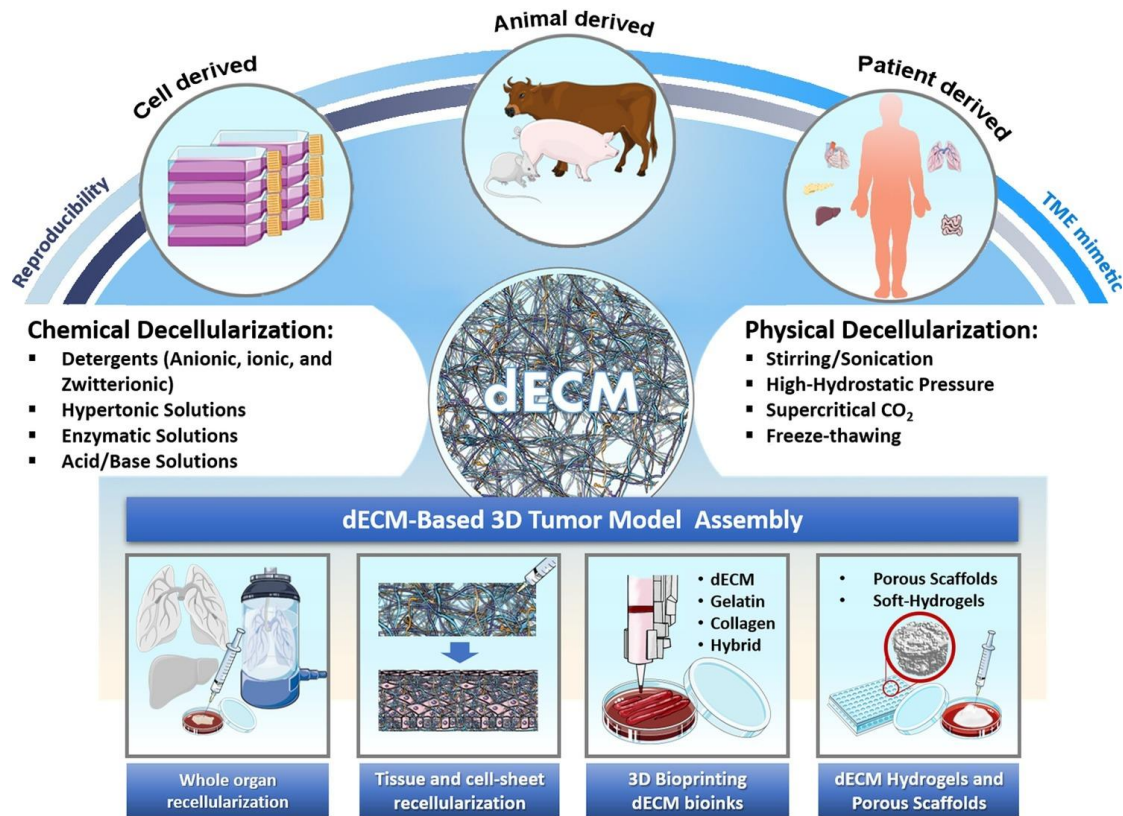


Figure 20. Overview of the main sources from which the dECMs are obtained and of the main methodologies used to obtain them, including the various modelling strategies to develop 3D disease models capable of summarizing the main characteristics of a tumour. Figure taken from “**Decellularised Extracellular Matrix for Bioengineering Physiomimetic 3D *in Vitro* Tumour Models**” by L.P. Ferreira *et al.*, *Trends in Biotechnology*, 38 (12), pp. 1397-1414, (2020).

4.22 Decellularisation methodologies

The composition and the architecture of the ECM vary according to the type of tumour and the progress of the disease itself (E. Mavrogonatou *et al.* 2019). Furthermore, tumour ECMs provide structural support to neoplastic cells and are also reservoirs of both pro- and anti-tumour factors, regulating cell differentiation, immune cell activity and tumour cell migration (A.D. Theocharis & N.K. Karamanos, 2019). For these reasons, ECM decellularisation procedures must be specifically developed in order to preserve both the microarchitecture and the biological functions of the ECM. In fact, if carefully developed, some dECM-based tumour models can preserve the properties of the native ECM, thus

allowing the study of the mechanical modifications of the ECM in controlled culture conditions, or to study key cell-ECM interactions that are established between the different components of the tumour microenvironment (M.L. Pinto *et al.* 2017).

Different decellularisation techniques have been used to obtain cell-free dECM biomaterials (D.A. Taylor *et al.* 2018). Regarding tumour ECMs, many of the decellularised matrices were obtained through chemical treatments with surfactants such as sodium dodecyl sulfate (SDS), sodium deoxycholate (SDC) and Triton-X100. These denaturing compounds are usually coupled with the use of enzymes and/or acidic/basic decellularising agents (L.P. Ferreira *e al.* 2020). The decellularisation process, in order to be considered effective, must specifically degrade the cellular material while preserving, instead, the microarchitecture of the ECM, its biochemical composition and its intrinsic bioactivity (A. Gilpin & Y. Yang, 2017). The decellularisation methods can be classified into three main categories: i) physical decellularisation, ii) enzymatic decellularisation and iii) chemical decellularisation. dECM derived from cells and tissues can be easily obtained within a few minutes up to 72 hours, depending on the thickness of the starting material and the methodology used (F.R. Maia *et al.* 2020). At the end of the process, dECMs are commonly sterilized using peracetic acid, ethanol, antibiotics and / or UV or gamma radiation prior to their use as scaffolds for cell culture (T. Hoshiba, 2018). The obtained dECMs are also tested for biochemical assays such as the evaluation of the total collagen and absence of DNA and RNA, to verify the success of the decellularisation process (I. Koh *et al.* 2018).

- Physical decellularisation. Decellularisation procedures based on physical methods include magnetic stirring, sonication, high hydrostatic pressure or freeze-thawing procedures aimed at destroying cell membranes (A. Gilpin & Y. Yang, 2017; D. Sun *et al.* 2018). Physical methodologies are rarely used alone, and very commonly they are combined with frequent washing steps and subsequently, chemical solutions are used (A. Gilpin & Y. Yang,

2017). The use of pressure gradients has proved so far the most promising method for physical decellularisation. Hydrostatic pressure can be applied to decellularisation procedures in combination with chemical agents to increase cell lysis, as well as promote the removal of cellular debris (N. Watanabe *et al.* 2019). At the same time, methods based on very critical CO₂-based decellularisation have been shown both to produce effective decellularisation and to preserve the native composition of the ECM (Figure 21), (D.M. Casali *et al.* 2018).

- **Chemical decellularisation.** Chemical treatment of the ECM is usually carried out with acid/base and hypertonic solutions and with detergents with the aim of destroying cell membranes and degrading cellular debris. The addition of acids, such as acetic acid and peracetic acid, and/or bases such as ammonium hydroxide, can increase the efficiency of decellularisation. Nevertheless, the strong pH that characterises these solutions used for the process can lead to the degradation of key biomolecules (H. Hasmad *et al.* 2018). On the other hand, bases are commonly used only during the initial steps of the process, especially in very dense samples, because they possess a marked aggressiveness in removing cellular and genetic material (M.T. Scherzer *et al.* 2015). However, both acidic and basic solutions, can lead to the degradation of components of the ECM, altering the structural stability of the matrix itself (H. Hasmad *et al.* 2018). For these reasons, the use of softer detergent-based decellularisation protocols is recommended (Figure 21), (L.P. Ferreira *et al.* 2020).

- **Detergent-based decellularisation.** Decellularisation methods based on the use of detergents are divided into ionic, non-ionic (based on polyoxyethylene or a glycoside) or zwitterionic (They carry a positively and a negatively charged group, but like nonionic surfactants, do not have a net charge). These detergents are able to solubilise cell membranes and degrade DNA through its dissociation from histonic proteins. Non-ionic detergents, such as Triton-X100 are considered soft detergents, capable of maintaining the native structure of

proteins and their enzymatic activity. Ionic detergents, such as SDS and Triton-X200, show a high decellularisation capacity, but are considered much more aggressive (R. Simsa *et al.* 2018). For these reasons, methods that combine different detergents can synergistically increase the biomechanical modifications of the ECM. In addition, in tissues characterized by a strong lipid component, the decellularisation methods based on the use of detergents are coupled with the use of methanol, ethanol or chloroform to promote the total lipids depletion (Figure 21), (H. Fairfield *et al.* 2018).

- Enzymatic_based decellularisation. Enzymatic-based decellularisation methods are based on the use of specific enzymes, such as trypsin, peptidases or nucleases, which can remove cells from the tissues of origin. This methodology is generally coupled with both physical and chemical decellularisation methods, to ensure the complete depletion of the genetic material (D.A. Taylor *et al.* 2018). This combination allows a correct conservation of the architecture and protein composition of complex tissues that are decellularised (Figure 21), (C.S. Scanlon *et al.* 2013).

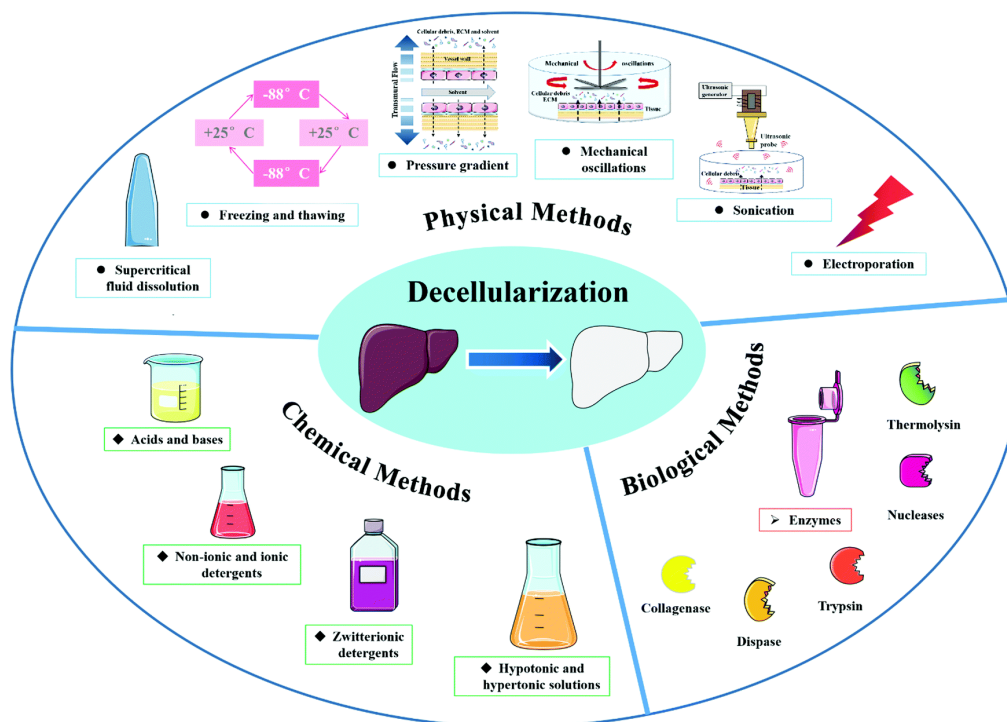


Figure 21. The main methods used for tissue decellularisation. The decellularisation process involves the total removal of the cellular component from the tissue, preserving the micro-architecture and biochemical properties of the native ECM. The main decellularisation methods can be divided into: i) physical type, ii) chemical type and iii) enzymatic type. The combination of different methods is frequently observed to increase decellularisation efficiency. Figure taken from “**Applications of decellularised materials in tissue engineering: advantages, drawbacks and current improvements, and future perspectives**” by J. Liao *et al.*, *Journal of Material Chemistry B*, Issue 44, (2020).

4.23 dECMs for *in vitro* tumour modelling

Models based on decellularised matrices have several important features, including a complex and advanced architecture, are easy to handle and to analyse and possess extremely relevant biological properties. In fact, there is a steady increase in works in which dECMs are used to reconstruct 3D tumour models *in vitro* (G. Rijal & W. Li, 2017; I. Koh *et al.* 2018; D. Sun *et al.* 2018; X. Tian *et al.* 2018), demonstrating the ability of dECMs to recapitulate the fundamental communications that underlie the interactions between tumour cells and the ECM. These interactions are the basis of key mechanisms for cancer development, such as tumour evolution, progression and metastatic potential (Figure 22), (L.P. Ferreira *et al.* 2020)

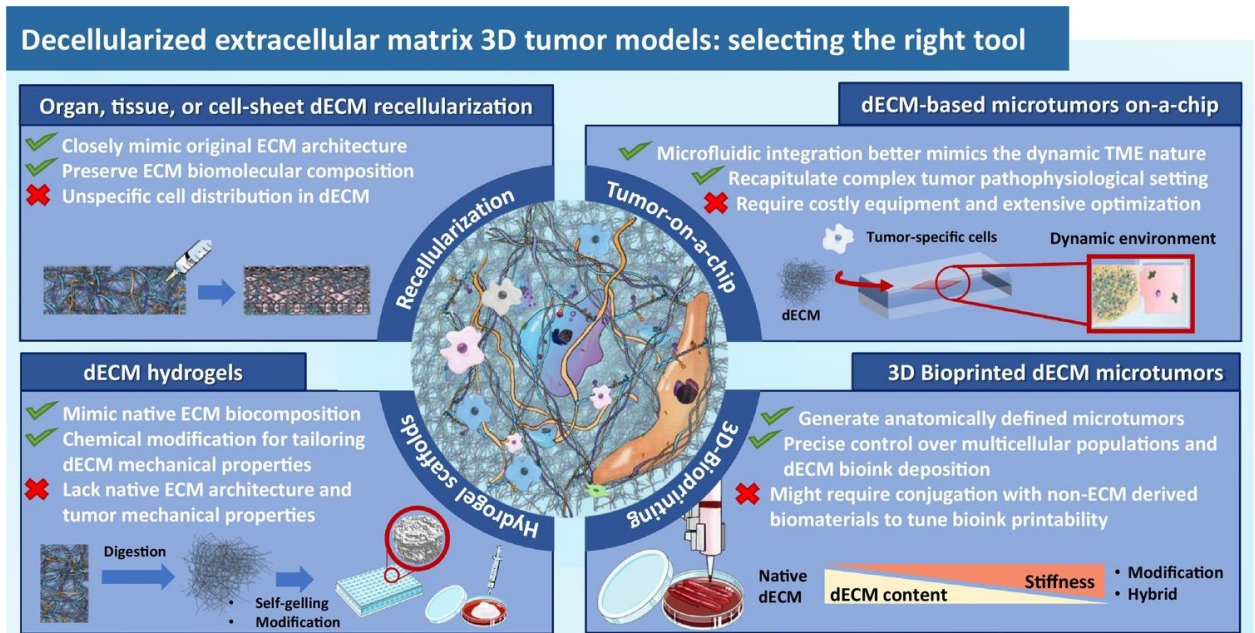


Figure 22. Principal strategies used to develop dECM-based 3D tumour models *in vitro*. The main advantages and limitations of all strategies are also indicated. Figure taken from “**Decellularised Extracellular Matrix for Bioengineering Physiomimetic 3D *in Vitro* Tumour Models**” by L.P. Ferreira *et al.*, *Trends in Biotechnology*, 38 (12), pp. 1397-1414, (2020).

- *In vitro* tumour models based on Repopulated dECMs. Given the complexity and space-time nature of tumour progression, *in vitro* tumour models able to mimic specific stages that characterise the malignant progression should be developed (C.S. Scanlon *et al.* 2013). These models should also represent the different alterations of composition and biomolecules (such as growth factors, ECM’s proteins, cytokine/chemokine), to which the ECM and the microenvironment in general are subject. Such *in vitro* models may recapitulate the complex networks and pathways involved in the processes of growth, invasion and metastasis (T. Brabletz *et al.* 2018). Tumour models based on the repopulation with tumour cells of dECM obtained from tissues exhibit a highly conserved fibrous microarchitecture, very similar to that observed in the tissues from which they were derived (S.J. Keeton *et al.* 2018). Therefore they can be used to study the mechanisms that lead tumour cells to invade the basement membrane in a highly fibrotic context given by the use of dECM (C.S. Scanlon *et al.* 2013),

allowing to correlate the composition of the ECM and its fibrillar arrangement with cell invasion. It is in fact widely recognized that the cancerous phenotype is influenced by the loss of specific biomolecules, present in the ECM, which support the neoplastic cells, even independently of the same fibrillar structure that presents the ECM (L. Genovese *et al.* 2014). For this reason, it is important to preserve these specific biomolecules within the dECM. However, models based on the repopulation of dECMs are still far from fully representing the complexity of the cellular organization of the microenvironment, as the repopulation process occurs randomly (L.P. Ferreira *et al.* 2020).

- *In vitro* tumour models using dECM-based hydrogels. Models constructed using hydrogel-based dECMs allow to precisely modify the mechanical properties and composition of the dECM. These “artificial” dECMs are generally used to study processes of invasion and metastatisation and to perform preclinical drug screening (G. Rijal & W. Li, 2017). Hydrogels are defined as highly hydrated polymer materials (>30% water by weight) that maintain structural integrity by physical and chemical crosslinks between polymer chains. The polymer chains can be synthetic (e.g., polyethylene oxide (PEO), poly(vinyl alcohol) (PVA), poly(acrylic acid) (PAA), poly(propylenefumarate-co-ethylene glycol) P(PF-co-EG)) or natural (e.g., alginate, chitosan, collagen, hyaluronic acid). Many hydrogels have been derived from components of the extracellular matrix (ECM) such as collagen, hyaluronic acid and elastin or complex mixtures of ECM proteins such as Matrigel (L.P. Ferreira *et al.* 2020)

The structural properties and composition of these dECMs promote survival, proliferation, migration and invasion much better than the classic assays used with 2D cultures. Furthermore, this type of dECM seems to show an advantage in terms of a better ability to reproduce the main histopathological characteristics of tumours and better predictive ability in the therapeutic response (G. Rijal & W. Li, 201). The development of hydrogels with

modifiable stiffness properties, allows a better reproduction of cell-ECM interactions (H.Y. Liu *et al.* 2018), representing a better model to study the mechanisms of invasion and metastatisation promoted by the mechanical modifications of the ECM (L.C. Bahlmann *et al.* 2020).

- ***In vitro* tumour models based on Patient-personalized dECMs.** The screening of pharmacological strategies that are more effective in the treatment of a tumour should be performed on patient-specific models, which can reproduce the dynamic landscape of the specific microenvironment and ECM of the tumour. *In vitro* models based on dECM mimic the specificity of tumour tissue and the heterogeneity of the tumour, thus serving as a platform for the development of personalized therapies (M. Arnedos *et al.* 2015). To do this, the patient's derived ECM samples must be grouped according to the patient's characteristics (i.e. stage, grade) and should be obtained using standardized protocols, to avoid the introduction of variations in their structural composition (G. Landberg *et al.* 2020). Models able to promote the growth of tumour cells and recapitulate the main morphological and genetic characteristics of the patient from which they were derived, have been developed (I. Koh *et al.* 2018). Finally single-cell RNA-seq analyses, have allowed a greater understanding of the intra and inter tumoural heterogeneity, leading to the discovery of new pathways of cell-cell and cell-ECM interactions fundamental for tumour progression. (A.M. Newman *et al.* 2019). For these reasons, exploiting this kind of information for the development of *in vitro* 3D models is fundamental to increase their degree of resolution and representation of the pathology (L.P. Ferreira *et al.* 2020).

- ***In vitro* tumour models based on Tumour-on-a-chip dECMs.** The tumour-on-a-chip models, are microfluidic devices that aim to recreate relevant features of the tumour physiology by combining the use of microfluidics, tissue engineering, and

microfabrication tools. They act as *in situ* platforms characterised by an adaptable environment and are particularly useful for the study of time-dependent and cell-cell-dependent dynamic interactions (C.P. Miller *et al.* 2020). The combination of dECM and tumour-on-a-chip models permits to obtain mimetic platforms of the microenvironment and tumour ECMs, where high-throughput screening of multiple therapeutic combinations and biomechanical and dynamic variations can be performed (L.P. Ferreira *et al.* 2020). These models could serve as patient-specific platforms to guide clinical decisions during patient follow-up (S.N. Ooft *et al.* 2019). For example, the integration of an automatable 3D-printed patient-derived dECM model coupled with a microfluidics system can lead patient-specific predictive models, capable of being used as *in vitro* therapeutic screening platforms for assessing patient-specific tumour response (H.G. Yi *et al.* 2019).

4.24 Conclusions

Decellularised tumour models are unique for studying specific interactions between tumour cells and the ECM. The conjugation of dECM scaffolds with cancer cells and other cell subpopulations associated with the microenvironment is fundamental for gaining a better understanding of cell-cell and cell-ECM interactions and, consequently, a better *in vitro* model of tumours (L.P. Ferreira *et al.* 2020). It is very important to standardize the decellularisation protocols, because a single variation of the composition of the ECM results in a strong alteration of the cellular phenotype. For this purpose, studies based on single-cell analysis and mass spectrometry can make a strong contribution to obtain highly precise snapshots of the development of models based on dECM (A.M. Newman *et al.* 2019). These models have already demonstrated their potential as testing platforms for screening drug libraries and their ability to recapitulate the stage and interactions of the specific patient microenvironment. Nevertheless, it has begun to become extremely clear how dECM-based models represent a great promise in the use of biomaterials such as scaffolds that will help

evolve *in vitro* tumour modelling towards personalized therapeutic approaches (L.P. Ferreira *et al.* 2020).

5. Hypothesis alongside the project and specific aims

I hypothesise that a 3D model integrating the main features of the tumour ECM coupled with PM-derived organoids could help in characterising the biological events that lead to the development of the metastatic niche in peritoneal metastatic disease (PM).

My PhD project was divided into three specific aims:

- **Aim_1:** To develop a panel of organoids representative of the spectrum of PM.
- **Aim _2:** To generate and characterise 3D-decellularised extracellular matrices (3D-dECMs) to mimic the peritoneal ECM niche.
- **Aim_3:** To combine the 3D-dECMs and organoids to develop and characterise an *ex vivo* PM lesion for studying PM disease.

6. Materials and Methods

6.1 Human tissues

Peritoneal tissue was collected from patients with peritoneal metastatic colorectal carcinoma who underwent surgical resection at the Peritoneal Malignancies Unit of our Institution. The patients were staged according to the WHO classification (I. Ubink *et al.* 2016). The study was approved by the Institutional review board (INT134/13; INTI249/19) and was conducted in accordance with the Declaration of Helsinki, 2009. Written informed consent was acquired. The main characteristics of the patients from which the PM organoids were derived are listed in Table 2.

Metastatic lesions and apparently normal tissue (> 10 cm from the metastatic lesions) were harvested. One part of the metastatic tissue (1 cm in diameter) was placed in ice-cold PBS (ThermoFisher Scientific, Waltham, MA) containing gentamicin (50 ng/ml, ThermoFisher Scientific) and amphotericin B (50 ng/ml, ThermoFisher Scientific) for the development of PM-derived organoids, while a second specimen was frozen in liquid nitrogen for molecular and histopathological analyses. The remaining tissue was frozen and used to develop 3D-decellularised matrices (3D-dECMs). Normal tissue was partly used to develop 3D-decellularised matrices and partly frozen for further studies. Formalin-fixed, paraffin-embedded (FFPE) blocks were prepared for immunohistochemical (IHC) analyses of normal and metastatic tissue.

ID	Diagnosis	Grade	Stage	Mutations	Microsatellite
S07-7576	Moderately differentiated infiltrating adenocarcinoma	G2	pT3N2M1	G12S KRAS; TP53	MSS
S11-2361	Poorly differentiated mucinous multiple intestinal adenocarcinoma	G3	pT4N2b M1	V600E BRAF; TP53	MSS
S16-8598	Intestinal mucinous adenocarcinoma	G3	pT4N2M1	G12S KRAS; TP53; FGFR1 amplification	MSS
S17-3963	Moderately differentiated adenocarcinoma	G3	T4aN2aM1b	G12S KRAS	MSS
S17-3610	Intestinal adenocarcinoma with mucinous component	G2	pT4aN0M1	G12S KRAS	MSS
S18-8607	Colloidal / gelatinous mucinous adenocarcinoma associated with hairy adenocarcinoma of high and low grade	G3	T4aN2bM1	G12S KRAS; TP53	MSS

Table 2: The main pathological characteristics of the patients from whom the tumour specimens were obtained. Mutational profiles were obtained by next generation sequencing (NGS) analyses, performed by Pathology Department of the Fondazione IRCCS, Istituto Nazionale dei Tumori, Milan. Microsatellite stability/instability was obtained by routinely analyses performed by the Pathology Department of the Fondazione IRCCS, Istituto Nazionale dei Tumori, Milan. Tumours grade and stage were determined by an expert pathology following the WHO classification for metastatic CRC.

6.2 Development of PM-derived organoids

Fresh PM tissue was processed following the protocol described by Fuji *et al.* (M. Fuji *et al* 2016; *Figure 23*). The tissue was cut into small pieces, washed with ice-cold PBS at least ten times, and then digested with 500 U/ml collagenase type II (Sigma Aldrich, St.Louis, Missouri, USA) in DMEM-F12 medium (ThermoFisher Scientific) for 1 hour at 37 °C with vigorous pipetting every 15 minutes. The remaining fragments were digested with 1 mg/ml trypsin, 5 mM EDTA (ThermoFisher Scientific) at 37 °C for 20 minutes. The supernatant was collected and centrifuged at 300 g for 5 minutes at 4 °C.

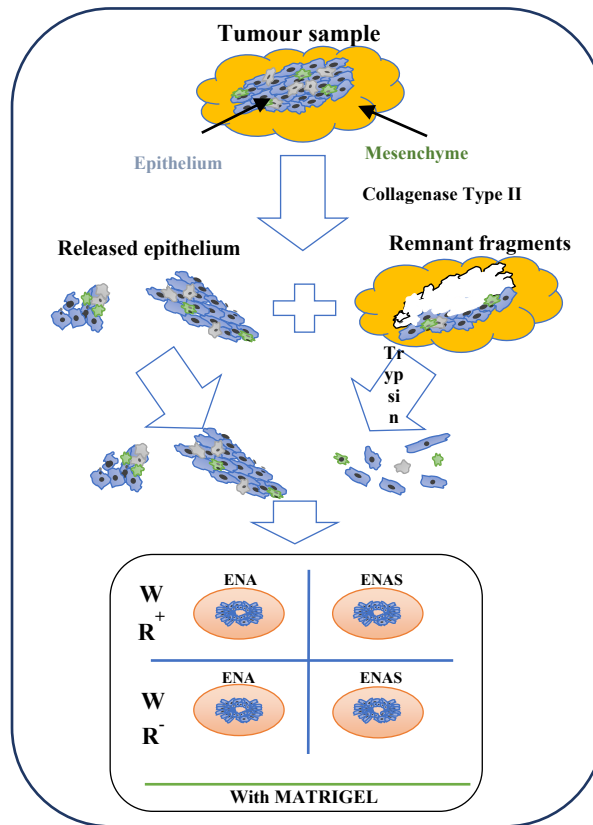


Figure 23. Schematic representation of the protocol used to develop CRC PM-derived organoids. Digested cells were cultured in presence of different growth factors, to mimic different niche factors conditions. (**ENA**: human EGF recombinant protein (**E**); human Noggin recombinant protein (**N**); A83-01, anti-p38 inhibitor (**A**); **ENAS**: ENA supplemented with SB201290 anti-Rock inhibitor (**S**); **WR+/-**: cell culture media supplemented with or without human Wnt3A recombinant protein (**W**) and human R-Spondin-1 recombinant protein (**R**)). Organoids developed under a specific culture medium condition, depending on the growth factors they needed.

The cell pellet was resuspended with Matrigel, growth factor reduced (Corning, NY, USA), and dispensed into 24-well cell culture plates (50 μ l/well). After Matrigel polymerization, the cells were overlaid with 500 μ l of basal cell culture medium consisting of Advanced DMEM-F12 (ThermoFisher Scientific) and supplemented with different growth factors (Table 3) to mimic different niche factor conditions.

Factor	Description	Vendor	Working Concentration
Gentamicin	Antibiotic	Thermo Fisher Scientific	50 ng/ml
HEPES	Buffer	Thermo Fisher Scientific	10 mM
L-Glutamine (GlutaMAX)	Cell culture supplement	Thermo Fisher Scientific	2 mM
B27	Cell culture supplement	Thermo Fisher Scientific	1:50
Gastrin-1, recombinant human	Recombinant protein	Sigma Aldrich	10 mM
N-acetylcysteine	Colonic niche factor	Wako	1 mM
EGF, recombinant human	Recombinant protein	Thermo Fisher Scientific	50 ng/ml
Noggin, recombinant human	Recombinant protein	Preprotech	100 ng/ml
R-spondin-1, recombinant human	Recombinant protein	Preprotech	100 ng/ml
Wnt3A, recombinant human	Recombinant protein	Preprotech	50 ng/ml
Prostaglandin E2	Colonic niche factor	Tocris	100 nM
A83-01	p38 inhibitor	Tocris	500 nM
SB202190	ROCK inhibitor	Sigma Aldrich	10 μ M

Table 3: List of growth factors, media supplements and concentrations used for PM-derived organoid cultures.

Incubation was performed at 20% O₂ and 5% CO₂. After expansion, the TDO were cultured in cell culture medium lacking growth factors, which was refreshed every three days. Optimal cell culture medium conditions were determined separately for each organoid culture (Table 4).

Organoid culture	Medium composition
C1	DMEM-F12; B27; Glutamax; N-acetylcysteine; prostaglandin-E2; gastrin-I
C2	DMEM-F12; B27; Glutamax
C3	DMEM-F12; B27; Glutamax; N-acetylcysteine; prostaglandin-E2; gastrin-I; A83-01
C4	DMEM-F12; B27; Glutamax; N-acetylcysteine; prostaglandin-E2; gastrin-I; EGF; A83-01; Noggin
C5	DMEM-F12; B27; Glutamax; N-acetylcysteine; prostaglandin-E2; gastrin-I; A83-01; SB202190; Noggin
C6	DMEM-F12; B27; Glutamax; N-acetylcysteine; prostaglandin-E2; gastrin-I; A83-01; Noggin

Table 4: The specific media composition for each PM-derived organoid culture.

Organoids were split every 1-2 weeks as follows: they were mechanically removed from the Matrigel by pipetting, incubated in Cell Recovery Solution (Corning) for 1 hour at 4 °C, washed twice with ice-cold PBS and seeded as described above.

Aliquots of each organoid culture were frozen or prepared for IHC analyses as follows: samples were fixed in 10% formalin at room temperature (RT) for 10 minutes and embedded into 200 µl Bio-Agar (Bio-Optica, Milan, Italy). The samples were then cooled at -20 °C until solidification. For each sample, sections of 3 µm were obtained.

6.3 Preparation of 3D-dECMs

3D-dECMs were derived from both PM and the corresponding normal peritoneum. Each experiment was conducted using three to ten different surgical specimens deriving from different patients.

The decellularisation was performed as shown in Figure 24, according to the protocol described by Genovese *et al.* (L. Genovese *et al.* 2014).

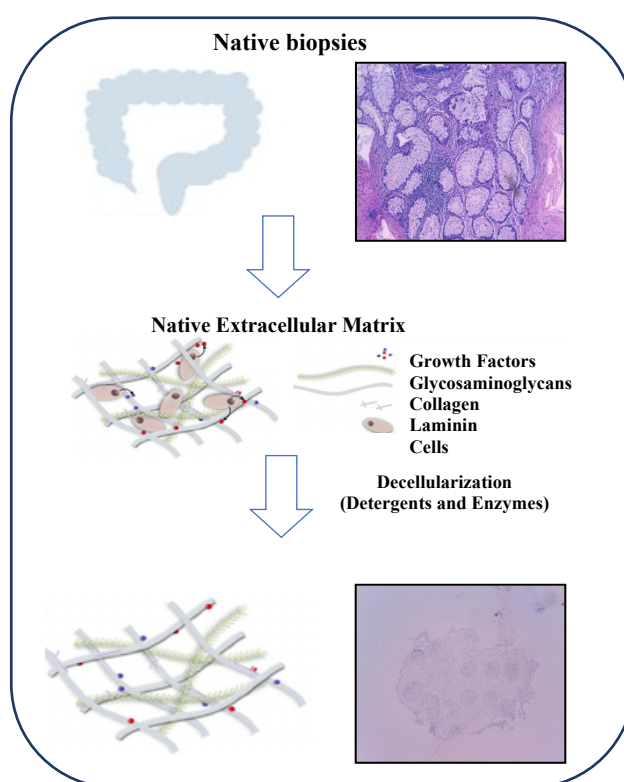


Figure 24. Diagram of established method. Schematic representation of the protocol used to obtain peritoneal-derived 3D-dECMs.

Briefly, both PM and normal peritoneum samples (60-100 mg wet weight) were kept in ice-cold PBS for 1 hour before processing. The specimens were split into two fragments, one of which was kept untreated for later comparison of the characteristics of the 3D-dECMs. For decellularisation, the fragments were washed with ice-cold PBS supplemented with 50 ng/ml gentamicin and 50 ng/ml amphotericin B, followed by treatment with solutions containing detergents and enzymatic agents (Table 5).

Solution	Composition	Mechanism of Action
Solution A	86 % 0.14 X PBS, 5 mM EDTA, 10 % DMSO, 1 % protease inhibitor cocktail, 1 % pen/strep, 1 % amphotericin B, 50 µg/ml gentamicin	Cell dissociation from the stroma and cell lysis
Solution B	96 % 0.1 X PBS, 1 % TrytonX-100, 1 % protease inhibitor cocktail, 1 % pen/strep, 1 % amphotericin B, 50 µg/ml gentamicin	Removal of membrane lipids and cell residues
Solution C	0.5 M NaCl in 0.1 X PBS	Dissociation of proteins from DNA
Solution D	10 mM sodium cholate hydrate in 0.1 X PBS	Solubilization of nucleic membranes
Solution E	50 mM Tris-HCL pH 8.0, 2 mM MgCl ₂	Conditioning with Tris buffer
Solution F	Solution E supplemented with 100 U/ml Benzonase	Degradation of DNA and RNA

Table 5: The specific composition of the solutions used for the decellularisation procedure and their relative mechanism of actions

The success of the decellularisation procedure was evaluated by analysing on an agarose gel the DNA content of the 3D-dECMs (see below). DNA from 20 mg of normal peritoneum and PMs, both decellularised and untreated, was used to evaluate the success of the decellularisation procedure. DNA was extracted using the DNeasy Blood&Tissue kit (QIAGEN) according to the manufacturer's instructions and quantified using Nanodrop 1000 (ThermoFisher Scientific) at 260/280 nm ratio. DNA from decellularised ECM, normal peritoneum, PM, and their corresponding non-decellularised samples was loaded onto a 1% agarose gel. The separated bands were visualized by exposing the gel to UV light and images were acquired using Gel Doc (Bio-Rad, Hercules, CA, USA). All the experiments were performed in triplicate. The 3D-dECMs were then washed with ice-cold PBS and either transferred into chilled freezing solution (90% DMEM-F12, 10% DMSO) and frozen for

storage or fixed for IHC and immunofluorescence (IF) analyses. All the decellularisation experiments were performed in triplicate, using at least three different samples, each derived from a different donor.

6.4 *ex vivo* engineered PM lesion

Engineered PM lesions were obtained from three organoid cultures (C1, C2 and C3). TDO were removed from the Matrigel as described above and dissociated into single-cell suspensions with Trypsin-EDTA by vigorous pipetting for 10 minutes. One million of dissociated cells were counted with an automatic cell counter (ThermoFisher Scientific). 3D-dECMs derived from normal peritoneal tissue and PM were incubated overnight at 37 °C in DMEM-F12 supplemented with 10% FBS (Euroclone, Milan, Italy) and 50 ng/ml gentamicin and amphotericin B. To reduce intra-sample variability, the 3D-dECMs were cut into fragments of comparable sizes.

TDO were resuspended in 50 µl of appropriate cell culture medium diluted 1:8 with Matrigel and seeded on the top of a 3D-dECMs (50mg). Repopulated matrices were placed in a 24-well cell culture plate (Corning) containing DMEM-F12 supplemented with 10% FBS and 50 ng/ml gentamicin and amphotericin B, followed by incubation for 2 hours at 37 °C. Each well was filled with 2 ml cell culture medium, which was changed every two days (Figure 25).

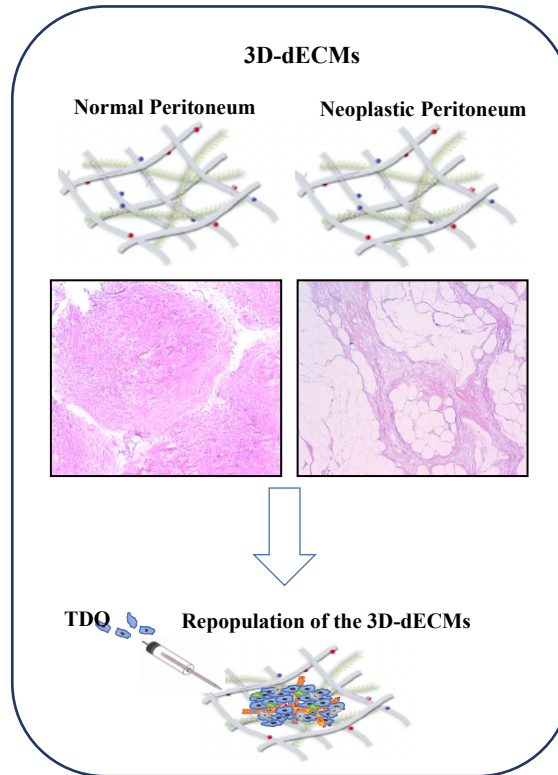


Figure 25. Experimental design used to develop the *ex vivo* 3D-engineered PM lesions.

Repopulated matrices were either frozen for RNA extraction or fixed for IHC and IF analyses. Representative sections of 3 μ m FFPE were cut at different depths to verify the presence of TDO in the inner part of the 3D-dECM scaffold. The repopulation experiments were performed in triplicate, using three different neoplastic and normal-derived matrices obtained from three different donors.

6.5 Nucleic acid extraction

DNA from FFPE sections of the PM-derived organoids and their tissue of origin was used for the mutational analysis. DNA was extracted using the Masterpure Complete DNA Purification Kit (Lucigen-Biosearch Technologies, Middleton, WI, USA) and quantified on the QIAxpert® spectrophotometer (QIAGEN, Hilden, Germany).

RNA from the three organoid cultures, grown both in Matrigel and on normal or neoplastic peritoneal 3D-dECMs, was used for RNA-seq analyses. Matrigel containing TDO was digested with Cell Recovery Solution (Corning) as described above. The pellet was washed three times with ice-cold PBS and suspended in 1 ml TRIzol™ reagent (QIAGEN). Instead, for the repopulated 3D-dECMs, the matrices were washed three times with ice-cold PBS and homogenized using the TISSUE Tearor Homogenizer (QIAGEN) in 500 µl TRIzol™ reagent (QIAGEN). Then, RNA was extracted following the manufacturer's instructions, quantified on a ND-1000 spectrophotometer (ThermoFisher Scientific) and stored at -80 °C.

6.6 Histochemistry (HC), IHC and IF

Before HC and IHC staining, FFPE sections were cut into slices and dewaxed in xylene, rehydrated through decreasing concentrations of ethanol, and washed with water. Slices were stained with hematoxylin and eosin for quality control. For HC analysis, sections were stained with Masson's trichrome (Aniline blue kit; Bio-Optica), Alcian blue stain (pH 2.5 kit, Bio-Optica), van Gieson trichrome (Bio-Optica), and Periodic Acid Schiff (PAS, Bio-Optica) following the manufacturers' instructions. IHC was performed using the following mouse anti-human monoclonal antibodies: Ki-67, CK19, CK20, CK AE1/AE3, CDX2, LGR5, and vimentin. Images were acquired with a DM6000B microscope (Leica). Staining was performed automatically, using the Autostainer Link 48 (Dako, Agilent, Santa Clara, CA, US). Dilutions and experimental conditions are listed in Table 3. For IF analyses, FFPE sections were stained with Alexa680-conjugated Wheat Germ Agglutinin (WGA) marker (ThermoFisher Scientific) for 1 h at RT in dark and DAPI (VECTASHIELD Mounting Medium with *DAPI*, Maravai LifeScencies, San Diego, CA, USA) for 1 h at RT in dark, with anti-human Ki-67 and LGR5 monoclonal antibodies, with anti-human Collagen-IV and anti-human monoclonal cCASPASE3 antibodies and DAPI overnight at 4°C, followed by Alexa488-conjugate goat anti-mouse or Alexa546-conjugated goat anti-rabbit IgG polyclonal

secondary antibodies for 1 hour at RT in dark (ThermoFisher Scientific). Images were acquired with a DM6000B microscope (Wetzlar, Germany Leica,) equipped with a 100 W mercury lamp, and analysed using Cytovision software (Leica). Dilutions and experimental conditions are listed in Table 6.

Antigen (human)	Host	Clone	Vendor	Dilution	Antigen retrieval solution
Ki-67	Mouse	MIB-1	Dako	1:400	5 mM EDTA (pH 8), 10 min, 96 °C
CK19	Mouse	A53-B/A2	Dako	1:1000	5 mM EDTA (pH 8), 15 min, 96°C
CK20	Mouse	Ks20.8	Dako	1:500	5 mM EDTA (pH 8), 30 min, 96°C
CK AE1/AE3	Mouse	AE1+AE3	Dako	1:100	10 mM Citrate (pH 6), 15 min, 96°C
CDX2	Mouse	CDX2_88	Dako	1:50	5 mM EDTA (pH 8), 30 min, 96°C
LGR5	Mouse	OTI2A2	Origene	1:250	10 mM Citrate (pH 6), 15 min, 96 °C
Vimentin	Mouse	V9	Dako	1:400	10 mM Citrate (pH 6), 15 min, 96°C
Collagen-IV	Rabbit	CIV-22	Abcam	1:200	5 mM EDTA (pH 8), 10 min, 96 °C
cCASPASE3	Rabbit	#9661	Cell Signaling	1:250	10 mM Citrate (pH 6), 15 min, 96 °C

Table 6: The primary antibodies and the experimental conditions used for IHC and IF analyses.

6.7 DNA sequencing

About 150–200 ng of genomic DNA (measured with the Qubit dsDNA HS assay kit, ThermoFisher Scientific), were sheared by the Sure Select Enzymatic Fragmentation kit (Agilent Technologies Inc., Santa Clara, CA, USA). NGS libraries were created using Sure Select XT2 Low input Custom library probes (Agilent Technologies Inc.). The probe set was custom designed by Cogentech (OncoPan panel) and includes the exonic regions of the following genes: APC, ATM, BARD1, BMPR1A, BRCA1, BRCA2, BRIP1, CDH1, CDKN2A (α and β isoform), CDK4 (exon 2), CHEK2, CTNNA1, EPCAM, FANCM, MLH1, MSH2, MSH3, MSH6, MUTYH, NBN, NHTL1, PALB2, PMS2, POLD1, POLE, PTEN, RAD51C, RAD51D, SMAD4, STK11, TP53, KRAS, NRAS, BRAF, EGFR, HER2 (ERBB2), and PIK3CA. Sequencing was performed on Illumina MiSeq platform, in PE mode (2 x 150 bp). Raw reads were demultiplexed and aligned to a reference genome (Human GRCh37) using a pipeline developed in-house in collaboration with enGenome Software Company and annotated with the eVai tool. Results were compared to find the percentage of common SNVs (Single Nucleotide Variants). Five PM-derived organoids (C1, C2, C3, C4 and C6) and their corresponding surgical samples were analysed. FFPE tissue for C5, unfortunately, was not available.

6.8 Morphological evaluation of the decellularised matrices

3D-dECMs from normal peritoneum and PM lesions were washed twice with 1X PBS and placed in a 60 mm petri dish. Samples were illuminated with a widefield lamp laser to visualize the architecture of the collagen fibers. An image format of 1024x1024 pixels was used and all images were acquired with Leica Application Suite X, ver. 3 software. 3D-dECMs FFPE sections deriving from normal and metastatic peritoneum was used to perform polarized light microscopy (PLM). FFPEs were analysed with an Olympus BX63 upright widefield microscope equipped with a motorized stage and a Hamamatsu OrcaAG camera,

using Metamorph software. UplanSApo 4X/0.16 N.A objective was used to acquire the mosaics of the sections. Insets were acquired with UplanSApo 10X/0.4 N.A. and UplanSApo 20X/0.75 N.A. objectives. All experiments were performed at least in duplicate. Confocal reflection microscopy images were acquired with a Leica TCS SP8 laser confocal scanner mounted on a Leica DMI8 microscope through a HC PL FLUOTAR 20×/0.5 NA.

6.9 Nanoscale topographical analysis of 3D-dECMs

The topographical evaluation of the 3D-dECMs was performed by Atomic Force Microscopy (AFM) on samples deriving from normal peritoneum and PM of three different patients. Before the AFM analysis, the 3D-dECM samples were embedded in optical cutting compound (OCT) and frozen with nitrogen-cooled 2-propanol for 10 seconds. Slices of 50 μm thickness were cut with a microtome (Leica) and attached to positively charged polylysine coated glass coverslips (ThermoFisher Scientific), exploiting the electrostatic interaction. After that, slides were left for 30 minutes at RT to dissolve the OCT compound. Then, the samples were carefully washed with ultrapure water and covered with 1X PBS buffer. AFM topographic measurements were carried out at RT using a NanoWizard3 AFM (JPK, Germany) coupled to an Olympus BX61 inverted microscope and equipped with tapping mode silicon ACTG AFM probes (APPNANO). The 50 μm thick tissue slices, instead, were mounted on polarized glass slides (ThermoFisher Scientific), left for 30 minutes at RT, and carefully washed with ultrapure water. The topography of each tissue was characterized by collecting at least 10 areas ($5 \times 5 \mu\text{m}^2$) of the sample surface with 512×512 points (scan speed $3,5 \mu\text{m s}^{-1}$).

6.10 Collagen and glycosaminoglycan quantification

Total collagen and sulphated glycosaminoglycan (sGAG) content on fresh and decellularised peritoneum (both normal and PM derived respectively) were quantified using the SIRCOL collagen assay (Biocolor, Carrickfergus, UK) and the Blyscan GAG assay kit (Biocolor), respectively. The experiments were performed in triplicate following the manufacturer's instruction. Data are the mean of three different neoplastic and normal-derived samples obtained from three different donors.

6.11 Nanoindentation measurements by AFM

AFM mechanical analysis was performed on 3D-dECMs deriving from normal peritoneum and PM of three patients. 3D-dECMs were embedded in OCT and frozen with nitrogen-cooled 2-propanol for 10 seconds. Slices of 100 μm thickness were cut with a microtome (Leica) and attached to positively charged poly-lysine coated glass coverslips (ThermoFisher Scientific), exploiting the electrostatic interaction. Nanomechanical tests were performed in liquid on samples covered by a PBS droplet confined by a circular ridge of hydrophobic two-component silicone paste (Leica). A Bioscope Catalyst AFM (Bruker) was used, which was resting on an active anti-vibration base (DVIA-T45, Daeil Systems) and put into an acoustic enclosure (Schaefer). The measurements were performed at RT.

Custom monolithic borosilicate glass probes consisting of spherical glass beads (SPI Supplies), with radii R in the range of 7.5–9.5 μm , were attached to tipless cantilevers (Nanosensor, TL-FM) with nominal spring constant $k = 2.8 \text{ N/m}$. Probes were fabricated and calibrated, in terms of tip radius, according to an established custom protocol (M. Indrieri *et al.* 2011). The spring constant was measured using the thermal noise calibration (M. Chighinzola *et al.* 2021; H.J. Butt *et al.* 1995) and corrected for the contribution of the added mass of the sphere (J. Laurent *et al.* 2013; J.L. Hutter and J. Bechhoefer, 1993). The deflection sensitivity was calibrated *in situ* and non-invasively before every experiment by

using the previously characterized spring constant as a reference, according to the SNAP procedure described in H. Schillers *et al.* (H. Schillers *et al.* 2017).

The mechanical properties of the 3D-dECMs were obtained by fitting the Hertz model to sets of force versus indentation curves (simply force curves, FCs), as described elsewhere (H. Schillers *et al.* 2017; M. Nebuloni *et al.* 2016; L. Puricelli *et al.* 2015; E. Shimshoni *et al.* 2020) to extract the value of the YM of elasticity, which measures ECM rigidity. FCs were collected in Point and Shoot (P&S) mode, selecting the regions of interest from optical images, exploiting the accurate alignment of the optical and AFM images obtained using the Miro software module integrated in the AFM software. Each set of FCs consisted of an array of $15 \times 15 = 225$ FCs spatially separated by approximately 10 μm , each FC containing 8192 points, with ramp length $L = 8 \mu\text{m}$, maximum load $F_{\text{max}} = 150 \text{ nN}$, and ramp frequency $f = 1 \text{ Hz}$. Typical maximum indentation was 3-4 μm . Typical probe velocity during indentation was 16 $\mu\text{m/s}$.

Three samples were characterized for each condition. In each sample, three P&S, each made of 225 FCs, were recorded in macroscopically separated locations, resulting in ~2000 FCs per patient condition.

6.12 Stem cell maintenance, proliferation, and apoptosis assays

Growing cells, stem cells and apoptotic cells were detected on FFPE sections. Growing cells, deriving from disaggregated TDO, were stained with anti-human Ki-67 monoclonal antibody (clone MIB-1) and DAPI overnight at 4°C, followed by Alexa488-conjugate goat anti-mouse polyclonal secondary antibodies for 1 hour at RT in dark (ThermoFisher Scientific), and their growth rate was expressed as the percentage of Ki-67-positive cells present in fields devoid of dead cells. Stem cells were stained with anti-human LGR5 monoclonal antibody (clone OTI2A2) and DAPI overnight at 4°C, followed by Alexa488-conjugate goat anti-mouse or Alexa546-conjugated goat anti-rabbit IgG polyclonal

secondary antibodies for 1 hour at RT in dark (ThermoFisher Scientific), and their density was expressed as the percentage of LGR5-positive cells present in fields devoid of dead cells. Apoptotic cells were stained with anti-human cCASPASE3 monoclonal antibody (clone 9661) and DAPI overnight at 4°C, followed by Alexa546-conjugated goat anti-rabbit IgG polyclonal secondary antibodies for 1 hour at RT in dark (ThermoFisher Scientific), and the apoptotic rate was calculated as the percentage of cCASPASE3-positive cells present in the field. The percentage of Ki-67-positive, LGR5-positive and cCASPASE3-positive cells was obtained by dividing the number of positive cells present in one field to the total number of cells in one field, multiplied by 100. Cells in three independent fields (40X magnification) were counted using ImageJ software. Dilutions and experimental conditions are listed in Table 6 (see above).

The experiments were performed in triplicate using three different neoplastic and normal-derived matrices obtained from three different donors.

6.13 RNA-seq analysis

Gene expression profiles were conducted on C1, C2 and C3 organoid cultures grown in Matrigel and on 3D-dECMs (Normal and Neoplastic-derived respectively). Total RNA was extracted using TRIzol™ reagent (QIAGEN) and tissue homogenizator (QUIAGEN) following the manufacturer's instructions. Qubit fluorimeter (ThermoFisher Scientific) and Agilent Bioanalyser 2100 (RIN > 8) were used to measure and assess RNA abundance and integrity, respectively. Indexed library preparation was performed starting with 500 ng total RNA with the TruSeq stranded mRNA (Illumina) according to the manufacturer's instructions. RNA-seq was performed in PE mode (2x75nt) on an Illumina NextSeq550 platform, generating an average of 55×10^6 PE reads per sample. For every condition (Matrigel, normal 3D-dCM and neoplastic 3D-dECM), two replicates per organoid were sequenced, for a total of 18 data points. Raw reads were aligned to the human transcriptome (hg38) with

STAR (A. Dobin *et al.* 2013) using the quantMode option to generate transcripts counts. STAR was developed as a stand-alone C++ code. STAR is capable of running parallel threads on multicore systems with close to linear scaling of productivity with the number of cores. It is a novel algorithm for aligning to a reference genome high-throughput long and short RNA-seq data, developed to overcome high mapping error rate, alignment biases, low sensitivity for unannotated transcripts, poor scalability with the read length, restrictions in the number of junctions/mismatches/indels per read, inability to detect non-linear transcripts (such as chimeric RNAs), and, crucially, low mapping throughput. Differentially expressed genes in the three growth conditions were identified with DESeq2 (H.A.N. Alshehri, 2018). All *p*-values were adjusted for false discovery rate with the Benjamini-Hochberg method.

6.14 Gene Set Enrichment Analysis

Gene Set Enrichment Analysis was performed with the enrichR R package (E.Y. Chen *et al.* 2013) and with GSEA tool (<https://www.gsea-msigdb.org>) on deregulated genes (absolute fold change > 2 and adjusted *p*-value <0.05). EnrichR is an easy to use intuitive enrichment analysis web-based tool providing various types of visualization summaries of collective functions of gene lists, and represents an alternative approach to rank enriched terms, and various interactive visualization approaches to display enrichment results using the JavaScript library, Data Driven Documents (D3). The software can also be embedded into any tool that performs gene list analysis. In particular, the enrichment for the Matrisome database was assessed, since transcriptomics experiments were conducted on samples grown on 3D-dECMs, mainly consisting of ECM proteins and ECM-related proteins. This database provides live cross-referencing to gene and protein databases for every ECM and ECM-associated gene, also integrating experimental proteomic data on ECM and ECM-associated proteins and genes from the ECM Atlas (A. Naba *et al.* 2016). Gene sets with adjusted *p*-value <0.05 were considered significantly enriched.

6.15 Treatment with cytotoxic drugs

For the *in vitro* simulation of HIPEC treatment, mitomycin-c (Kyowa Kirin Co., Ltd., Tokyo, Japan) was used at a concentration of 35 mg/m², which corresponds to 17.5 mg/l for *in vitro* treatments (I. Ubink *et al.* 2019). Mitomycin-c was dissolved in DMSO to obtain a 100 mg/l stock solution and diluted to the working concentration in the cell culture medium. The final solvent concentration was <0.1% for all samples, including controls. The experiments were performed in triplicate, using three different neoplastic and normal-derived matrices obtained from three different donors.

6.16 *ex vivo* PM lesion to test HIPEC efficacy *in vitro*

The *in vitro* surrogate model of PM disease mimicking HIPEC intervention was designed as reported by Ubink *et al.* (I. Ubink *et al.* 2019). An *ex vivo* engineered micrometastasis that reproduces the binding of CRC circulating metastatic cells to the peritoneum was obtained by growing PM-derived organoids on 3D-dECMs from neoplastic peritoneum. In the model, PM-derived organoids were in contact with the drug, as during HIPEC. Briefly, PM-derived organoids were grown on the top of neoplastic 3D-dECMs in a 24-well cell culture plate for 12 days in order to allow a complete colonization of the matrix (H.J. Chen *et al.* 2016, L. Genovese *et al.* 2014, H. Weijing *et al.* 2021). TDO grown in Matrigel were used as control to evaluate the impact of native 3D-dECMs on the HIPEC treatment. The engineered PM lesions were treated with preheated (42.5 °C) mitomycin-c at a concentration of 17.5 mg/l for 1 hour at 42.5 °C, which is in line with the current standard protocol used for HIPEC at Fondazione IRCCS Istituto Nazionale dei Tumori - Milano. washed three times with 1X PBS and incubated for 48 hours with appropriate cell growth medium (Figure. 26).

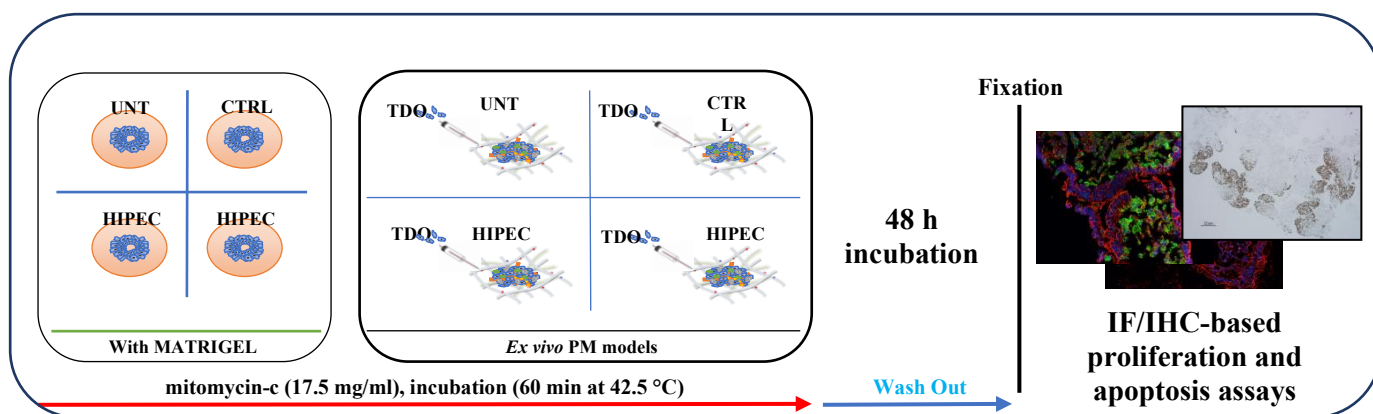


Figure 26. Workflow chart representing the experimental design used to reproduce *in vitro* HIPEC treatments (UNT: untreated group; CTRL: control group, mitomycin-c vehicle: physiological solution; **HIPEC**: Hyperthermic Intraperitoneal Chemotherapy; **TDQ**: tumour-derived organoid; **IF**: Immunofluorescence; **IHC**: Immunohistochemistry).

Samples were fixed in formalin and FFPE sections were obtained as described above. The impact of HIPEC treatment on TDQ proliferation and the activation of an apoptotic program were determined by Ki-67 and cCASPASE3 immunostaining, respectively as described above. All experiments were performed in triplicate using three different neoplastic and normal-derived matrices obtained from three different donors.

6.17 MMT Assay and 3D-dECMs lyophilization

CRC-derived DLD-1, HT-29 and HCT-116 cell lines were obtained from the American Type Culture Collection (ATCC, Rockville, MD, USA) and were authenticated by the Cell Culture Facility at the FIRC Institute of Molecular Oncology (IFOM, Milan, Italy) with the StemElite ID system (Promega) following the manufacturer's instructions. Cells were routinely tested for mycoplasma and cultured following the recommended ATCC's protocols. The 3D-dECMs were placed at -80°C overnight, lyophilized using freeze-drier cycles following standard procedures, and then added to the culture media of the three cell lines. During the experiments, three different concentrations of lyophilized 3D-dECMs were tested and cell viability was evaluated after 72 hours of growth by MTT (3-(4, 5-

dimethylthiazol-2-yl)-2, 5-diphenyltetrazolium bromide) assay (Sigma Aldrich), following the manufacturer's instructions.

6.18 Statistical analyses

Statistical analyses were performed using GraphPad Prism software (version 8.4.1 (676), GraphPad Software, San Diego, USA). Data are expressed as mean and SEM. A two-sided Student's *t*-test was used to compare paired groups. Differences among groups were evaluated using two-way ANOVA.

In the case of AFM mechanical experiments, for each patient and each condition tested, the median values of the YM were extracted from each measured location, and the associated effective errors were calculated by using the procedure described in Cramer et al (E. Shimshoni *et al.* 2020, H. Cramer, 1999). The distributions of the measured YM values were obtained by grouping all values measured in all locations, for each patient and each condition tested. The statistical significance of differences between results obtained for the two conditions was estimated by applying the two-tailed *t*-test. A *p*-value <0.05 was considered statistically significant.

7. Results

7.1 Development of PM-derived organoids

I developed a panel of PM-derived organoids that resemble the main characteristics of PM disease. Following established protocols for *ex vivo* organoid cultures (M. Fujii *et al.* 2017; van De Wetering *et al.* 2016), I established six organoid cultures (named from C1 to C6). The main characteristics of their tumour of origin are listed in table 2. TDO were able to grow in the absence of key growth factors for CRC-derived organoids, such, and R-spondin-1 and Wnt3A and this was in line with other published papers where it has been highlighted how organoids derived from tumours at advanced stages progressively lose colonic niche factor dependency (M. Fujii *et al.* 2017; F. Bozzi *et al.* 2017). The composition medium appeared to be correlated with the molecular characteristics of the tumour of origin. In fact, C2 organoids, *BRAF*-mutant, grew in media with minimal requirements for niche factors; C3 organoids, carrying *FGR1* amplification, grew in medium without EGF, while C1, C4, C5 and C6 organoids, *KRAS*-mutant, required EGF or noggin-1 supplementation (Table 4). Of note, I was able to develop PM-derived organoids from both patients undergoing adjuvant chemotherapy and from those who had not received treatment before surgery. All these observations reflect the evidence previously described by Ganesh *et al.*, in which clinical variables are unable to predict the success or failure of organoid development (Ganesh *et al.* 2019). The main characteristics of the organoids derived from the six PM patients are summarized in Table 2.

7.2 PM-derived organoid characterisation

A key feature of TDO is to fully recapitulate the main characteristics of their tumour of origin, both in terms of genetic landscape and expression of cancer-related proteins, also preserving the tumour heterogeneity. Thus, I compared the six PM-derived organoids with

their corresponding surgical samples looking at the expression of the colorectal specific markers CKA1-CKA3, CK19, CK20 and CDX2, routinely used in clinics for metastatic colorectal cancer . IHC analysis showed how PM-derived organoids retain the expression of these markers, with the same pattern present in their corresponding clinical specimens. Moreover, I observed that the expression signal displayed by the organoids was comparable with the one from the patient from which they were derived (Figure 26 and Appendix A: Figure 1A)

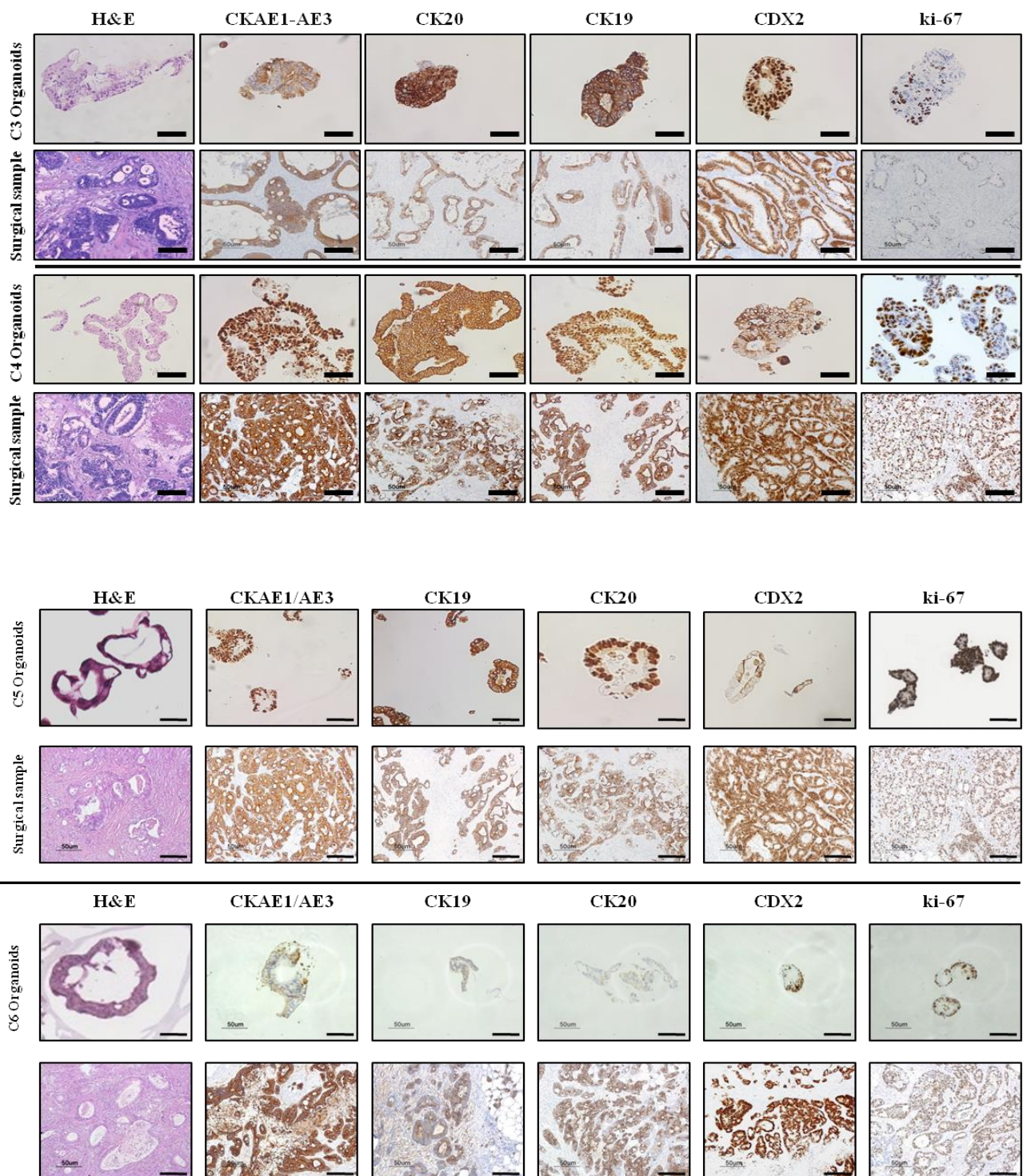


Figure 26: Comparative histological and IHC analysis of PM-derived organoids and their tissue of origin, using H&E staining and CK AE1/AE3, CK20, CK19, CDX2, and Ki-67 immunostaining showing that PM-derived organoids retain the main features of their tissue of origin. PM tissues generally present a tumour epithelium surrounded by stromal-derived cells, while organoids consist exclusively of epithelial cells. Scale bar: 100 μ m.

As for the morphological aspects, I observed that the obtained PM-derived organoids displayed the typical glandular features found in the corresponding surgical sample, including signet-ring cells, nest-like growth pattern, nuclear atypia, cuboidal nuclear morphology and pleomorphism, and were also characterised by a similar degree of differentiation with respect to the parental cancer. In fact, organoids derived from undifferentiated tumours, such as C4, showed a typical monolayer organization of the epithelial cells, while TDO derived from moderately undifferentiated cultures (for example C3) displayed a multi-layered epithelium with the presence of branches that resemble the colonic villous (Figures 27 and Appendix A).

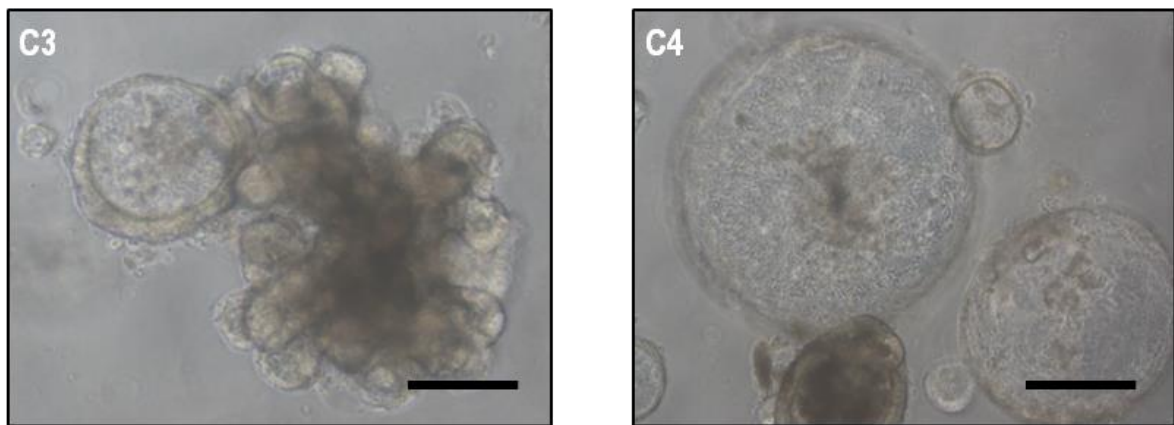


Figure 27. Bright-field images depicting the phenotypes of two PM-derived organoids. The left micrograph shows a glandular-like branched organoid, while the right one shows a spherical-like cohesive organoid. Scale bar: 100 μ m

I investigated the expression of LGR5 protein in the organoid cultures through an IHC approach. The protein was present both in TDO and in their corresponding clinical samples (Figure 28 and Appendix A: Figure 1B and 1C).

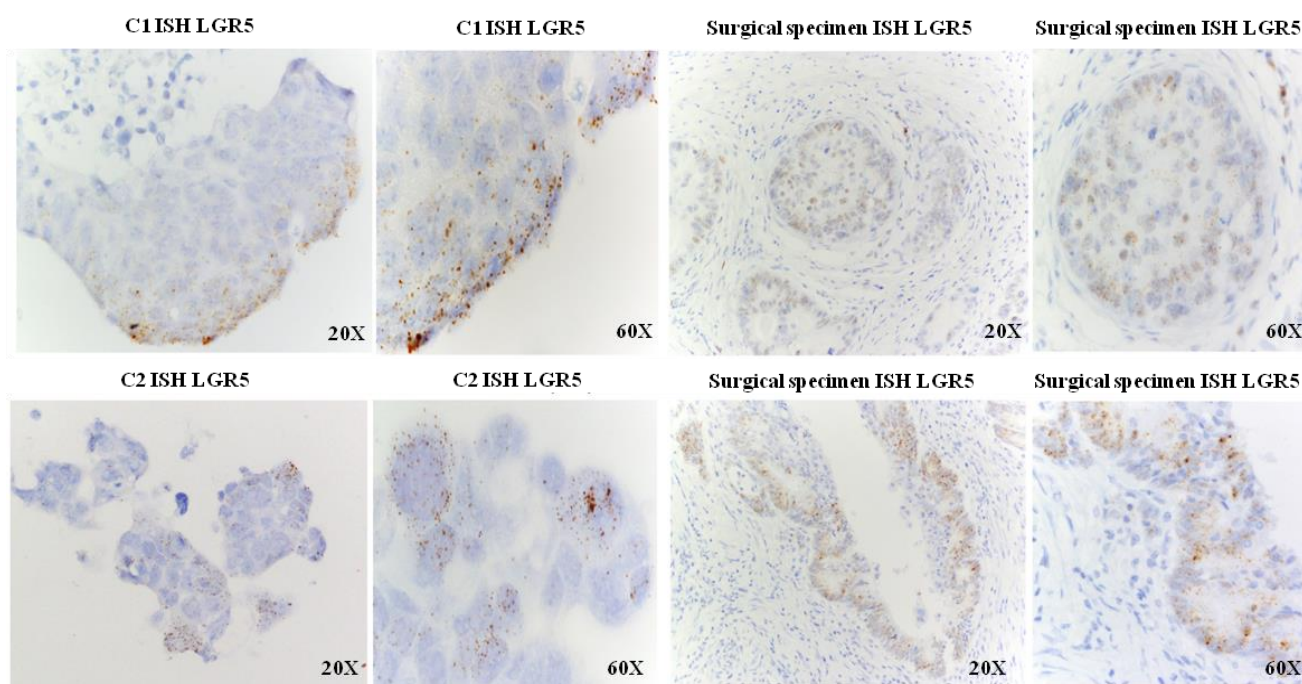


Figure 28 In situ hybridization (ISH) of C1 and C2 organoids and corresponding surgical samples, using LGR5 immunostaining (20X magnification). The images were previously published by Bozzi et al.

Furthermore, I analysed the expression of Ki-67 in the PM-derived organoids, demonstrating that all cultures expressed this protein, with a pattern comparable to that observed in patient-derived samples (Figure 26, Appendix A: Figure 1A). This result suggests that PM-derived organoids were in active proliferative state.

Finally, I confirmed that all PM-derived organoids had the same characteristics of the parental cancer tissue by analysing their mutational profile, together with that of their tissue of origin, for 32 genes frequently mutated in several cancers, including CRC. I observed that TDO maintained the mutational profile of the tumour from which they were generated, with a similarity ranging from 87 % to 100 % (Figure 29, Appendix A: Figure 1D).

	C1	C2	C3	C4	C6
% of Similarity	97,92	91,84	100	87,18	93,85
<i>APC</i>					
<i>ATM</i>					
<i>BARD1</i>					
<i>BMPR1A</i>					
<i>BRAF</i>					
<i>BRCA1</i>					
<i>BRCA2</i>					
<i>BRIP1</i>					
<i>CDH1</i>					
<i>CDKN2A</i>					
<i>CHEK2</i>					
<i>CTNNA1</i>					
<i>EGFR</i>					
<i>ERBB2</i>					
<i>FANCM</i>					
<i>KRAS</i>					
<i>MLH1</i>					
<i>MSH2</i>					
<i>MSH3</i>					
<i>MSH6</i>					
<i>MUTYH</i>					
<i>NBN</i>					
<i>PALB2</i>					
<i>PIK3CA</i>					
<i>PMS2</i>					
<i>POLD1</i>					
<i>POLE</i>					
<i>RAD51C</i>					
<i>RAD51D</i>					
<i>SMAD4</i>					
<i>TP53</i>					

Figure 29. Mutational analysis of 32 cancer-related genes, analysed by target DNA sequencing. Red boxes indicate the genes presenting acquired mutations in TDOs with respect to their tumour of origin. The percentage of similarity of each TDO with its tumour of origin was reported. Passage numbers of the organoid lines were: C1: P11; C2: P13; C3: P10; C4: P14; C6: P10.

7.3 Development of 3D decellularised scaffolds

I generated 3D-dECMs from the tissue surrounding the peritoneal metastases and from normal peritoneum, following the established protocol by Genovese *et al.* (L. Genovese *et al.* 2014). The first requirement of a decellularised matrix is to have a depletion of 95% or greater, of the nucleic acid content of the tissue of origin. Therefore, I verified that the protocol used for tissue decellularization completely removed the DNA by extracting DNA from the 3D-dECM and checking its yield on agarose gel and at the spectrophotometer. Results showed a complete removal of DNA was completely removed in both the experiments. (***) $p < 0.001$; Figure 30).

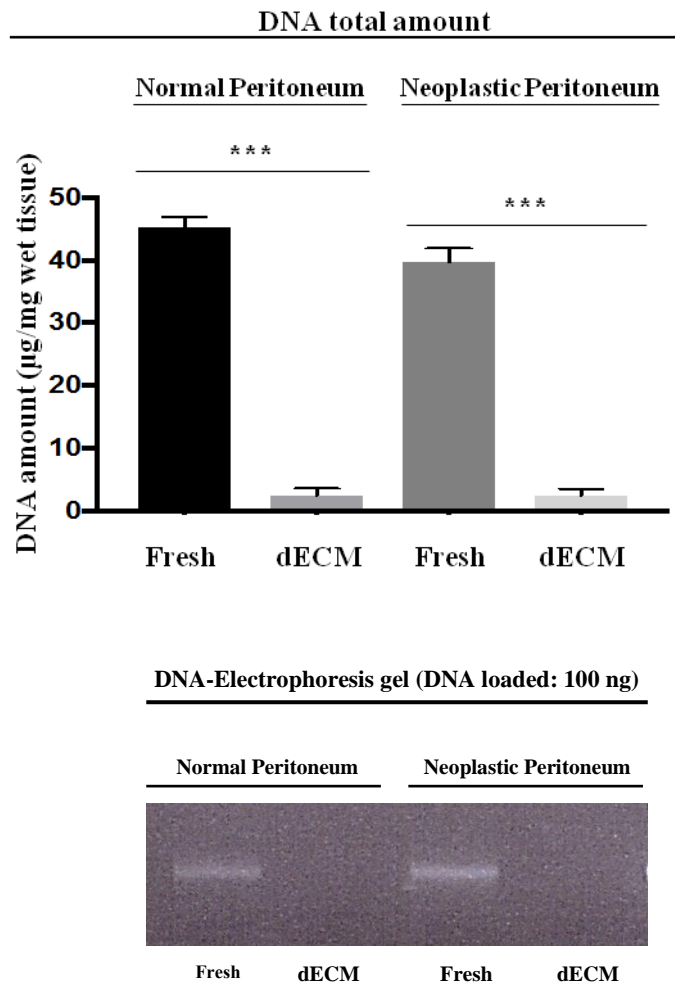


Figure 30. DNA quantification of normal and neoplastic peritoneal tissue samples before (fresh) and after the decellularisation treatment (dECM), showing a high DNA depletion. Student's *t*-test ($***p<0.001$). The electrophoresis gel showed the absence of DNA in dECM samples, indicating the success of the decellularization procedure. The experiments were performed in triplicate.

After that, I performed a fluorescence analysis of FFPE sections derived from both normal and neoplastic peritoneum, decellularised and not decellularised, to verify the complete removal of the lipid that form the cellular membranes and have a visual confirmation of the complete depletion of the DNA. I stained the sections with DAPI, a nuclear marker, and with WGA, a lipid's membrane marker, and observed a clear fluorescence signal for both markers only in the non-decellularised samples (Figure 31)

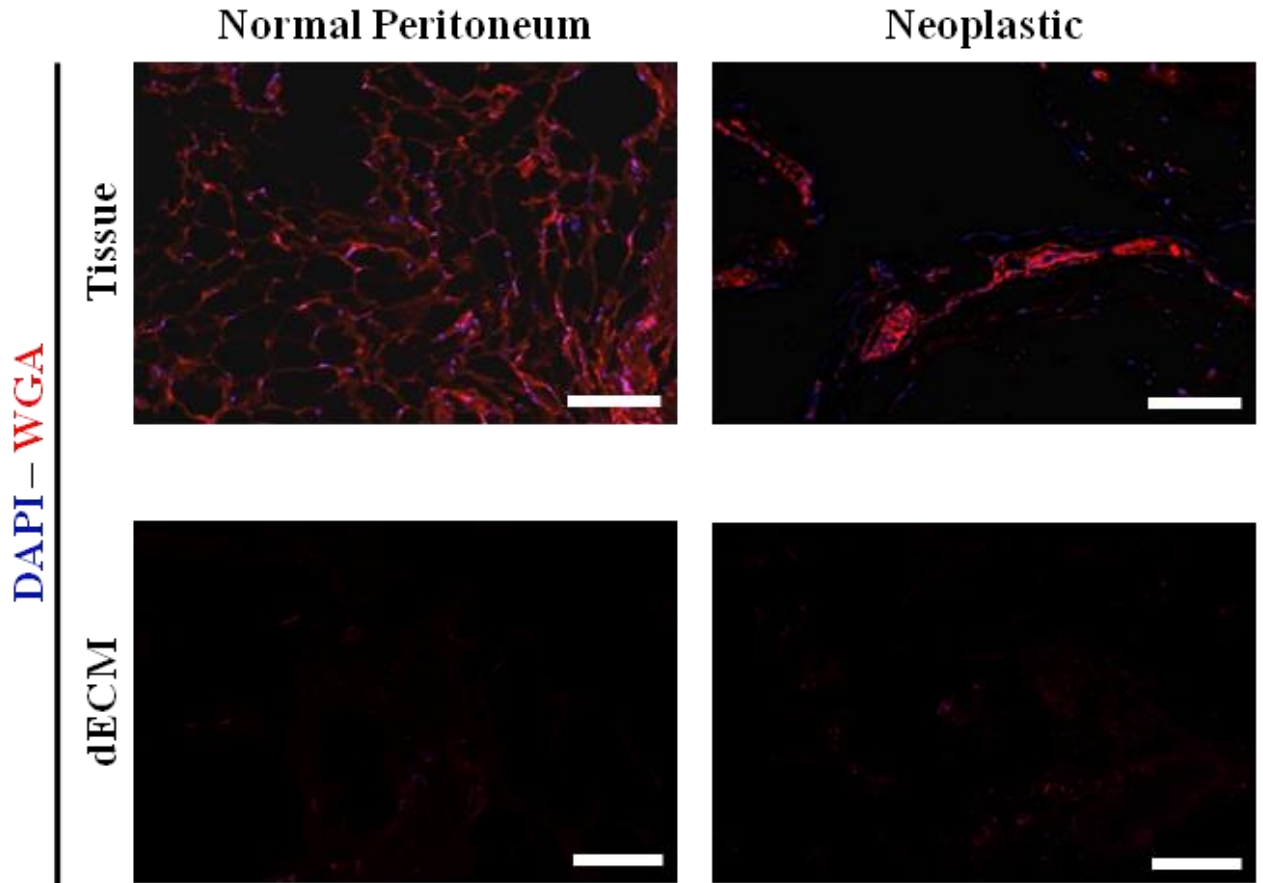


Figure 31. Fluorescence analysis of normal and neoplastic peritoneal samples before and after the decellularisation procedure using the WGA (Wheat Germ Agglutinin), a marker for glycoproteins in lipid membranes; red) antibody. The samples were counterstained with DAPI (blue). Scale bar: 100 μ m.

The second most important requirement for obtaining 3D-dECMs that can be used as scaffolds for cell cultures is that they must preserve their 3D structures and the main structural proteins that constitute the ECM. I performed Hematoxylin and Eosin staining, to verify if the decellularisation procedures preserved the ECM architecture. Results revealed that both the normal and neoplastic decellularized peritoneum completely retained the architectural structure of the corresponding non-decellularised samples (Figure 32). Then, I verified the complete depletion of the epithelial and mesenchymal cells by IHC analysis of cytokeratin and vimentin respectively. Finally, I checked the preservation of one of the main structural

proteins that compose the ECM, collagen-IV, via collagen-IV immunostaining. The IHC analysis showed that the 3D-dECMs of both normal and neoplastic peritoneum did not express cytokeratin and vimentin when compared to their corresponding non decellularised tissue, indicating the absence of both epithelial and mesenchymal cells in the decellularised samples (Figure 32). As regarding collagen-IV expression, I observed that it was retained after decellularisation, also maintaining the original distribution, as showed in Figure 32.

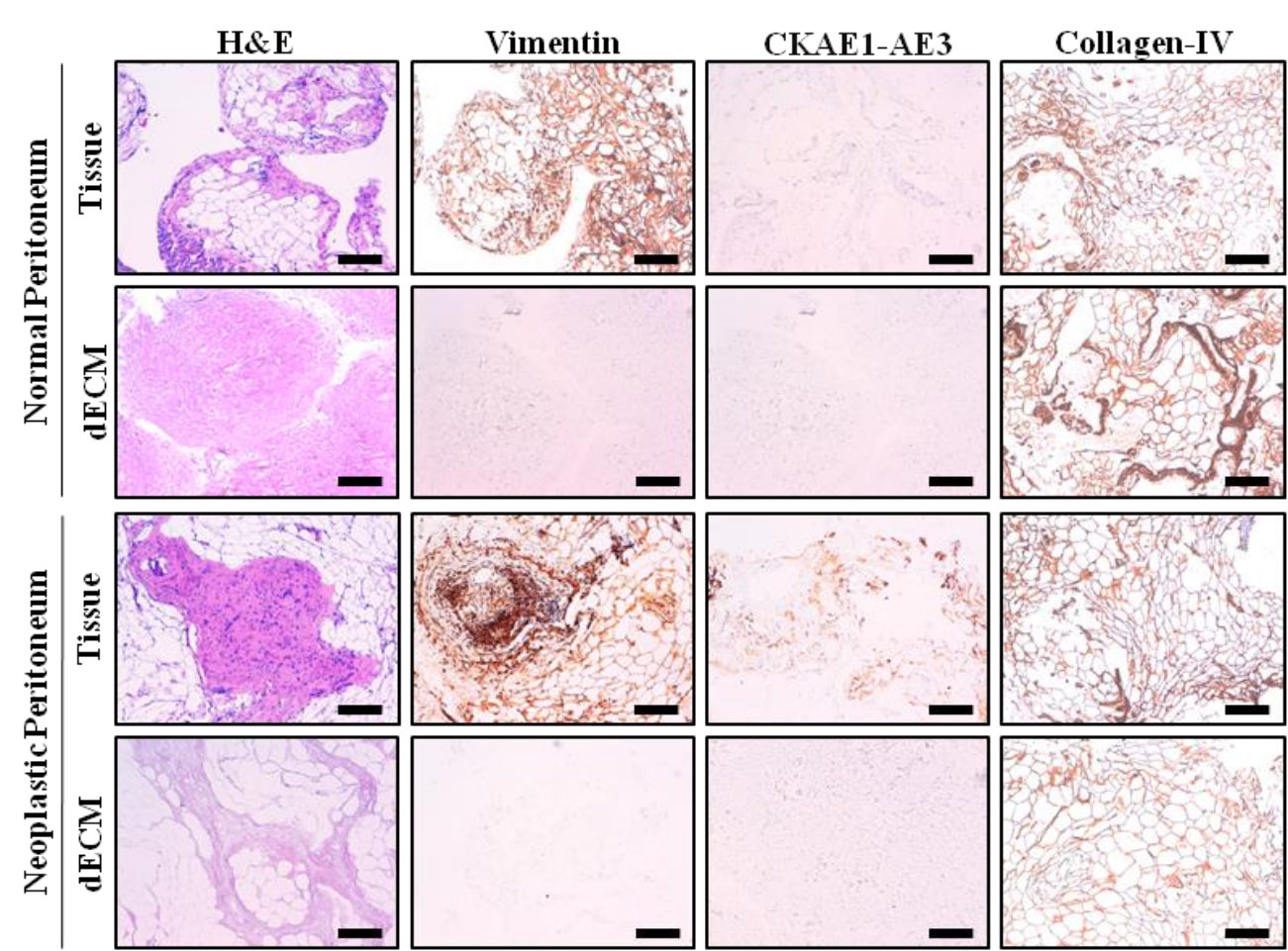


Figure 32. IHC analysis of fresh peritoneal-derived tissues and the corresponding decellularised samples using H&E staining and vimentin, pan-Cytokeratin (CK AE1/AE3), and collagen-IV immunostaining. Scale bar: 200 μ m.

I also confirmed that the tissue architecture was similar to that of the tissue of origin by van staining 3D-dECMs with Gienson and Masson trichrome that allowed the visualization of the

organization of the collagen fibers. Finally, I confirmed the presence of Glycosaminoglycans (GAG) by Alcian blue and periodic acid – Schiff (PAS) stains (Figure 33).

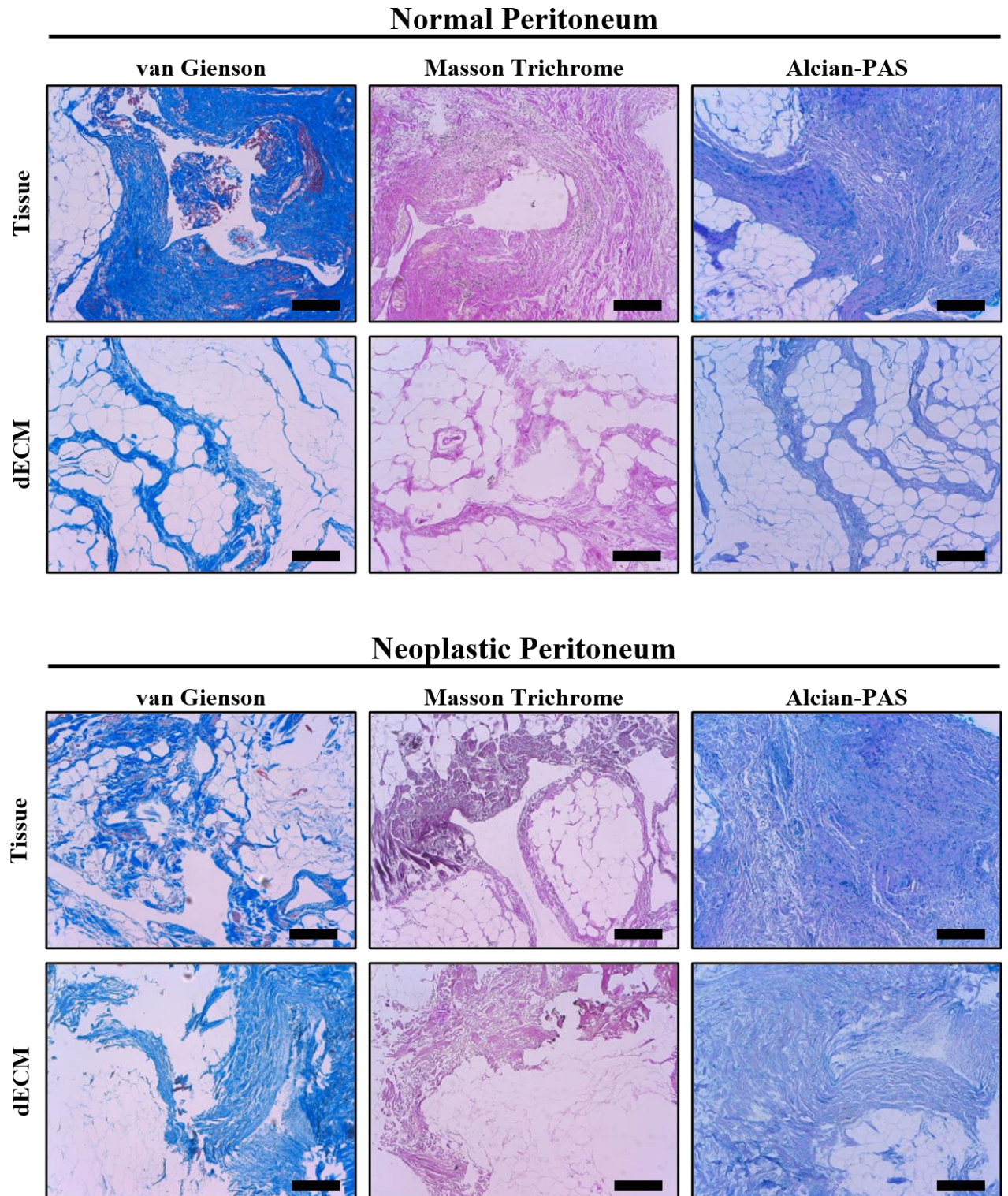


Figure 33. Van Gienson, Masson's Trichrome and Alcian-PAS stains for the detection of collagens, polysaccharides, glycoproteins, and structural tissue preservation on fresh and decellularised peritoneal-derived samples. Scale bar: 200 μ m.

Since the obtained 3D-dECMs will be used as a scaffold for PM-derived organoids, I tested whether the reagents and/or procedures used for the decellularisation can affect cell growth. I lyophilized 3D-dECMs and added them to the culture media of three CRC commercially available cell lines (DLD-1, HT-29 and HCT-116) and evaluated changes in cell growth through an MTT assay. I observed no differences between cells cultured with and without the matrices after 72 hours of growth, demonstrating that the lyophilized 3D-dECMs do not affect cell growth. These results indicate that the decellularisation protocol I used is safe for cell growth and that the 3D-dECMs can be used as a scaffold for TDO (Figure 34).

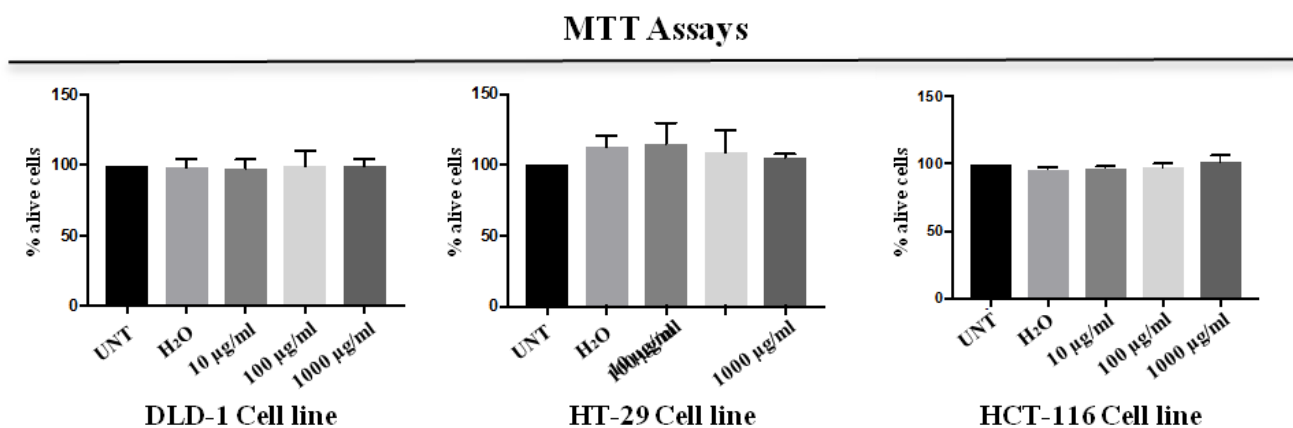


Figure 34. MTT assay showing no differences in cell viability between cells cultured with or without lyophilized 3D-dECM, highlighting that the decellularisation procedure is safe for cell growth. The experiments were performed at least in duplicate.

7.4 3D-dECMs: morphological features and mechanical properties

I investigated the main morphological features of the obtained 3D-dECMs using confocal reflection and polarized light microscopy techniques, which allow the visualization of the entire conformation of the decellularised samples. I observed that the differences between normal and neoplastic-derived tissues obtained from three different PM

patients were related both to the tissue texture and to the distribution and integrity of the single collagen fiber (Figure 34).

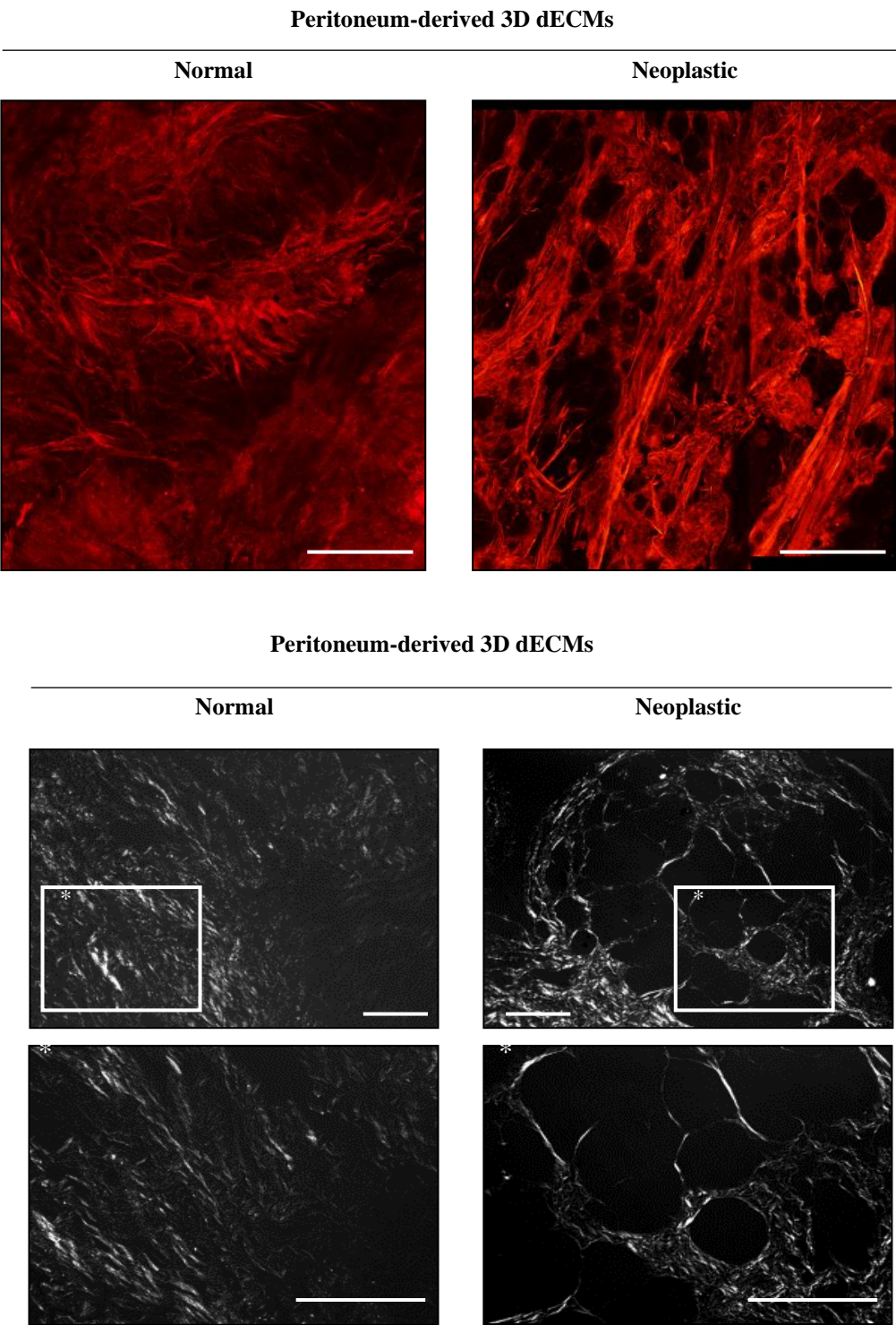


Figure 35. Confocal reflectionl and polarized light microscopy analysis of the peritoneal-derived 3D-dECMs samples. Scale bar: 50 μ m.

The data I obtained show that the 3D-dECMs of normal tissues had a higher density and clusters of collagen fibers, with random relative orientation. In the neoplastic 3D-dECMs the collagen structure appeared more irregular and porous, although a tendency towards fiber alignment and formation of bundles on a larger scale can be observed (Figure 35).

After that, I performed a topographical analysis of the decellularised matrices using the AFM technique. I observed an asymmetric distribution of collagen at the micrometer scale: matrices derived from normal tissues are organized in groups of very thin, intersecting fibers (with diameters below 50nm), characterised by a variety of orientations, while matrices derived from neoplastic tissues had a more corrugated and disordered surface pattern (Figure 36).

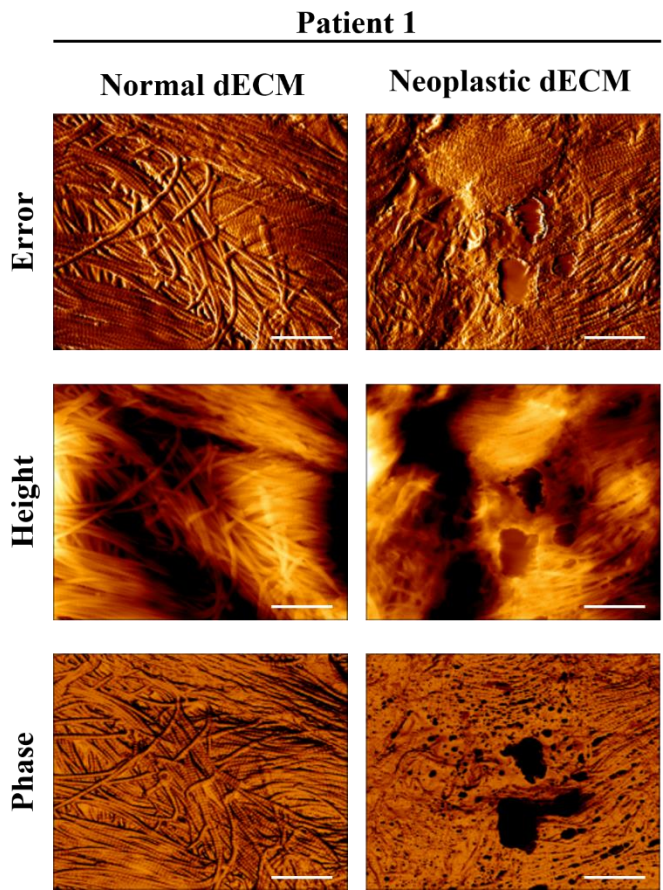


Figure 36. Topography analysis of peritoneal-derived 3D-dECMs. Phase, height, and peak force error images of both normal and neoplastic decellularised matrices are shown. Scale bar: 1 μm .

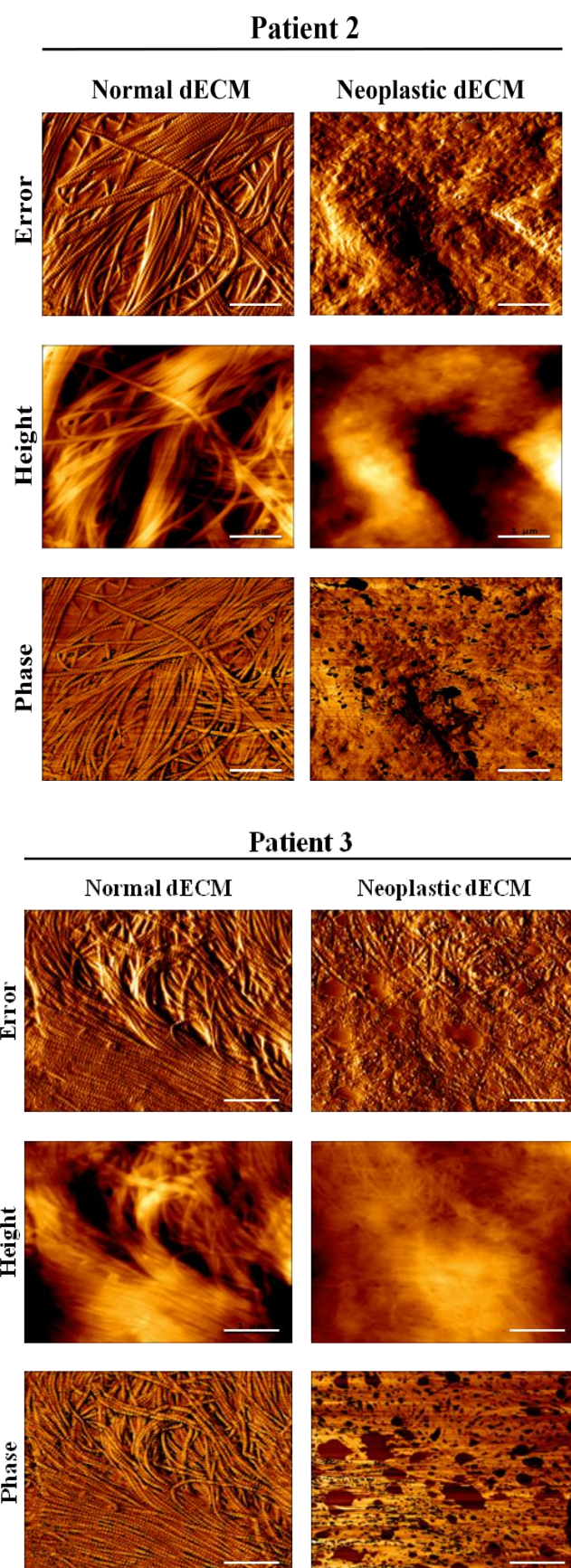


Figure 36. Topography analysis of peritoneal-derived 3D-dECMs. Phase, height, and peak force error images of both normal and neoplastic decellularised matrices are shown. Scale bar: 1 μm .

In contrast to what was published in a previous work on 3D-dECMs from CRC, where there was a clear tendency of collagen fiber to form aligned bundles as well as an increase in the anisotropy of the neoplastic tissue (M. Nebuloni et al. 2015), the collagen fibers of the PM-derived neoplastic 3D-dECMs did not form aligned bundles, although at this small scale the neoplastic matrix appears structurally more compact than the normal ECM. More importantly, the increased anisotropy of the ECM structure, in the case of the CRC, is more evident in the optical confocal image of the neoplastic sample, as I showed in Figure 35, according with data already published (M. Nebuloni *et al.* 2015).

To check if the decellularisation protocol can modify the total protein level of the fundamental components of the ECM, I verified the total amount of collagen and GAG in the 3D-dECMs derived from normal and neoplastic PM tissue. As showed in Figure 37, I noticed that collagen was less abundant in neoplastic tissue than in normal tissue; however the latter showed higher levels of glycosaminoglycans, GAGs. This finding is very important, indicating that the ECM derived from tumour tissue is enriched in GAG composition. GAGs are a fundamental player in the metastatic process; In fact, GAGs are the most source of chondroitin sulphate, which is involved in the bond with the CD44 receptor, widely expressed by the circulating neoplastic cells, that has a role in tumour spreading.

Moreover, I verified that both collagen and GAG levels decreased in the decellularised samples, indicating that the decellularisation procedure resulted in a loss of collagen and GAGs of about 20%, in line with other similar results on 3D-dECMs (L. Genovese *et al.* 2014, M. Piccoli *et al.* 2018, Chen *et al.* 2016, M. Nebuloni *et al.* 2015, Pozzobon *et al.* 2016) (** $p < 0.01$; Figure 37).

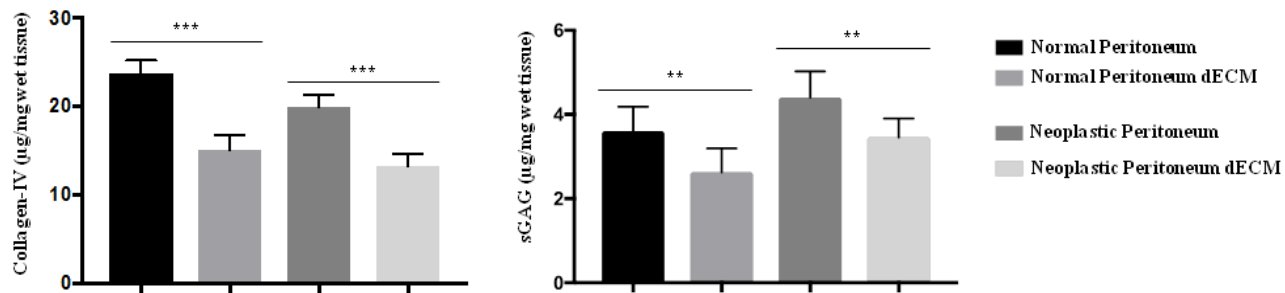


Figure 37. Quantification of total collagens I/IV (left) and total sulphated glycosaminoglycans (sGAG), (right) on fresh and decellularised peritoneal tissues. Student's *t*-test (** $p < 0.001$ and ** $p < 0.01$).

Finally, I studied the variations in the stiffness of the decellularised matrices, both neoplastic and normal, comparing their values. The results obtained showed that the neoplastic 3D-dECMs presented a broader distribution of Young Modulus (YM) values and were markedly stiffer than the normal 3D-dECMs (Figure 38).

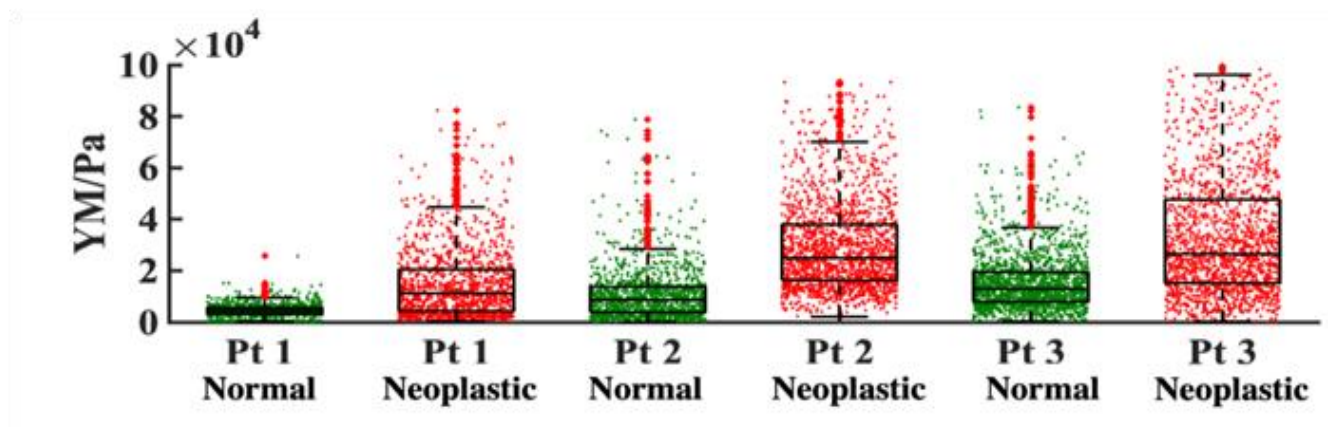


Figure 38. Distribution of the YM/Pa (Young Modulus/Pascal) values obtained for each patient (Pt) and condition (Normal and Neoplastic). Box plots: each dot represents the YM value from a single FC (Force Curve); the quartile group, outliers and median values are highlighted.

I noticed that the YM distributions are considerably scattered, and a significant overlap is present between the normal and the neoplastic 3D-dECMs. This finding highlight that the ECM is a complex system that remains locally heterogeneous on the scale of several typical

cellular lengths, i.e., 10-100 μm , because the transition from the normal to the neoplastic condition, in terms of change of stiffness and structural organization, is not uniform across the whole tissue (Figure 39). Despite this observed heterogeneity, the median values of the YM measured in the different conditions indicated that the stiffening is statistically significant for all the three patients used for the analysis. In fact, the data showed in Figure 40 confirmed these observations, where the results were normalized to the mean YM value of the normal-derived samples.

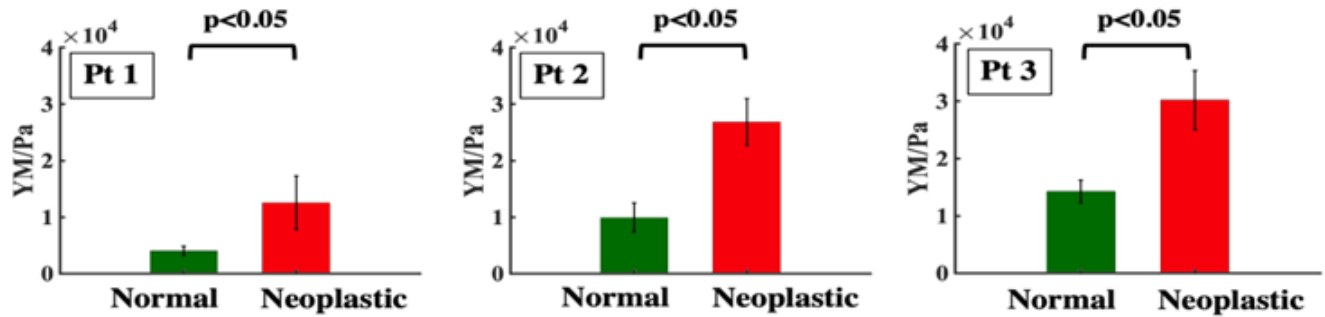


Figure 39. Result of the statistical analysis of the YM value for each patient and condition tested. The bars and error bars represent mean, median YM values and effective SEM (Standard Error of the Mean), respectively, calculated as described in Materials and Methods.

Of Note, the strongest relative stiffening in the tumor tissue, with an increase in the YM value of more than 200%, was measured in the tumor sample of the the youngest patient. Overall, the YM and the relative increase in stiffness correlate with the age of the patients: the YM tends to increase with age, although its relative increase is smaller, suggesting a greater propensity for ECM remodeling in younger individuals. The stiffness of healthy tissues increases with the age of the patient. The relative stiffening in the neoplastic tissues appears to be related to the aggressiveness of the tumor, which, in our study, was greater in the younger patient, confirming that tumor stiffness favors its metastatic spread (Figure 41).

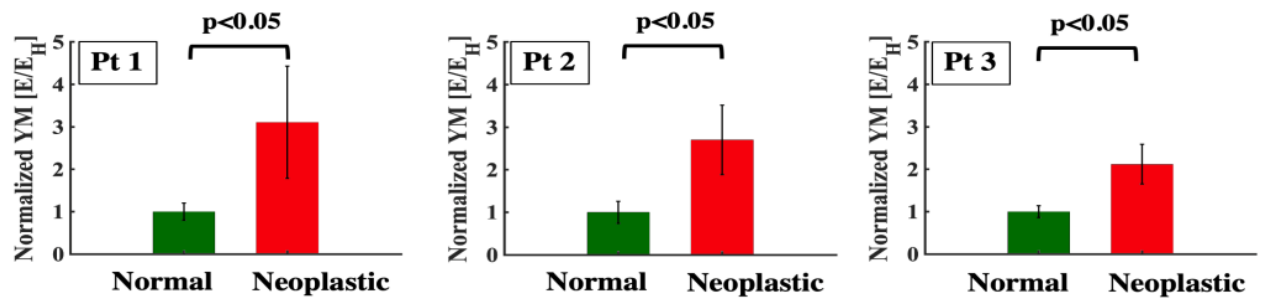


Figure 40. Results of the statistical analysis normalized to the YM value of the normal samples. The bars and error bars represent mean, median YM values and effective SEM (Standard Error of the Mean), respectively, calculated as described in Materials and Methods.

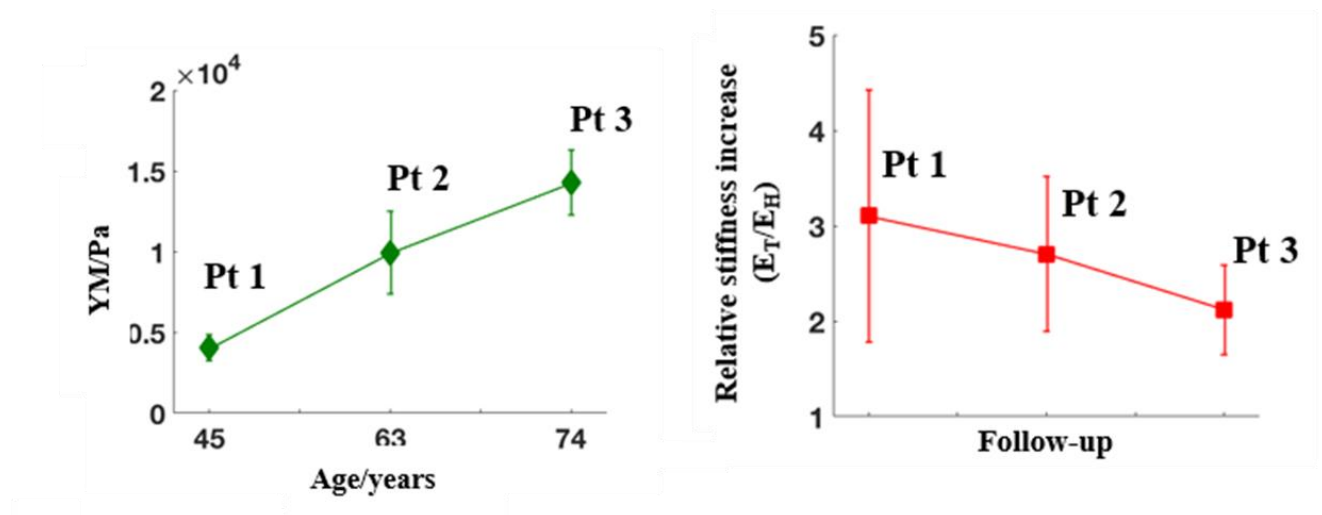


Figure 41. YM values of the cases analysed. The rigidity of the healthy tissues clearly increases with the age of the patient (e.g., the YM value of the neoplastic 3D-dECM of Pt1 is comparable to the YM of healthy 3D-dECM) (left panel). Instead, on the right, the relative stiffening seems to be associated with tumour aggressiveness (right panel)

7.5 Decellularised scaffolds sustain PM-derived organoid growth

To develop an *in vitro* model of the PM disease, I repopulated the 3D-dECMs, derived from normal and neoplastic samples with three TDO lines with mutational profiles that

resemble the most common gene alterations in CRC: the *KRAS*-mutant C1 line, the *BRAF*-mutant C2 line and the *FGFR1* amplified C3 line.

Based on literature data, which show that colonization of decellularised matrices takes eight to twelve days, I chose to grow organoids on the matrices for five, 12 and 21 days (Chen *et al.* 2016, L. Genovese *et al.* 2014, M. Nebuloni *et al.* 2015, E. Weijing *et al.* 2021). The results showed that, five days after seeding, C1 organoids were localized along the perimeter of the 3D-dECMs generated from normal peritoneum. I observed a similar distribution 12 and 21 days after seeding, with a slight increase in the number of cells in the stromal region. Regarding the 3D-dECMs generated from neoplastic peritoneum, instead, C1 TDO were distributed throughout the matrix five days after seeding, and colonization was evident with high stromal infiltration on day 21 (Figure 42 and Appendix B, Figure 1A).

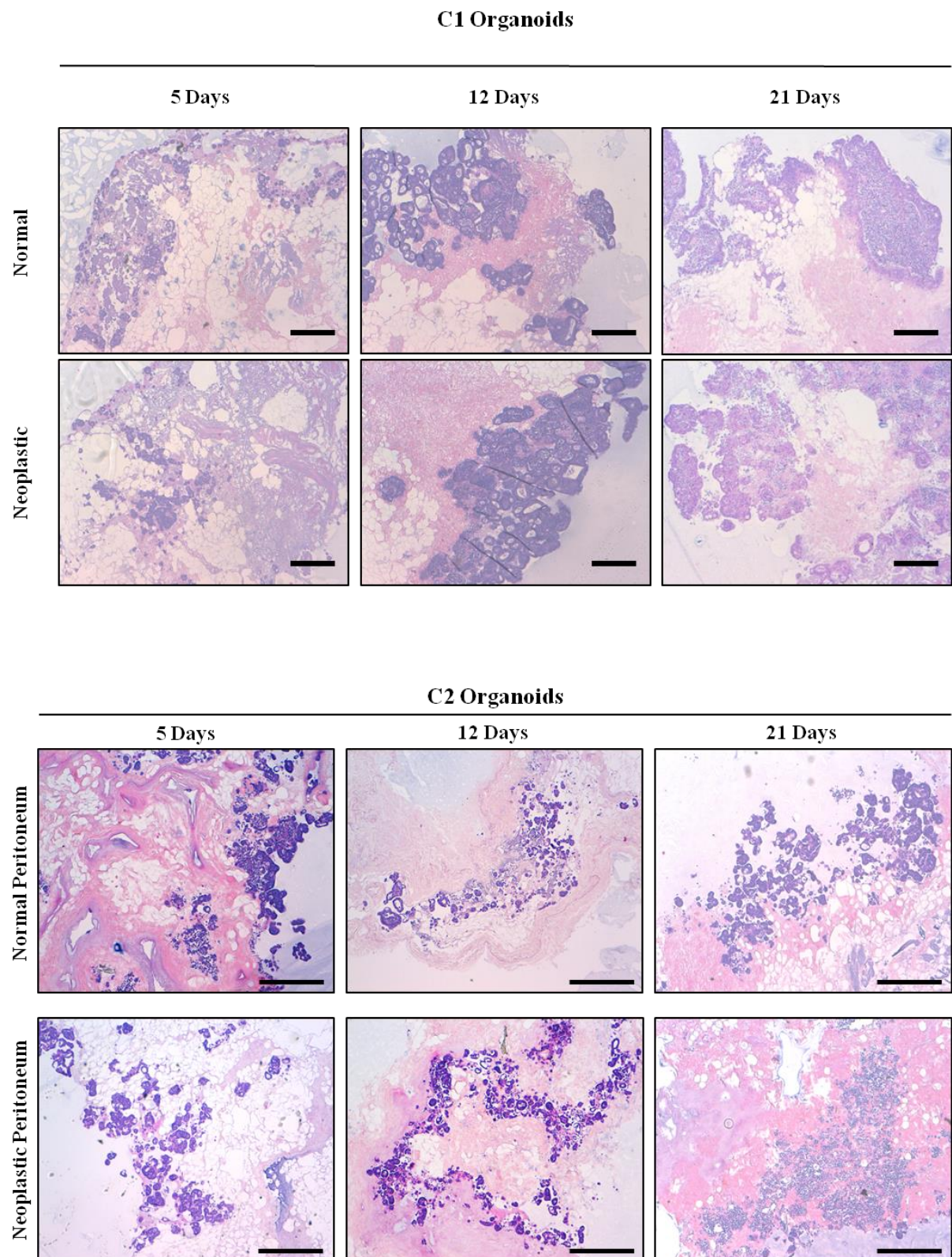


Figure 42. H&E staining of Peritoneum-derived 3D-dECM matrices derived from normal (top) or neoplastic (bottom) peritoneum repopulated with PM-TDO (C1 upper panel, C2 lower panel) as indicated. Scale bar: 50 μ m. The repopulation experiments were performed in triplicate.

I noticed that the morphological characteristics and the efficiency of TDO infiltration appears to be related to the pathologic grade and differentiation state of their tumours of origin. In fact, organoids deriving from a metastatic grade III/G2 lesion, with a moderate undifferentiating and low invasive ability (C1), infiltrated into the 3D-dECM as single cells, while organoids originating from grade IV/G3 poorly undifferentiated tumours with either BRAF mutation (C2) or FGFR1 amplification (C3) infiltrated into the 3D-dECMs and maintained the spheroid shape (Figure 42, Appendix B: Figure 1A).

7.6 3D decellularised scaffolds support the proliferation of organoids

I investigated the different contribution of both normal and neoplastic-derived 3D-dECMs on the TDO proliferation rate and on their ability to maintain the stem cell pool through an immunofluorescence analysis on FFPE sections derived from the repopulated 3D-dECMs using antibodies that recognize Ki-67 and LGR5 proteins to mark proliferating and stem cells, respectively. Results showed that 3D-dECMs generated from neoplastic peritoneum had a significantly higher percentage of Ki-67-positive cells 5 and 12 days ($***p<0.001$) after seeding, indicating that these organoids underwent a faster growth (Figure 43 and Appendix B: Figure 1B, 1D, 1E).

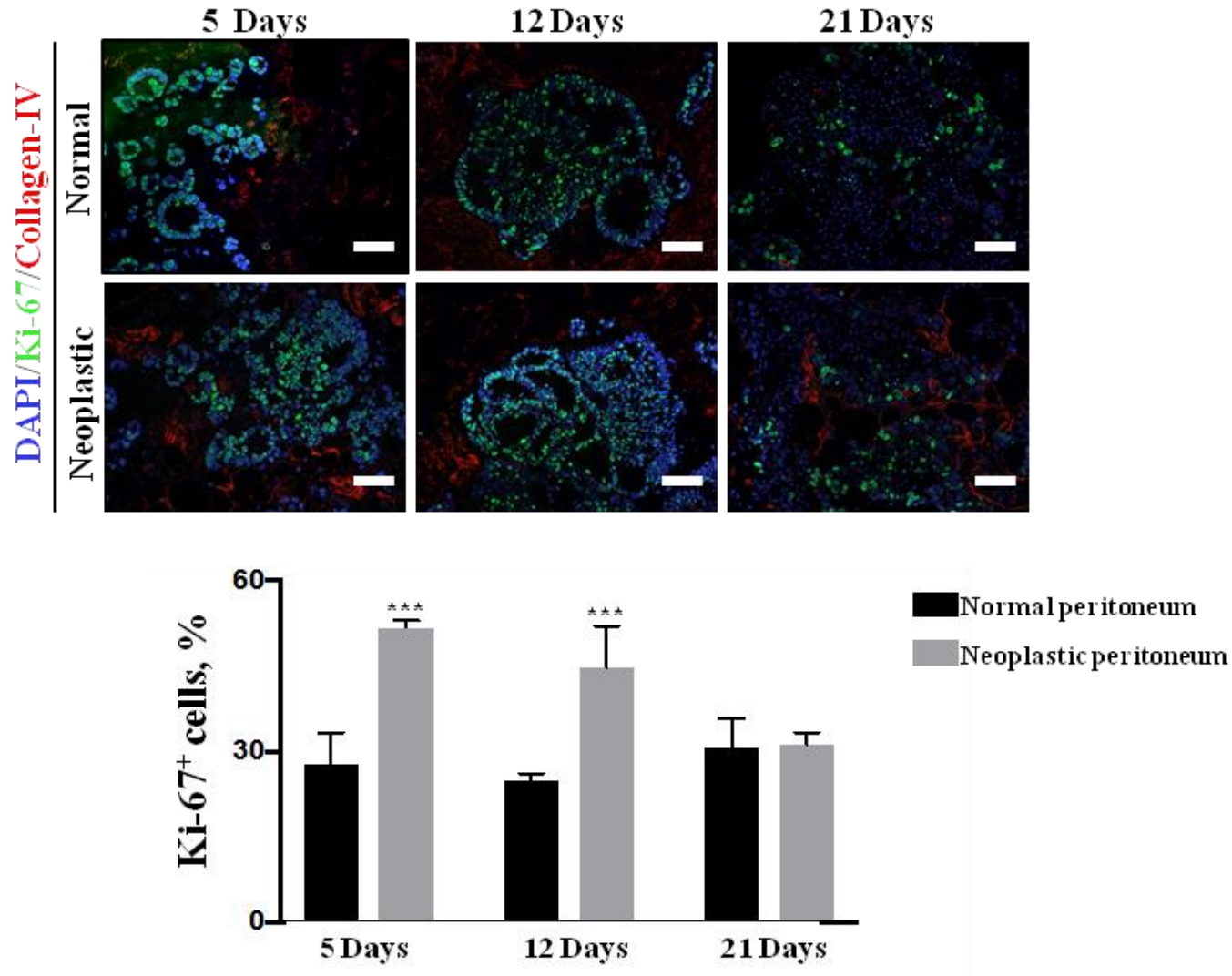


Figure 43. IF analysis of 3D decellularised matrices derived from normal and neoplastic peritoneum repopulated with PM-derived organoids (C1) using Ki-67-positive (green) and collagen IV-positive (red). The samples were counterstained with DAPI (blue). Scale bar: 20 μ m. The bar plot shows the proliferation rate of PM-derived organoids measured as the percentage of Ki-67⁺ cells present in fields devoid of dead cells. Five fields per experiment (40X magnification) were counted. Data are presented as median and SD for surgical specimens of three patients. One-way ANOVA (***) $p < 0.001$.

After 12 days of growth, the positive fraction for Ki-67, was lower than that of cells cultured for five days; however, at both timepoints the Ki-67-positive fraction was greater in cells grown on a neoplastic matrix than in those cultured on normal matrix, showing that the neoplastic 3D-dECM promotes TDO proliferation.

I did not observe any differences in TDO proliferation 21 days after seeding, probably because the organoids had reached plateau condition, no longer having the physical space needed to grow.

Regarding the maintenance of the stem cell pool of the TDO grown on the 3D-dECMs, the LGR5-positive staining showed that the stem cell pool was maintained in both the normal and neoplastic 3D-dECMs five and 12 days after seeding. At day 21 the stem cell pool was significantly lower in 3D-dECMs generated from the normal peritoneum compared to the 3D-dECMs generated from neoplastic peritoneum (Figure 44, Appendix B: Figure 1C, 1E and 1F). Most likely, after 21 days of growth, the cells are at confluence and the pool of stem cells grown on the neoplastic matrix has an environment that favours the maintenance of its phenotype.

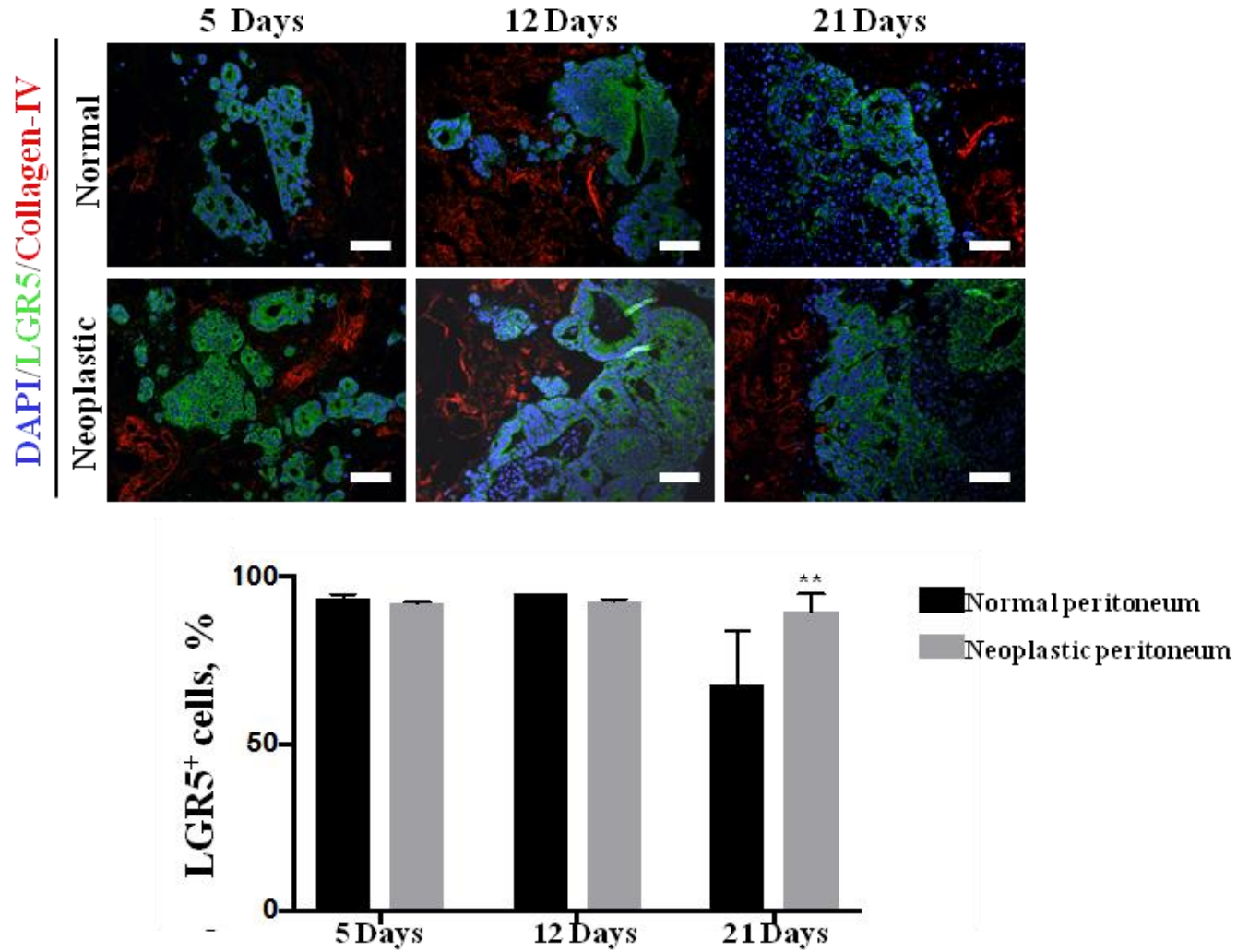


Figure 44. IF analysis of 3D decellularised matrices derived from normal and neoplastic peritoneum, repopulated with PM-derived organoids (C1) using LGR5-positive (green) and collagen IV-positive (red) antibodies as indicated. The samples were counterstained with DAPI (blue). Scale bar: 20 μ m. The bar plot shows the amount of stem cells in PM-derived organoids, measured as the percentage of LGR5⁺ cells present in fields devoid of dead cells. Five fields per experiment (40X magnification) were counted. Data are presented as median and SD for surgical specimens of three patients. One-way ANOVA (** $p < 0.01$).

7.7 *ex vivo* engineered PM lesions reproduce the patient's PM

To compare the similarities of C1, C2 and C3 PM-derived organoids grown on 3D-DECMs derived from the neoplastic peritoneum with the original patient lesions, I tested by IHC the colorectal markers CKA1-CKA3, CK19, CK20 and CDX2 on the organoids, on tissue derived from the PM of origin and on the repopulated 3D-DECMs.

The data obtained clearly demonstrated that the repopulated 3D-dECMs derived from the neoplastic tissue summarise the main characteristics of their tumour of origin. In particular, they preserve the same protein expression, usually observed in the corresponding patient lesion (Figure 45 and Appendix C: Figure 1A and 1C).

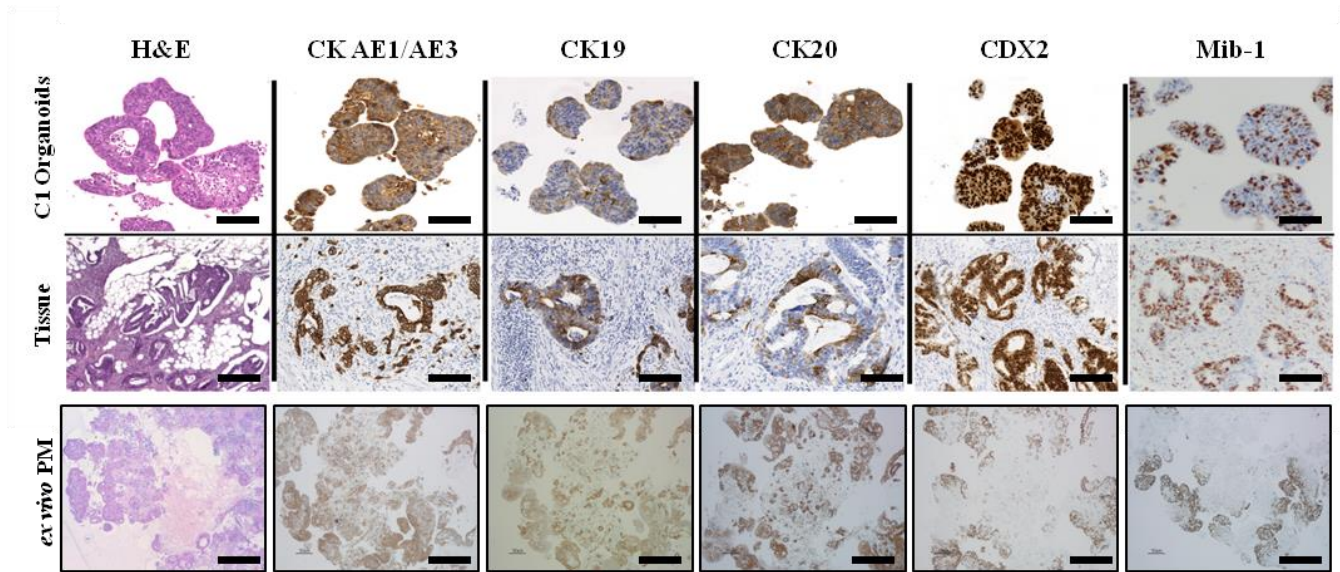


Figure 45. Comparative histological and immunohistochemical images of PM-derived organoids (C1) versus their corresponding tumour of origin and the *ex vivo* engineered PM lesion. Samples were analysed for the expression of the CRC-specific markers: CK AE1/AE3, CK19, CK20, CDX2, and Mib-1. Scale bar: 100 μ M. Images in the first two lanes were previously published (F. Bozzi *et al.* 2017).

Regarding the main morphological characteristics, I noticed that the repopulated 3D-dECMs of neoplastic derivation presented the typical histological features observed in PM patients, such as: i) signet ring cells, ii) bizarre mitotic figures, iii) necrotic debris, iv) pleomorphic cell size and shape and v) multinucleated cells (Figure 46 and Appendix C: Figure 1B and 1D). Interestingly, signet ring cells have only been reported once in an *ex vivo* model system (X. Tian *et al.* 2018), highlighting that the *ex vivo* engineered PM lesion model I generated recapitulates almost all the features typically present in the *in vivo* lesions.

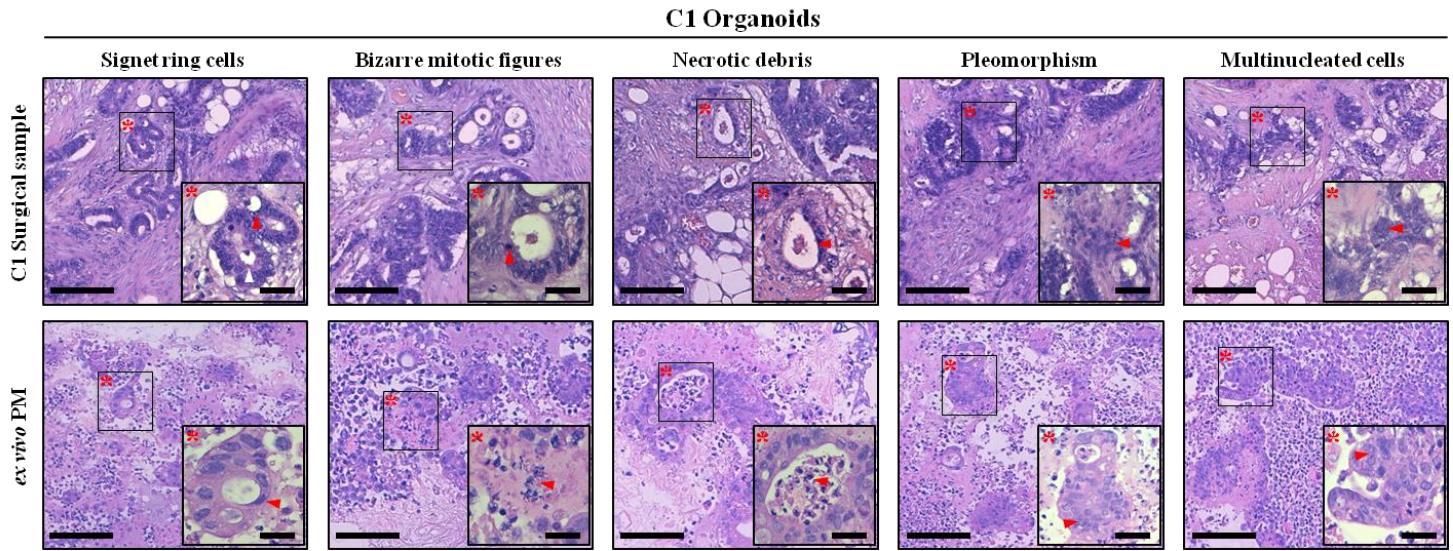


Figure 46. Histological analysis of peritoneal metastasis and neoplastic-derived 3D-dECMS repopulated with C1 PM-derived organoids. The *ex vivo* engineered PM lesions present histological features that are typical of PMs of gastrointestinal origin. Asterisks and arrows indicated the main morphological features. Scale bar: 20 μ m.

Interestingly, signet ring cells have been reported only once in an *ex vivo* model system (X. Tian *et al.* 2018), highlighting that the *ex vivo* engineered PM lesion model I generated recapitulates almost all the features typically present in the *in vivo* lesions.

7.8 Gene expression analysis of engineered PM lesions

To better understand the role of the ECM in the development of the peritoneal metastatic niche I performed a 3' RNA-sequencing (RNA-seq) to address the contribution of the different substrates (normal-derived 3D-dECM, neoplastic-derived 3D-dECM and Matrigel) on the behavior of organoid cultures. Analyses of the transcriptomic data were performed using the following datasets: GO BP, KEGG and Reactome. Moreover, we applied also the Matrisome dataset, which is a searchable database that provides live cross-referencing to gene and protein databases for every ECM and ECM-associated gene (A. Naba *et al.* 2016, Shao *et al.* 2019). Results highlighted differences between TDO grown on 3D-dECMs and Matrigel substrates. 327 differentially expressed genes (DEGs, 153 genes were up-regulated, while 174 genes were down-regulated) were identified in TDO grown on

normal 3D-dECMs, and 144 DEGs (106 genes were up-regulated, while 38 genes were down-regulated) were identified in TDO grown on neoplastic 3D-dECMs compared to TDO grown in Matrigel ($|FC| > 1.5$ and adjusted p -value < 0.05). The most represented biological processes include cell-cell/cell-matrix interactions, organoid behavior and interactions with the ECM, angiogenesis, metal ion homeostasis, and response to external stimuli. 3D-dECMs deregulated many genes fundamental for the 3D-architecture/organization of the ECM. Many of the up-regulated genes identified in TDO grown on neoplastic 3D-dECM were assigned to the Matrisome database (67% for neoplastic versus normal 3D-dECM, and 25% for neoplastic 3D-dECM versus Matrigel). Only 8% of the up-regulated genes identified in TDO grown on normal 3D-dECM versus TDO grown in Matrigel belonged to the Matrisome database (Figure 47).

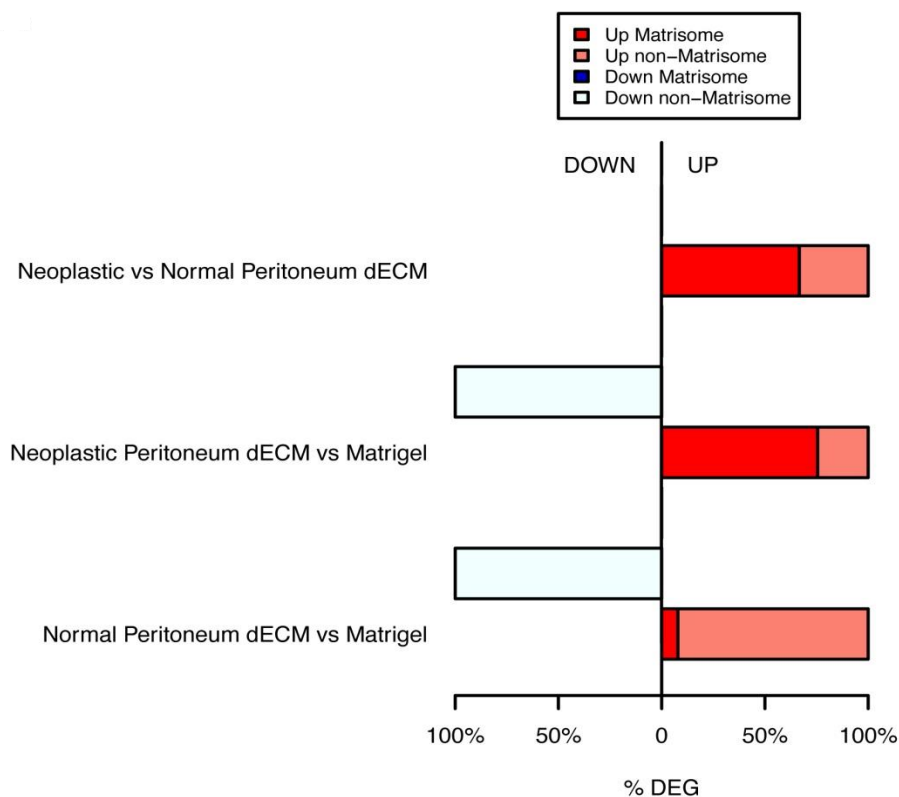


Figure 47. Percentage of up- and down-regulated genes belonging to the Matrisome dataset, in organoids grown on 3D-dECMs compared to Matrigel or in neoplastic versus normal 3D-dECM.

Unsupervised hierarchical clustering of TDO highlighted a clear separation between neoplastic 3D-dECM and Matrigel substrates, with normal 3D-dECM closer to the Matrigel, (Figure 48)

An unbiased analysis of GOs evidenced multiple functional categories related to processes like cell-cell/cell-matrix interactions and crosstalk, tumour-like environment, and ECM interaction/remodeling. I analysed the relative expression of the DEGs of these GOs across the different substrates and the results showed that both normal and neoplastic-derived 3D-dECMs presented an over-representation of DEGs involved in the composition, regulation and modulation of the ECM when compared to Matrigel. Organoids grown on Matrigel instead showed a downregulation of DEGs related to the Matrisome dataset. When compared to the Matrigel, peritoneal-derived scaffolds also up-regulate genes involved in the regulation of the angiogenesis process, the response to cytokine stimuli, the integrin pathway and copper and zinc metabolism. Moreover, the neoplastic-derived 3D-dECMs up-regulate the same GOs compared to the normal 3D-dECM (Figure 48, 49 and Appendix D: Figure 1A, 1B, 1C and 1D).

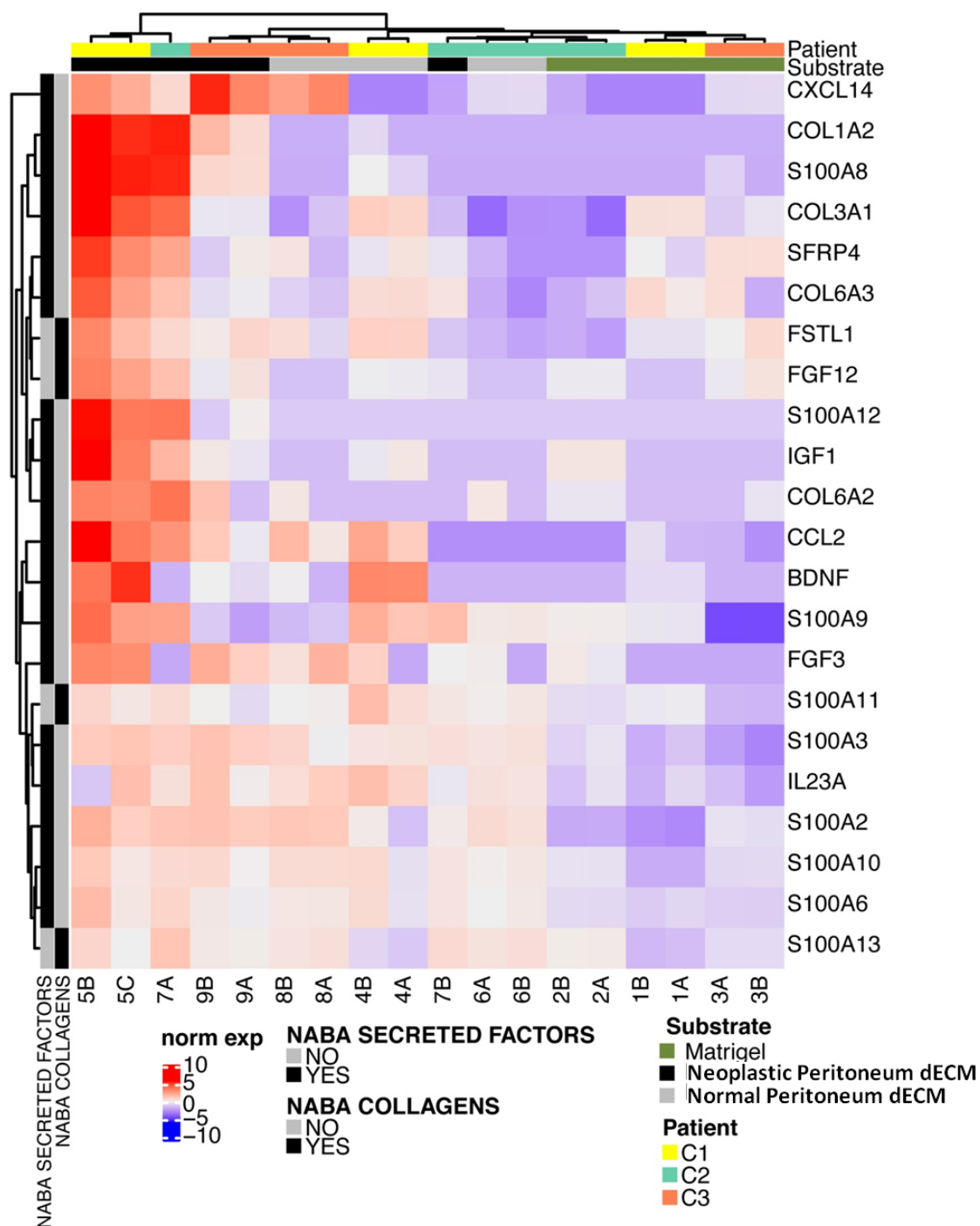


Figure 48. Unsupervised hierarchical clustering of the TDO growing onto neoplastic 3D-dECM vs normal 3D dECM vs Matrigel, according to the expression of the top DEGs included in Naba Secreted Factors and in Naba Collagens categories, which are the more functionally related categories to ECM functions. ($|FC| > 1.5$ and adjusted p -value < 0.05).

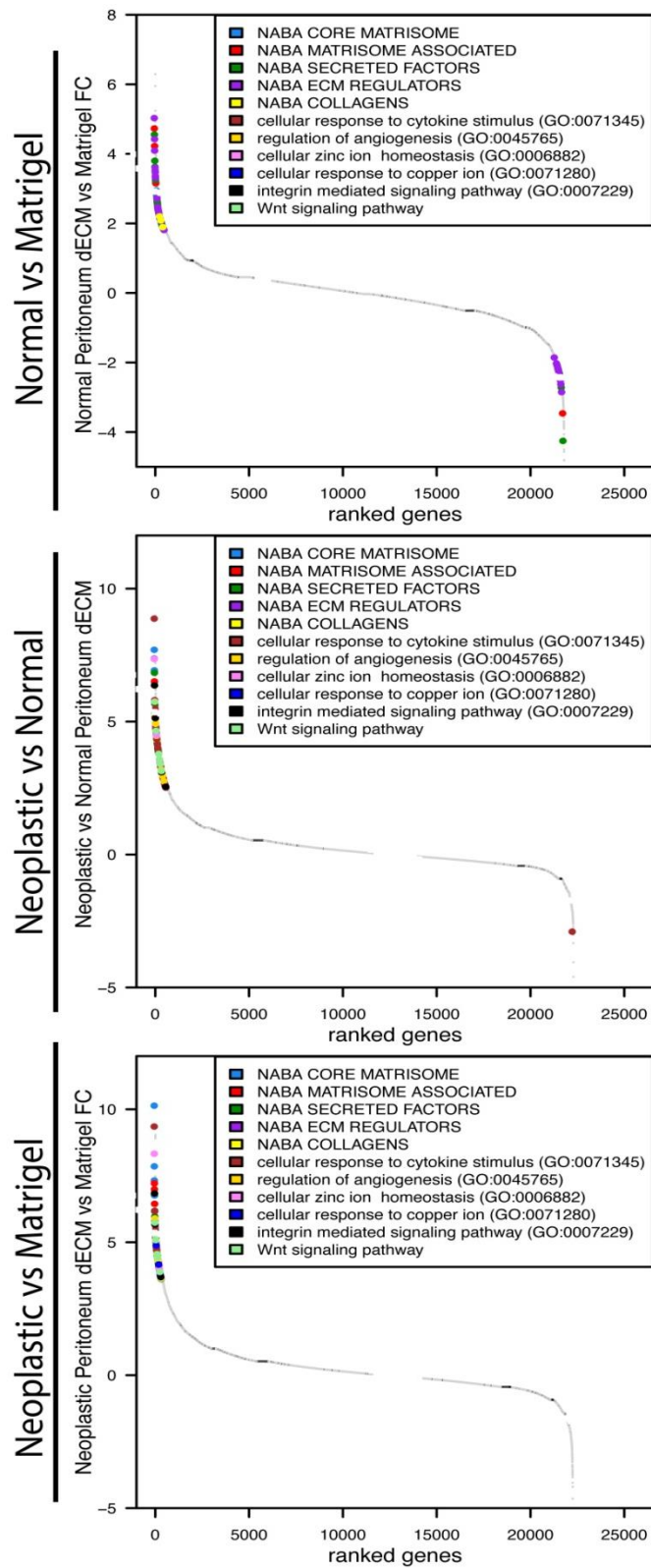


Figure 49. Expression levels of the top 100 deregulated genes belonging to the indicated gene sets identified in the comparisons of NvsM, NvsN and NvsM. Gene ranks for relative fold change are shown on the x-axis and the logFCs on the y-axis.

After that, I selected some gene sets related to the matrisome dataset, such as Naba Core Matrisome, Naba Secreted Factors, Nab ECM Regulators, Naba Glycoproteins, Naba Proteoglycans and Naba Collagens, all mediating several key features of the ECM’s remodeling during cancer development. I found that all these gen sets were differentially expressed in peritoneal-derived 3D-dECMs when compared with Matrigel. I also noticed that Neoplastic-derived 3D-dECMs overexpressed some genes related to the categories “core composition of the ECM” (COL1A2, POSTN, SRGN, MFAP4, SPARC, *p-value: 0.003365*) and “interactions/regulation of the ECMs through secretion of specific factors” (S100A8, S100A12, SFRP2, IGF1, CCL21, HTRA3, SERPFIN1, VEGF, *p-value: 0.00365*) (Figure 50 and Appendix D, Figure 1E, 1F, 1G and 1H).

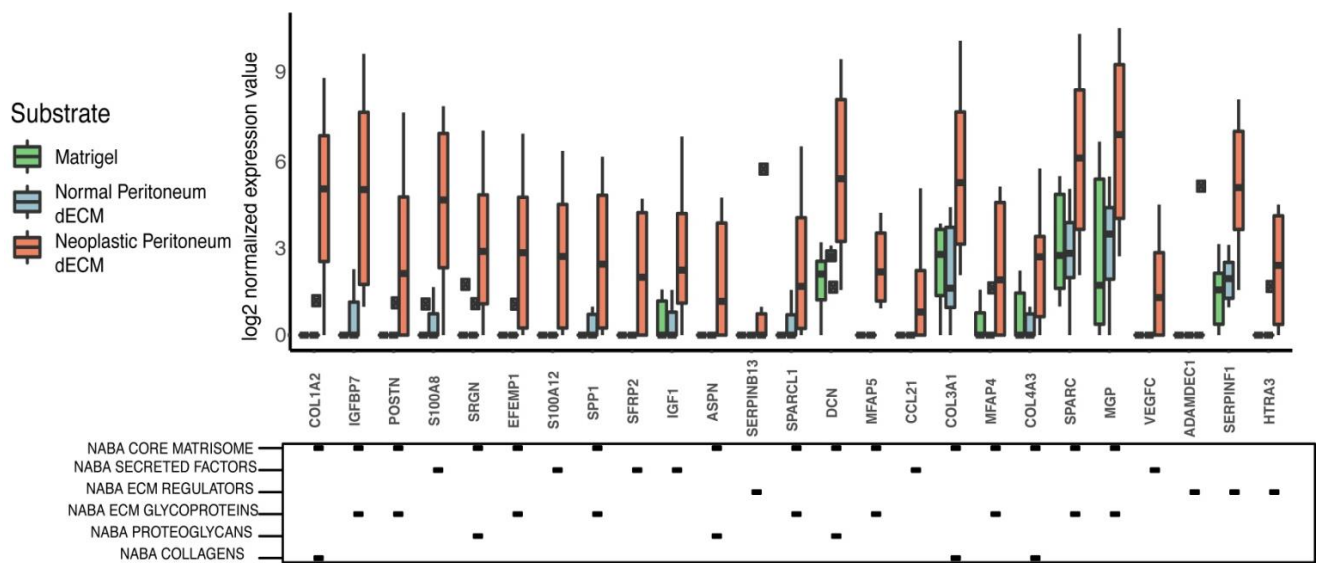


Figure 50. Box plot showing the expression of genes selected for their involvement in the indicated processes of the Naba Matrisome datasets. The median and interquartile range are displayed as horizontal lines. The black squares in the bottom panel indicate which category the genes belong to.

I also observed that peritoneal-derived 3D-dECMs, and in particular the neoplastic ones, showed higher expression of genes involved in the categories “stem cells pathways” (SFRP2, WNT7A,SERPFIN1, CAMK2A), in “cellular response to cytokine and zinc/cooper ions”

(S100A8, MMP3, COL1A2, MT1MCCL2, DCN) and in genes related to the KEGG categories “integrin pathway” and “regulation of angiogenesis” (THY1, PLEK, COL3A1, VEGF) when compared with normal-derived 3D-dECM and Matrigel (Figure 51 and Appendix D: Figure 1E, 1F, 1G and 1H). These results showed that the PM-derived organoids cultured in neoplastic-derived 3D-dECMs were different from those cultured in normal-derived 3D-dECMs and Matrigel, with up-regulation of genes related to ECMs regulation/composition and relevant biological processes such as cytokine stimuli, integrin pathway, zinc ion homeostasis, regulation of angiogenesis (Figure 51 and Appendix D: Figure 1E, 1F, 1G and 1H).

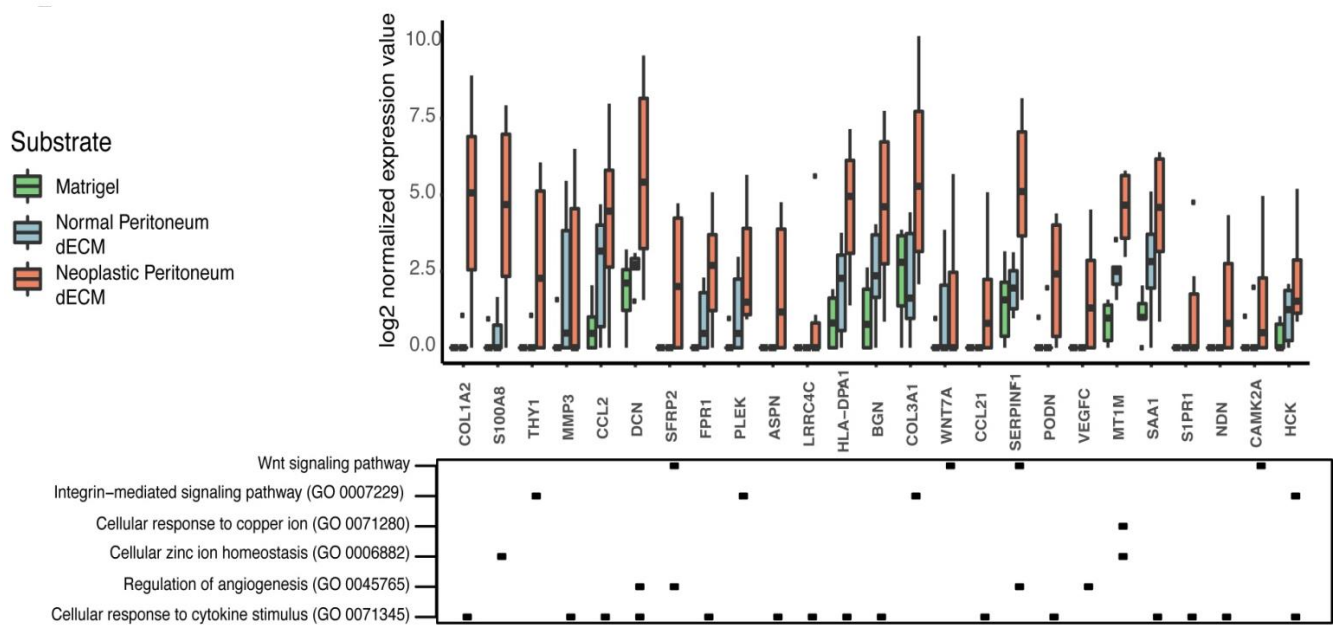


Figure 51. Expression of genes selected for their involvement in the indicated processes of GO BP and KEGG databases. The median and interquartile range are displayed as horizontal lines. The black squares in the bottom panel indicate which category the genes belong to.

Finally, I analysed the expression levels of some genes involved in the mechanisms of cell-cell/cell-matrix interaction (FBN2, VWF, EFEMP1, ASPN, THBS2, EDIL3, DPT, IGFBP1), regulation of the stiffness of the ECM (COL1A2, DCN, FBN2, VCAM1, SERPINE1) and in the mechanisms of drug resistance (S100A8, MGP, NNMT, TNFR, LOX). I found that most of

these genes were differentially expressed, with greater upregulation when PM-derived organoids were cultured on neoplastic-derived 3D-dECMs (Figure 52).

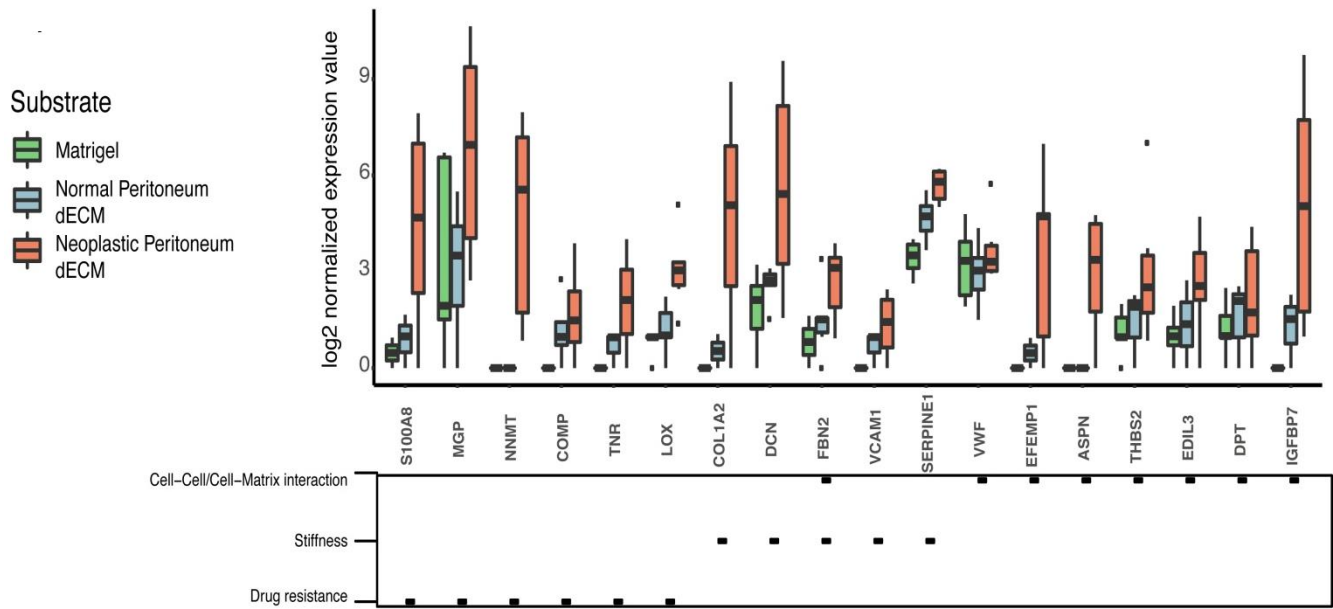


Figure 52. Expression of genes related to the following biological processes: cell-cell/cell-matrix interactions, extracellular matrix stiffness and drug resistance in the three conditions analysed. The median and interquartile range are displayed as horizontal lines. The black squares in the bottom panel indicate which category the genes belong to.

7.9 3D-dECMs decrease the efficacy of HIPEC treatments

To test the hypothesis that recurrence observed after CRS-HIPEC could be caused by the active role of the tumour ECM in response to the drug treatment, I simulated an HIPEC treatment on the repopulated 3D-dECMs using mitomycin-c (MMC) at 35 mg/m², the dose commonly used during CRS/HIPEC for PM patients in our institution. I analysed C1, C2 and C3 TDO grown on Matrigel or on 3D-dECMs of neoplastic peritoneal derivation. I observed that MMC was able to induce cellular disruption in both the conditions analysed, characterised by the presence of nuclear material at cytoplasmic level in both C1 and C3 organoids (Figure 52 and 53).

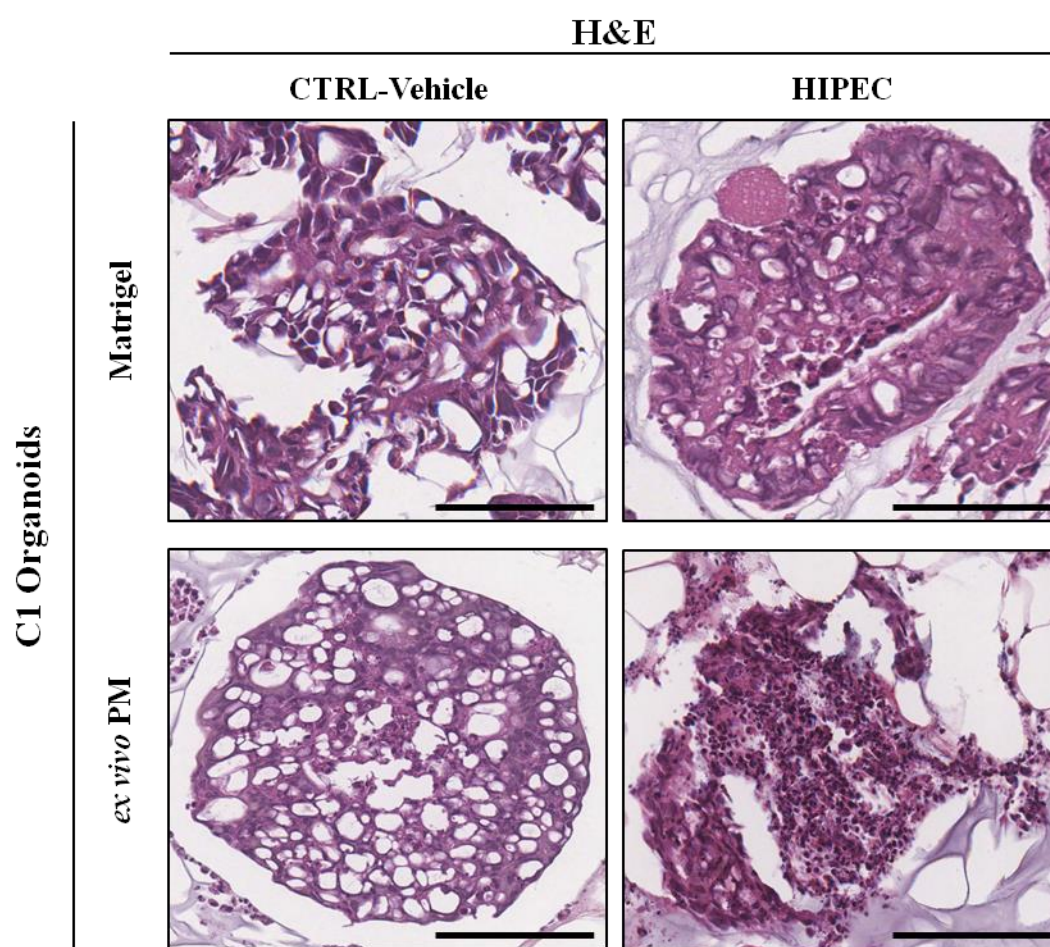


Figure 52. H&E staining of C1 PM-derived organoids cultured in Matrigel and on neoplastic-derived peritoneal 3D-dECMs after *in vitro* HIPEC treatments. Scale bar: 50 μ m.

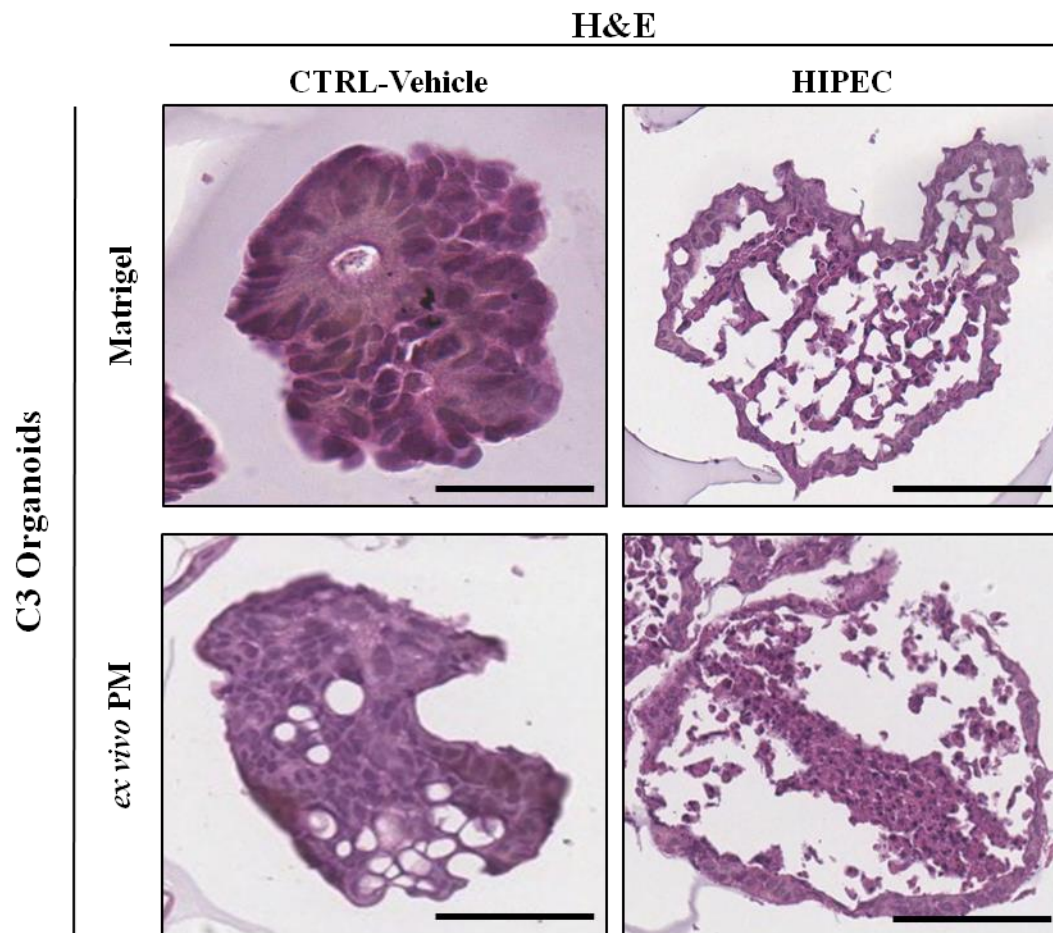


Figure 53. H&E staining of C3 PM-derived organoids cultured in Matrigel and on neoplastic-derived peritoneal 3D-dECMs after *in vitro* HIPEC treatments. Scale bar: 50 μ m.

After that, I evaluated the effects of MMC treatment on proliferation of these two TDO lines by performing IHC immunostaining of Ki-67 and found that the intensity of Ki-67 decreased after treatment with the drug (Figure 54)

Ki-67

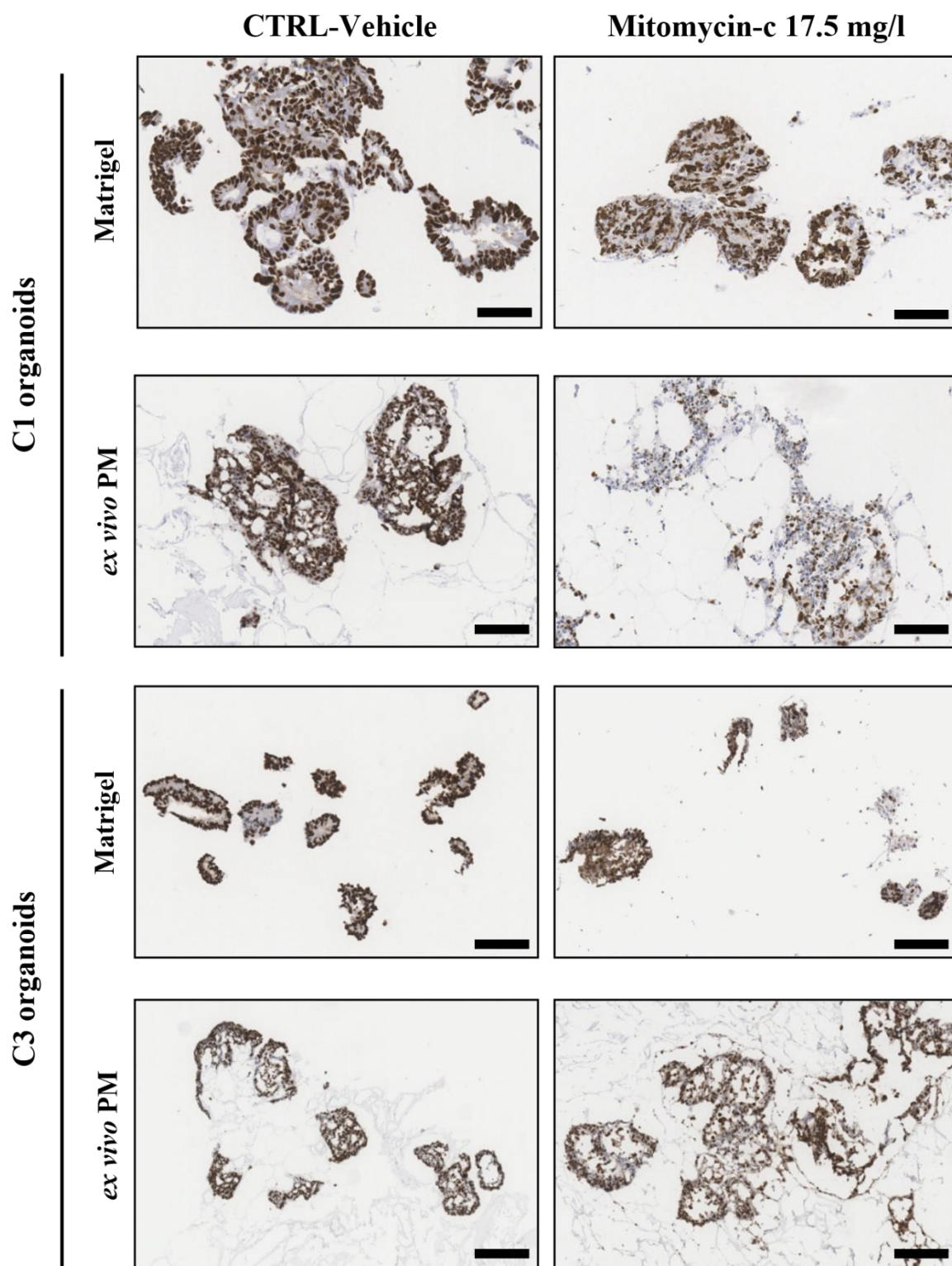


Figure 54. IHC analysis of C1 and C3 PM-derived organoids cultured in Matrigel and on neoplastic-derived peritoneal 3D-dECMs, after *in vitro* HIPEC treatments, using Ki-67 immunostaining showing that presence of the 3D-dECM scaffold decreases treatment efficacy. Scale bar: 50 μ m.

I noticed that the treatment significantly decreased the number of Ki-67-positive cells in C1 TDO cultured both in Matrigel and on the neoplastic-derived 3D-dECMs by 95 % and by 72 % respectively (** $p<0.01$; Figure 54). Also, C3 TDO showed a significant reduction in Ki-67-positive cells, after MMC treatment, of 80 % when cultured in Matrigel, and 66 % when cultured using the neoplastic-derived 3D-dECMs (** $p<0.01$; Figure 54). Moreover, I noticed that 3D-dECM leads to an increase in Ki-67-positive cells after mitomycin treatment (* $p<0.05$, Figure 55).

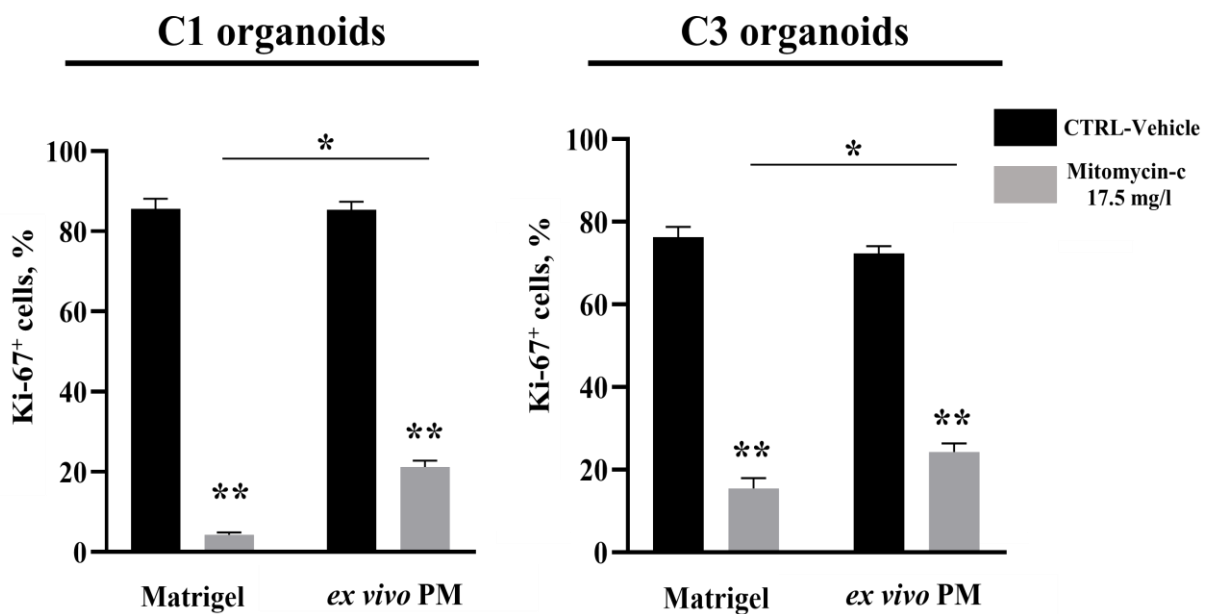


Figure 55. Proliferation rate of PM-derived organoids (C1, left panel; C3, right panel) measured as the percentage of Ki-67⁺ cells present in fields devoid of dead cells. Five fields per experiment (40X magnification) were counted. Data are presented as median and SD for surgical specimens of three patients. One-way ANOVA (* $p<0.05$, ** $p<0.01$).

The data obtained suggest an impact of the ECM on the response to HIPEC treatment.

7.10 HIPEC treatments lead to apoptosis in PM-derived organoids

MMC is an antineoplastic antibiotic that selectively inhibits the synthesis of DNA by cross-linking guanine and cytosine, generating oxygen radicals, alkylates DNA and interstrand DNA cross-links, thereby inhibiting DNA synthesis and favouring cell death through apoptosis (J.B. Barnett *et al.* 2011, I. Ubink *et al.* 2017). For these reasons, I investigated by immunofluorescence the cell death mechanism induced by MMC treatment by analysing the presence of the cleaved form of caspase3 protein, a marker of presence of apoptosis. C1, C2 and C3 TDO cultures were seeded both in Matrigel and onto neoplastic-derived 3D-dECMs and treated with 35 mg/m² MMC. Immunofluorescence staining with cCASPASE-3 of FFPE sections of the samples showed that treatment with MMC induced cleavage of caspase-3 in C1 and C3 TDO (Figure 56). After HIPEC treatment, the percentage of cCASPASE3 positive cells was around 80% for both C1 and C3 TDO lines grown on Matrigel and 60 % 55 % respectively, for C1 and C3 cultured on 3D-dECM of neoplastic derivation (Figure 57). Moreover, data showed that the 3D-dECM leads to a decrease in cCASPASE3-positive cells after mitomycin-c treatment ($p < 0.05$, Figure 56). Taken together, these data demonstrate that HIPEC simulation induces cell death in TDO mainly through apoptotic mechanisms and that the presence of a 3D-dECM of neoplastic derivation results in a lower response to chemotherapy.

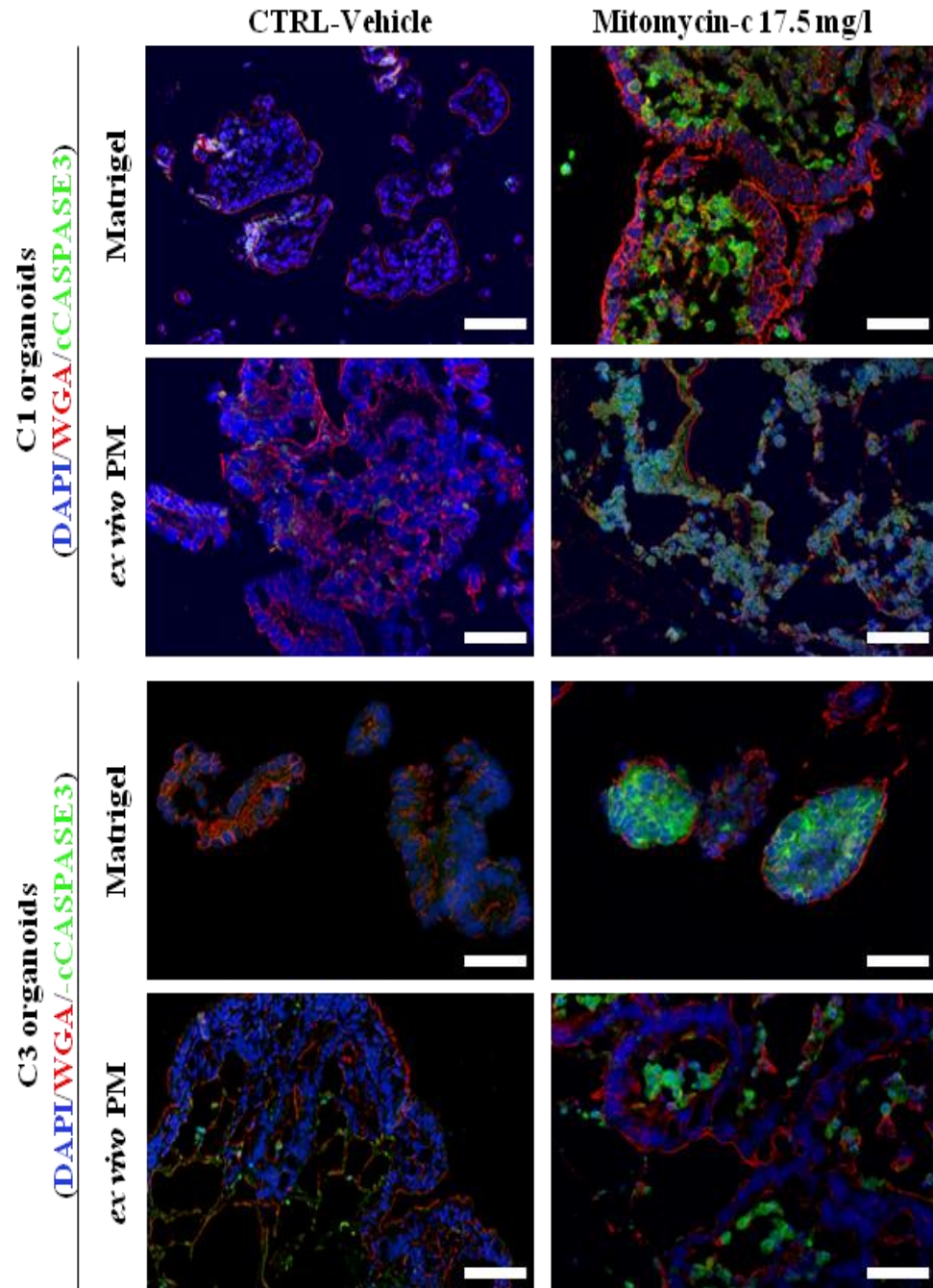


Figure 56. Immunofluorescence analysis of C1 and C3 TDO cultured in Matrigel and on neoplastic-derived peritoneal 3D-dECMs, after HIPEC treatment including mitomycin C and XX as control, using cCASPASE-3 antibody (green). The samples were counterstained with WGA (red) and DAPI (blue). Scale bar: 20 μ m.

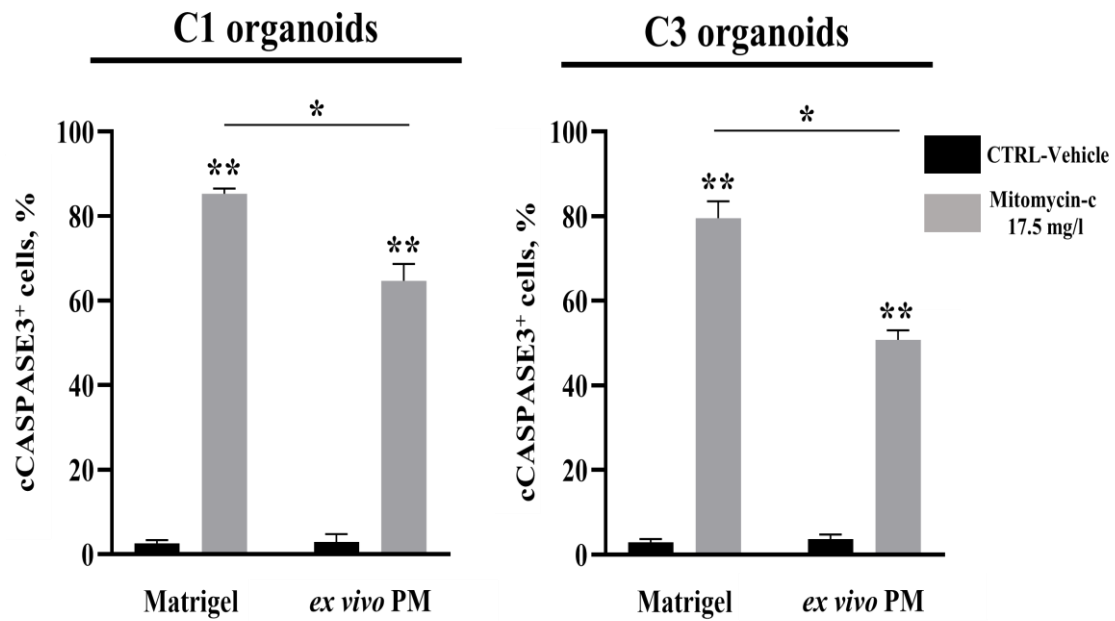


Figure 57. Rate of apoptotic PM-derived organoids (C1, left panel; C3, right panel) measured as the percentage of cCASPASE-3⁺ cells present in selected fields. Five fields per experiment (40X magnification) were counted. Data are presented as median and SD of results from three different experiments. One-way ANOVA (* p <0.05, ** p <0.01).

Regarding C2 TDO, I did not observe presence of cCASPASE3 after MMC treatments both in presence of Matrigel or of neoplastic-derived 3D-dECMs, indicating that they are resistant to MMC treatment (Figure 58).

C2 organoids
(DAPI/WGA/cCASPASE3)

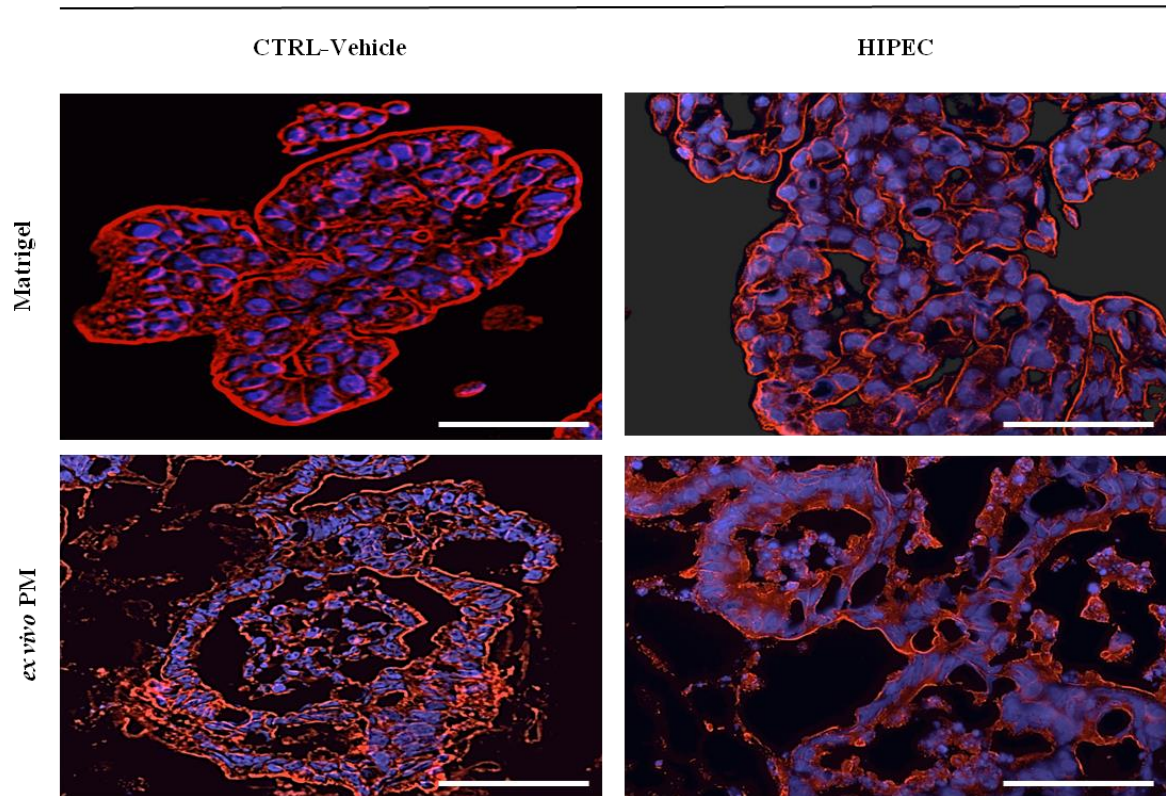


Figure 58. IF analysis of C2 PM-derived organoids cultured in Matrigel and on neoplastic-derived peritoneal 3D-dECMs after *in vitro* HIPEC treatments, using cCASPASE3 (green) antibody. The samples were counterstained with WGA (red) and DAPI (blue). Scale bar: 50 μ m.

8. Discussion

In this thesis I described the engineered model I have developed, which combines key features of TDO within the microenvironment, enabling the recapitulation of the PM niche under physiological conditions. The development of organoids from PM is highly relevant for colorectal cancer patients suffering for a widespread peritoneal disease.

Transcriptome analysis showed that organoids grown on peritoneal matrices express genes involved in pathways that favor the implantation into the matrix and remodelling of the ECM which are less represented when the organoids are grown in Matrigel. The 3D-dECM models reproduce the complex tissue architecture and cell-matrix interactions of the native environment of PM, as evidenced by its full colonization by TDO. 3D-dECMs derived from the neoplastic peritoneum allow the development of a tissue microenvironment that preserves the stem cell pool of TDO, enhancing their proliferation and favoring a repopulation pattern similar to that usually observed *in vivo*. These findings are in line with previous works showing that cancer-derived ECM sustains the proliferation and invasion of CRC cell lines (E. D'Angelo *et al.* 2020).

I also noticed that scaffolds deriving from neoplastic peritoneum showed greater rigidity than those derived from normal peritoneum. The increased rigidity and crosslinking of the perilesional ECM was identified as an environmental modification predisposing CRC invasion (M. Nebuloni *et al.* 2016). The observed stiffening of the neoplastic ECM can be partially attributed to the more compact fine structure of the matrix and to the linearization of the fibers into bundles, as observed in Nebuloni *et al.* (M. Nebuloni *et al.* 2016). Of note, I observed an increase in GAGs in the perilesional ECM. This evidence can also be related to the increase of the rigidity. Moreover, some authors have highlighted the relation between GAGs and matrix stiffness, showing that negatively charged GAGs provide a repulsive force opposing compression and shear in the ECM (M.D. Buschmann & A.J. Grodzinsky 1995). It has been also demonstrated that GAGs capacity to retain high amounts of water and hydrated

cations confers resistance to compressive forces (M.D. Buschmann & A.J. Grodzinsky 1995), leading to a higher stiffness, especially in tumour-derived samples.

I found that the rigidity of healthy tissues increases with the age of the patient (L.P Ferreira *et al.* 2020); indeed aging has been demonstrated to have a role in fibrotic tissue deposition, leading to an increase of the tissue-stiffness. On the other hand, the relative stiffening in neoplastic tissues seems to be related to the aggressiveness of the cancer, which, in my study, was greater in the younger patient, confirming that tumour stiffness favors its metastatic spread (J. Winkler *et al.* 2020). The high amount of GAGs that I observed in the neoplastic tissues could be a result of the metastatic transformation. In fact, GAGs are the main source of chondroitin-sulfate, which is the main binding site for the isoform v of CD44 that is involved in the metastatic dissemination (F. Zanconato *et al.* 2019). With the transcriptome analysis I also confirmed higher expression of GAGs in the repopulated neoplastic 3D-dECMs. These preliminary results support further investigations with more donors to confirm the observed trends. Moreover, during the last decade, it has been demonstrated that the mechanical properties of the ECM could be involved in the direct reprogramming of the epithelial cells, conferring them neoplastic features via the interactions between YAP/TAZ and specific oncogene aberrations such as RAS signalling (T. Panciera *et al.* 2020). However, GSEA analysis of genes from the YAP/TAZ signaling did not show an enrichment of this specific pathway in the repopulated matrices. To better clarify this result, I have planned to study the localisation of YAP/TAZ proteins in the model by IF analysis.

I noticed that the expression of specific genes that are fundamental for tissue architecture and stiffness, ECM remodelling, fibril generation, epithelial cell differentiation, resistance to compression and regulation of angiogenesis (S.V. Glavey *et al.* 2017, K.A. Robinson *et al.* 2017, H. Nistala *et al.* 2010, M. Schlesinger & G. Bendas 2015, K. Bajou *et al.* 2008) was higher in 3D-dECMs developed from neoplastic tissue compared with 3D-dECMs generated from normal tissue or Matrigel, confirming the ability of the model that I obtained, to

reproduce the PM microenvironment. Through morphological and topographical experiments, I could observe that the neoplastic scaffold undergoes to complex structural modifications that enhance TDO adhesion and proliferation. In support of this concept, both normal and tumour 3D-dECMs showed an upregulation of genes involved in zinc and copper metabolism and homeostasis, which was higher in the neoplastic-derived peritoneal matrix. It is interesting to note that these metal ions are involved in the regulation and activation of the metalloproteinase enzymes, which are the main modulators of the ECM through a proteolytic activity (W. Ceelen *et al.* 2020) and could play a role in the activation of ECM remodeling pathways for the formation of the metastatic niche. All these observations make the model that I develop during my PhD project more attractive than the conventional culture methods with collagen-based scaffolds, which do not mimic real tissue conditions.

Transcriptomic analyses, allow me to demonstrated that repopulated 3D-dECMs presented features typical of the PM disease (D.G. Jayne *et al.* 2002, R. Siegel *et al.* 2014) and expressed genes involved in ECM remodelling, such as NABA Matrisome and stem cell-related genes, ECM regulators and genes involved in the response to cytokine and pro-inflammatory stimuli, integrin interactions and collagen/proteoglycans modifications. These pathways were less represented in normal 3D-dECMs and absent in Matrigel samples, confirming a previous study showing that growth on the ECM of normal colon organoids transfected with mutant *APC* induces features typically associated with CRC progression (H.J. Chen *et al.* 2016). The deregulation of genes belonging to pathways involved in the metastatic process, linked to metastatic spread and the development of the metastatic niche (L. Lemoine *et al.* 2016, S. Varghese *et al.* 2007) observed, is in agreement with the fact that I derived the oganoids from PM metastatic lesions, where the cells activate a series of pathways to better adapt to the niche.

HIPEC simulation experiments highlighted the potential role of the neoplastic ECM in the development of drug resistance. In fact, from the transcriptome analysis I noticed the

activation of mechanisms correlated with drug resistance along with the modification of the mechanical properties of the ECM. In addition, growth on scaffolds increased the expression of anti-apoptotic and pro-survival genes, as well as genes involved in resistance to platin-based drugs. I also observed high expression of stiffness-related genes in PM organoids grown on neoplastic derived 3D-dECMs. It is also clear how the treatment response of the TDO reflects the characteristics of the patient of origin, highlighting how PM-derived organoids could be used as patient avatars for personalized treatment. The engineered model based on the combination between TDO technology and 3D-dECM-derived scaffolds could therefore be a drug screening tool that more faithfully recapitulates the tumour microenvironment and response to treatment for tailored therapies than the classical monoculture 2D models, still used, or even 3D-cultures (C. M. Ghajar 2015).

However, the model that I developed presents some limitations, as it still does not reach a resolution level that allows it to mimic the PM niche in all its constituents. In fact, the other components of the microenvironment play a fundamental role in the spread of PM (M. Bleijs *et al.* 2019, G.S. Hussey *et al.* 2017), such as immune surveillance and the vascular system (C.T. Seebauer *et al.* 2016, L. Mohrmann *et al.* 2020). Moreover, Seebauer and collaborators demonstrated that a failure of immune surveillance during the metastatic remodelling induces senescence of PM cells and promotes overexpression of VEGF-A (C.T. Seebauer *et al.* 2016). Pericytes and mesenchymal stem/stromal cells localized around the blood vessels regulate many functions in response to tumour dissemination, such as inflammation, immune cell activity and angiogenesis, favouring the dissemination of the circulating tumour cells and the development of dormant niches (D. Correa, 2016). For these reasons, further optimization of the model will, therefore, imply the reconstruction of a specialized physiological microenvironment by incorporating vascular networks, the immune system, as well as organ-specific microbes. In addition, the replacement of patient-derived 3D-dECM with a synthetic support with the same biochemical and physical characteristics of the components of the

decellularised matrix will improve the reproducibility of the model and could be used together with TDO, to set up personalized drug tests for selecting the most active drugs to administer to the patient.

The 3D model that I developed could be used as a pre-clinical platform to study the role of tumour ECM in the development of the PM niche. In fact, it represents a physiological tool that can aid the identification of key players in the metastatic development, and may allow the selection of new therapeutic strategies in a biologically relevant setting , also providing a new tool to boost the bench-to-bed-side process to improve patient care. Finally, the approach described here might be used to generate other types of *ex vivo* metastatic niches from different organs, allowing the development of different metastatic niche platforms to study the key biological events that sustain the metastatic spread in a more relevant context.

9. Conclusions

During my PhD thesis, I was able to demonstrate how organoids, obtained from patients suffering from metastases to the peritoneum derived from CRC are able to recapitulate the pathology of the tissue of origin, both in morphological and genetic terms. In fact, the organoids showed positivity to the main histochemical markers commonly used for the diagnosis of this disease, maintaining a mutational profile substantially comparable to that of their tissue of origin. Regarding the use of 3D-dECMs, it was possible to highlight how the decellularisation protocol was able to preserve the main morphological and physical properties of the native ECM. Indeed, the experiments conducted with AFM, showed how the decellularised matrices had morphology and mechanical properties comparable to that of the tissues from which they were derived. This allowed me to use the 3D-dECMs as a scaffold for the growth of TDO and to develop an *ex-vivo* model of the peritoneal metastases with characteristics very close to those commonly observed “*in vivo*”. Finally, I showed that the 3D-dECMs are able to modulate organoid behavior, both in terms of proliferation and

expression of stem cell markers, which is fundamental for maintaining the self-renewal characteristics. All this underlines how these scaffolds are natural substrates that faithfully reproduce a physiological environment typical of metastatic lesions to the peritoneum. In this regard, I verified how the TDO grown on 3D-dECM, obtained from the peritoneum, recapitulate the main lesions and morphologies, typically observed *in vivo*, recreating structures such as signet ring cells, showing pleomorphism, bizarre mitotic features and many others. All this underlines how the model is capable of mimicking a peritoneal metastasis *in vitro*, providing a useful tool for the study of the main biological mechanisms involved in the development of PM disease. Finally, simulating HIPEC treatment on the model, I showed how the ECM is able to modulate the pharmacological response, giving protection to the organoids from the drug. This highlights the fundamental role that the ECM plays in the response to pharmacological treatment and paves the way for the development of new therapeutic regimens, based on the targeting of the ECM, which could enhance patient's response. In conclusion, the engineered model I have developed could be used as a predictive platform for patient specific drug treatment response. To achieve this, it will be necessary to fully characterize the physical and biological properties of the peritoneal ECM, especially using fine investigation techniques, such as mass spectrometry, in order to obtain exhaustive information on its composition and its involvement in the modulation of biological events during the development of metastatic lesions on the peritoneal cavity. All this information will allow the development of standardized 3D-dECMs that summarize the main features of the tumour peritoneal cavity, to be used as devices for pharmacological screening and for the study of biological phenomena that play a fundamental role in PM disease.

10 References

- A. Bertotti & F. Sassi
Molecular pathways: sensitivity and resistance to anti-EGFR antibodies
Clin. Cancer Res., 21 (15) (2015), pp. 3377–383.
- A. Cano, *et al.*
Transcription factor Snail controls epithelial—mesenchymal transitions by repressing E-cadherin expression
Nat. Cell Biol., 2 (2000), pp. 76–83
- A. Chronopoulos, *et al.*
Syndecan-4 tunes cell mechanics by activating the kindlin- integrin-RhoA pathway *Nat. Mater.*, 19 (2020), pp. 669–78
- A. Dobin, *et al.*
STAR: ultrafast universal RNA-seq aligner
Bioinformatics, 29(1) (2013), pp. 15-21
- A. Fumagalli, *et al.*
Genetic dissection of colorectal cancer progression by orthotopic transplantation of engineered cancer organoids
Proc. Natl. Acad. Sci. USA, 114 (2017), pp. E2357–E364
- A. Gilpin & Y. Yang
Decellularization strategies for regenerative medicine: from processing techniques to Applications
Biomed. Res. Int., 1 (2017), pp. 1–13
- A. Hoshino, *et al.*
Tumour exosomes integrins determine organotropic metastasis
Nature, 27 (7578) (2015), pp. 329-35
- A. Kamb
What's wrong with our cancer models?
Nat. Rev. Drug Discov., 4 (2005), pp. 161-65
- A. Kasi, *et al.*
Molecular Pathogenesis and Classification of Colorectal Carcinoma
Dig. Dis. Sci., 60 (3) (2015), pp. 762-72
- A. Madamanchi, *et al.*
Flipping the switch: integrin switching provides metastatic competence
Sci. Signal., 7 (2019), pe9
- A. Mayorca- Guiliani, *et al.*
ISDoT: in situ decellularization of tissues for high- resolution imaging and proteomic analysis of native extracellular matrix
Nat. Med., 23 (2017), pp. 890–98
- A. Naba, *et al.*
The extracellular matrix: Tools and insights for the "omics" era
Matrix Biol., 49 (2016), pp. 10-24
- A. Naba, *et al.*
The matrisome: in silico definition and in vivo characterization by proteomics of normal and tumor extracellular matrices
Mol. Cell Proteomics, 11 (2012), M111.014647

- A. Parekh, *et al.*
Sensing and modulation of invadopodia across a wide range of rigidities
Biophys. J., 100 (2011), 573 – 82
- A.D. Theocharis & N.K. Karamanos
Proteoglycans remodeling in cancer: underlying molecular mechanisms
Matrix Biol., 75–76 (2019), pp. 220–59
- A.E. Miller, *et al.*
Feeling things out: bidirectional signaling of the cell- ECM interface, implications in the mechanobiology of cell spreading, migration, proliferation, and differentiation
Adv. Healthc. Mater., 9 (8) (2020), e1901445
- A.G. Kerscher, *et al.*
Impact of peritoneal carcinomatosis in the disease history of colorectal cancer management: a longitudinal experience of 2406 patients over two decades
Br. J. Cancer, 108 (2012), pp. 1432–439
- A.H. Yang, *et al.*
Myofibroblastic conversion of mesothelial cells
Kidney Int., 63 (4) (2003), pp. 1530-9
- A.M. Kuijpers, *et al.*
Perioperative systemic chemotherapy in peritonealcarcinomatosis of lymph node positive colorectal cancer treated withcytoreductive surgery and hyperthermic intraperitoneal chemotherapy
Ann.Oncol., 25 (2014), 864–69
- A.M. Newman, *et al.*
Determining cell type abundance and expression from bulk tissues with digital cytometry
Nat. Biotechnol., 37 (2019), pp. 773–82
- A.N. Gargalionis, *et al.*
Polycystin-1 and polycystin-2 are involved in the acquisition of aggressive phenotypes in colorectal cancer
Int. J. Cancer, 136 (7) (2015), pp. 1515-527
- A.P. Wasnik, *et al.*
Primary and secondary disease of the peritoneum and mesentery: review of anatomy and imaging features
Abdom. Imaging, 40 (2015), pp. 626-42
- A.U. Blackham, *et al.*
Metastatic colorectal cancer: survival comparison of hepatic resectionversus cytoreductive surgery and hyperthermic intraperitoneal chemotherapy
Ann. Surg. Oncol., 21 (2014), 2667–674
- A.Zuidema, *et al.*
Crosstalk between cell adhesion complexes in regulation of mechanotransduction *Bioessays* , 42 (11) (2020), e2000119
- B. Chen, *et al.*
Small molecule- mediated disruption of Wnt- dependent signaling in tissue regeneration and Cancer
Nat. Chem. Biol., 5 (2) (2009), pp. 100-7

- B. Costa-Silva, *et al.*
Pancreatic cancer exosomes initiate pre-metastatic niche formation in the liver
Nat. Cell Biol., 17 (6) (2015), pp. 816-26
- B. Piersma, *et al.*
Fibrosis and cancer: a strained relationship
Biochim. Biophys. Acta Rev. Cancer, 1873 (2020), 188356
- B. Weigelt, *et al.*
HER2 signaling pathway activation and response of breast cancer cells to HER2-targeting agents is dependent strongly on the 3D microenvironment
Breast Cancer Res. Treat., 122 (2010), 35-43
- B.A. Pereira, *et al.*
CAF subpopulations: a new reservoir of stromal targets in pancreatic cancer
Trends Cancer, 5 (2019), pp. 724–41
- B.K. Koo, *et al.*
Porcupine inhibitor suppresses paracrine Wntdriven growth of Rnf43; Znr3-mutant neoplasia
Proc. Natl. Acad. Sci. USA, 112 (2015), pp. 7548–550
- B.N. Lourenço, *et al.*
CD44v6 increases gastric cancer malignant phenotype by modulating adipose stromal cellmediated ECM remodeling
Integr. Biol. (Camb.), 10 (2018), pp. 145–58
- B.T. Beaty & J. Condeelis J
Digging a little deeper: the stages of invadopodium formation and maturation
Eur. J. Cell Biol., 93 (10-12) (2014), pp. 438-44
- C. Greenman, *et al.*
Patterns of somatic mutation in human cancer genomes
Nature, 446 (2007), pp. 153–58
- C. Millan, *et al.*
3D culture of cancer cells in a polysaccharide-based hydrogel drastically alters the protein and RNA cargo EVs
Selected talk, ISEV 2018
- C. Pauli, *et al.*
Personalized in vitro and in vivo cancer models to guide precision medicine
Cancer Discov., 7 (2017), pp. 462-77
- C. Tetta, *et al.*
Extracellular vesicles as an emerging mechanism of cell-to-cell communication *Endocrine*, 44 (1) (2013), pp. 11–19
- C. Tian, *et al.*
Proteomic analyses of ECM during pancreatic ductal adenocarcinoma progression reveal different contributions by tumor and stromal cells
Proc. Natl. Acad. Sci. USA, 116 (2019), pp. 19609–618
- C. Vennin, *et al.*
Transient tissue priming via ROCK inhibition uncouples pancreatic cancer progression, sensitivity to chemotherapy, and metastasis
Sci. Transl. Med., 9 (2017), eaai8504
- C.D.K. Nguyen & C. Yi
YAP/TAZ signaling and resistance to cancer therapy
Trends Cancer, 5 (2019), pp. 283-296

- C.M. Ghajar
Metastasis prevention by targeting the dormant niche
Nat. Rev. Cancer, 15 (4) (2015), pp. 238-47
- C.P. Carmignani, *et al.*
Intraperitoneal cancer dissemination: mechanisms of the patterns of spread
Cancer Metastasis Rev., 22 (2003), pp. 465-72
- C.P. Miller, *et al.*
Engineering microphysiological immune system responses on chips
Trends Biotechnol., 38 (2020), pp. 857–872
- C.Q. Huang, *et al.*
Cytoreductive surgery plus hyperthermic intraperitoneal chemotherapy improves survival of patients with peritoneal carcinomatosis from colorectal cancer: a case-control study from a Chinese center
J. Surg. Oncol.; 109 (2014a), pp. 730–39
- C.S. Fuchs, *et al.*
Plasma insulin-like growth factors, insulin-like binding protein-3, and outcome in metastatic colorectal cancer: results from intergroup trial N9741
Clin. Cancer Res., 14 (2008), pp. 8263-269
- C.S. Scanlon, *et al.*
Characterization of squamous cell carcinoma in an organotypic culture via subsurface non-linear optical molecular imaging
Exp. Biol. Med., 238 (2013), pp. 1233–241
- C.S. Scanlon, *et al.*
Characterization of squamous cell carcinoma in an organotypic culture via subsurface non-linear optical molecular imaging
Exp. Biol. Med., 238 (2013), pp. 1233–241
- C.S. Verissimo, *et al.*
Targeting mutant RAS in patient derived colorectal cancer organoids by combinatorial drug screening
eLife, 5 (2016), pii: e18489
- C.T. Seebauer, *et al.*
Peritoneal carcinomatosis of colorectal cancer is characterized by structural and functional reorganization of the tumor microenvironment inducing senescence and proliferation arrest in cancer cells
Oncoimmunology, 5 (12) (2016), pp. e1242543
- C.Z. Li, *et al.*
Inhibition of CD44 expression by small interfering RNA to suppress the growth and metastasis of ovarian cancer cells in vitro and in vivo
Folia Biol., 54 (2008), pp. 180-86
- Cancer Genome Atlas Network
Comprehensive molecular characterization of human colon and rectal cancer
Nature, 487 (2012), pp. 330–37
- D. Ait Ouakrim, *et al.*
Trends in colorectal cancer mortality in Europe: retrospective analysis of the WHO mortality database
BMJ, 351 (2015), pp. h4970

- D. Baratti, *et al.*
Cost analysis of the combined procedure of cytoreductive surgery and hyperthermic intraperitoneal chemotherapy (HIPEC)
Eur. J. Surg. Oncol., 36 (2010), pp. 463–69
- D. Baratti, *et al.*
Postoperative complications after cytoreductive surgery and hyperthermic intraperitoneal chemotherapy affect long-term outcome of patients with peritoneal metastases from colorectal cancer: a two-center study of 101 patients
Dis. Colon Rectum, 57 (2014), 858–68
- D. Baratti, *et al.*
Progress in treatments for colorectal cancer peritoneal metastases during the years 2010-2015. A systematic review
Crit. Rev. Oncol. Hematol., 100 (2016), pp. 209-22
- D. Barras, *et al.*
BRAF V600E mutant colorectal cancer subtypes based on gene expression
Clin. Cancer Res., 23 (1) (2017), pp. 104–15
- D. Caccia, *et al.*
Bioinformatics tools for secretome analysis
Biochim. Biophys. Acta, 1834 (11) (2013), pp. 2442-453
- D. Correa
Mesenchymal Stem Cells During Tumor Formation and Dissemination
Cur. Stem Cell Rep., 2 (2016), pp. 174–82
- D. Elias, *et al.*
Heated intraoperative intraperitoneal oxaliplatin after complete resection of peritoneal carcinomatosis: pharmacokinetic and tissue distribution.
Ann. Oncol., 13 (2002), pp. 267–72
- D. Elias, *et al.*
Peritoneal colorectal carcinomatosis treated with surgery and peri-operative intraperitoneal chemotherapy: retrospective analysis of 523 patients from a multicenteric French study
J. Clin. Oncol., 28(2010), pp. 63–68
- D. Gao, *et al.*
Organoid cultures derived from patients with advanced prostate cancer
Cell, 159 (2014), pp. 176–87
- D. Jayne
Molecular biology of peritoneal carcinomatosis
Cancer Treat. Res., 134 (2007), pp. 21-33
- D. Nassar & C. Blanpain
Cancer stem cells: basic concepts and therapeutic implications
Ann. Rev. Pathol., 11 (2016), pp. 47–76
- D. Sun, *et al.*
Novel decellularized liver matrix-alginate hybrid gel beads for the 3D culture of hepatocellular carcinoma cells
Int. J. Biol. Macromol., 109 (2018), pp. 1154–163
- D.A. Taylor, *et al.*
Decellularized matrices in regenerative medicine
Acta Biomater., 74 (2018), pp. 74–89

- D.G. Jayne, *et al.*
A three dimensional in-vitro model for the study of peritoneal tumour metastasis
Clin. Exp. Metastasis, 17 (1999), pp. 515-23
- D.G. Jayne, *et al.*
Peritoneal carcinomatosis from colorectal cancer
Br. J. Surg., 89 (12) (2002), pp. 1545-550
- D.J. Cheon & S. Orsulic
Mouse models of cancer
Annu. Rev. Pathol., 6 (2011), pp. 95–119
- D.K. Mishra, *et al.*
Small cell and non small cell lung cancer form metastasis on cellular 4D lung model *BMC Cancer*, 18 (2018), pp. 1–9
- D.M. Casali, *et al.*
A novel supercritical CO₂-based decellularization method for maintaining scaffold hydration and mechanical properties
J. Supercrit. Fluids, 131 (2018), pp. 72–81
- E. Batlle, *et al.*
Transcription factor Snail is a repressor of E-cadherin gene expression in epithelial tumour cells
Nat. Cell Biol., 2 (2000), pp. 84–89
- E. D'Angelo, *et al.* **Patient-Derived Scaffolds of Colorectal Cancer Metastases as an Organotypic 3D Model of the Liver Metastatic Microenvironment** *Cancers (Basel)*, 12(2) (2020)
- E. Dekker, *et al.*
Colorectal cancer
The Lancet, 19 (394) (10207) (2019), pp. 1467-480
- E. Fessler, *et al.*
TGFβ signaling directs serrated adenomas to the mesenchymal colorectal cancer Subtype
EMBO Mol. Med., 8 (2016), pp. 745–60
- E. Hansen, *et al.*
Tumor cells in blood shed from the surgical field
Arch. Surg., 130 (1995), pp. 387-93
- E. Mavrogonatou, *et al.*
Extracellular matrix alterations in senescent cells and their significance in tissue homeostasis
Matrix Biol., 75–76 (2019), pp. 27–42
- E. Pretzsch, *et al.*
Mechanisms of Metastasis in Colorectal Cancer and Metastatic Organotropism: Hematogenous versus Peritoneal Spread
J. of Oncol., 19 (2019), pp. 1-13
- E. Shimshoni, *et al.*
Distinct extracellular-matrix remodeling events precede symptoms of inflammation *Matrix Biol.*, s0945-053X (30) (2020), pp. 30103-0107
- E.C. Filipe, *et al.*
Charting the unexplored extracellular matrix in cancer
Int. J. Exp. Pathol., 99 (2018), pp. 58–76
- E.I. Andaloussi, *et al.*
Extracellular vesicles: biology and emerging therapeutic opportunities
Nat. Rev. Drug. Discov., 12 (5) (2013), pp. 347-57

- E.I. Benizri, *et al.*
Small bowel involvement is a prognostic factor in colorectal carcinomatosis treated with complete cytoreductive surgery plus hyperthermic intraperitoneal chemotherapy *World J. Surg. Oncol.*, 10 (2012), pp. 56
- E.J. Hoffmann & S.M. Ponik
Biomechanical contributions to macrophage activation in the tumor microenvironment *Front. Oncol.*, 10 (2020), pp. 787
- E.M. Grasset, *et al.*
Matrix stiffening and EGFR cooperate to promote the collective invasion of cancer cells *Cancer Res.*, 78 (2018), pp. 5229–242
- E.Y. Chen, *et al.*
Enrichr: interactive and collaborative HTML5 gene list enrichment analysis tool *BMC Bioinformatics*, 14 (2013), pp. 128
- F. Ballet
Hepatotoxicity in drug development: detection, significance and solutions *J. Hepatol.*, 26 (1997), (Suppl. 2), pp. 26–36
- F. Blokzijl, *et al.*
Tissue- specific mutation accumulation in human adult stem cells during life *Nature*, 538 (2016), pp. 260-64
- F. Bozzi, *et al.*
MIF/CD74 axis is a target for novel therapies in colon carcinomatosis *J. Exp. Clin. Cancer Res.*, 36(1) (2017), pp. 16
- F. Bray, *et al.*
Global cancer statistics 2018: GLOBOCAN estimates of incidence and mortality worldwide for 36 cancers in 185 countries *CA Cancer J. Clin.*, 68 (2018), pp. 394–424
- F. Kai, *et al.*
The extracellular matrix modulates the metastatic journey *Dev. Cell*, 49 (2019), pp. 332-46
- F. Petrelli, *et al.*
Prognostic survival associated with left-sided vs right-sided colon cancer: a systematic review and meta-analysis *JAMA Oncol.*, 3 (2) (2017), pp. 211–19
- F. Sensi, *et al.*
Preclinical three-dimensional colorectal cancer model: the next generation of in vitro drug efficacy evaluation *J. Cell. Physiol.*, 234 (2017), pp. 181–91
- F. Zanconato, *et al.*
YAP and TAZ: a signalling hub of the tumour microenvironment *Nat. Rev. Cancer*, 19 (8) (2019), pp. 454-64
- F.R. Maia, *et al.*
Decellularized hASCs-derived matrices as biomaterials for 3D in vitro approaches *Methods Cell Biol.*, 156 (2020), pp. 45–58
- G. Binnig, *et al.*
Atomic Force Microscope *Phys. Rev. Lett.*, 56 (1986), pp. 930

- G. Caponigro & W.R. Sellers
Advances in the preclinical testing of cancer therapeutic hypotheses
Nat. Rev. Drug Discov., 10 (2011), pp. 179–87
- G. Dalagiorgou, *et al.*
Polycystin-1: function as a mechanosensor
Int. J. Biochem. Cell. Biol., 42 (2010), pp. 1610-613
- G. Landberg, *et al.*
Patient-derived scaffolds uncover breast cancer promoting properties of the microenvironment
Biomaterials, 235 (2020), 119705
- G. Passot, *et al.*
Progression following neoadjuvant systemic chemotherapy may not be a contraindication to a curative approach for colorectal carcinomatosis
Ann. Surg., 256 (2012), pp. 125–29
- G. Rijal & W. Li
A versatile 3D tissue matrix scaffold system for tumor modeling and drug screening *Sci. Adv.*, 3 (2017), pp. 1–17
- G. Vasiukov, *et al.*
Myeloid cell- derived TGF- beta signaling regulates ECM deposition in mammary carcinoma via adenosine- dependent mechanisms
Cancer Res., 15 (80) (12) (2020), pp. 2628-638
- G. Vlachogiannis, *et al.*
Patient-derived organoids model treatment response of metastatic gastrointestinal cancers
Science, 359 (2018), pp. 920–26
- G.S. Hussey, *et al.*
The extracellular matrix of the gastrointestinal tract: a regenerative medicine platform *Nat. Rev. Gastroenterol. Hepatol.*, 14 (9) (2017), pp. 540-552
- H. Clevers
The intestinal crypt, a prototype stem cell compartment
Cell, 154 (2013), pp. 274–84
- H. Clevers
Modeling Development and Disease with Organoids
Cell, 165 (7) (2016), pp. 1586-895
- H. Cramer.
Mathematical methods of statistics
Princeton University Press, (1999)
- H. Davies, *et al.*
HRDetect is a predictor of BRCA1 and BRCA2 deficiency based on mutational signatures
Nat. Med., 23 (2017), pp. 517–25
- H. Fairfield, *et al.*
Development of a 3D bone marrow adipose tissue model
Bone, 118 (2018), pp. 77–88
- H. Gao, *et al.*
Multi- organ site metastatic reactivation mediated by non- canonical discoidin domain receptor 1 signaling
Cell, 166 (2016), pp. 47–62

- H. Hamidi & J. Ivaska
Every step of the way: integrins in cancer progression and metastasis
Nat. Rev. Cancer, 18 (2018), pp. 533–48
- H. Hasmad, *et al.*
Human amniotic membrane with aligned electrospun fiber as scaffold for aligned tissue regeneration
Tissue Eng. C Methods, 24 (2018), pp. 368–78
- H. Hoffmeister, *et al.*
The human polycystin-2 protein represents an integral membrane protein with six membrane-spanning domains and intracellular N- and C-termini
Biochem. J., 433 (2011), pp. 285–94
- H. Nistala, *et al.*
Fibrillin-1 and -2 differentially modulate endogenous TGF-beta and BMP bioavailability during bone formation
J. Cell. Biol., 190 (6) (2010), pp. 1107–121
- H. Peinado, *et al.*
Melanoma exosomes educate bone marrow progenitor cells toward a pro-metastatic phenotype through MET
Nat. Med., 18 (6) (2012), pp. 883–91
- H. Peinado, *et al.*
The secreted factors responsible for pre-metastatic niche formation: old sayings and new thoughts
Semin. Cancer Biol. 21 (2) (2011), pp. 139–46
- H. Schillers, *et al.*
Standardized Nanomechanical Atomic Force Microscopy Procedure (SNAP) for Measuring Soft and Biological Samples
Sci. Rep., 11;7(1) (2017), pp. 5117
- H. Weijing, *et al.*
In vitro bone metastasis dwelling in a 3D bioengineered niche
Biomaterials, 269 (2021): 120624
- H.A.N. Alshehri
Compare and Contrast of Differential Gene Expression Software Packages of RNA-Seq.
Computational Science and Computational Intelligence (CSCI). Las Vegas, NV, USA: IEEE; 2018
- H.G. Yi, *et al.*
A bioprinted human-glioblastoma-on-achip for the identification of patient-specific responses to chemoradiotherapy
Nat. Biomed. Eng., 3 (2018), pp. 509–19
- H.H. Yan, *et al.*
RNF43 germline and somatic mutation in serrated neoplasia pathway and its association with BRAF mutation
Gut, 66 (2016), pp. 1645–656
- H.J. Butt & M. Jaschke
Calculation of thermal noise in atomic force microscopy
Nanotechnology, 6 (1) (1995), pp. 1–15
- H.J. Chen, *et al.*
A recellularized human colon model identifies cancer driver genes
Nat. Biotechnol., 34 (8) (2016), pp. 845–851

- H.Y. Liu, *et al.*
Biomimetic and enzyme-responsive dynamic hydrogels for studying cell-matrix interactions in pancreatic ductal adenocarcinoma
Biomaterials, 160 (2018), pp. 24–36
- I. Koh, *et al.*
The mode and dynamics of glioblastoma cell invasion into a decellularized tissue-derived extracellular matrix-based three-dimensional tumor model
Sci. Rep., 8 (2018), pp. 1–12
- I. Ubink, *et al.*
Organoids from colorectal peritoneal metastases as a platform for improving hyperthermic intraperitoneal chemotherapy
Br. J. Surg., 106 (10) (2019), pp. 1404–414
- I.A. Khawar, *et al.*
Improving drug delivery to solid tumors: priming the tumor microenvironment
J. Control. Release, 201 (2015), pp. 78–89
- J. Comijn, *et al.*
Two-handed E box binding zinc finger protein SIP1 downregulates E-cadherin and induces invasion
Mol. Cell, 7 (2001), pp. 1267–278
- J. Drost & H. Clevers
Organoids in cancer research
Nat. Rev. Cancer, 18 (7) (2018), pp. 407–18
- J. Drost, *et al.*
Use of CRISPR- modified human stem cell organoids to study the origin of mutational signatures in cancer
Science, 358 (2017), pp. 234–38
- J. Guinney, *et al.*
The consensus molecular subtypes of colorectal cancer
Nat. Med., 21 (11) (2015), pp. 1350–356
- J. L. Young, *et al.*
Integrin subtypes and nanoscale ligand presentation influence drug sensitivity in cancer cells
Nano Lett., 20 (2020), pp. 1183–191
- J. Laurent, *et al.*
Functionalized AFM probes for force spectroscopy: eigenmode shapes and stiffness calibration through thermal noise measurements.
Nanotechnology, 7 (24) (22) (2013), pp. 225504
- J. Mikula-Pietrasik, *et al.*
The peritoneal “soil” for a cancerous “seed2: a comprehensive review of the pathogenesis of intraeritoneal cancer metastases
Cel.l Mol. Life Sci., 75 (3) (2018), pp. 509–25
- J. Pagetti, *et al.*
Exosomes released by chronic lymphocytic leukemia cells induce the transition of stromal cells into cancer-associated fibroblast
Blood, 126 (9) (2015), pp. 1106–117
- J. Segelman, *et al.*
Incidence, prevalence and risk factors for peritoneal carcinomatosis from colorectal Cancer.
Br. J. Surg., 99 (2012), pp. 699–05

- J. Tabernero, *et al.*
Association of prognostic value of primary tumor location in stage III colon cancer with RAS and BRAF mutational status
JAMA Oncol., 4 (7) (2018), pp. e173695
- J. Winkler, *et al.*
Concepts of extracellular matrix remodelling in tumour progression and metastasis *Nat. Commun.*, 11 (1) (2020), pp. 5120
- J. Yang, *et al.*
Twist, a master regulator of morphogenesis, plays an essential role in tumor metastasis *Cell*, 117 (7) (2004), pp. 927–39
- J.B. Bramsen, *et al.*
Molecular-subtype-specific biomarkers improve prediction of prognosis in colorectal cancer
Cell Rep., 19 (6) (2017), pp. 1268–80
- J.B. van der Wal & J. Jeekel
Biology of the peritoneum in normal homeostasis and after surgical trauma
Colorectal Dis., 9 (2007), Suppl 2: pp. 9-13
- J.F. Hastings, *et al.*
The extracellular matrix as a key regulator of intracellular signalling networks
Br. J. Pharmacol., 176 (2019), pp. 82-92
- J.F.E. Grey, *et al.*
The use of decellularised animal tissue to study disseminating cancer cells
J. Cell Sci., 132 (2019), jcs219907
- J.L. Hutter & J. Bechhoefer
Calibration of atomic-force microscope tips
Rev. of Sci. Instrum., 64 (1868) (1993), pp. 1-10
- J.L. Leight, *et al.*
Matrix rigidity regulates a switch between TGF-beta1-induced apoptosis and epithelial-mesenchymal transition
Mol. Biol. Cell, 23 (2012), pp. 781–91
- J.P. Medema
Cancer stem cells: the challenges ahead
Nat. Cell. Biol., 15 (2013), pp. 338–44
- J.P. Webber, *et al.*
Differentiation of tumourpromoting stromal myofibroblasts by cancer exosomes *Oncogene*, 34 (2015), pp. 290–302
- J.T. Neal, *et al.*
Organoid modeling of the tumor immune microenvironment
Cell, 175 (2018), pp. 1972–988
- J.T. Parsons, *et al.*
Cell adhesion: integrating cytoskeletal dynamics and cellular tension
Nat. Rev. Mol. Cell Biol., 11 (2010), pp. 633-43
- J.W. Dobbie
Morphology of the peritoneum in CAPD
Blood Purif., 7 (1989), pp. 74-85
- J.Z. Kechagia, *et al.*
Integrins as biomechanical sensors of the microenvironment
Nat. Rev. Mol. Cell Biol., 20 (2019), pp. 457-73

- K. Bajou, *et al.*
Plasminogen activator inhibitor-1 protects endothelial cells from FasL-mediated apoptosis
Cancer Cell, 14 (4) (2008), pp. 324-34
- K. Hayashi, *et al.*
Real-time imaging of tumor-cell shedding and trafficking in lymphatic channels *Cancer Res.*, 67 (2007), pp. 8223-228
- K. Ksiazek, *et al.*
Oxidative stress-dependent increase in ICAM-1 expression promotes adhesion of colorectal and pancreatic cancers to the senescent peritoneal mesothelium
Int. J. Cancer., 127 (2) (2010), pp. 293-303
- K. Michailova, *et al.*
Scanning and transmission electron microscopic study of visceral and parietal peritoneal regions in the rat
Ann. Anat., 181 (1999), pp. 253-60
- K. Thanki, *et al.* Nicholls
Consensus molecular subtypes of colorectal cancer and their clinical implications
Int. Biol. Biomed. J., 3 (3) (2017), pp. 105–11
- K. Van der Speeten, *et al.*
Pharmacology of perioperative intraperitoneal and intravenous chemotherapy in patients with peritoneal surface malignancy
Surg. Oncol. Clin. N. Am., 21 (2012), pp. 577–97
- K. Wang, *et al.*
Whole- genome sequencing and comprehensive molecular profiling identify new driver mutations in gastric cancer
Nat. Genet., 46 (2014), pp. 573–82
- K.A. Robinson, *et al.*
Decorin and biglycan are necessary for maintaining collagen fibril structure, fiber realignment, and mechanical properties of mature tendons
Matrix Biol., 64 (2017), pp. 81-93
- K.E. Kadler, *et al.*
Collagens at a glance
J. Cell Sci., 120 (2007), pp. 1955–958
- K.G. Chen, *et al.*
Human pluripotent stem cell culture: considerations for maintenance, expansion, and therapeutics
Cell Stem Cell, 14 (2014), pp. 13–26
- K.W. McCracken, *et al.*
Modelling human development and disease in pluripotent stem-cell-derived gastric organoids
Nature, 516 (2014), pp. 400–04
- L. Broutier, *et al.*
Human primary liver cancer-derived organoid cultures for disease modeling and drug screening
Nat. Med., 23 (2017), pp. 1424–435
- L. Cao, *et al.*
Omental milky spots in screening gastric cancer stem cells
Neoplasma, 58 (2011), pp. 20-26

- L. Genovese, *et al.*
Cellular localization, invasion, and turnover are differently influenced by healthy and tumor-derived extracellular matrix
Tissue Eng. Part. A, 20 (13-14) (2014), pp. 2005-018
- L. Hood, *et al.*
Exosomes released by melanoma cells prepare sentinel lymph nodes for tumor metastasis
Cancer Res., 71 (11) (2011), pp. 3792-801
- L. Lemoine *et al.*
Pathophysiology of colorectal peritoneal carcinomatosis down-regulates expression of overall CD44 isoforms and inhibits tumor growth and metastasis in highly metastatic colon carcinoma cells
Int. J. Cancer, 91 (2001), pp. 67-75
- L. Lemoine, *et al.*
Pathophysiology of colorectal peritoneal carcinomatosis: Role of the peritoneum
World J. Gastroenterol., 22 (34) (2016), pp. 7692-707
- L. Lemoine, *et al.*
Pathophysiology of colorectal peritoneal carcinomatosis mouse omentum. II. Kinetic features and metabolic requirements
Exp. Cell. Res., 69 (1971), pp. 313-23
- L. Liu, *et al.*
Stromal myofibroblasts are associated with poor prognosis in solid cancers: a meta- analysis of published studies
PLoS ONE, 11 (2016), e0159947
- L. Mohrmann, *et al.*
A perivascular niche in the bone marrow hosts quiescent and proliferating tumorigenic colorectal cancer cells
Int. J. Cancer., 147 (2) (2020), pp. 519-31
- L. Puricelli, *et al.*
Nanomechanical and topographical imaging of living cells by atomic force microscopy with colloidal probes
Rev. Sci. Instrum., 86 (3) (2015), pp. 033705
- L. Rivoltini, *et al.*
TNF-Related Apoptosis-Inducing Ligand (TRAIL)-Armed Exosomes Deliver Proapoptotic Signals to Tumor Site
Clin. Cancer Res., 22 (14) (2016), pp. 3499-512
- L. Wei, *et al.*
Cancer- associated fibroblasts promote progression and gemcitabine resistance via the SDF-1/SATB-1 pathway in pancreatic cancer
Cell Death Dis, 9 (2018), pp. 1065
- L.C. Bahlmann, *et al.*
Designer biomaterials to model cancer cell invasion in vitro: predictive tools or just pretty pictures?
Adv. Funct. Mater., 16 (2020), pp. 1-11
- L.P. Ferreira, *et al.*
Decellularized Extracellular Matrix for Bioengineering Physiomimetic 3D in Vitro Tumor Models
Trends Biotechnol., 38 (12) (2020), pp. 1397-414
- L.R. Smith, *et al.*
Stem cell differentiation is regulated by extracellular matrix mechanics
Physiology, 33 (2018), pp. 16–25

- M. Arnedos, *et al.*
Precision medicine for metastatic breast cancer-limitations and solutions
Nat. Rev. Clin. Oncol., 12 (2015), pp. 693–704
- M. Arnold, *et al.*
Global patterns and trends in colorectal cancer incidence and mortality
Gut., 66 (2017), pp. 683–91
- M. Bleijis, *et al.*
Xenograft and organoid model systems in cancer research
EMBO J., 38 (15) (2019), pp. e101654
- M. Chighizola, *et al.*
Large colloidal probes for atomic force microscopy: Fabrication and calibration issues *J. Mol. Recognit.*, 34 (1) (2021), pp. e2879
- M. Deraco, *et al.*
Surgical technique of parietal and visceral peritonectomy for peritoneal surfacemalignancies
J. Surg. Oncol., 100 (2009), pp. 321–28
- M. Eiraku & Y. Sasai
Self-formation of layered neural structures in three-dimensional culture of ES cells *Curr. Opin. Neurobiol.*, 22 (2012), pp. 768–77
- M. Fujii, *et al.*
A Colorectal Tumor Organoid Library Demonstrates Progressive Loss of Niche Factor Requirements during Tumorigenesis.
Cell Stem Cell., 18 (6) (2016), pp. 827-38
- M. Fujii, *et al.*
Efficient genetic engineering of human intestinal organoids using electroporation
Nat. Protoc., 10 (10) (2015), pp. 1474-485
- M. Ii, *et al.*
Role of matrix metalloproteinase-7 (matrilysin) in human cancer invasion, apoptosis, growth, and angiogenesis
Exp. Biol. Med., 231 (2006), pp. 20-27
- M. Indrieri, *et al.*
Adhesive-free colloidal probes for nanoscale force measurements: production and Characterization
Rev. Sci. Instrum., 82 (2) (2011), pp. 1-15
- M. Janiszewska, *et al.*
Cell adhesion in cancer: beyond the migration of single cells
J. Biol. Chem., 295 (2020), pp. 2495–505
- M. Maimets, *et al.*
Long- term in vitro expansion of salivary gland stem cells driven by wnt signals
Stem Cell Rep., 6 (2016), pp. 150–62
- M. Matano *et al.*
Modeling colorectal cancer using CRISPR- Cas9-mediated engineering of human intestinal organoids
Nat. Med., 21 (2015), pp. 256–62
- M. Nebuloni, *et al.*
Insight On Colorectal Carcinoma Infiltration by Studying Perilesional Extracellular Matrix
Sci. Rep., 4 (6) (2016), pp. 22522

- M. Parri & P. Chiarugi
Rac and Rho GTPases in cancer cell motility control
Cell Commun. Signa., 18 (2011), pp. 23
- M. Pocard, *et al.*
Single alteration of p53 or E-cadherin genes can alter the surgical resection benefit in an experimental model of colon cancer
Dis. Colon Rectum., 44 (2001), pp. 1106-112
- M. Schlesinger & G. Bendas
Vascular cell adhesion molecule-1 (VCAM-1) an increasing insight into its role in tumorigenicity and metastasis
Int. J. Cancer, 136 (11) (2015), pp. 2504-514
- M. Shimokawa, *et al.*
Visualization and targeting of LGR5(+) human colon cancer stem cells
Nature, 545 (2017), pp. 187–92
- M. Takasato, *et al.*
Kidney organoids from human iPS cells contain multiple lineages and model human nephrogenesis
Nature, 526 (2015), pp. 564–68
- M. Tampellini, *et al.*
Co-expression of EGF receptor, TGFalpha and S6 kinase is significantly associated with colorectal carcinomas with distant metastases at diagnosis
Virchows Arch., 450 (2007), pp. 321-28
- M. van de Wetering, *et al.*
Prospective derivation of a living organoid biobank of colorectal cancer patients
Cell, 161 (2015), pp. 933–45
- M. Xia & H. Land H
Tumor suppressor p53 restricts Ras stimulation of RhoA and cancer cell motility
Nat. Struct. Mol. Biol., 14 (2007), 215 – 23
- M. Yilmaz & G. Christofori
EMT, the cytoskeleton, and cancer cell invasion
Cancer Metastasis Rev., 28 (2009), pp. 15-33
- M.A. Lancaster & J.A. Knoblich
Organogenesis in a dish: modeling development and disease using organoid technologies
Science, 345 (2014), pp.1247125
- M.D. Buschmann & A.J. Grodzinsky
A molecular model of proteoglycan-associated electrostatic forces in cartilage mechanics
J. Biomech. Eng., 117 (2) (1995), pp. 179-92
- M.D. Roycik, *et al.*
A fresh prospect of extracellular matrix hydrolytic enzymes and their substrates
Curr. Pharm. Des., 15 (2009), pp. 1295-308
- M.E. Bracke
Role of adhesion molecules in locoregional cancer spread
Cancer Treat: Res., 134 (2007), pp. 35-49
- M.E. Fedorko, *et al.*
Studies on transport of macromolecules and small particles across mesothelial cells of the peritoneum
World J. Gastroenterol., 22 (2016), pp. 7702

- M.E. Salem, *et al.*
Comparative molecular analyses of left-sided colon, rightsided colon, and rectal cancers
Oncotarget, 8 (49) (2017), pp 86356–368
- M.J. Koppe, *et al.*
Peritoneal carcinomatosis of colorectal origin: incidence and current treatment strategies
Ann. Surg., 243 (2006), pp. 212–22
- M.J. Koppe, *et al.*
Recent insights into the pathophysiology of omental metastases
J. Surg. Oncol., 110 (2014), pp. 670-75
- M.J. Wheelock, *et al.*
Cadherin switching
J. Cell Sci., 121 (2008), pp. 727–35
- M.L. Pinto, *et al.*
Decellularized human colorectal cancer matrices polarize macrophages towards an anti-inflammatory phenotype promoting cancer cell invasion via CCL18
Biomaterials, 124 (2018), pp. 211–24
- M.M. Olcina, *et al.*
H3K9me3 facilitates hypoxia-induced p53-dependent apoptosis through repression of APAK
Oncogene, 35 (2016), pp. 793-99
- M.R. Stratton, *et al.*
The cancer genome
Nature, 458 (2009), pp. 719–24
- M.T. Scherzer, *et al.*
Fibroblast-derived extracellular matrices: an alternative cell culture system that increases metastatic cellular properties
PLoS One, 10 (2015), pp. 1–17
- M.W. Conklin, *et al.*
Collagen alignment as a predictor of recurrence after ductal carcinoma in situ
Cancer Epidemiol. Biomarkers Prev., 27 (2018), pp. 138–45
- M.W. Pickup, *et al.*
The extracellular matrix modulates the hallmarks of cancer
EMBO reports, 15 (12) (2014), pp. 1243-253
- N. Barker, *et al.*
Lgr5(+ve) stem cells drive self-renewal in the stomach and build long-lived gastric units in vitro
Cell Stem Cell, 6 (2010), pp. 25–36
- N. Gjorevski, *et al.*
Designer matrices for intestinal stem cell and organoid culture
Nature, 539 (2016), pp. 560–64
- N. Harada, *et al.*
Introduction of antisense CD44S CDNA
World J. Gastroenterol., 22 (2016)
- N. Hugen, *et al.*
Metastatic pattern in colorectal cancer is strongly influenced by histological subtype *Ann. Oncol.*, 25 (2014), pp. 651-57
- N. McGranahan & C. Swanton
Clonal heterogeneity and tumor evolution: past, present, and the future
Cell, 168 (2017), pp. 613–28

- N. Sachs, *et al.*
A living biobank of breast cancer organoids captures disease heterogeneity
Cell, 172 (2017), pp. 373–386.e10
- N. Watanabe, *et al.*
Comparison of high-hydrostatic pressure decellularized versus freeze-thawed porcine menisci
J. Orthop. Res., 37 (2019), pp. 2466–475
- N.A Alkhamesi, *et al.*
Induction of Proteases in Peritoneal Carcinomatosis, the Role of ICAM-1/CD43 Interaction
Biomark. Insights, 2 (2007), pp. 377-84
- N.A. Alkhamesi, *et al.* Ziprin
ICAM-1 mediated peritoneal carcinomatosis, a target for therapeutic intervention
Clin. Exp. Metastasis, 22 (2005), pp. 449-59
- N.A. Bhowmick, *et al.*
Stromal fibroblasts in cancer initiation and progression
Nature, 432 (2004), pp. 332-37
- N.S. Wang
The regional difference of pleural mesothelial cells in rabbits
Am. Rev. Respir. Dis., 110 (1974), pp. 623-33
- O. Chaudhuri, *et al.*
Substrate stress relaxation regulates cell spreading
Nat. Commun., 6 (2015), pp. 6364
- P. Benien & A. Swami
3D tumor models: history, advances and future perspectives
Future Oncol., 10 (2014), pp. 1311–327
- P. Jaquet & P.H. Sugarbaker
Current methodologies for clinical assessment of patients with peritoneal carcinomatosis
J. Exp. Clin. Cancer Res., 15 (1996), pp. 49–58
- P. Jess, *et al.*
A nationwide Danish cohort study challenging the categorisation into right-sided and leftsided colon cancer
BMJ Open., 3 (5) (2013) pp. e002608
- P.C. Ma, *et al.*
c-Met: structure, functions and potential for therapeutic inhibition
Cancer Metastasis Rev., 22 (2003), pp. 309-25
- P.H. Sugarbaker
Observations concerning cancer spread within the peritoneal cavity and concepts supporting an ordered pathophysiology
Cancer Treat. Res., 82 (1996), pp. 79-100
- P.H. Sugarbaker & D.P. Ryan
Cytoreductive surgery plus hyperthermic perioperative chemotherapy to treat peritoneal metastases from colorectal cancer: standard of care or an experimental approach
Lancet Oncol., 13 (2013), pp. e362–69
- P.H. Sugarbaker
Peritonectomy procedures
Ann. Surg., 221 (1995), pp. 29–42

- P.H. Sugarbaker
Peritoneum as the first-line of defense in carcinomatosis
J. Surg. Oncol., 95 (2007), pp. 93-96
- P.M. Kasi, *et al.*
Rising proportion of young individuals with rectal and colon cancer
Clin. Colorectal Cancer, 18 (2019), pp. e87-95
- P.M. Polanco, *et al.*
Does obesity affect outcomes of cytoreductive surgery and hyperthermic intraperitoneal chemoperfusion for disseminated mucinous appendiceal neoplasms *Ann. Surg. Oncol.*, 21 (2014), pp 3963-969
- P.R. Kuninty, *et al.*
ITGA5 inhibition in pancreatic stellate cells attenuates desmoplasia and potentiates efficacy of chemotherapy in pancreatic cancer
Sci. Adv., 5 (2019), eaax2770
- Q. Peng, *et al.*
Identification of genomic expression differences between rightsided and left-sided colon cancer based on bioinformatics analysis
OncoTargets Ther., 11 (2018), pp. 609-18
- R. Kalluri
The biology and function of fibroblasts in cancer
Nat. Rev. Cancer, 16 (2016), pp. 582-98
- R. Kalluri
The biology and function of fibroblasts in cancer
Nat. Rev. Cancer, 16 (2016), pp. 582-98
- R. Siegel *et al.*
Colorectal cancer statistics, 2014
CA Cancer. J. Clin., 64 (2) (2014), pp. 104-17
- R. Simsa, *et al.*
Systematic in vitro comparison of decellularization protocols for blood vessels
PLoS One, 13 (2018), e0209269
- R. Warn, *et al.*
HGF/SF induces mesothelial cell migration and proliferation by autocrine and paracrine pathways
Exp. Cell. Res., 267 (2001), pp. 258-66
- R. Warn, *et al.*
HGF/SF induces mesothelial cell migration and proliferation by autocrine and paracrine pathways
Exp. Cell Res., 267 (2001), pp. 258-66
- R.L. Siegel, *et al.*
Colorectal cancer incidence patterns in the United States, 1974-2013
J. Nat. Cancer. Inst., 109 (2017), pp. djw322
- R.M. Heath, *et al.*
Tumour-induced apoptosis in human mesothelial cells: a mechanism of peritoneal invasion by Fas Ligand/Fas interaction
Br.J. Cancer, 90 (2004) pp. 1437-442
- R.O. Hynes
The extracellular matrix: not just pretty fibrils
Science, 326 (2009), pp. 1216-219

- R.P. Sticca & B.W. Dach
Rationale for hyperthermia with intraperitoneal intraoperative chemotherapy agents *Surg. Oncol. Clin. N. Am.*, 12 (2005), pp. 689–00
- R.S. Lindoso, *et al.*
Proteomics of cell-cell interactions in health and disease *Proteomics*, 16 (2) (2016), pp. 328–44
- S. Alexander, *et al.*
An atomic-resolution atomic-force microscope implemented using an optical lever *J. of Appli. Phys.*, 65 (1989), pp. 164
- S. Behjati, *et al.*
Genome sequencing of normal cells reveals developmental lineages and mutational Processes *Nature*, 513 (2014), pp. 422–25
- S. González-Moreno, *et al.*
Hyperthermic intraperitoneal chemotherapy: methodology and safety considerations *Surg. Oncol. Clin. N. Am.*, 21 (2012), pp. 543–57
- S. Kusamura, *et al.*
Drugs carrier solutions and temperature in hyperthermic intraperitoneal chemotherapy *J. Surg. Oncol.*, 98 (2008), pp. 247–52
- S. Stintzing, *et al.*
Understanding the role of primary tumour localisation in colorectal cancer treatment and outcomes *Eur. J. Cancer.*, 84 (2017), pp. 69–80
- S. Van Ruth, *et al.*
Pharmacokinetics of intraperitoneal mitomycin C *Surg. Oncol. Clin. N. Am.*, 12 (2003), pp. 771–80
- S. Varghese, *et al.*
Site-specific gene expression profiles and novel molecular prognostic factors in patients with lower gastrointestinal adenocarcinoma diffusely metastatic to liver or peritoneum *Ann. Surg. Oncol.*, 14 (12) (2007), pp. 3460–471
- S.A. Gerber, *et al.*
Preferential attachment of peritoneal tumor metastases to omental immune aggregates and possible role of a unique vascular microenvironment in metastatic survival and growth *Am. J. Pathol.*, 169 (2006), pp. 1739–752
- S.E. Mutsaers, & S. Wilkosz
Structure and function of mesothelial cells *Cancer Treat. Res.*, 134 (2007), pp. 1–19
- S.E. Mutsaers, *et al.*
Changes in the concentration of microvilli on the free surface of healing mesothelium are associated with alterations in surface membrane charge *J. Pathol.*, 180 (1996), pp. 333–39
- S.J. Keeton, *et al.*
Compressed collagen and decellularized tissue - novel components in a pipeline approach for the study of cancer metastasis *BMC Cancer*, 18 (2018), pp. 1–12

- S.J.P. Pratt, *et al.*
The mechanical microenvironment in breast cancer
Cancers, 12 (2020), pp. 1452
- S.N. Ooft, *et al.*
Patient-derived organoids can predict response to chemotherapy in metastatic colorectal cancer patients
Sci. Transl. Med., 11(2019), eaay2574
- S.V. Bayer, *et al.*
DDR2 controls breast tumor stiffness and metastasis by regulating integrin mediated mechanotransduction in CAFs
eLife, 8 (2019), e45508
- S.V. Glavey, *et al.*
Proteomic characterization of human multiple myeloma bone marrow extracellular matrix
Leukemia, 31(11) (2017), pp. 2426-2434
- T. Brabletz, *et al.*
EMT in cancer
Nat. Rev. Cancer, 18 (2018), pp. 128–34
- T. Celià-Terrassa, *et al.*
Epithelial-mesenchymal transition can suppress major attributes of human epithelial tumor initiating cells
J. Clin. Invest. 122 (2012), pp. 1849 – 868
- T. Gawain, *et al.*
Measuring the mechanical properties of living cells using atomic force microscopy
J. Vis. Exp., 76 (2013), 50497
- T. Hoshiba & M. Tanaka
Optimization of the tissue source, malignancy, and initial substrate of tumor cell-derived matrices to increase cancer cell chemoresistance against 5- fluorouracil *Biochem. Biophys. Res. Commun.*, 457 (2015), pp. 353–57
- T. Katsuda, *et al.*
Conversion of terminally committed hepatocytes to culturable bipotent progenitor cells with regenerative capacity
Cell Stem Cell, 20 (2016), pp. 41–55
- T. Liu, *et al.*
Cancer-associated fibroblasts build and secure the tumor microenvironment
Front. Cell Dev. Biol., 7 (2019), pp. 1-20
- T. Panciera, *et al.*
Reprogramming normal cells into tumour precursors requires ECM stiffness and oncogene-mediated changes of cell mechanical properties
Nat. Mater., 19 (7) (2020), pp. 797-806
- T. R. Cox
The matrix in cancer
Nat. Rev. Cancer, 21 (2021), pp. 217-38
- T. Sato, *et al.*
Long-term expansion of epithelial organoids from human colon, adenoma, adenocarcinoma, and Barrett's epithelium
Gastroenterology, 141 (2011), pp. 1762–772
- T. Sato, *et al.*
Single Lgr5 stem cells build crypt-villus structures in vitro without a mesenchymal niche
Nature, 459 (2009), pp. 262–65

- T. Weber, *et al.*
Current status of cytoreductive surgery with hyperthermic intraperitoneal chemotherapy in patients with peritoneal carcinomatosis from colorectal cancer
Clin. Colorectal Cancer, 11 (2012), pp. 167–76
- T.C. Chua, *et al.*
Should the treatment of peritoneal carcinomatosis by cytoreductive surgery and hyperthermic intraperitoneal chemotherapy still be regarded as a highly morbid procedure?: a systematic review of morbidity and mortality
Ann. Surg., 249 (2009), pp. 900–07
- T.M. Bodenstine & D.R. Welch
Metastasis suppressors and the tumor microenvironment
Cancer Microenviron., 1 (2008), pp. 1–11
- T.R. Cox & J.T. Erler
Molecular pathways: connecting fibrosis and solid tumor metastasis
Clin. Cancer Res., 20 (2014), pp. 3637–643
- T.R. Shenoy, *et al.*
CHD1 loss sensitizes prostate cancer to DNA damaging therapy by promoting errorprone double-strand break repair
Ann. Oncol., 28 (2017), pp. 1495–507
- T.Y. Feinberg, *et al.*
Divergent matrix- remodeling strategies distinguish developmental from neoplastic mammary epithelial cell invasion programs
Dev. Cell, 47 (2018), pp. 145–160.e6
- U. Ben- David, *et al.*
Patient- derived xenografts undergo mouse- specific tumor evolution
Nat. Genet., 49 (2017), pp. 1567–575
- U. Klinge, *et al.*
Different matrix micro-environments in colon cancer and diverticular disease
Int. J. Colorectal Dis., 22 (2007), pp. 515–20
- U. Lindberg, *et al.*
The microfilament system and malignancy
Semin. Cancer Biol., 18 (2008), pp. 2–11
- Ubink, *et al.*
Histopathological and molecular classification of colorectal cancer and corresponding peritoneal metastases
Br. J. Surg., 105 (2) (2018), pp. e204–e211
- V. Sanz-Moreno, *et al.*
Rac activation and inactivation control plasticity of tumor cell movement
Cell, 135 (2008), pp. 510 – 23
- V.E. Lemmens, *et al.*
Predictors and survival of synchronous peritoneal carcinomatosis of colorectal origin: a population-based study
Int. J. Cancer, 128 (2011), pp. 2717–25
- W. Ceelen
HIPEC with oxaliplatin for colorectal peritoneal metastasis: The end of the road?
Eur. J. Surg. Oncol., 45 (2019), pp. 400–2

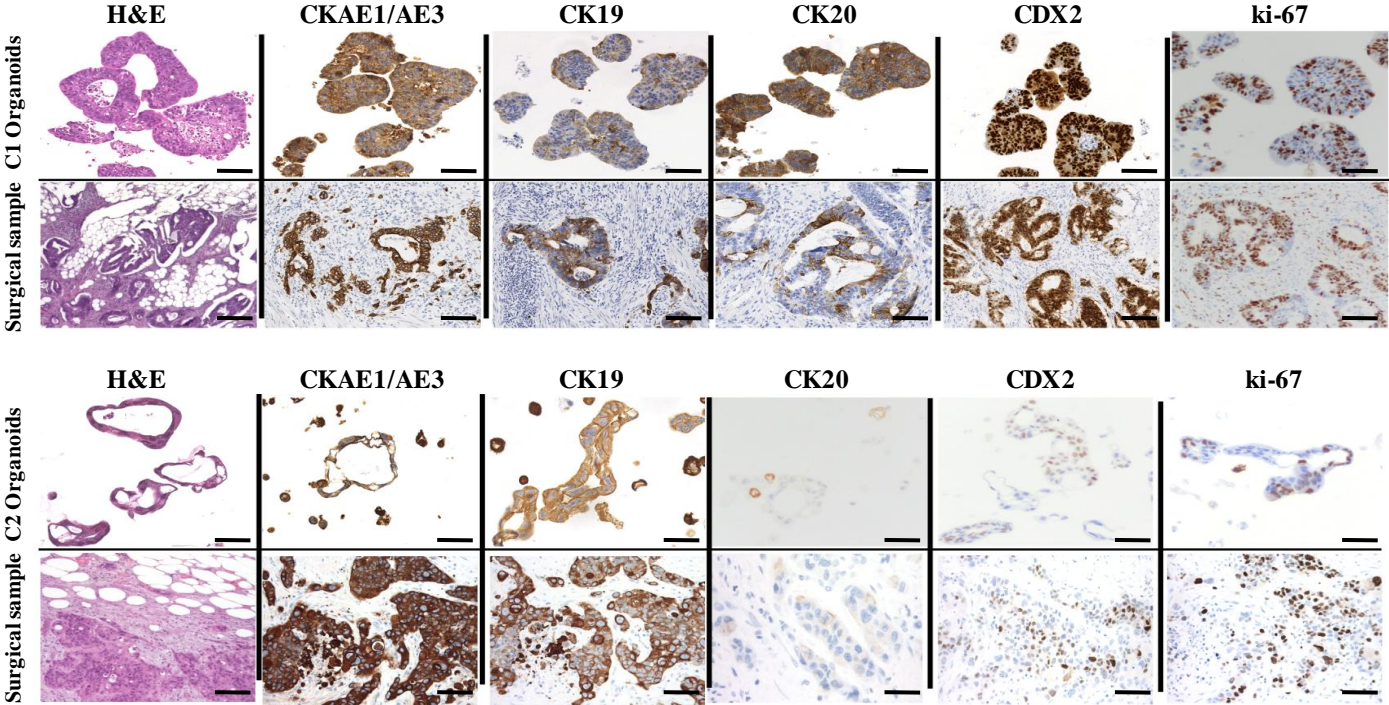
- W. Ceelen, *et al.*
Targeting the Tumor Microenvironment in Colorectal Peritoneal Metastases
Trends Cancer, 6 (3) (2020), pp. 236-46
- W. Gang, *et al.*
Strategy to targeting the immune resistance and novel therapy in colorectal cancer
Cancer Med., 7 (5) (2018), pp.1578–603
- W. Guo, *et al.*
Beta 4 integrin amplifies ErbB2 signaling to promote mammary tumorigenesis
Cell, 126 (2006), pp. 489-502
- W.M. van Grevenstein, *et al.*
Inflammatory cytokines stimulate the adhesion of colon carcinoma cells to mesothelial monolayers
Dig. Dis. Sci., 52 (2007), pp. 2775-783
- X. Garcia-Albeniz, *et al.*
Serum matrilysin correlates with poor survival independently of KRAS and BRAF status in refractory advanced colorectal cancer patients treated with irinotecan plus cetuximab
Tumour Biol., 32 (2011), pp. 417-24
- X. Li, *et al.*
Oncogenic transformation of diverse gastrointestinal tissues in primary organoid culture
Nat. Med., 20 (2014), pp. 769–77
- X. Tian, *et al.*
Organ-specific metastases obtained by culturing colorectal cancer cells on tissue-specific decellularized scaffolds
Nat. Biomed. Eng., 2 (2018), pp. 443-52
- X. Yin, *et al.*
Engineering stem cell organoids
Cell Stem Cell, 18 (2016), pp. 25–38
- Y. Miyauchi, *et al.*
A novel three-dimensional culture system maintaining the physiological extracellular matrix of fibrotic model livers accelerates progression of hepatocellular carcinoma cells
Sci. Rep., 7 (2017), pp. 1–9
- Y. Yonemura, *et al.*
Prognostic factors of peritoneal metastases from colorectal cancer following cytoreductive surgery and perioperative chemotherapy
Sci. World J., 2013, pp. 978394
- Y.R. van Gestel, *et al.*
Metachronous peritoneal carcinomatosis after curative treatment of colorectal cancer *Eur. J. Surg. Oncol.*, 40 (2014), pp. 963–69
- Z. Gong, *et al.*
Matching material and cellular timescales maximizes cell spreading on viscoelastic substrates
Proc. Natl. Acad. Sci. USA, 115 (2018), pp. E2686–E695

11 Appendix

Appendix A

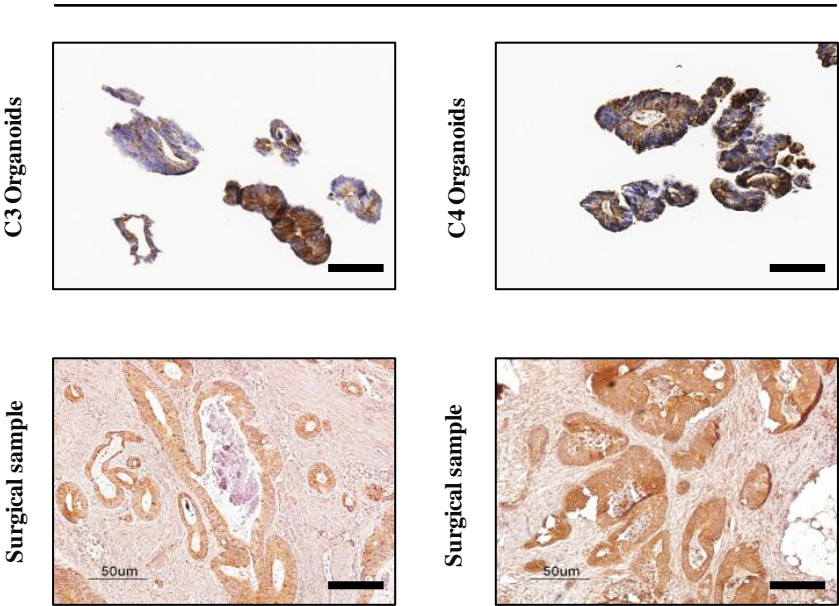
Appendix Figure 1

A



B

LGR5

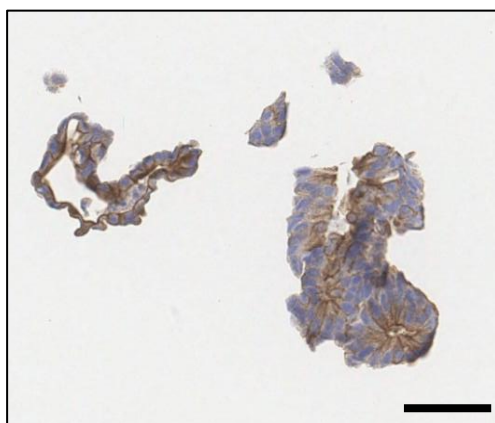


Appendix Figure 1. (A) IHC analysis of C1 and C2 organoids and corresponding surgical samples, using H&E staining and CK AE1/AE3, CK19, CK20, CDX2 and Ki-67 immunostaining (20X magnification). The images were previously published by Bozzi et al. (B) IHC analysis of PM-derived organoids (top) and their tissue of origin (bottom), using LGR5 immunostaining. LGR5-positive cells found in PM tissue are retained in the derived organoids. Scale bar: 50 μ m.

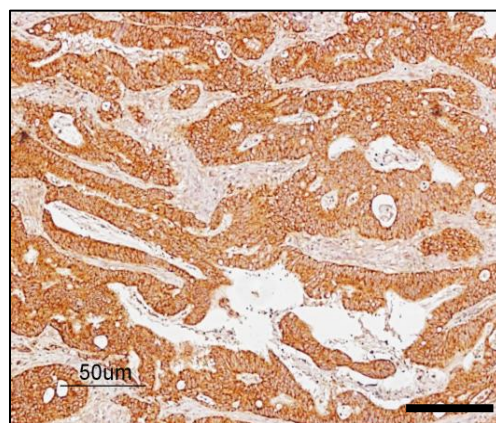
C

LGR5

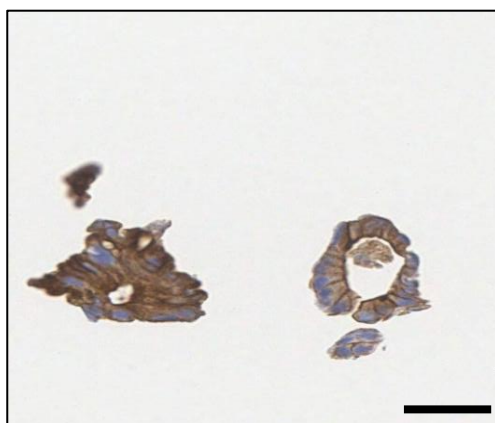
C5 Organoids



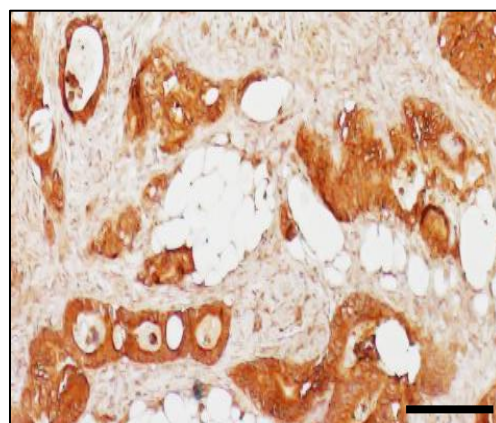
Surgical sample



C6 Organoids



Surgical sample



Appendix Figure 1. (C) IHC analysis of C5 and C6 organoid cultures and their tumor of origin, using LGR5 immunostaining. Scale bar: 50 μ m.

D

Genes	C1 Organoid	Tissue of origin
MSH3 (A62P)		
BRCA2 (G267Q)		
BRCA2 (S2414S)		
POLE (L1903L)		
PMS2 (S260S)		
BRCA2 (K1132K)		
RAD51C (D253H)		
POLE (A252V)		
BRCA2 (V2466A)		
ATM (D1853N)		
BRCA1 (E1038G)		
BRCA2 (V2171V)		
EGFR (N158N)		
ERBB2 (A356D)		
BRCA1 (S694S)		
BRCA1 (K1183R)		
BRCA1 (L771L)		
BRCA1 (D693N)		
BRCA1 (P871L)		
BRCA1 (S1436S)		
BRIP1 (Y1137Y)		
EGFR (T629T)		
BRCA1 (S1613G)		
KRAS (R161R)		
ATM (N1983S)		
BRCA1 (S1040N)		
ERBB2 (P1140A)		
POLD1 (K738N)		
MSH3 (E949R)		
BRCA2 (L1521L)		
EGFR (A613A)		
MSH6 (G39Q)		
BRIP1 (Q879Q)		
TP53 (R213R)		
BRIP1 (S919P)		
CDH1 (A692A)		
EGFR (T903T)		
KRAS (Q61H)		
POLE (A1510A)		
POLE (T1052T)		
POLE (S2084S)		
BARD1 (H506H)		
APC (S1411S)		
TP53 (P72R)		
EGFR (Q787Q)		
TP53 (R175H)		
BARD1 (T351T)		
PMS2 (K541E)		

% of Similarity: 97.92 %

Genes	C2 Organoid	Tissue of origin
MSH2 (L556L)		
PALB2 (T1100T)		
BMPR1A (P2T)		
PALB2 (E559R)		
APC (E260)		
MLH1 (I219V)		
APC (T1556fs)		
PMS2 (V280V)		
PALB2 (G998Q)		
MSH6 (D180D)		
MSH6 (P92P)		
POLD1 (T495T)		
PIK3CA (I391M)		
CTNNA1 (L180L)		
MSH6 (R62R)		
BRCA2 (V2466A)		
KRAS (R162R)		
BARD1 (A40V)		
MSH3 (I78V)		
BRCA2 (V1269V)		
PALB2 (E672Q)		
FANCM (I1460V)		
ATM (S1270C)		
BRCA2 (I3412V)		
BRAF (G643G)		
BRCA2 (V2171V)		
MSH3 (Q949R)		
FANCM (V878L)		
ATM (N1983S)		
EGFR (T629T)		
BRAF (V600E)		
ATM (D1853N)		
MSH3 (A1045T)		
POLE (P1548T)		
BRCA2 (L1521L)		
CTNNA1 (S740S)		
EGFR (T903T)		
FANCM (S175F)		
BRIP1 (E879E)		
NBN (D399D)		
BARD1 (P24S)		
CDH1 (A692A)		
BARD1 (H506H)		
TP53 (R273H)		
PMS2 (K541E)		
EGFR (Q787Q)		
EGFR (R521K)		
FANCM (P1812A)		
TP53 (P72R)		

% of Similarity: 91.84 %

Appendix Figure 1. (D) List of the gene mutations acquired in the TDOs compared to the tumor of origin (red boxes). The percentage of similarity is also reported. Passage numbers of the organoid lines were: C1: P11; C2: P13; C3: P10; C4: P14; C6: P10.

D

Genes	C3 Organoid	Tissue of origin
PMS2 (K541E)		
PMS2 (P470S)		
PMS2 (S260S)		
TP53 (R273C)		
TP53 (P72R)		
CDKN2A (A148T)		
PALB2 (V932M)		
KRAS (R161R)		
BRCA2 (N372H)		
BRCA2 (K1132K)		
BRCA2 (L1521L)		
BRCA2 (V2171V)		
BRCA2 (S2414S)		
BRCA2 (V2466A)		
RAD51D (R24R)		
ERBB2 (I625V)		
ERBB2 (P1104A)		
BRCA1 (S1613G)		
BRCA1 (S1436S)		
BRCA1 (K1183R)		
BRCA1 (E1038G)		
BRCA1 (P871L)		
BRCA1 (L771L)		
BRCA1 (S694S)		
BRCA1 (D693N)		
FANCM (S175F)		
FANCM (V878L)		
FANCM (I1460V)		
FANCM (I1742V)		
FANCM (P1812A)		
MSH6 (R62R)		
MSH6 (P92P)		
MSH6 (D180D)		
EGFR (N158N)		
EGFR (T903T)		
BRIP1 (Y1137Y)		
BRIP1 (S919P)		
BRIP1 (E879E)		
CDH1 (A692A)		
MSH3 (A55A del)		
MSH3 (A61P dup)		
MSH3 (P67P69 del)		
MSH3 (I79V)		
MSH3 (Q949R)		
MSH3 (A1045T)		
BMPR1A (P2T)		
NBN (P672P)		
NBN (D399D)		
NBN (E185Q)		
NBN (L34L)		
ATM (N1983S)		
APC (Q48Q)		
APC (D774D)		
APC (I1417fs)		
APC (V1822D)		
POLE (S2084S)		
POLE (A1510A)		
POLE (T1052T)		
CTNNA1 (A179V)		
PIK3CA (Q546R)		

% of Similarity: 100 %

Genes	C4 Organoid	Tissue of origin
KRAS (R161R)		
KRAS (G12S)		
BRCA2 (K1132L)		
BRCA2 (L1521L)		
BRCA2 (T1915M)		
BRCA2 (V2171V)		
BRCA2 (S2414)		
BRCA2 (V2466A)		
MSH6 (R62R)		
MSH6 (P92P)		
MSH6 (D180D)		
MSH6 (R1034Q)		
SMAD4 (D351N)		
POLD1 (T495T)		
EGFR (T903T)		
EGFR (D994D)		
BRIP1 (Y1137Y)		
BRIP1 (S919P)		
BRIP1 (E879E)		
CDH1 (T379M)		
CDH1 (A692A)		
MSH3 (A55A60 del)		
MSH3 (P67P69 del)		
MSH3 (I79V)		
MSH3 (Q949R)		
BMPR1A (P2T)		
ATM (N1983S)		
APC (Y486Y)		
APC (A545A)		
APC (S835fs)		
APC (L1488)		
APC (T1493T)		
APC (G1678G)		
APC (S1756S)		
APC (V1822D)		
APC (P1960P)		
POLE (S2084S)		
BRAF (G643G)		
BARD1 (V507M)		

% of Similarity: 87.18 %

Appendix Figure 1. (D) List of the gene mutations acquired in the TDOs compared to the tumor of origin (red boxes). The percentage of similarity is also reported. Passage numbers of the organoid lines were: C1: P11; C2: P13; C3: P10; C4: P14; C6: P10.

D

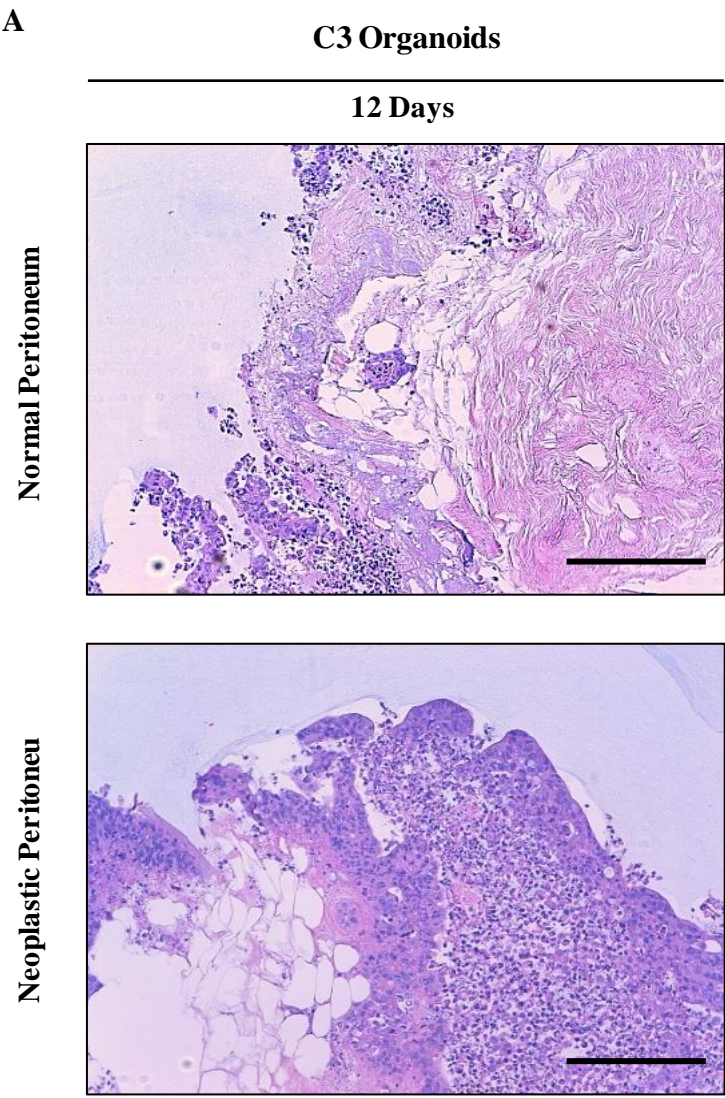
Genes	C6 organoid	Tissue of origin
PMS2 (P470S)		
PMS2 (S260S)		
TP53 (G245V)		
TP53 (P72A)		
CDKN2A (A148T)		
KRAS (R161R)		
KRAS (G12A)		
BRCA2 (N372H)		
BRCA2 (K1132K)		
BRCA2 (L1521L)		
BRCA2 (T1915M)		
BRCA2 (V2171V)		
BRCA2 (S2414S)		
BRCA2 (V2466A)		
RAD51D (R145C)		
MLH1 (I219V)		
ERBB2 (P1140A)		
BRCA1 (S1613G)		
BRCA1 (S1436S)		
BRCA1 (K1183R)		
BRCA1 (E1038G)		
BRCA1 (P871L)		
BRCA1 (L771L)		
BRCA1 (S694S)		
MUTYH (S515F)		
MUTYH (Q338H)		
MSH6 (R62R)		
MSH6 (P92P)		
MSH6 (D180D)		
MSH6 (Y214Y)		
SMAD4 (D315H)		
EGFR (N158N)		
EGFR (R521K)		
EGFR (Q787Q)		
EGFR (R836R)		
EGFR (T903T)		
BRIP1 (Y1137Y)		
BRIP1 (S919P)		
BRIP1 (E879E)		
CDH1 (A692A)		
MSH3 (A55A60del)		
MSH3 (P67P69del)		
MSH3 (I79V)		
MSH3 (Q949R)		
MSH3 (A1045T)		
BMPR1A (P2T)		
ATM (D1853N)		
ATM (N1983S)		
APC (Y486Y)		
APC (A545A)		
APC (L1129S)		
APC (Q1406fs)		
APC (T1493T)		
APC (G1678G)		
APC (S1756S)		
APC (V1822D)		
APC (P1960P)		
POLE (S2084S)		
POLE (A1510A)		
POLE (N1396S)		
POLE (T1052T)		
CTNNA1 (S740S)		
BRAF (G643G)		
BARD1 (H506H)		
BARD1 (T351T)		

% of Similarity: 93.85 %

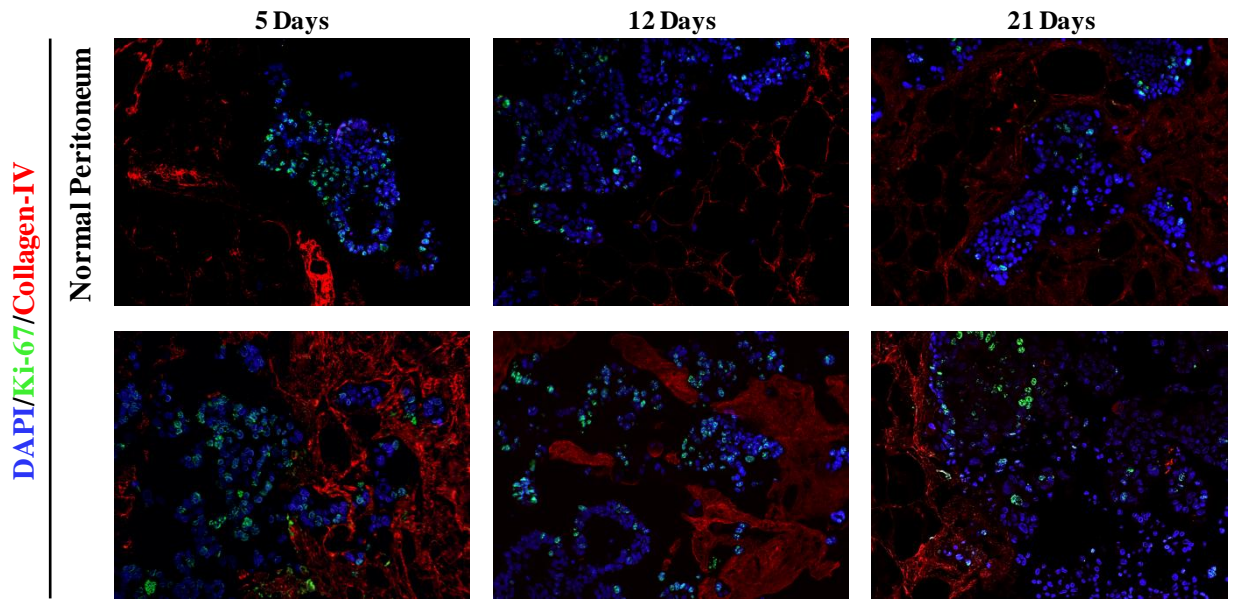
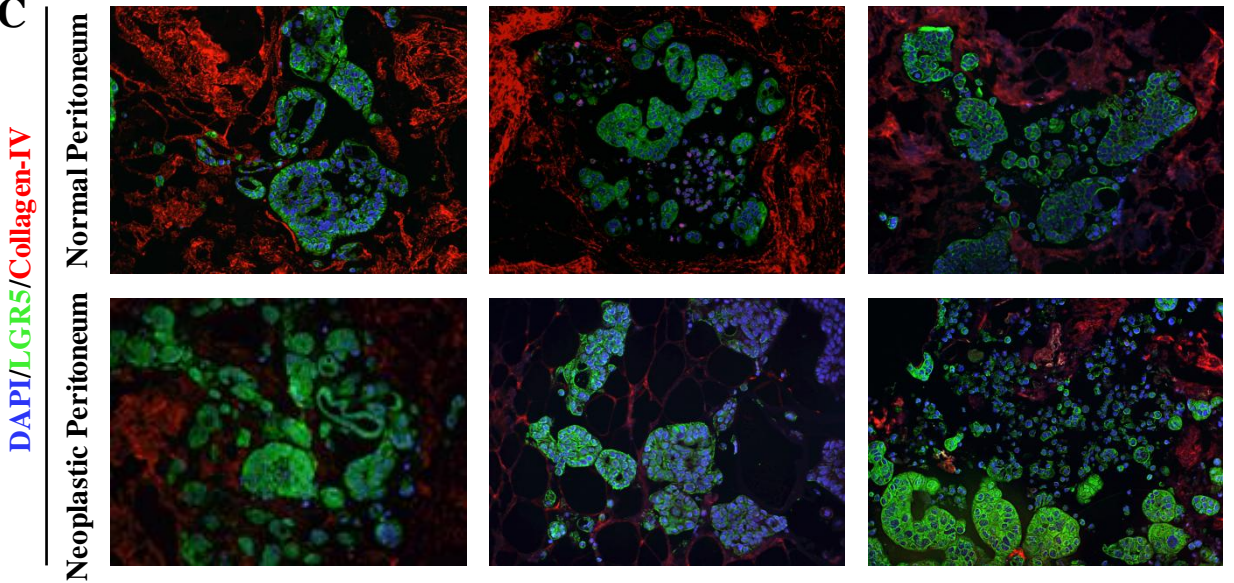
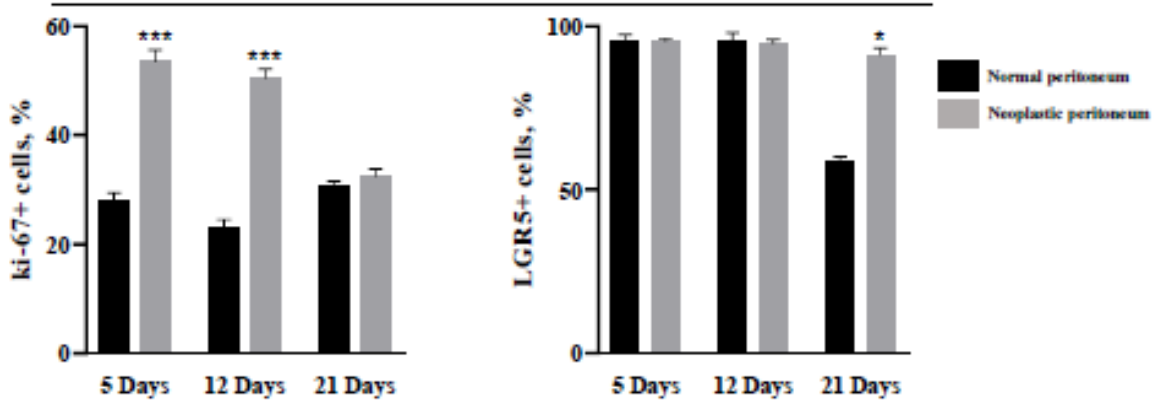
Appendix Figure 1. (D) List of the gene mutations acquired in the TDOs compared to the tumor of origin (red boxes). The percentage of similarity is also reported. Passage numbers of the organoid lines were: C1: P11; C2: P13; C3: P10; C4: P14; C6: P10.

Appendix B

Appendix B Figure 1



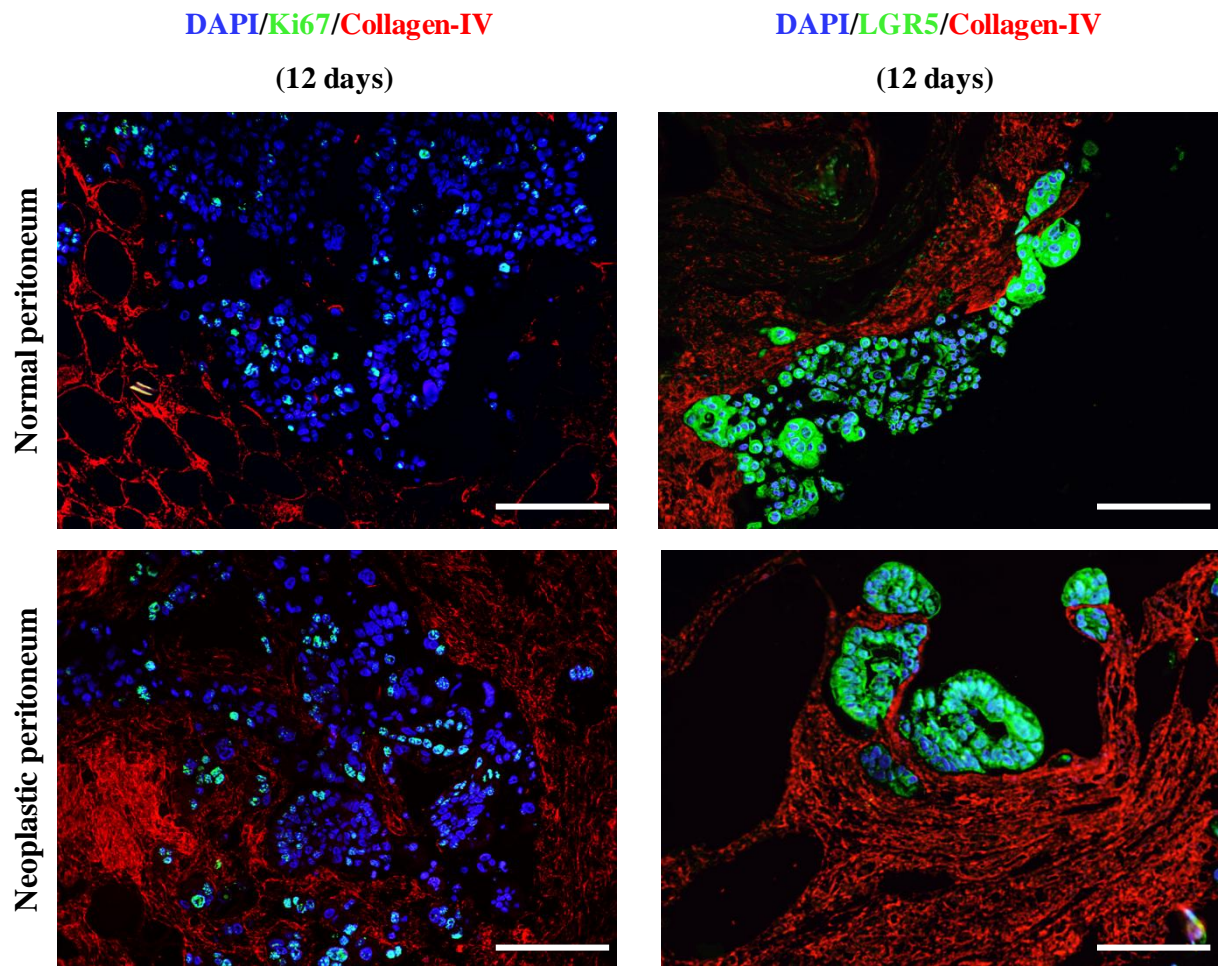
Appendix Figure 1. (A) H&E staining of decellularized matrices derived from normal (top) or neoplastic (bottom) peritoneum repopulated with PM-derived organoids (C3) on day 12. Scale bar: 100 μm . The repopulation experiments were performed in triplicate.

B**C2 Organoids****C****D****C2 Organoids**

Appendix Figure. 1. (B) IF analysis of 3D-dECMs derived from normal (top) and neoplastic (bottom) peritoneum repopulated with PM-derived organoids (C2) at different time points as indicated, using Ki-67 (green) and collagen IV (red) antibodies. Scale bar: 50 μ m. The experiments were performed in triplicate. **(C)** IF analysis of 3D-dECMs derived from normal (top) and neoplastic (bottom) peritoneum repopulated with PM-derived organoids (C2) at different time points as indicated, using LGR5 (green) and collagen IV (red) antibodies. Scale bar: 50 μ m. The experiments were performed in triplicate. **(D) Left panel:** proliferation rate of PM-derived organoids, measured as the percentage of Ki-67⁺ cells present in fields devoid of dead cells. Five fields per experiment (40X magnification) were counted. Data are presented as median and SD for surgical specimens of three patients. One-way ANOVA (*** p < 0.001). **Right panel:** amount of stem cells in PM-derived organoids, measured as the percentage of LGR5⁺ cells present in fields devoid of dead cells. Five fields per experiment (40X magnification) were counted. Data are presented as median and SD for surgical specimens of three patients. One-way ANOVA (* p < 0.05). The experiments were performed in triplicate.

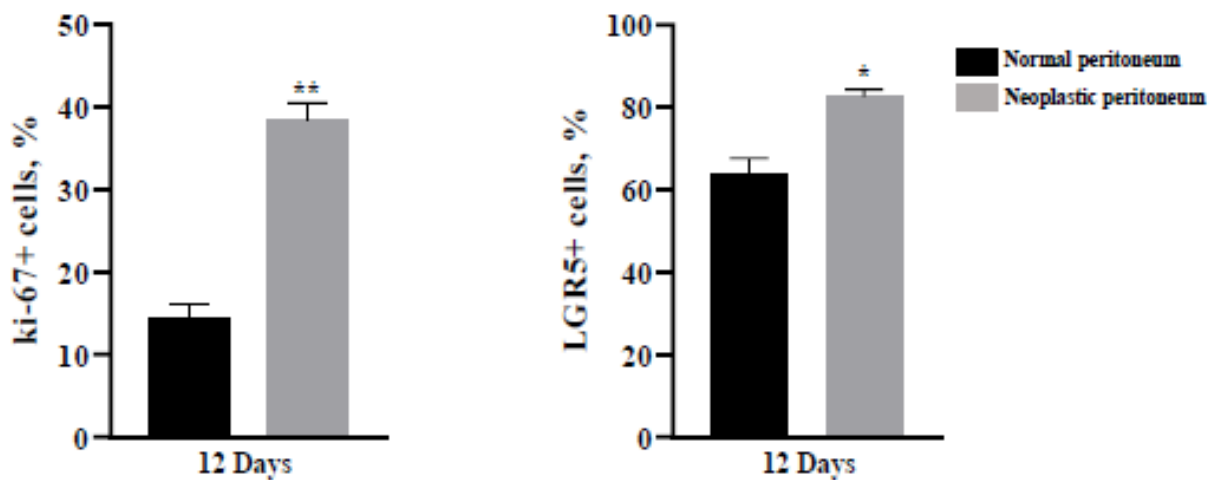
E

C3 Organoids



F

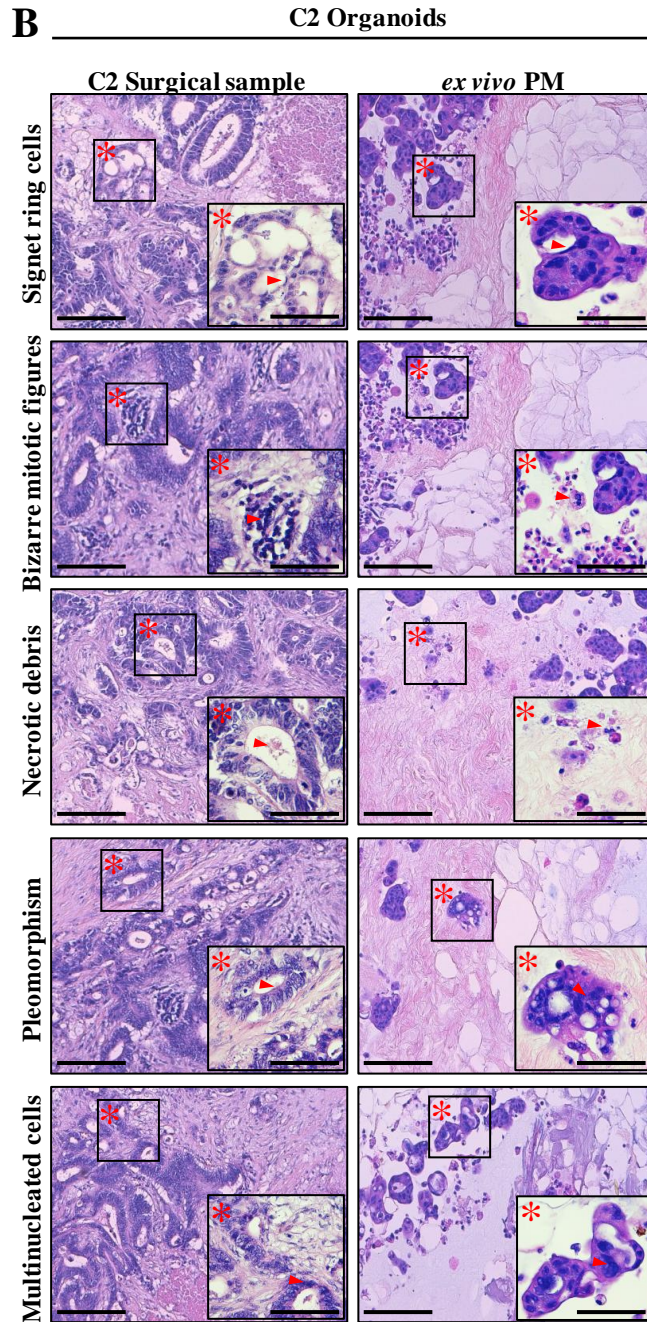
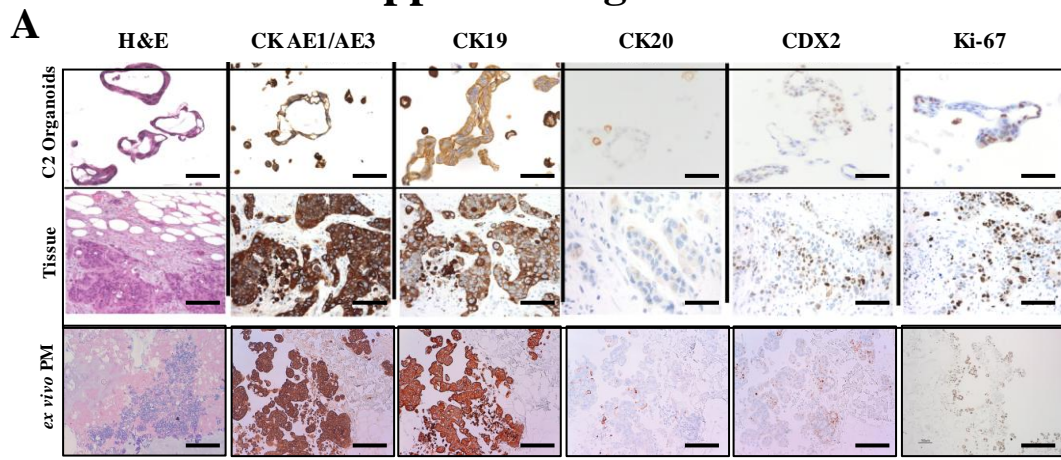
C3 Organoids



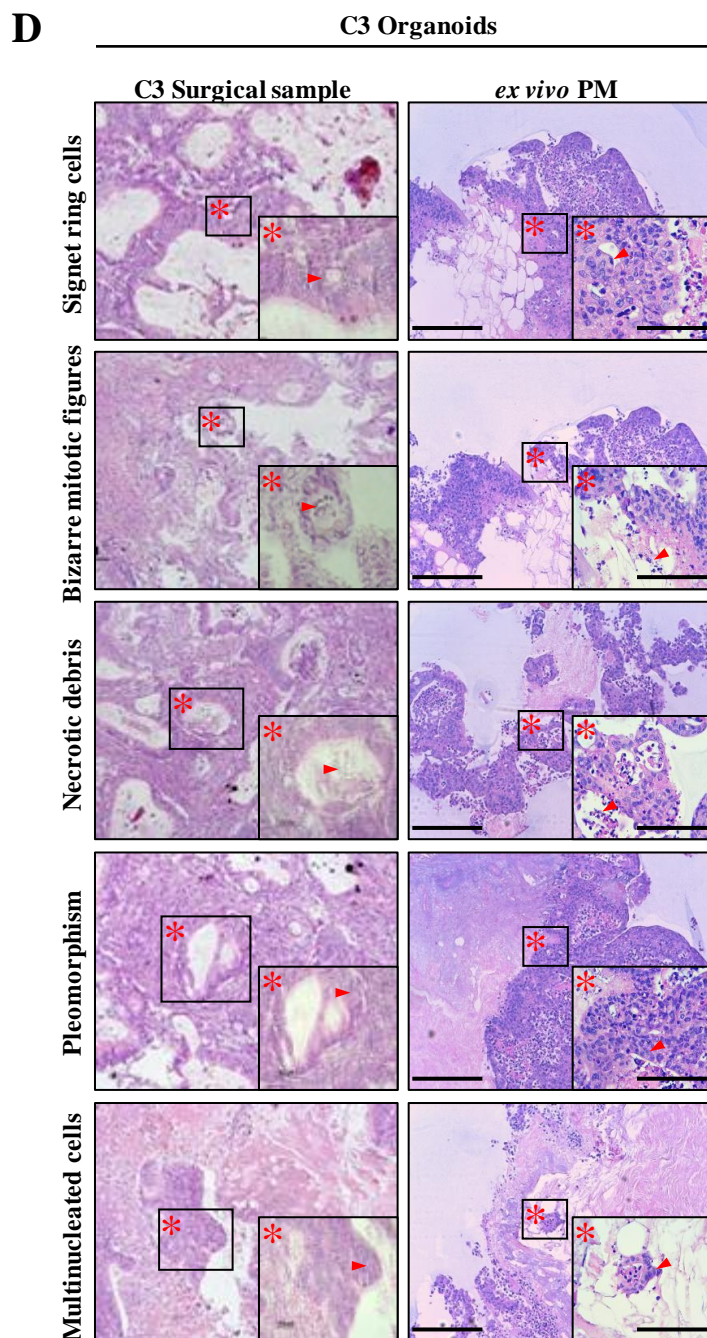
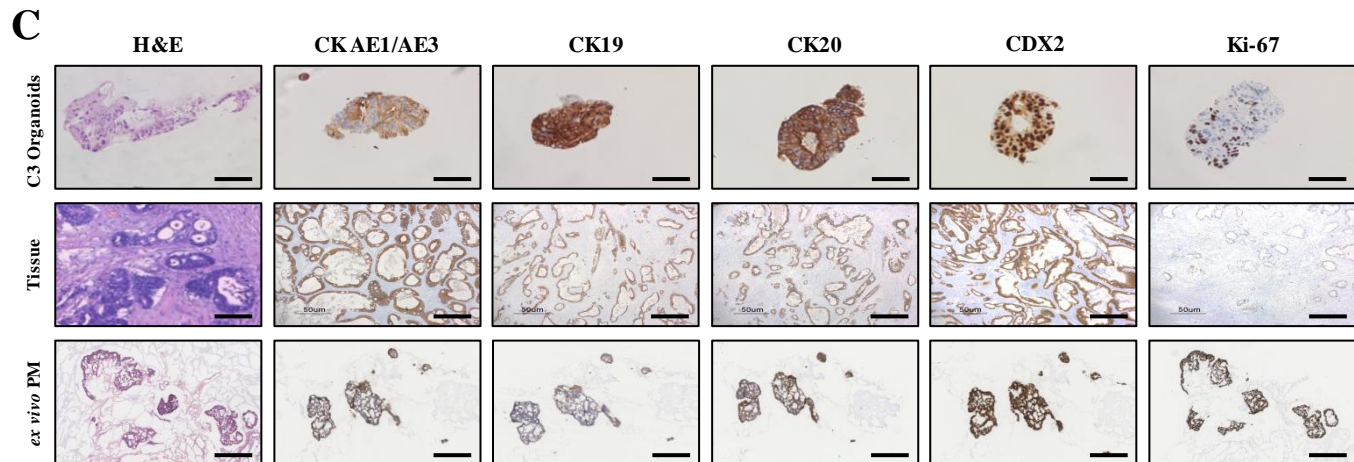
Appendix Figure 1. (E) IF analysis of 3D decellularized matrices derived from normal (top) and neoplastic (bottom) peritoneum repopulated with PM-derived organoids (C3) on day 12, using Ki-67 (green) and collagen IV (red) (left panel), and LGR5 (green) and collagen IV (red) (right panel) antibodies. Scale bar: 50 μ m. The experiments were performed in triplicate. **(F) Left panel:** proliferation rate of PM-derived organoids measured as the percentage of Ki-67⁺ cells present in fields devoid of dead cells. Five fields per experiment (40X magnification) were counted. Data are presented as median and SD for surgical specimens of three patients. Student's *t*-test (** $p < 0.01$). **Right panel:** Amount of stem cells in PM-derived organoids, measured as the percentage of LGR5⁺ cells present in fields devoid of dead cells. Five fields per experiment (40X magnification) were counted. Data are presented as median and SD for surgical specimens of three patients. Student's *t*-test (* $p < 0.05$). The experiments were performed in triplicate.

Appendix C

Appendix Figure 1



Appendix Figure 1. (A) Comparative histological and immunohistochemical analysis of PM-derived organoids (C2) versus their corresponding tumor of origin and the *ex vivo* engineered PM lesion. Samples were analyzed for the expression of the CRC-specific markers as indicated. Scale bar: 50 μ m. Images in the first two lanes were previously published by Bozzi et al¹¹. **(B)** Histological analysis of PM and neoplastic-derived 3D-dECM repopulated with C2 PM-derived organoids. The *ex vivo* engineered PM lesions present histological features that are typical of PMs of gastrointestinal origin. Asterisks and arrows indicated the main morphological features. Scale bar: 20 μ m.

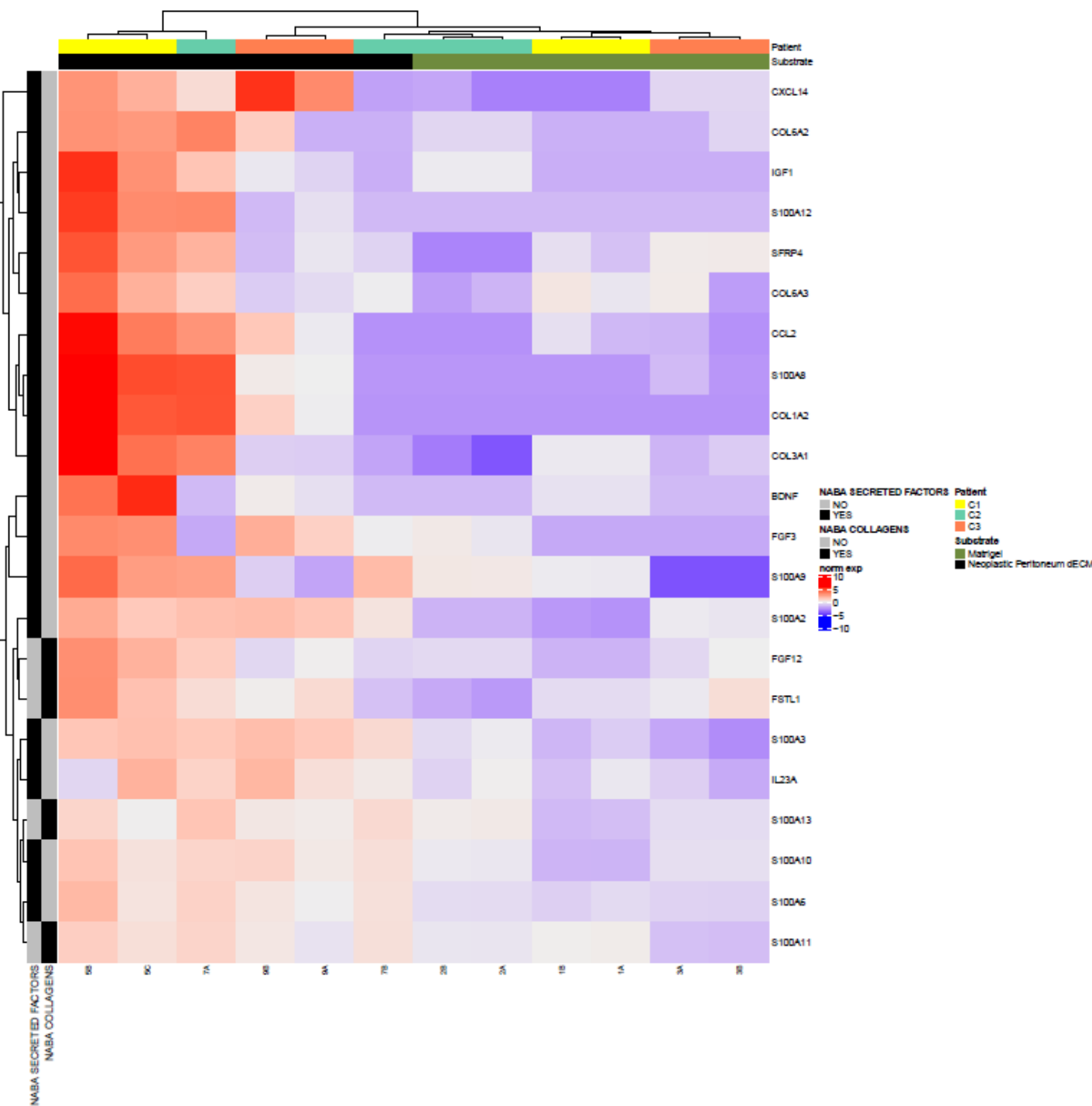


Appendix Figure 1. (C) Comparative histological and immunohistochemical analysis of PM-derived organoids (C3) versus their corresponding tumor of origin and the *ex vivo* engineered PM lesion. Samples were analyzed for the expression of the CRC-specific markers as indicated. Scale bar: 50 μ m. **(D)** Histological analysis of peritoneal metastasis and neoplastic-derived 3D-DECMS repopulated with C3 PM-derived organoids. The *ex vivo* engineered PM lesions present histological features that are typical of PMs of gastrointestinal origin. Asterisks and arrows indicated the main morphological features. Scale bar: 20 μ m.

Appendix D

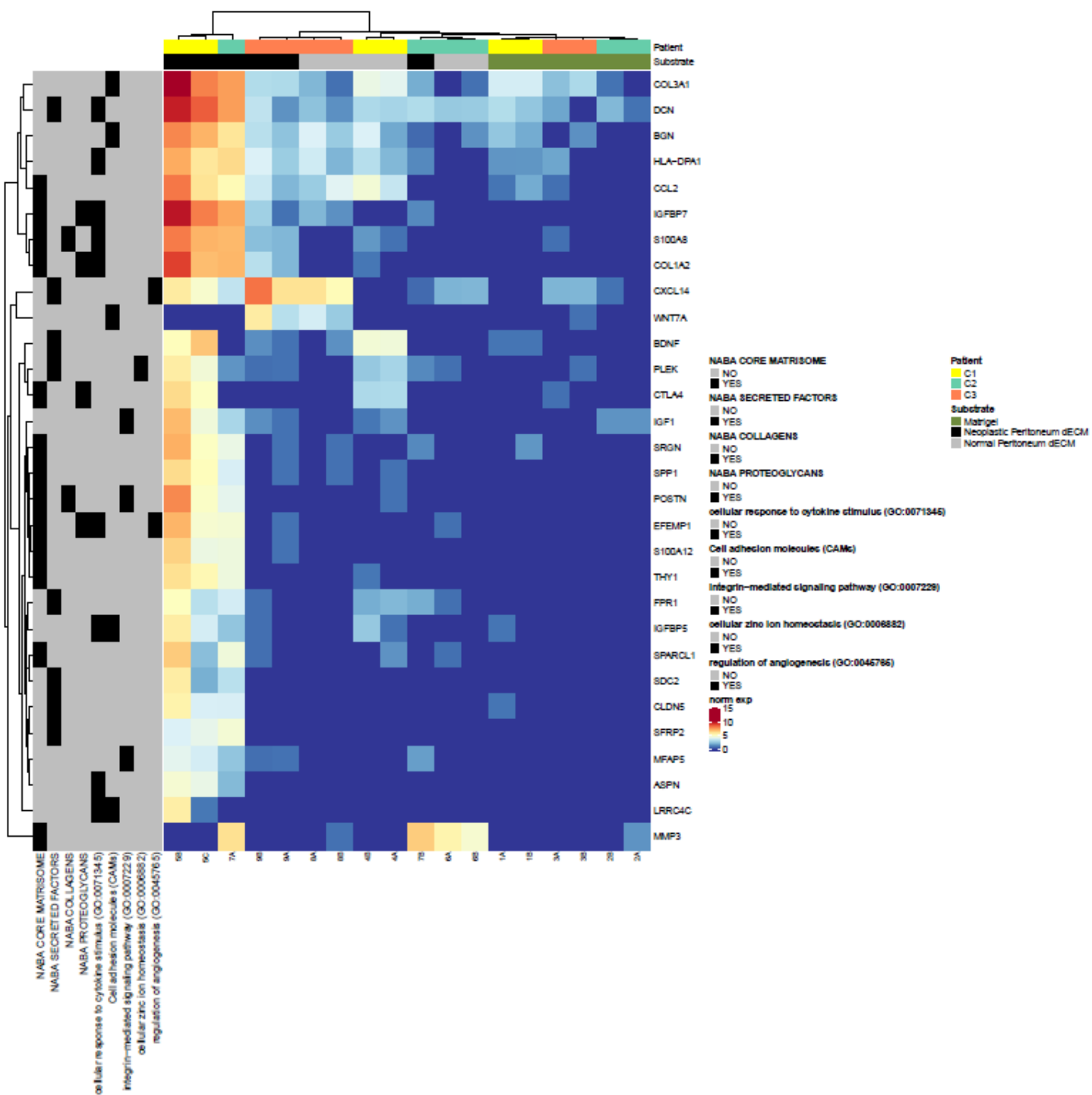
Appendix D Figure 1

A



Appendix D Figure.1. (A) Unsupervised hierarchical clustering of organoids based on the expression of the top DEGs between organoids grown on neoplastic 3D-dECM and in Matrigel, and present in Naba Secreted Factors or Naba Collagen categories.

B



Appendix D Figure 1. (B) Unsupervised hierarchical clustering of organoids based on the expression of the top DEGs between organoids grown on neoplastic 3D-dECM, normal 3D-dECM and in Matrigel, and present in Naba Core Matrisome, Naba Secreted Factors, Naba Collagen categories, Naba Proteoglycan categories, cellular response to cytokine stimulus, cell adhesion molecules, integrin mediated signaling pathway, cellular zinc ion homeostasis, and regulation of angiogenesis categories.

C

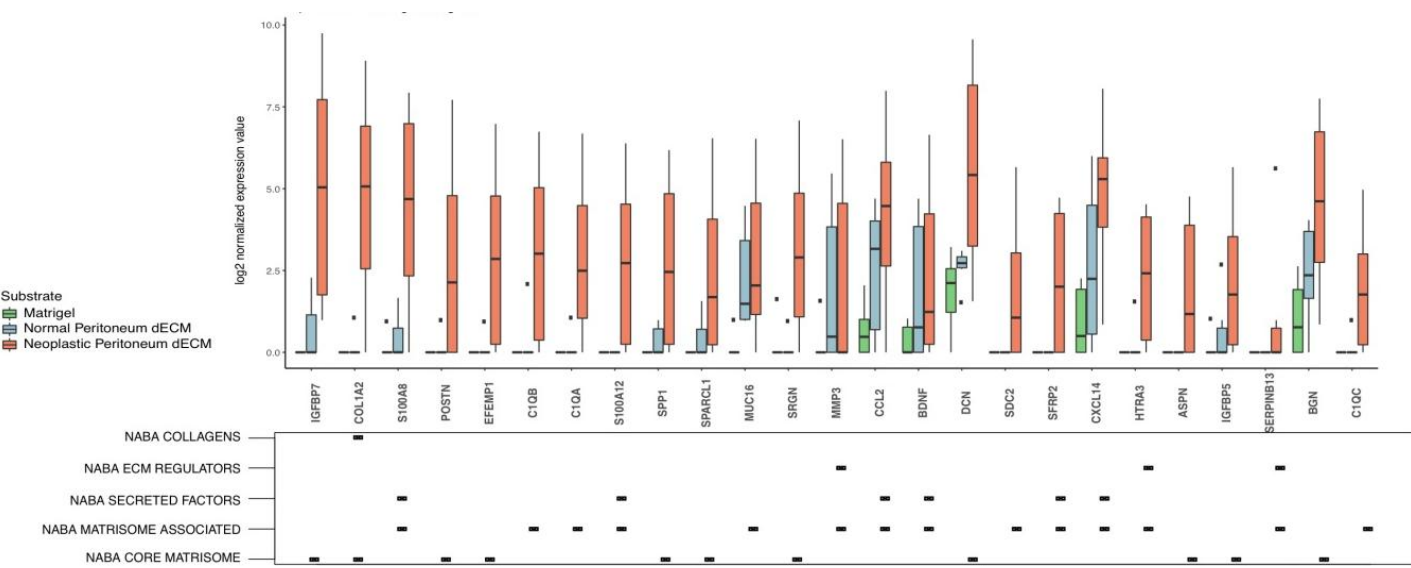
	Collection	ID	Term	Adjusted <i>p</i> -value	Leading Edge genes (%)	# Genes
Neoplastic 3D-dECM Vs Matrigel	GO BP	GO:0071345	Cellular response to cytokine stimulus	0.003365	27.1	413
	GO BP	GO:0045765	Regulation of angiogenesis	0.003365	19.3	171
	GO BP	GO:0006882	Cellular zinc ion homeostasis	0.003365	46.7	30
	GO BP	GO:0071280	Cellular response to copper ion	0.003365	55.0	20
	GO BP	GO:0007229	Integrin-mediated signaling pathway	0.011230	19.6	56
	KEGG		Wnt signaling pathway	0.022987	20.5	151
Normal 3D-dECM Vs Matrigel	GO BP	GO:0071280	Cellular response to copper ion	0.006015	55.0	20
	GO BP	GO:0071294	Cellular response to zinc ion	0.006015	64.7	17
	KEGG		Cell adhesion molecules (CAMs)	0.006015	32.8	128
Neoplastic 3D-dECM Vs Normal 3D-dECM	KEGG		ECM-receptor interaction	0.004499	25.0	80
	GO BP	GO:0045765	Regulation of angiogenesis	0.009176	15.2	171
	KEGG		Cell adhesion molecules (CAMs)	0.020511	22.7	132
	Reactome	R-HSA-5660526	Response to metal ions Homo sapiens	0.040965	81.8	11
	GO BP	GO:0030198	Extracellular matrix organization	0.002740	25.3	221

D

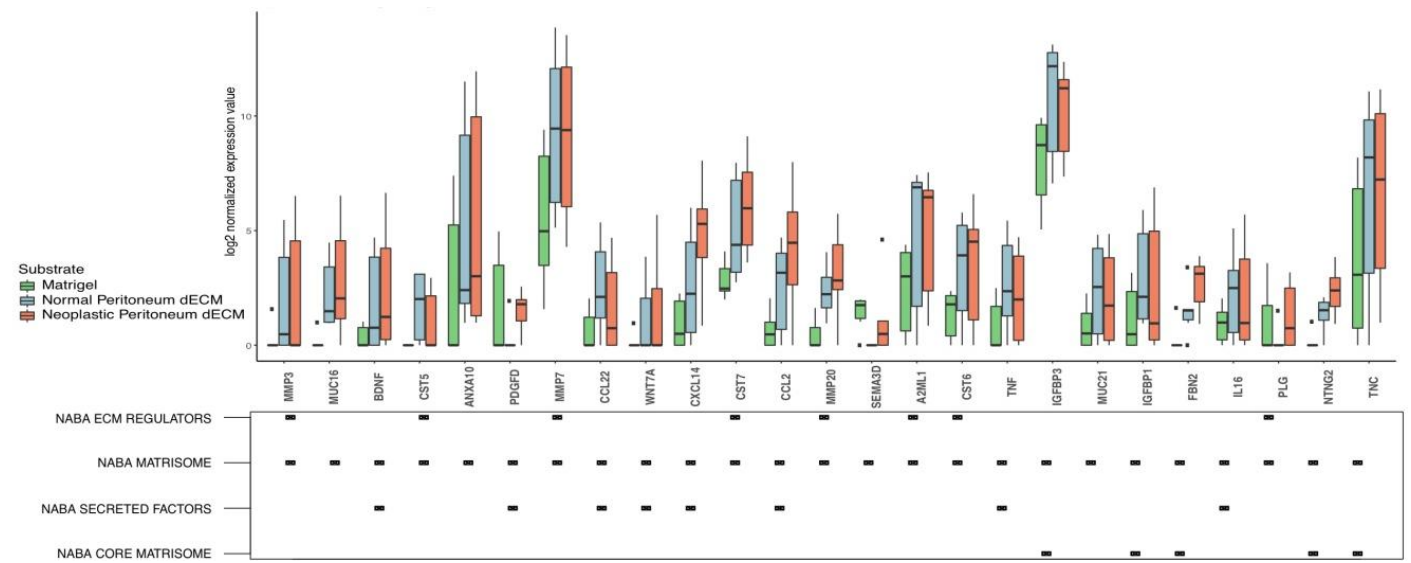
	Collection	Term	Adjusted <i>p</i> -value	Leading Edge genes (%)	# Genes
Neoplastic 3D-dECM Vs Matrigel	NABA MATRISOME	Naba Matrisome Associated	0.003365	38.2	663
	NABA MATRISOME	Naba Core Matrisome	0.003365	36.1	266
	NABA MATRISOME	Naba ECM Regulators	0.003365	30.6	222
	NABA MATRISOME	Naba Secreted Factors	0.003365	45.1	288
	NABA MATRISOME	Naba Collagens	0.004307	31.2	44
Normal 3D-dECM Vs Matrigel	NABA MATRISOME	Naba ECM Regulators	0.0060150	39.2	217
	NABA MATRISOME	Naba Core Matrisome	0.006015	22.7	256
	NABA MATRISOME	Naba Secreted Factors	0.006015	34.7	274
	NABA MATRISOME	Naba Matrisome	0.006024	32.9	897
Neoplastic 3D-dECM Vs Normal 3D-dECM	NABA MATRISOME	Naba Core Matrisome	0.002740	26.3	266
	NABA MATRISOME	Naba Secreted Factors	0.002740	39.2	291
	NABA MATRISOME	Naba ECM Glycoproteins	0.002740	21.9	192
	NABA MATRISOME	Naba Collagens	0.002740	40.9	44
	NABA MATRISOME	Naba Proteoglycans	0.002740	53.3	30
	NABA MATRISOME	Naba ECM Regulators	0.024908	28.2	16

Appendix Figure 1. (C) Selected categories enriched in DEGs between organoids grown on neoplastic 3D-dECM, normal 3D-dECM and in Matrigel involved in relevant biological processes according to GO Biological Process, KEGG and Reactome databases. (D) Selected Matrisome categories enriched in DEGs between organoids grown on neoplastic 3D-dECM, normal 3D-dECM and in Matrigel involved in relevant biological processes according to Naba Maatrisome dataset.

E

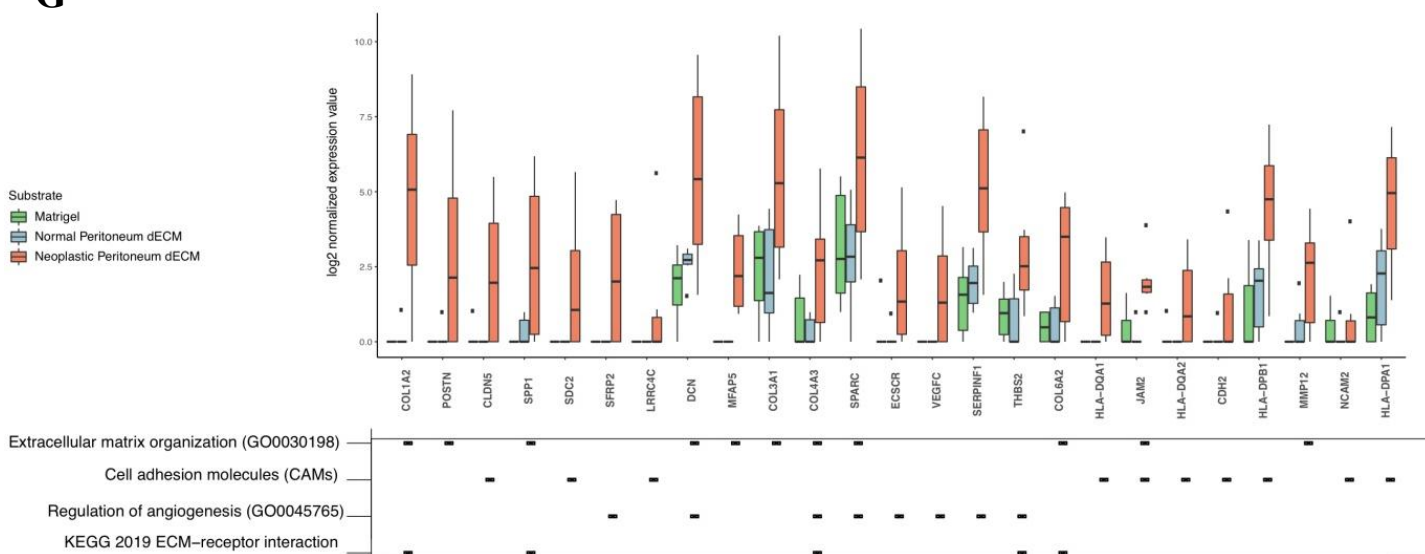


F

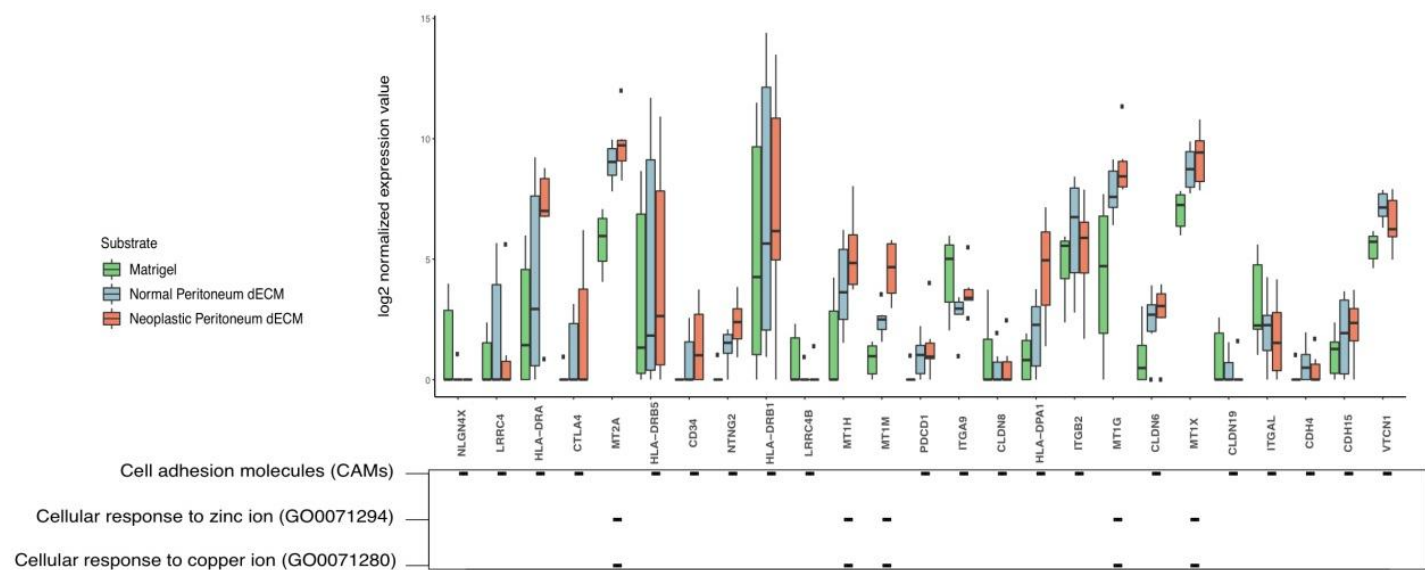


Appendix Figure 1. (E) Box plot showing the expression in organoids grown on neoplastic 3D-dECM and in Matrigel, of DEGs selected based on their involvement in the indicated processes of the Naba Matrisome geneset. DEGs expression in organoids grown on normal 3D-dECM is also shown. Median and interquartile range are displayed as horizontal lines. Black squares in the bottom panel indicate which category the genes belong to. **(F)** Box plot showing the expression, in organoids grown on normal 3D-dECM and in Matrigel, of DEGs selected based on their involvement in the indicated processes of the Naba Matrisome geneset. DEGs expression in organoids grown on neoplastic 3D-dECM is also shown. Median and interquartile range are displayed as horizontal lines. Black squares in the bottom panel indicate which category the genes belong to.

G



H



Appendix Figure 1. (G) Box plot showing the expression in organoids grown on normal 3D-dECMs and in Matrigel, of DEGs selected based on their involvement in the indicated processes of GO Biological Process, KEGG and Reactome databases. DEGs expression in organoids grown on neoplastic 3D-dECM is also shown. Median and interquartile range are displayed as horizontal lines. Black squares in the bottom panel indicate which category the genes belong to. **(H)** Box plot showing the expression levels of genes selected based on their involvement in the indicated processes. The expression levels of the selected genes were compared in organoids grown in Matrigel, on neoplastic 3D-dECM and on normal 3D-dECM. Median and interquartile range are displayed as horizontal lines. Black squares in the bottom panel indicate which category the genes belong to.